

**Fluorescence-Based Methods to Study Rapid Dynamics and
Conformational Flexibility in Peptides**

INAUGURALDISSERTATION

zur

Erlangung der Würde eines Doktors der Philosophie

vorgelegt der

Philosophisch-Naturwissenschaftlichen Fakultät

der

UNIVERSITÄT BASEL

von

FANG HUANG

aus Gongcheng (Guangxi), China

Basel, 2004

Genehmigt von der Philosophisch-Naturwissenschaftlichen Fakultät

auf Antrag von

Prof. Dr. Jakob Wirz und Prof. Dr. Helma Wennemers

Basel, den 30.03.2004

Prof. Dr. M. Tanner
Dekan

*To the memory of my beloved mother,
who passed away in January 1997.*

Acknowledgement

First of all, I would like to deeply express my gratitude to my supervisor, Prof. Werner Nau, for giving me the opportunity to work in his group and allowing me to work on this interesting project. He guided me throughout this thesis with stimulating suggestions, fruitful discussions and encouragements.

I thank Prof. Jakob Wirz and Prof. Helma Wennemers in their function as referees and Prof. Hanspeter Huber in his function as chairman.

I sincerely thank Prof. Robert R. Hudgins (York University, Canada) for introducing me into the “peptide world”, for his constructive collaboration and constant support also after he accepted a faculty position in Toronto.

Prof. Elisha Haas and his group members (Bar-Ilan University, Israel) are appreciated for their kind collaboration in the data analysis within our FRET project.

I am indebted to the kind support from Prof. Joachim Seelig and his group members (Biozentrum, Universität Basel). All the CD experiments were carried out in his group.

I would like to express my thanks to the group members of Prof. Werner Nau and Prof. Jakob Wirz for their help and for providing a friendly working environment.

I must thank the financial support from the Swiss National Science Foundation. Without this financial support, I would not have been able to finish my thesis.

A particular acknowledgement goes to my parents, sisters, brother and all my friends for their help and encouragement.

Finally, my deepest appreciation goes to my dear wife, Xiaojuan, for her love, support and encouragement in the past years.

Contents

1. Abstract	(6)
2. Introduction	(9)
2.1. General background	(9)
2.2. Techniques to study the dynamics and folding of proteins and peptides	(11)
3. DBO-based fluorescence methodologies to study peptide dynamics	(19)
3.1. A fluorescence method based on a contact quenching mechanism	(19)
3.2. A method based on intramolecular fluorescence resonance energy transfer	(22)
4. Length dependence of end-to-end collision rates in peptides	(24)
5. A flexibility scale for amino acids in peptides	(27)
6. Primary and secondary structure dependence of peptide flexibility	(30)
7. Intramolecular energy transfer in peptides	(33)
8. Ongoing project: Helix-coil transition of an alanine-rich peptide	(37)
9. Summary	(42)
10. A brief experimental description	(43)
11. Publications	(44)
12. Presentations at conferences	(45)
13. Appendix	(47)
14. Curriculum Vitae	

1. Abstract

Intramolecular collision of polypeptides is the primary step in protein folding, the dynamics of which is of importance for understanding this fascinating topic. In this thesis the rapid dynamics and flexibility of several sets of peptides were experimentally investigated with a fluorescence-based method, where the long-lived, hydrophilic fluorophore, 2,3-diazabicyclo[2.2.2]oct-2-ene (DBO), was employed, which can be selectively and efficiently quenched by tryptophan (Trp) through contact. An asparagine derivative, Fmoc-DBO, was synthesized and applied to standard solid-phase peptide synthesis to obtain DBO/Trp-labeled peptides. The end-to-end collision rates can then be directly related to the intramolecular quenching of DBO by Trp. [Hudgins, R. R.; Huang, F.; Gramlich, G.; Nau, W. M. *J. Am. Chem. Soc.* **2002**, *124*, 556-564 (Appendix I); Nau, W. M.; Huang, F.; Wang, X.; Bakirci, H.; Gramlich, G.; Marquez, C. *Chimia* **2003**, *57*, 161-167 (Appendix III); Marquez, C.; Huang, F.; Nau, W. M. *IEEE Trans. Nanobiosci.* **2004**, *3*, 39-45 (Appendix V)]

This method has been further improved by establishing a dual quencher system, i.e., tyrosine (Tyr) was employed as an additional quencher, which can react with DBO upon contact but with a lower efficiency than Trp. The combination of two probe/quencher pairs with different quenching efficiency as well as the theoretical results for intermolecular diffusion allows the extrapolation of the microscopic rate constants for formation and dissociation of the end-to-end encounter complex even in the absence of diffusion-controlled quenching. [Nau, W. M.; Huang, F.; Wang, X.; Bakirci, H.; Gramlich, G.; Marquez, C. *Chimia* **2003**, *57*, 161-167 (Appendix III); Huang, F.; Hudgins, R. R.; Nau, W. M. **2004**, Submitted for publication (Appendix VI)]

We first applied this fluorescence-based method to measure the end-to-end collision rate constants in flexible Gly-Ser peptides with varying length. The results suggest that the behavior of real peptides deviates significantly from that of the ideal chain model and the speed limit for protein folding should be faster than that reported previously. [Hudgins, R. R.; Huang, F.; Gramlich, G.; Nau, W. M. *J. Am. Chem. Soc.* **2002**, *124*, 556-564 (Appendix I)]

We also investigated the end-to-end collision rates of another series of peptides composed of different types of amino acids in the backbone but with identical length. The experimental results have led to a conformational flexibility scale for amino acids in

peptides and suggested that the flexibility of peptides is mainly determined by the atoms and groups in close proximity to the backbone, while the more remote atoms and groups have a smaller effect on the peptide dynamics due to their larger conformational space. [Huang, F.; Nau, W. M. *Angew. Chem. Int. Ed.* **2003**, *42*, 2269-2272 (Appendix II); Huang, F.; Nau, W. M. *Res. Chem. Intermed.* **2004**, submitted for publication (Appendix VII)]

Further investigations on peptides derived from the *N*-terminal β -hairpin of ubiquitin were also carried out. The end-to-end collision rates in these peptides showed significant dependence on the secondary structure, i.e., the turn segment is much more flexible than the strand segments, which supports a previous proposal that the β -turn is the initiator for the formation of the whole β -hairpin. Activation energies for end-to-end collision of these peptides showed a good agreement with the collision rate constants, which indicates that the activation energy may also be a measure of the flexibility of peptides although it is not as sensitive as the collision rate. [Huang, F.; Hudgins, R. R.; Nau, W. M. **2004**, Submitted for publication (Appendix VI)]

Additionally, to get more detailed structural information of our peptides and to reveal the underlying reasons for the deviation of the experimental length dependence of end-to-end collision rates from the theoretical prediction, intramolecular fluorescence resonance energy transfer (FRET) was applied as an independent approach to investigate the dynamics in peptide chains. Two energy donor/acceptor pairs with small Förster critical radius, where either naphthalene or Trp serves as energy donor and DBO as energy acceptor, were employed. Energy transfer between naphthalene and DBO was first investigated at a very short distance, where DBO and naphthalene were separated by dimethylsiloxy. It was found that the Dexter mechanism might dominate in this system due to the close proximity of donor and acceptor, the high flexibility of the tether, and the nonviscous solvent employed. [Pischel, U.; Huang, F.; Nau, W. M. *Photochem. Photobiol. Sci.* **2004**, *3*, 305-310 (Appendix IV)] However, when naphthalene and DBO were covalently attached to the opposite ends of peptides and studied in water, control experiments in the presence of cucurbit[7]uril as an encapsulating host suggested that FRET was the dominant mechanism, which allowed us to apply the FRET technique to recover the intramolecular end-to-end distance distribution and diffusion coefficient by means of global analysis. In the investigation with naphthalene/DBO energy

donor/acceptor pair, slower diffusion coefficients in shorter chains were found for the series of flexible Gly-Ser peptides, suggesting that shorter chains may exhibit a larger internal friction limiting the conformational change. Additionally, the intramolecular energy transfer efficiency have been measured with the Trp/DBO pair and the effective average end-to-end distances were calculated, which provided a lower limit for the mean end-to-end distance of peptides for the global data analysis and offered a complementary approach to interpret the end-to-end collision rates determined with the same pair but based on a collision-induced quenching mechanism. [Huang, F.; Wang, X.; Haas, E.; Nau, W. M. **2004**, In preparation (Appendix VIII)]

The fluorescence-based method based on contact quenching mechanism has some other potential applications. It has potential to be applied for high-throughput screening of protease activity and to investigate the helix-coil transition in peptides.

2. Introduction

2.1. General background

Proteins can only be functional under their correctly folded three-dimensional or “native” structure.¹ As one of the “holy grails” of the physical and life sciences, protein folding attracts great interest and research in the field has made significant progress in both theoretical²⁻⁴ and experimental aspects.⁵⁻⁷ However, interdisciplinary questions are still standing: How do proteins fold? How fast do proteins fold? How does the primary sequence of proteins determine their native structure and functions?

Several mechanisms for protein folding have been proposed, such as the framework model, hydrophobic collapse model, and nucleation-condensation model.⁸⁻¹² A framework model assumes that secondary structures are formed first, which are only dependent on the primary sequence. The secondary structures form and determine the tertiary structures. A hydrophobic collapse model, on the other hand, supports a hydrophobic collapse as the first step in the folding pathway, through which proteins form a molten globule. The following rearrangement of the compact structure results in the tertiary structure. The nucleation-condensation model assumes that a small nucleus is necessary at the beginning of protein folding, which works as a template for the subsequent steps in protein folding and which is assumed to be the rate-limiting step. Detailed investigations on the kinetics of the primary steps or early processes in protein folding can provide experimental evidence in favor of each of the various mechanisms.

It is also a long-standing controversy whether protein folding is kinetically or thermodynamically controlled.¹³⁻¹⁶ In principle, one may be able to clarify kinetic control and thermodynamic control by computing the global energy minimum of proteins and the entire energy surface of protein folding. It is, however, impossible at present due to the extremely long computational time required to reliably search for the global energy minimum. Kinetic studies of protein folding as well as studies of intermediates in the folding pathway are therefore the most promising approaches to protein folding at present.

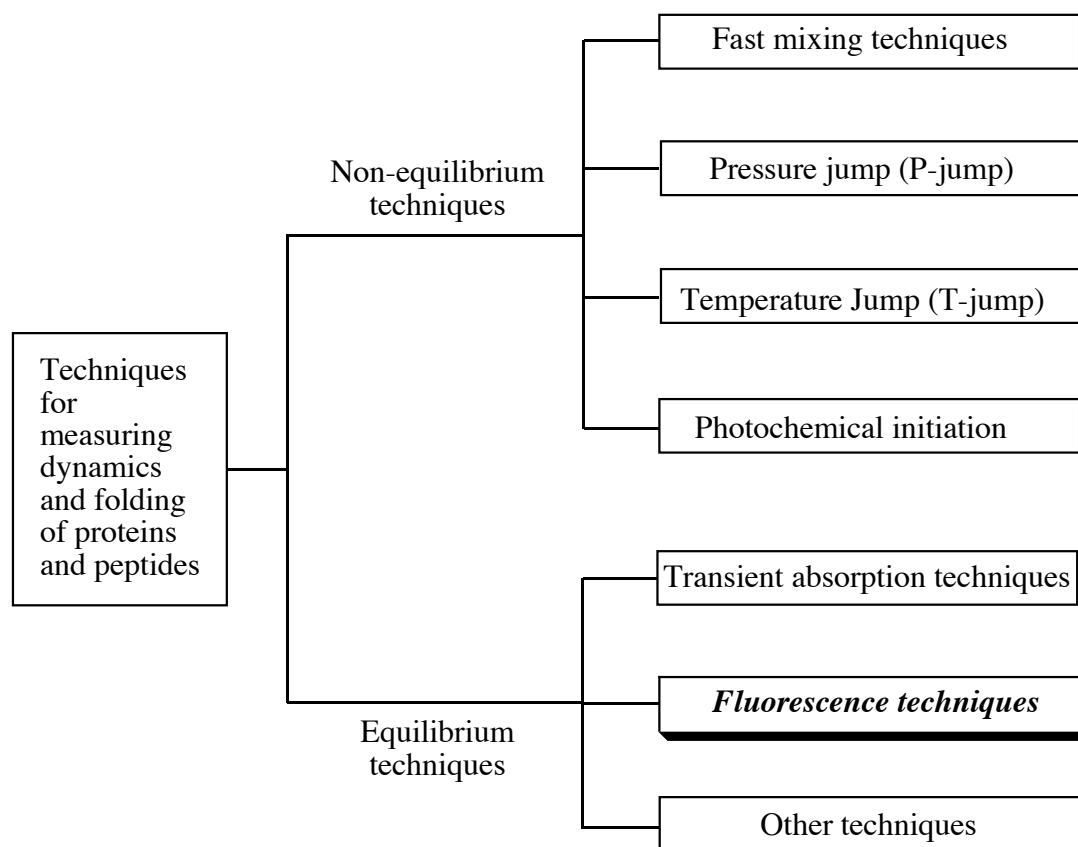
To comprehensively understand protein folding and functions, it is invaluable to investigate the intramolecular motions of proteins and peptides and their kinetics.¹⁷⁻²⁰ Knowledge of the kinetics of peptide and protein conformational changes is also essential to provide benchmarks for computational simulations of protein folding^{21,22} and to

examine theoretical predictions of the folding rates.²³⁻²⁵ On the other hand, the molecular flexibility of proteins is a crucial factor in determining their biological activity,²⁶⁻²⁹ including binding affinity, antigenicity, and enzymatic activity. The study of the flexibility of different segments of proteins is also essential to understand the functions of proteins and to tackle the *de novo* design of peptides and proteins, which has attracted intensive research interest.³⁰⁻³² The present thesis focuses on the kinetics of peptide conformational changes and peptide flexibility in an effort to explore some fundamental questions in protein folding and functions.

2.2. Techniques to study the dynamics and folding of proteins and peptides

There are various techniques available to investigate the dynamics and folding of proteins and peptides, which are summarized in Scheme 2-1 and classified into two major groups: non-equilibrium techniques and equilibrium techniques. According to the characteristics of the investigated system and the requirements for time resolution, different techniques can be selected.

Scheme 2-1. Techniques for measuring dynamics and folding of proteins and peptides.



The different techniques have their advantages and disadvantages and are complementary to each other. This thesis aims to develop new fluorescence-based techniques and to measure the dynamics of peptides. The strength of our techniques will become more evident by comparison with conventional techniques. This section will therefore give a brief introduction to the different techniques.

2.2.1. Conventional non-equilibrium techniques for fast protein folding

Fast mixing techniques include stopped-flow and continuous-flow, which initiate protein folding by changing the composition of a protein solution. The former has a typical time resolution of milliseconds,^{33,34} and the latter extends the limit down to a few 10 μ s and has become one of the most important techniques in the study of protein folding.³⁵⁻³⁷ One of the major advantages of the continuous-flow technique is that it is applicable to a very broad range of proteins because the folded/unfolded equilibrium of most proteins can be changed by a variation of the concentration of denaturants or the pH of the solution. However, the time resolution of this technique is still limited to several 10 μ s. On the other hand, additional reagents are always introduced during the folding/unfolding processes for both techniques and continuous-flow normally requires large amounts of sample.

The volume changes in any protein folding/unfolding process renders the equilibrium also dependent on pressure in addition to temperature and solvent composition,³⁸ which allows another method, pressure jump (P-jump), to initiate the protein folding/unfolding process.³⁹ A modern P-jump apparatus with a stack of piezoelectric crystals can complete a jump of 200 bar within 50 ms,⁴⁰ which results in a similar time resolution as stopped-flow. The major advantages of the P-jump technique lie in its two-directional jump (increasing or decreasing pressure) and long-time stability after the jump (up to tens of seconds).⁴¹

Temperature jump (T-jump) is another common technique used for non-equilibrium processes. After a temperature jump, the conformational distribution undergoes a change (relaxation) from the initial to the target temperature, i.e., folding or unfolding is induced. The time resolution for conventional temperature jump techniques with resistive capacitive heaters was limited to microseconds. With the application of lasers, the temperature jump can be accomplished in nanoseconds or even faster,⁴²⁻⁴⁶ which depends on the rate of complete thermal equilibration of solvent and solute as well as on the width of the laser pulse. Laser-assisted T-jump has a much better time resolution than fast mixing and P-jump, but its upper limit is determined by the rate of heat diffusion. To span a large time range, the combination of different T-jump relaxation spectrometers covering different time ranges is also usually required.⁴⁷

Recently, trigger techniques based on photochemistry, such as photodissociation and photochemical electron transfer, have been developed. The first photodissociation method was established based on the different stability of cytochrome *c* in the presence and absence of a CO ligand.⁴⁸ At a particular concentration of guanidinium chloride, fast photodissociation of CO from an unfolded cytochrome *c* interrupts the equilibrium and triggers the folding process. The dissociation can be accomplished in <1 ps after the laser pulse. In addition, Hagen et al. applied a laser pulse to dissociate the heme-ligand complex in cytochrome *c*, and then monitored the rebinding of the heme and ligand.^{49,50} On the other hand, due to the different stability of reduced and oxidised cytochromes, another method based on photochemical electron transfer was established,^{51,52} where the time resolution is determined by the electron transfer from Ru²⁺ to the oxidized cytochrome *c* (< 1 ms), and the upper limit is dependent on the re-oxidation of reduced cytochromes. Another method based on photochemical triggers was realized by introducing a non-native aryl disulfide cross-linking group into the ends of a peptide, which prevents the peptide from going into folded conformations.⁵³ The folding of peptides is triggered by breaking the disulfide bond with a laser of 270 nm under physiological conditions. This technique can be used for different peptides and proteins and can trigger protein folding very fast. However, the formation of the disulfide bonds presumably induces some unexpected conformations,⁵⁴ which will obstruct the observation of real rates for the secondary structure formation. Additionally, the laser pulse with wavelength at 270 nm is strongly absorbed also by the aromatic amino acids.

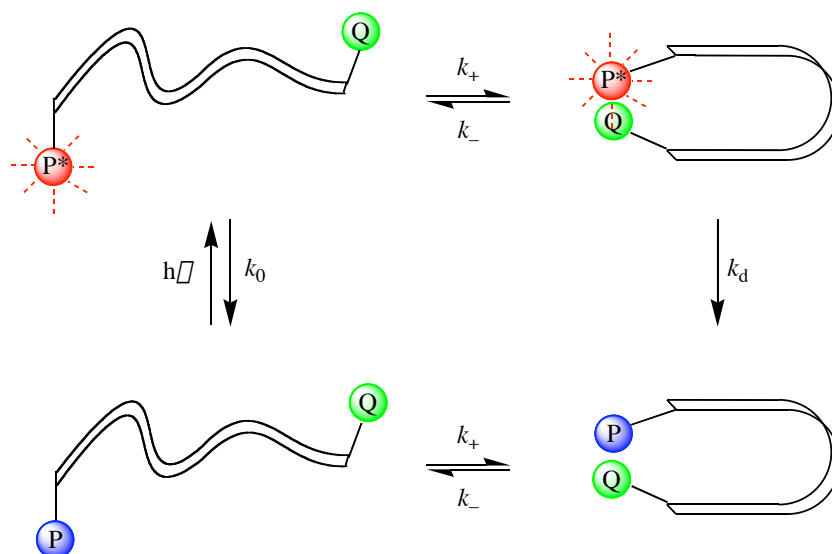
2.2.2. Equilibrium techniques based on contact quenching mechanisms

The conventional techniques, especially the laser-assisted techniques, used for protein folding have many important advantages. However, to initiate folding or unfolding, one always either needs very specialized techniques or has to introduce external reagents to the system, or both. Furthermore, in many cases, the time resolution becomes the major limitation for fast kinetic studies. Therefore, there is still an intensive quest for alternative ways to observe very fast kinetics, in particular for some special processes in the folding of proteins and nucleic acids that cannot be detected by conventional means. Equilibrium methods can compensate for the deficiencies of conventional non-equilibrium ways. They are particularly suitable for studies on intramolecular collision in random-coiled chains and they in principle can access the time range from picoseconds to microseconds. Equilibrium techniques include dynamic NMR,^{55,56} photophysical

techniques,⁵⁷⁻⁶⁰ as well as single-molecule techniques.⁶¹⁻⁶⁴ Dynamic NMR techniques are limited to the microsecond time scale. Single-molecule techniques are interesting but they are currently limited to large chromophores, and therefore are not suitable for systems requiring small probes,⁶⁵ such as very short peptides. The common equilibrium approaches for measuring the dynamics of peptides and elementary steps in protein folding are photophysical techniques.

Intramolecular reactions in polymers under diffusion-control have been extensively studied theoretically.⁶⁶⁻⁷⁷ The first photophysical method applied to polymers under equilibrium was motivated by the theoretical studies of Wilemski and Fixman.⁷⁸ From then on, experimental studies on polymer dynamics have led to great achievements.⁷⁹⁻⁸³ However, the transfer of the probe/quencher methodology from polymers to biopolymers has proven to be the opposite of straightforward, since there are a number of additional constraints in polypeptides and oligonucleotides. For example, polar probes and quenchers should be used to reduce hydrophobic effects and the probe/quencher system must allow measurement in aqueous solution. These are not fulfilled for the traditional chromophores like pyrene and anthracene,⁸³⁻⁸⁵ which has led to a quest for suitable probe/quencher systems for biopolymers.^{57,58,86,87}

Scheme 2-2. Principle of photophysical techniques for measuring end-to-end collision rates.



Photophysical methods have a general principle, which can be simply described as Scheme 2-2. A photophysical probe (P) and a quencher (Q) are introduced at the opposite ends of a peptide with random-coiled structure. The excited probe, P^* , can be obtained with a short light pulse (top-left structure), which can decay spontaneously with the

intrinsic decay rate constant k_0 or be quenched by the quencher through contact. The apparent decay of P^* , which can be followed through its characteristic emission or absorption, will reflect the rate of intrinsic excited-state decay (k_0) and the intramolecular quenching rate constant (k_q) (Equation 2-1). In the case that intermolecular quenching is excluded, a kinetic analysis gives Equation 2-2, where k_d is the quenching rate constant for P^* in contact with Q. Equation 2-2 contains a steady-state approximation for the concentration of the encounter complex. For a diffusion-controlled reaction, where $k_d \gg k_{\square}$, Equation 2-2 can be simplified to Equation 2-3.

$$k_q = \frac{1}{\square} \square \frac{1}{\square_0} \quad (2-1)$$

$$k_q = \frac{k_+ \cdot k_d}{k_{\square} + k_d} \quad (2-2)$$

$$k_q \square k_+ \quad (\text{for } k_d \gg k_{\square}) \quad (2-3)$$

It should be noted that the methodology shown in Scheme 2-2 is subject to several additional assumptions and requirements. 1) It assumes that the excited probe imposes little effect on the kinetics of the bio-molecules, which requires that any strong interaction between excited probe and quencher or the residues in the chain should be excluded. 2) It requires that the introduced probe and quencher have only a small effect on the kinetics of chain motion; very small probe and quencher molecules or, preferably, an intrinsic probe and quencher are desirable. 3) The excited probe must be sufficiently long-lived. 4) The excited probe is quenched by the quencher at the other end of the chain only through contact.

The principle of measurement relies on a random-coiled chain. If there are any secondary structures or any thermodynamically stable conformations, one will not be able to extract the end-to-end collision rate directly from the fluorescence lifetime; however, with a suitable model one may be able to obtain the kinetics for the transition between random-coil and secondary structure.

References:

- (1) Dobson, C. M. *Nature* **2003**, 426, 884-890.
- (2) Shakhnovich, E. I. *Curr. Opin. Struct. Biol.* **1997**, 7, 29-40.
- (3) Mayor, U. et al. *Nature* **2003**, 421, 863-867.
- (4) Klimov, D. K.; Thirumalai, D. *Proc. Natl. Acad. Sci. USA* **2000**, 97, 2544-2549.
- (5) Chow, C. C. et al. *Biochemistry* **2003**, 42, 7090-7099.
- (6) Daggett, V.; Fersht, A. R. *Trends Biochem. Sci.* **2003**, 28, 18-25.
- (7) Schuler, B.; Lipman, E. A.; Eaton, W. A. *Nature* **2002**, 419, 743-747.
- (8) Pain, R. H., Ed. *Mechanisms of Protein Folding*; second ed.; Oxford University Press: Oxford, 2000.
- (9) Volk, M. *Eur. J. Org. Chem.* **2001**, 2001, 2605-2621.
- (10) Fersht, A. R. *Proc. Natl. Acad. Sci. USA* **1995**, 92, 10869-10873.
- (11) Dyson, H. J.; Wright, P. E. *Curr. Opin. Struct. Biol.* **1993**, 3, 60-65.
- (12) Wetlaufer, D. B. *Proc. Natl. Acad. Sci. USA* **1973**, 70, 697-701.
- (13) Anfinsen, C. B. *Science* **1973**, 181, 223-230.
- (14) Baker, D.; Agard, D. A. *Biochemistry* **1994**, 33, 7505-7509.
- (15) Baskakov, I. V.; Legname, G.; Prusiner, S. B.; Cohen, F. E. *J. Biol. Chem.* **2001**, 276, 19687-19690.
- (16) Cruzeiro-Hansson, L.; Silva, P. A. S. *J. Biol. Phys.* **2001**, 27, S6-S8.
- (17) Bieri, O.; Kiefhaber, T. *Biol. Chem.* **1999**, 380, 923-929.
- (18) Eaton, W. A.; Munoz, V.; Thompson, P. A.; Henry, E. R.; Hofrichter, J. *Acc. Chem. Res.* **1998**, 31, 745-753.
- (19) Eaton, W. A. et al. *Annu. Rev. Biophys. Biomol. Struct.* **2000**, 29, 327-359.
- (20) Ferguson, N.; Fersht, A. R. *Curr. Opin. Struct. Biol.* **2003**, 13, 75-81.
- (21) Baker, D.; Sali, A. *Science* **2001**, 294, 93-96.
- (22) Brooks, C. L., III *Acc. Chem. Res.* **2002**, 35, 447-454.
- (23) Debe, D. A.; Goddard, W. A., III *J. Mol. Biol.* **1999**, 294, 619-625.
- (24) Makarov, D. E.; Keller, C. A.; Plaxco, K. W.; Metiu, H. *Proc. Natl. Acad. Sci. USA* **2002**, 99, 3535-3539.
- (25) Thirumalai, D. *J. Phys. Chem. B* **1999**, 103, 608-610.
- (26) Huber, R. *Biochem. Soc. Trans.* **1987**, 15, 1009-1020.
- (27) Braddock, D. T.; Louis, J. M.; Baber, J. L.; Levens, D.; Clore, G. M. *Nature* **2002**, 415, 1051-1056.
- (28) Taschner, N. et al. *J. Mol. Biol.* **2001**, 310, 169-179.
- (29) Závodszy, P.; Kardos, J.; Svingor, A.; Petsko, G. A. *Proc. Natl. Acad. Sci. USA* **1998**, 95, 7406-7411.
- (30) Karplus, P. A.; Schulz, G. E. *Naturwissenschaften* **1985**, 72, 212-213.
- (31) Bhaskaran, R.; Ponnuswamy, P. K. *Int. J. Peptide Protein Res.* **1988**, 32, 241-255.

- (32) Vihinen, M.; Torkkila, E.; Riikonen, P. *Proteins* **1994**, *19*, 141-149.
- (33) Nau, W. M.; Wang, X. *ChemPhysChem* **2002**, *3*, 393-398.
- (34) Beechem, J. M.; Sherman, M. A.; Mas, M. T. *Biochemistry* **1995**, *34*, 13943-13948.
- (35) Teilum, K.; Maki, K.; Kragelund, B. B.; Poulsen, F. M.; Roder, H. *Proc. Natl. Acad. Sci. USA* **2002**, *99*, 9807-9812.
- (36) Chan, C.-K. et al. *Proc. Natl. Acad. Sci. USA* **1997**, *94*, 1779-1784.
- (37) Shastry, M. C. R.; Luck, S. D.; Roder, H. *Biophys. J.* **1998**, *74*, 2714-2721.
- (38) Herberhold, H.; Winter, R. *J. Phys.: Condens. Matter* **2002**, *14*, 11485-11488.
- (39) Desai, G.; Panick, G.; Zein, M.; Winter, R.; Royer, C. A. *J. Mol. Biol.* **1999**, *288*, 461-475.
- (40) Jacob, M. et al. *Biochemistry* **1999**, *38*, 2882-2891.
- (41) Mohana-Borges, R.; Silva, J. L.; Ruiz-Sanz, J.; de Prat-Gay, G. *Proc. Natl. Acad. Sci. USA* **1999**, *96*, 7888-7893.
- (42) Jas, G. S.; Eaton, W. A.; Hofrichter, J. *J. Phys. Chem. B* **2001**, *105*, 261-272.
- (43) Dyer, R. B.; Gai, F.; Woodruff, W. H. *Acc. Chem. Res.* **1998**, *31*, 709-716.
- (44) Phillips, C. M.; Mizutani, Y.; Hochstrasser, R. M. *Proc. Natl. Acad. Sci. USA* **1995**, *92*, 7292-7296.
- (45) Schindler, T.; Schmid, F. X. *Biochemistry* **1996**, *35*, 16833-16842.
- (46) Thompson, P. A.; Eaton, W. A.; Hofrichter, J. *Biochemistry* **1997**, *36*, 9200-9210.
- (47) Callender, R.; Dyer, R. B. *Curr. Opin. Struct. Biol.* **2002**, *12*, 628-633.
- (48) Jones, C. M. et al. *Proc. Natl. Acad. Sci. USA* **1993**, *90*, 11860-11864.
- (49) Hagen, S. J.; Hofrichter, J.; Szabo, A.; Eaton, W. A. *Proc. Natl. Acad. Sci. USA* **1996**, *93*, 11615-11617.
- (50) Hagen, S. J.; Hofrichter, J.; Eaton, W. A. *J. Phys. Chem. B* **1997**, *101*, 2352-2365.
- (51) Pascher, T.; Chesick, J. P.; Winkler, J. R.; Gray, H. B. *Science* **1996**, *271*, 1558-1560.
- (52) Pascher, T. *Biochemistry* **2001**, *40*, 5812-5820.
- (53) Volk, M. et al. *J. Phys. Chem. B* **1997**, *101*, 8607-8616.
- (54) Adam, W. et al. *J. Org. Chem.* **2002**, *67*, 6041-6049.
- (55) Wang, M. et al. *J. Am. Chem. Soc.* **2003**, *125*, 6032-6033.
- (56) Huang, G. S.; Oas, T. G. *Proc. Natl. Acad. Sci. USA* **1995**, *92*, 6878-6882.
- (57) Bieri, O. et al. *Proc. Natl. Acad. Sci. USA* **1999**, *96*, 9597-9601.
- (58) Lapidus, L. J.; Eaton, W. A.; Hofrichter, J. *Proc. Natl. Acad. Sci. USA* **2000**, *97*, 7220-7225.
- (59) McGimpsey, W. G.; Chen, L.; Carraway, R.; Samaniego, W. N. *J. Phys. Chem. A* **1999**, *103*, 6082-6090.
- (60) Hudgins, R. R.; Huang, F.; Gramlich, G.; Nau, W. M. *J. Am. Chem. Soc.* **2002**, *124*, 556-564.

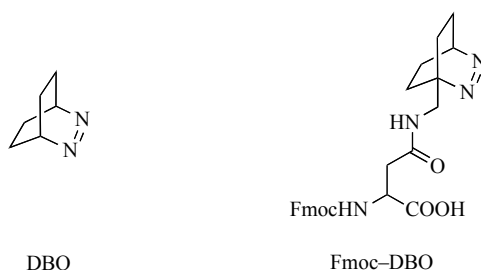
- (61) Xie, S. *Single Mol.* **2001**, 2, 229-236.
- (62) Weiss, S. *Nat. Struct. Biol.* **2000**, 7, 724-729.
- (63) Zhuang, X. et al. *Science* **2000**, 288, 2048-2051.
- (64) Neuweiler, H.; Schulz, A.; Boehmer, M.; Enderlein, J.; Sauer, M. *J. Am. Chem. Soc.* **2003**, 125, 5324-5330.
- (65) Fenton, W. A.; Horwich, A. L. *Q. Rev. Biophys.* **2003**, 36, 229-256.
- (66) Jacobson, H.; Stockmayer, W. H. *J. Chem. Phys.* **1950**, 18, 1600-1606.
- (67) Flory, P. J. *Principles of polymer chemistry*; Cornell University Press: Ithaca, 1953.
- (68) Flory, P. J.; Suter, U. W.; Mutter, M. *J. Am. Chem. Soc.* **1976**, 98, 5733-5739.
- (69) Wilemski, G.; Fixman, M. *J. Chem. Phys.* **1973**, 58, 4009-4019.
- (70) Wilemski, G.; Fixman, M. *J. Chem. Phys.* **1974**, 60, 866-877.
- (71) Wilemski, G.; Fixman, M. *J. Chem. Phys.* **1974**, 60, 878-890.
- (72) Doi, M. *Chem. Phys.* **1975**, 9, 455-466.
- (73) Szabo, A.; Schulten, K.; Schulten, Z. *J. Chem. Phys.* **1980**, 72, 4350-4357.
- (74) Cuniberti, C.; Perico, A. *Prog. Polym. Sci.* **1984**, 10, 271-316.
- (75) Perico, A.; Ganazzoli, F.; Allegra, G. *J. Chem. Phys.* **1987**, 87, 3677-3686.
- (76) Perico, A.; Beggiato, M. *Macromolecules* **1990**, 23, 797-803.
- (77) Friedman, B.; O'Shaughnessy, B. *Macromolecules* **1993**, 26, 4888-4898.
- (78) Cuniberti, C.; Perico, A. *Eur. Polym. J.* **1977**, 13, 369-374.
- (79) Mita, I.; Horie, K.; Takeda, M. *Macromolecules* **1981**, 14, 1428-1433.
- (80) Lee, S.; Winnik, M. A. *Macromolecules* **1997**, 30, 2633-2641.
- (81) Redpath, A. E. C.; Winnik, M. A. *Journal of the American Chemical Society* **1982**, 104, 5604-5607.
- (82) Winnik, M. A.; Redpath, T.; Richards, D. H. *Macromolecules* **1980**, 13, 328-335.
- (83) Winnik, M. A. *Chem. Rev.* **1981**, 81, 491-524.
- (84) Zachariasse, K. A.; Macanita, A. L.; Kuehnle, W. *J. Phys. Chem. B* **1999**, 103, 9356-9365.
- (85) Horie, K.; Schnabel, W.; Mita, I.; Ushiki, H. *Macromolecules* **1981**, 14, 1422-1428.
- (86) Krieger, F.; Fierz, B.; Bieri, O.; Drewello, M.; Kiefhaber, T. *J. Mol. Biol.* **2003**, 332, 265-274.
- (87) Buscaglia, M.; Schuler, B.; Lapidus, L. J.; Eaton, W. A.; Hofrichter, J. *J. Mol. Biol.* **2003**, 332, 9-12.

3. DBO-based fluorescence methodologies to study peptide dynamics

3.1. A fluorescence method based on a contact quenching mechanism

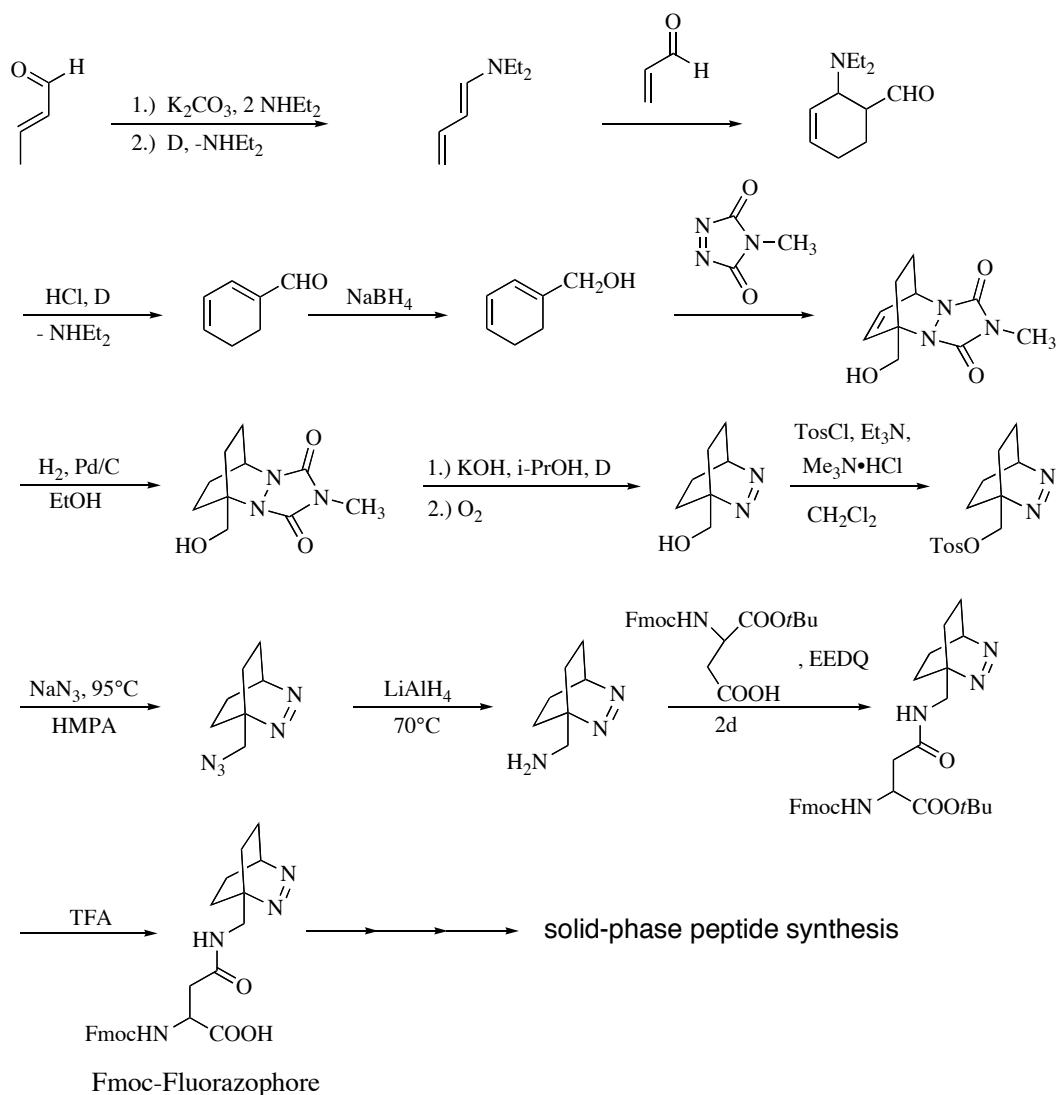
Photophysical techniques based on transient absorption have been previously applied to investigate the intramolecular collision rates in peptides.¹⁻⁴ To fulfill the requirements for establishing a photophysical method and to take the full advantage of fluorescence over transient absorption, we selected 2,3-diazabicyclo[2.2.2]-oct-2-ene (DBO) (Scheme 3-1) as a fluorescent probe and Trp or Tyr as a quencher to measure the dynamics of peptides. DBO is characterized by an exceedingly long fluorescence lifetime (up to 1 ns), small size, high chemical and photophysical stability, good solubility in water, as well as by a contact quenching mechanism by Trp and Tyr. The bimolecular quenching rate constants for DBO by 20 natural amino acids were measured. It was found that Trp, Cys, Met, and Tyr are efficient quenchers. Trp can quench DBO most efficiently with $2.0 \times 10^9 \text{ M}^{-1}\text{s}^{-1}$ in D_2O , which allows DBO to be quenched selectively by this quencher in peptides. In the following projects, Trp was selected as an efficient intrinsic quencher and Tyr was selected as a complementary, less efficient quencher.

Scheme 3-1. Structures of DBO and Fmoc-DBO.



DBO was introduced into peptides through Fmoc-DBO (Scheme 3-1), an asparagine derivative, which has good compatibility with solid-phase peptide synthesis. The synthetic route for Fmoc-DBO in 10% overall yield is shown in Scheme 3-2 (the details can be found in Appendix I).

Scheme 3-2. Synthetic route for Fmoc-DBO.



The fluorescence decay traces in the presence of quencher in random-coiled peptides are all monoexponential, which allows us to extract the dynamics of peptides directly from the fluorescence lifetime. In peptides with secondary structure, the decay is much more complex, but the model-assisted data analysis provides kinetics for transition between secondary structure and random-coil. Shown in Figure 3-1 are the typical fluorescence decay traces for random-coiled peptides.

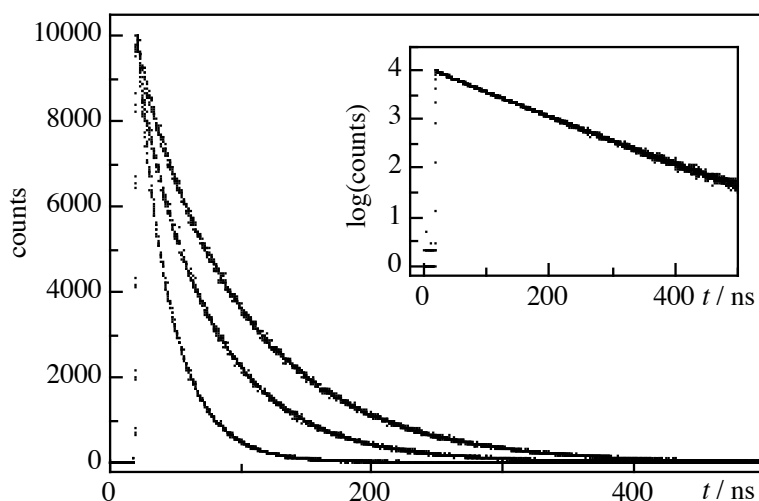


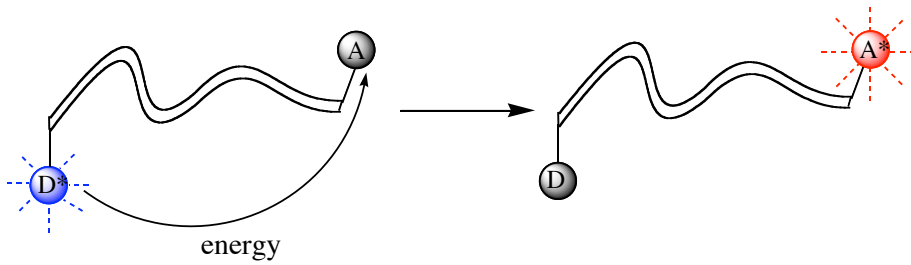
Figure 3-1. Typical fluorescence decay traces for random-coiled peptides. The traces from the upper to the lower one are for WQIFVK-DBO, WTITLE-DBO, and WTLTGK-DBO. Shown in the inset is the decay for WQIFVK-DBO on a semilogarithmic scale.

Trp is the best quencher among the natural amino acids for measuring the end-to-end collision rates of peptides due to its high quenching efficiency of DBO and its contact quenching mechanism. The contact quenching mechanism has been proven by a series of control experiments.⁵ For example, after the addition of cucurbit[7]uril, which complexes DBO selectively and quantitatively ($K = 4 \times 10^5 \text{ M}^{-1}$) and prevents the collision of DBO and Trp, the fluorescence lifetime of DBO in the peptide Trp-(Gly-Ser)₂-DBO increases from 19.5 ns to 1030 ns, suggesting that the quencher is not able to quench the excited probe at all (Appendix III and V). This result provides strong evidence for the view that quenching requires intimate contact. If quenching would occur through space or through the solvent it should have also been mediated through the supramolecular wall.

3.2. A method based on intramolecular fluorescence resonance energy transfer

DBO can not only serve as a long-lived fluorescent probe, which is selectively quenched by Trp or Tyr upon collision, but can also accept energy from Trp or naphthalene, which allows us to establish a complementary method to investigate peptide dynamics based on intramolecular fluorescence resonance energy transfer (FRET).⁶⁻⁹ This is wonderful since in the method based on the contact quenching mechanism DBO works as probe and Trp as quencher, but in the method based on FRET DBO serves as acceptor (quencher) and Trp or its analogue naphthalene as donor (probe), which allows us to keep the chemical structure of the peptides identical and to compare the results obtained from the two independent methods. The principle of the energy transfer method is shown in Scheme 3-3, where energy transfer occurs without direct contact of donor and acceptor.

Scheme 3-3. Principle of the intramolecular fluorescence resonance energy transfer.



The intrachain energy transfer efficiency from donor to acceptor depends on both the donor-acceptor distance and the fluctuation of the donor/acceptor during the lifetime of the excited donor. The time-resolved excited donor population decay can be analyzed by the following equation.¹⁰⁻¹²

$$\frac{\partial}{\partial t} g_N^*(r, t) = -\frac{1}{\tau_0} g_N^*(r, t) + \frac{R_0}{r} g_N^*(r, t) + D \frac{1}{r^2} \frac{\partial}{\partial r} r^2 \frac{\partial}{\partial r} g_N^*(r, t) + D \frac{1}{r^2} \frac{\partial}{\partial r} r^2 g_N^*(r, t) \frac{\partial}{\partial r} \ln U(r) \quad (3-1)$$

D is the mutual intramolecular end-to-end diffusion coefficient. τ_0 is the product of Boltzman constant and temperature ($\tau_0 = 1/k_B T$), and $U(r)$ is the potential energy of the chain possessing an end-to-end distance r . If the equilibrium distribution $g_N(r)$ is known, the potential energy can be obtained according to Equation 3-2:^{12,13}

$$\ln U(r) = -\ln g_N(r) \quad (3-2)$$

The survival probability density of the excited donor can be calculated according to Equation 3-1 and then integrated according to Equation 3-3 to fit the time-resolved fluorescence decay.

$$I = I_0 \int_0^{\infty} 4\pi r^2 g_N^*(r,t) dr \quad (3-3)$$

FRET experiments can in principle yield both of the end-to-end distance distribution and the intrachain diffusion coefficient. However, since these parameters are highly correlated, the recovery of both distribution and diffusion coefficient from the donor fluorescence decay becomes unreliable. A global analysis of the fluorescence decay traces of not only the donor but also the acceptor in the presence and absence of FRET was suggested to decrease the correlation between the parameters (See also Appendix VIII for details).¹⁴

References:

- (1) Bieri, O.; Wirz, J.; Hellrung, B.; Schutkowski, M.; Drewello, M.; Kiefhaber, T. *Proc. Natl. Acad. Sci. USA* **1999**, *96*, 9597-9601.
- (2) Lapidus, L. J.; Eaton, W. A.; Hofrichter, J. *Proc. Natl. Acad. Sci. USA* **2000**, *97*, 7220-7225.
- (3) Krieger, F.; Fierz, B.; Bieri, O.; Drewello, M.; Kiefhaber, T. *J. Mol. Biol.* **2003**, *332*, 265-274.
- (4) Buscaglia, M.; Schuler, B.; Lapidus, L. J.; Eaton, W. A.; Hofrichter, J. *J. Mol. Biol.* **2003**, *332*, 9-12.
- (5) Nau, W. M.; Huang, F.; Wang, X.; Bakirci, H.; Gramlich, G.; Marquez, C. *Chimia* **2003**, *57*, 161-167.
- (6) Stryer, L.; Haugland, R. P. *Proc. Natl. Acad. Sci. USA* **1967**, *58*, 719-726.
- (7) Lakowicz, J. R. *Principles of Fluorescence Spectroscopy*; 2nd ed.; Kluwer Academic/Plenum Publishers: New York, 1999.
- (8) Deniz, A. A.; Laurence, T. A.; Beligere, G. S.; Dahan, M.; Martin, A. B.; Chemla, D. S.; Dawson, P. E.; Schultz, P. G.; Weiss, S. *Proc. Natl. Acad. Sci. USA* **2000**, *97*, 5179-5184.
- (9) Schuler, B.; Lipman, E. A.; Eaton, W. A. *Nature* **2002**, *419*, 743-747.
- (10) Wang, X.; Bodunov, E. N.; Nau, W. M. *Opt. Spectrosc.* **2003**, *95*, 560-570.
- (11) Lakowicz, J. R.; Kusba, J.; Gryczynski, I.; Wiczak, W.; Szmajdzinski, H.; Johnson, M. L. *J. Phys. Chem.* **1991**, *95*, 9654-9660.
- (12) Haas, E.; Katchalski-Katzir, E.; Steinberg, I. Z. *Biopolymers* **1978**, *17*, 11-31.
- (13) Szabo, A.; Schulten, K.; Schulten, Z. *J. Chem. Phys.* **1980**, *72*, 4350-4357.
- (14) Beechem, J. M.; Haas, E. *Biophys. J.* **1989**, *55*, 1225-1236.

peptide is not the fastest one, i.e., a maximum is reached at $N = 4$. This significant inversion immediately speaks against the assumption that the fluorescence of DBO is quenched by Trp through long-range electron transfer or fluorescence resonance energy transfer, both of which are highly distance-dependent and therefore expected to occur faster for the shortest peptide. This is consistent with our other control experiments in favor of a contact quenching mechanism (*cf.* Appendix III and V).^{13,14}

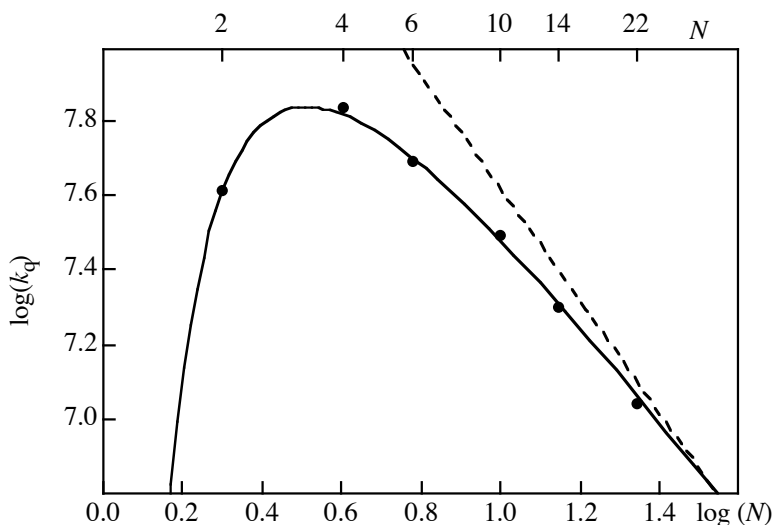


Figure 4-1. Double-logarithmic plot of the intramolecular quenching rate constant (k_q) of Trp-(Gly-Ser)_n-DBO polypeptides *versus* the peptide length. The dashed line has a slope of -1.5 and is shown to illustrate the deviation from the theoretical behavior.

References:

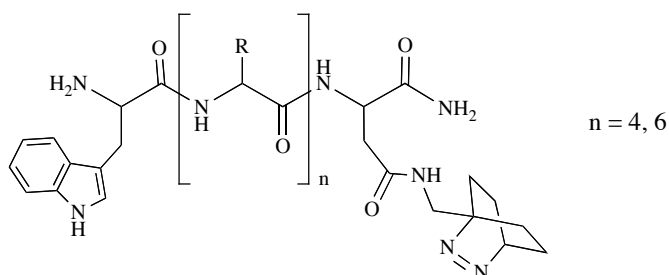
- (1) Flory, P. J.; Suter, U. W.; Mutter, M. *J. Am. Chem. Soc.* **1976**, *98*, 5733-5739.
- (2) Suter, U. W.; Mutter, M.; Flory, P. J. *J. Am. Chem. Soc.* **1976**, *98*, 5740-5745.
- (3) Wilemski, G.; Fixman, M. *J. Chem. Phys.* **1974**, *60*, 866-877.
- (4) Wilemski, G.; Fixman, M. *J. Chem. Phys.* **1974**, *60*, 878-890.
- (5) Szabo, A.; Schulten, K.; Schulten, Z. *J. Chem. Phys.* **1980**, *72*, 4350-4357.
- (6) Friedman, B.; O'Shaughnessy, B. *Macromolecules* **1993**, *26*, 4888-4898.
- (7) Bieri, O.; Wirz, J.; Hellrung, B.; Schutkowski, M.; Drewello, M.; Kiefhaber, T. *Proc. Natl. Acad. Sci. USA* **1999**, *96*, 9597-9601.
- (8) Lapidus, L. J.; Eaton, W. A.; Hofrichter, J. *Proc. Natl. Acad. Sci. USA* **2000**, *97*, 7220-7225.
- (9) Wang, X.; Bodunov, E. N.; Nau, W. M. *Opt. Spectrosc.* **2003**, *95*, 560-570.
- (10) McGimpsey, W. G.; Chen, L.; Carraway, R.; Samaniego, W. N. *J. Phys. Chem. A* **1999**, *103*, 6082-6090.
- (11) Krieger, F.; Fierz, B.; Bieri, O.; Drewello, M.; Kiefhaber, T. *J. Mol. Biol.* **2003**, *332*, 265-274.
- (12) Huang, F.; Wang, X.; Haas, E.; Nau, W. M. **2004**, In preparation.
- (13) Nau, W. M.; Huang, F.; Wang, X.; Bakirci, H.; Gramlich, G.; Marquez, C. *Chimia* **2003**, *57*, 161-167.
- (14) Marquez, C.; Huang, F.; Nau, W. M. *IEEE Trans. Nanobiosci.* **2004**, *3*, 39-45.

5. A flexibility scale for amino acids in peptides

Molecular flexibility includes local (positional) flexibility and global (conformational) flexibility.¹ The former reflects the local vibration occurring on a femtosecond time scale within a local energy minimum, while the latter comprises real conformational changes and reflects the hindrance during conformational changes. The molecular flexibility of proteins is a crucial factor in determining their biological activity, including binding affinity, antigenicity, and enzymatic activity.²⁻⁵ The prediction of the flexibility of peptides and protein segments is therefore essential for understanding and predicting the functions of proteins, which is significant for *de novo* peptide design. Additionally, the knowledge of the flexibility of amino acids will provide important benchmark values for theoretical studies of peptide dynamics as well as the simulation of protein functions.

Some positional flexibility scales for amino acids have been obtained from X-ray diffraction crystallographic data.⁶⁻⁸ However, conformational flexibility is more important in biological processes where conformational changes are required. We reported a conformational flexibility scale for amino acids in peptides according to the end-to-end collision rates.

Scheme 5-1. General structure for peptides used for setting up a flexibility scale.



To measure the flexibility of peptides, DBO and Trp were separated by a sequence of identical amino acids (Scheme 5-1). With the assumption that the end-to-end distance for the equally long peptides is similar, which is supported by our more recent study based on FRET,⁹ it is reasoned that the end-to-end collision rate of peptides should be an excellent measure of the conformational flexibility of the backbones. A series of end-to-end collision rate constants were obtained as a function of the amino acid type, which provide the following flexibility scale for amino acids in peptides:

Gly > Ser > Asp, Asn, Ala > Thr, Leu > Phe, Glu, Gln > His, Arg > Lys > Val > Ile > Pro

This conformational flexibility scale indicates that the introduction of Gly gives the most flexible peptide, while Pro makes it most rigid, which is in line with the expectations from conformational space.¹⁰ A general trend between the residue size and flexibility was found, i.e., larger residues lead on average to a lower flexibility. A slight charge effect was observed in the 6-mer peptides, in which all of the residues are charged. In another experiment carried out with peptides with only two charged residues, the end-to-end collision rate did not show a systematic effect,⁹ indicating that interactions between two charges are too minute to result in experimentally significant effects on the end-to-end collision rates (< 10 %). Both of the experiments strongly suggest that charge does not impose a significant effect on the end-to-end collision rate although it may affect the thermodynamic parameters of the peptides. The reason for the very weak charge effect is not clear yet. However, it is reasonable to expect that the hindrance to the backbone rotation is mainly due to the atoms or groups in close proximity to the backbone, while atoms or groups more remote from the backbone, no matter how their structure or charge status is, have a much smaller effect on the internal friction, due to the larger conformational space. This is consistent with the observation that the β -branched amino acid Ile was found to reduce peptide flexibility significantly, while the amino acid with very similar but γ -branched structure, Leu, gives rise to a much more flexible peptide.

Statistical,¹¹⁻¹³ theoretical,¹⁴ and experimental^{15,16} analyses have revealed that particular amino acids have a different preference to appear in secondary protein structures, such as α -helices, β -strands, and β -turns. According to the statistical results¹¹ Met, Glu, Leu, Ala, Gln, Lys, His and Cys prefer α -helices, Val, Ile, Phe, Tyr, Thr and Trp favor β -sheets, and Pro, Gly, Asp, Ser and Asn have higher abundance in β -turns. This secondary structure preference closely correlates with the conformational flexibility obtained, i.e., most flexible amino acids, including Gly, Ser, Asn and Asp, are β -turn forming amino acids, and the most rigid amino acids, namely Val and Ile, are β -sheet forming amino acids. The exception from this correlation is Pro, which is the most rigid one but prefers β -turns. Its cyclic structure restricts the dihedral angle about the N-C β bond (ϕ angle) to -60° , which allows this amino acid to fulfill the requirements for a β -turn in the $i+2$ position without conformational distortion.

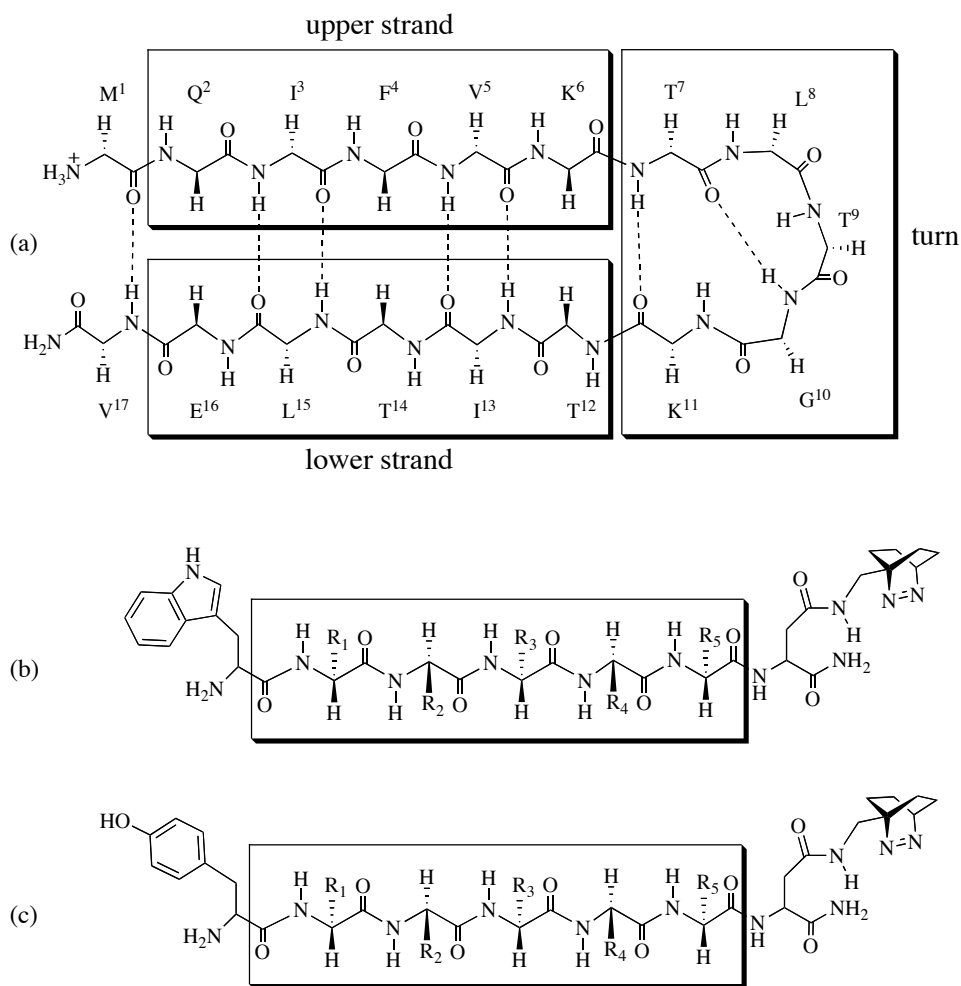
References:

- (1) Koca, J. *Prog. Biophys. Mol. Biol.* **1998**, *70*, 137-173.
- (2) Huber, R. *Biochem. Soc. Trans.* **1987**, *15*, 1009-1020.
- (3) Braddock, D. T.; Louis, J. M.; Baber, J. L.; Levens, D.; Clore, G. M. *Nature* **2002**, *415*, 1051-1056.
- (4) Taschner, N.; Müller, S. A.; Alumella, V. R.; Goldie, K. N.; Drake, A. F.; Aebi, U.; Arvinte, T. *J. Mol. Biol.* **2001**, *310*, 169-179.
- (5) Závodszky, P.; Kardos, J.; Svingor, A.; Petsko, G. A. *Proc. Natl. Acad. Sci. USA* **1998**, *95*, 7406-7411.
- (6) Karplus, P. A.; Schulz, G. E. *Naturwissenschaften* **1985**, *72*, 212-213.
- (7) Bhaskaran, R.; Ponnuswamy, P. K. *Int. J. Peptide Protein Res.* **1988**, *32*, 241-255.
- (8) Vihinen, M.; Torkkila, E.; Riikonen, P. *Proteins* **1994**, *19*, 141-149.
- (9) Huang, F.; Hudgins, R. R.; Nau, W. M. **2004**, *submitted for publication*.
- (10) Chakrabarti, P.; Pal, D. *Prog. Biophys. Mol. Biol.* **2001**, *76*, 1-102.
- (11) Levitt, M. *Biochemistry* **1978**, *17*, 4277-4285.
- (12) Hutchinson, E. G.; Thornton, J. M. *Protein Sci.* **1994**, *3*, 2207-2216.
- (13) Muñoz, V.; Serrano, L. *Proteins* **1994**, *20*, 301-311.
- (14) Koehl, P.; Levitt, M. *Proc. Natl. Acad. Sci. USA* **1999**, *96*, 12524-12529.
- (15) Monné, M.; Hermansson, M.; von Heijne, G. *J. Mol. Biol.* **1999**, *288*, 141-145.
- (16) Pace, C. N.; Scholtz, J. M. *Biophys. J.* **1998**, *75*, 422-427.

6. Primary and secondary structure dependence of peptide flexibility

It is very important to apply our established fluorescence-based method to explore some fundamental questions in protein folding. In this project, we investigated the flexibility of peptides relevant to the protein folding of ubiquitin,^{1,2} namely the two strand parts and the turn segment of the *N*-terminal β -hairpin. Ubiquitin is a protein with 76 amino acids and found in all eukaryotic cells.³ Its primary sequence in the *N*-terminal β -hairpin is shown in Scheme 6-1.^{1,2} The investigated peptides were derived from the turn and strand segments of this hairpin and were labeled with DBO and Trp or Tyr (Scheme 6-1).

Scheme 6-1. Structure of the *N*-terminal β -hairpin (1–17) of ubiquitin (a) and general structure of the peptides labeled with DBO/Trp (b) or DBO/Tyr (c).



The combination of quenchers with different quenching efficiency, namely Trp and Tyr, as well as the theoretical results for intermolecular encounter complex formation

(*cf.* Appendix III),⁴ allows the extrapolation of the absolute rate constants for end-to-end collision and dissociation. The extrapolated end-to-end collision rates, which are only slightly larger than the experimental quenching rate constants for the DBO/Trp probe/quencher system, provide an important measure of the conformational flexibility of the peptide backbone and support our previous assumption that the intramolecular quenching of DBO by Trp is almost diffusion-controlled.⁵ The chain flexibility is found to be strongly dependent on the type of secondary structure that the peptides represent. The collision rates for peptides derived from the β -strand motifs (ca. $1 \times 10^7 \text{ s}^{-1}$) are ca. 4 times slower than that derived from the β -turn, which implies that the thermodynamically β -turn favoured peptides are more flexible. The results provide further support for the hypothesis that chain flexibility is an important factor in the preorganization of protein segments during protein folding. The measured activation energies for fluorescence quenching ($16\text{--}24 \text{ kJ mol}^{-1}$), which are larger than the activation energy for viscous flow ($15\text{--}16 \text{ kJ mol}^{-1}$) and which are peptide-sequence dependent, demonstrate that the end-to-end collision process in peptides is partially controlled by internal friction within the backbone, while the collision rates at various viscosities indicate that solvent friction is an additional important factor in determining the collision rate. Mutations of Gly in the β -turn peptide to Ala, Phe, Thr or Val, respectively, show that a subtle sequence change strongly affects the flexibility of peptides, which decreases in the order Gly > Ala, Phe, Thr > Val, in line with expectations from the flexibility scale,⁶ yet somewhat less pronounced than in the flexibility-scale study (See Chapter 5 and Appendix II) since only a single amino acid was exchanged. Effective end-to-end distances obtained by intramolecular FRET from Trp to DBO (See Appendix VI and VIII)⁷ suggest that the equally long peptides have quite similar end-to-end distances, and the difference for the end-to-end collision rates is therefore presumably not due to the difference of the conformational equilibrium but to the dynamics of the peptides. This result also supports our previous assumption for deriving the flexibility scale for amino acids in peptides.⁶ Charges do not show systematical effect on end-to-end collision rates in peptides with two chargeable residues, consistent with the observation of weak charge effect in peptides with 6 chargeable residues (*cf.* Appendix II and VI).⁶

References:

- (1) Cox, J. P. L.; Evans, P. A.; Packman, L. C.; Williams, D. H.; Woolfson, D. N. *J. Mol. Biol.* **1993**, *234*, 483-492.
- (2) Zerella, R. et al. *Protein Sci.* **1999**, *8*, 1320-1331.
- (3) Mathews, C. K.; van Holde, K. E.; Ahern, K. G. *Biochemistry*; 3rd ed.; Benjamin/Cummings: San Francisco, 2000.
- (4) Nau, W. M. et al. *Chimia* **2003**, *57*, 161-167.
- (5) Hudgins, R. R.; Huang, F.; Gramlich, G.; Nau, W. M. *J. Am. Chem. Soc.* **2002**, *124*, 556-564.
- (6) Huang, F.; Nau, W. M. *Angew. Chem. Int. Ed.* **2003**, *42*, 2269-2272.
- (7) Huang, F.; Wang, X.; Haas, E.; Nau, W. M. **2004**.

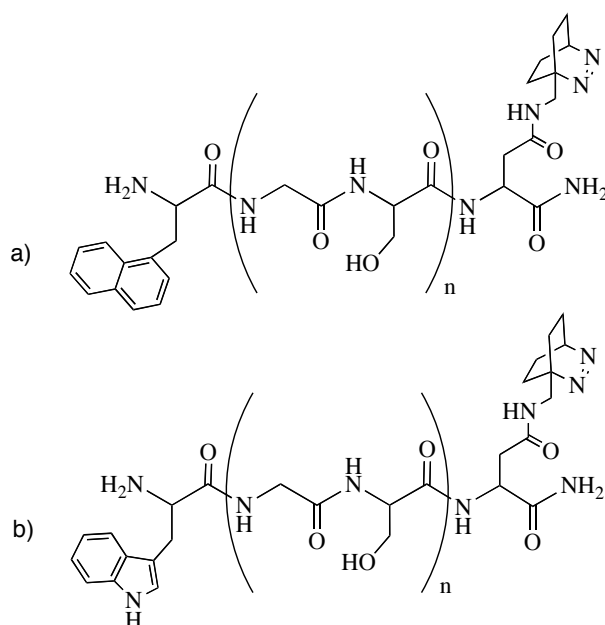
7. Intramolecular energy transfer in peptides

Fluorescence resonance energy transfer (FRET) is one of the most important photochemical techniques applied in the biochemical sciences. FRET cannot be used to measure intramolecular collision rates, since the quenching of the donor (probe) does not need direct contact with the acceptor (quencher). However, the strong distance dependence of the energy transfer efficiency allows one to apply this technique as a spectroscopic ruler to measure the site-to-site distance with Equation 7-1.¹⁻³

$$\eta_{\text{ET}} = \frac{R_0^6}{R_0^6 + R^6} \quad (7-1)$$

where η_{ET} is the energy transfer efficiency, which can be measured from the fluorescence intensity of the donor, R_0 is the critical distance, and R is the average distance between donor and acceptor. In the case without diffusion R is the actual mean distance, while in the case that donor and acceptor diffuse during FRET process, R is shorter than the equilibrium average distance and also related to the diffusion coefficient, which provides the opportunity to measure the diffusion coefficient with FRET.

Scheme 7-1. General structure for donor/acceptor labeled peptides, a) Nal-(Gly-Ser)_n-DBO (Nal = Naphthylalanine), b) Trp-(Gly-Ser)_n-DBO, $n = 0, 1, 2, 4, 6, 10$.



It is a particular challenge to apply FRET to peptides with short end-to-end distance (ca. 10 Å), which are not compatible with normal FRET donor/acceptor pairs,

with R_0 ranging from 20 to 90 Å,⁴ due to both the strong distance dependence of energy transfer efficiency and the requirements of a relatively small critical radius in the theoretical models employed in the data analysis.⁵ To apply the FRET technique in such special systems, we selected FRET donor/acceptor pairs with very short critical distance (~ 10 Å), naphthalene/DBO or Trp/DBO, for the Gly-Ser peptide series, which have the same sequence as those used in Chapter 4⁶ (Scheme 7-1).

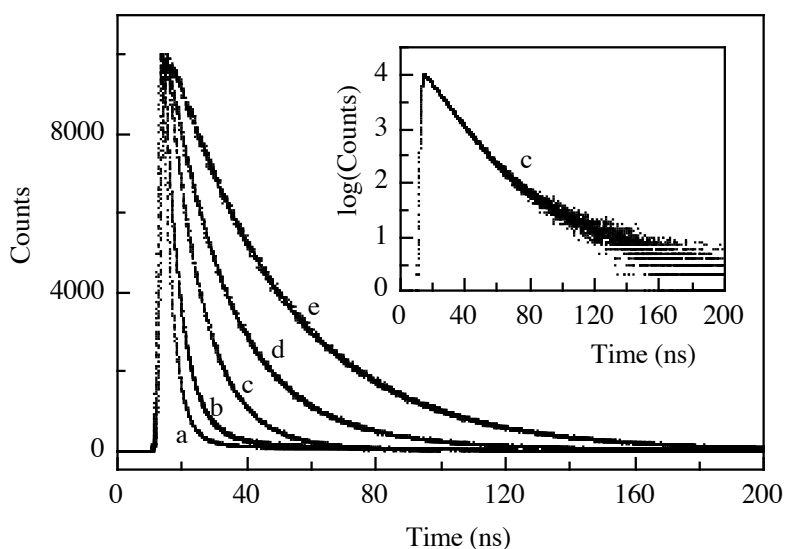


Figure 7-1 Typical time-resolved fluorescence decays ($\lambda_{ex} = 285\text{nm}$, $\lambda_{em} = 335\text{nm}$) of naphthalene peptides a) Nal-DBO, b) Nal-(Gly-Ser)₂-DBO, c) Nal-(Gly-Ser)₆-DBO, d) Nal-(Gly-Ser)₁₀-DBO, and e) Nal-(Gly-Ser)₆. The inset shows a semi-logarithmic plot for Nal-(Gly-Ser)₆-DBO.

The energy transfer between naphthalene and DBO was investigated first at a very short distance, where DBO and naphthalene were separated by a dimethylsiloxy group. In that investigation, it was found that exchange energy transfer might be dominant due to the close proximity of donor and acceptor, the high flexibility of the tether, and the nonviscous solvent employed. However, in the case of peptides, due to the larger separation and higher viscosity in D₂O, FRET is expected to become dominant. This was supported by the control experiment in the presence of CB7, which prevents the contact of naphthalene and DBO efficiently (*cf.* Appendix III and V), but which cannot exclude the energy transfer between naphthalene and DBO (Appendix VIII).⁷

The fluorescence decay traces of the naphthalene peptides in the presence of FRET are characteristically non-monoexponential, which prevents one to assign a fluorescence lifetime, and they show a strong length dependence (Figure 7-1). These fluorescence decay traces can be fitted with a biexponential function, from which average lifetimes can

be obtained. If these average lifetimes are applied to calculate the end-to-end collision rates approximately with equations 2-1 and 2-3, much larger end-to-end collision rates than those obtained with method based on contact quenching will be obtained (Figure 7-2), suggesting that faster “end-to-end collision” could be observed when probe/quencher pairs based on non-contact quenching mechanism or those with large reaction distance are applied in end-to-end collision measurements.

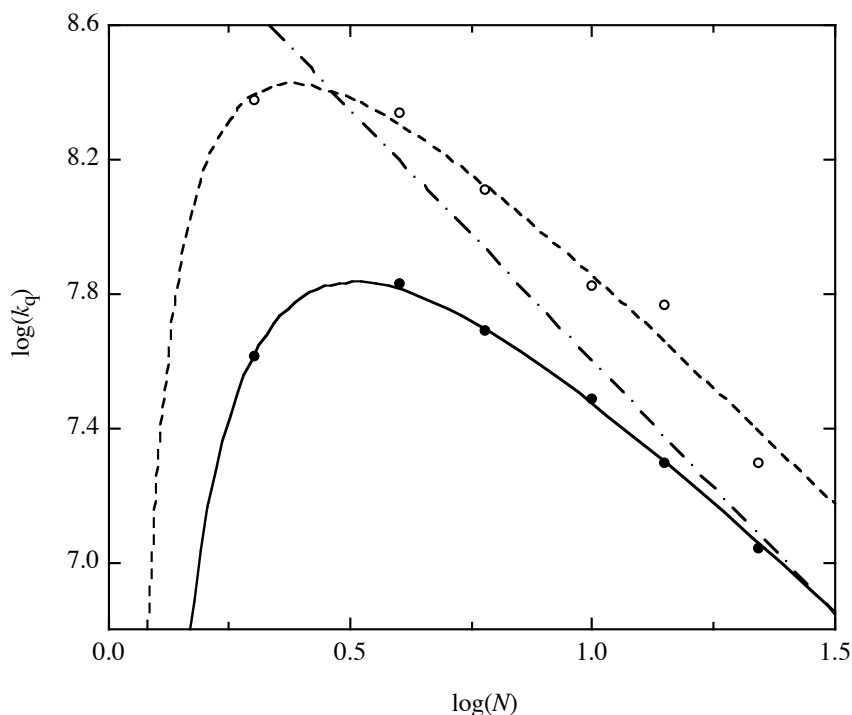


Figure 7-2. Double logarithmic plot of $k_{q,ET}$ (open cycle) and k_q (solid cycle) versus peptide length (data taken from Table 1). A function of the type $y = a - 1.5x - b/x$ was fitted to the experimental data ($a = 9.37$, $b = 0.392$ for data obtained from collision-based experiments,⁶ and $a = 9.57$, $b = 0.229$ for data obtained from experiments based on singlet-singlet energy transfer from current work). The dash-dot-dash line has a slope of -1.5 and is shown to illustrate the deviation from the theoretical behavior.

The fluorescence decay traces for the donor and acceptor in the presence and absence of FRET were globally analyzed (*cf.* Chapter 3.2). However, due to the extremely short end-to-end distance, which cannot prevent alternative energy transfer through a Dexter mechanism, and the high correlation between parameters, the analysis is subject to a quite large uncertainty. To reduce the correlation between the parameters, a theoretical

prediction for end-to-end distance was combined into the global data analysis. Results show that the diffusion coefficient decreases significantly for shorter peptides, which is expected to be the reason for the deviation of the distance dependence in real peptides from that expected for ideal chains (Figure 7-2, See also Appendix VIII).

The emission spectrum of Trp is very broad and overlaps with that of DBO, which prevents the use of the Trp/DBO pair for a similar global data analysis. However, the Trp/DBO energy donor/acceptor pair is very useful due to the very short lifetime of Trp. In the lifetime of Trp, the conformational change of peptides is expected to be not significant, especially for rigid peptides. As mentioned above, in the absence of diffusion or conformational change, the site-to-site distance can be obtained directly from the energy transfer efficiency with Equation 7-1. In the case of Gly-Ser peptides the diffusion cannot be completely excluded due to the high flexibility, but the average distance obtained from the energy transfer efficiency from Trp to DBO provides a lower limit for the end-to-end distance for the global data analysis and a unique way to estimate the end-to-end distance distribution function and to interpret the end-to-end collision rates measured with the same sequence but by employing Trp as collision-induced quencher of DBO.

References:

- (1) Stryer, L.; Haugland, R. P. *Proc. Natl. Acad. Sci. USA* **1967**, *58*, 719-726.
- (2) Deniz, A. A. et al. *Proc. Natl. Acad. Sci. USA* **2000**, *97*, 5179-5184.
- (3) Schuler, B.; Lipman, E. A.; Eaton, W. A. *Nature* **2002**, *419*, 743-747.
- (4) Lakowicz, J. R. *Principles of Fluorescence Spectroscopy*; 2nd ed.; Kluwer Academic/Plenum Publishers: New York, 1999.
- (5) Srinivas, G.; Yethiraj, A.; Bagchi, B. *J. Chem. Phys.* **2001**, *114*, 9170-9178.
- (6) Hudgins, R. R.; Huang, F.; Gramlich, G.; Nau, W. M. *J. Am. Chem. Soc.* **2002**, *124*, 556-564.
- (7) Nau, W. M.; Huang, F.; Wang, X.; Bakirci, H.; Gramlich, G.; Marquez, C. *Chimia* **2003**, *57*, 161-167.

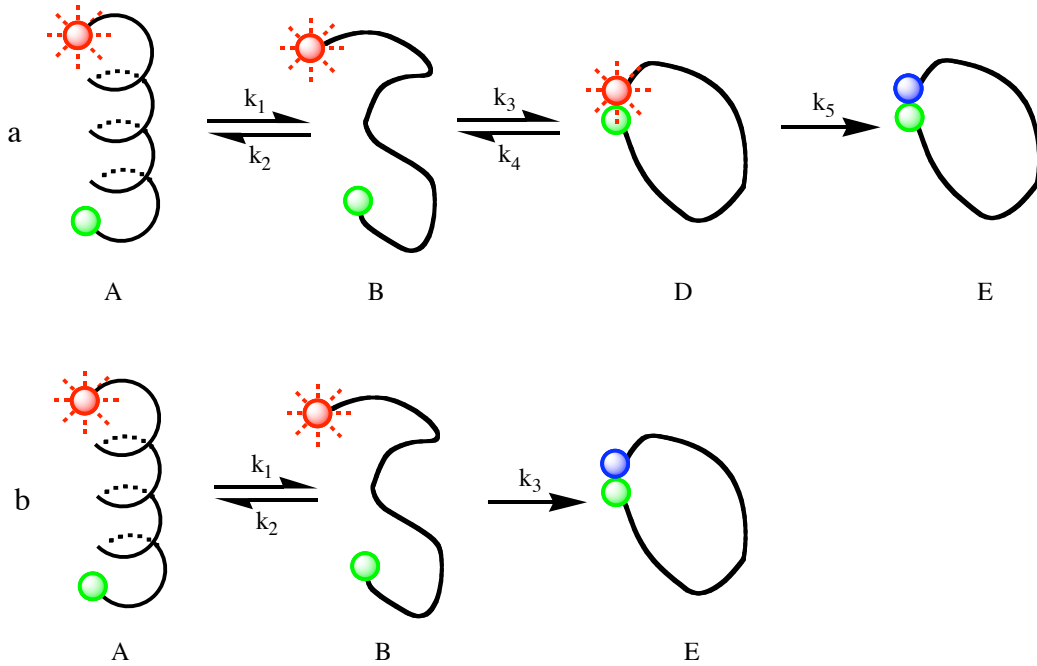
8. Ongoing project: Helix-coil transition of an alanine-rich peptide

α -Helices and α -hairpins are the most common secondary structures in proteins and are essential in protein folding, stability, and functions. Investigations on their folding rates and mechanisms are very important for understanding how proteins fold. Laser-assisted techniques have allowed to directly monitor the formation of α -helices and α -hairpins.¹⁻⁴ Although the helix-coil transition has been investigated with both temperature jump and photophysical methods and found to be a monoexponential process, theoretical results suggest that a non-monoexponential process should occur in the early stages.⁵ The helix-coil transition is therefore worthy of a more detailed investigation.

Our fluorescence-based technique for measuring intramolecular collision can, in principle, have a time resolution of picoseconds.^{6,7} The application of this new technique may be able to reveal this elusive process in the helix-coil transition that is too fast to be observed by the T-jump and triplet-triplet transient absorption techniques, which are limited in time resolution to > 5 ns.^{8,9}

The principle to apply our fluorescence-based technique to investigate a helix-coil transition is shown in Scheme 8-1. A fluorescent probe (DBO) and an efficient quencher (Trp) are attached at the opposite ends of a α -helix forming peptide. The excited probe cannot be quenched by the quencher at the opposite end of the peptide in the helical conformation because a) the probe can only be quenched through contact⁶ and b) the helix is rigid and the two ends cannot get into contact in the short time range.⁸ Once the helix unfolds to a random coil, its ends can collide and then the excited probe can be quenched through collision with Trp. The deactivation rate of the excited probe (k_q) is related to the helix-coil transition rates (k_1 and k_2), the end-to-end collision rates (k_3 and k_4), the deactivation rate of the contacted excited probe/quencher pair (k_5) as well as the intrinsic deactivation rate of the excited probe (k_0). By measuring the fluorescence decay, one can get information on these individual rates. From our previous study, the quenching of DBO by Trp is almost diffusion-controlled in a random-coiled peptide chain, which means that the whole rate constant for the last two steps in Scheme 8-1a equals k_3 in a good approximation (*cf.* Chapter 2 and Appendix VI). Scheme 8-1a therefore can be simplified to Scheme 8-1b.

Scheme 8-1. Principle for measuring helix-coil transition kinetics under equilibrium.



From Scheme 8-1b, a pair of differential equations (Equations 8-1 and 8-2) can be obtained, which describe the temporal evolution of A and B, respectively.

$$\frac{dA}{dt} = k_2 B - k_1 A - k_0 A \quad (8-1)$$

$$\frac{dB}{dt} = k_1 A - (k_0 + k_2 + k_3) B \quad (8-2)$$

The integrated functions to describe the decay of A and B can be obtained by solving Equations 8-1 and 8-2:

$$[A] = C_1 e^{\square k_n t} + C_2 e^{\square k_m t} \quad (8-3)$$

$$[B] = \frac{C_1}{2k_2} (k_1 - k_2 - k_3 + w) e^{\square k_n t} + \frac{C_2}{2k_2} (k_1 - k_2 - k_3 - w) e^{\square k_m t} \quad (8-4)$$

where

$$k_m = k_0 + \frac{1}{2} (k_1 + k_2 + k_3 + \sqrt{k_1^2 + k_2^2 + k_3^2 + 2k_1 k_2 + 2k_2 k_3 - 2k_1 k_3}) \quad (8-5)$$

$$k_n = k_0 + \frac{1}{2} (k_1 + k_2 + k_3 - \sqrt{k_1^2 + k_2^2 + k_3^2 + 2k_1 k_2 + 2k_2 k_3 - 2k_1 k_3}) \quad (8-6)$$

$$w = \sqrt{k_1^2 + k_2^2 + k_3^2 + 2k_1k_2 + 2k_2k_3 + 2k_1k_3} \quad (8-7)$$

and C_1 and C_2 are integration constants.

Accordingly, the decay of the fluorescence can be obtained as Equation 8-8

$$I = f \left[\frac{C_1}{2k_2} (k_1 + k_3 + k_2 + w) + C_1 \right] e^{-k_1 t} + f \left[\frac{C_2}{2k_2} (k_1 + k_3 + k_2 + w) + C_2 \right] e^{-k_m t} \quad (8-8)$$

where f is a constant. The initial concentration of A and B are described as Equations 8-9 and 8-10.

$$[A]_0 = C_1 + C_2 \quad (8-9)$$

$$[B]_0 = \frac{C_1}{2k_2} (k_1 + k_2 + k_3 + w) + \frac{C_2}{2k_2} (k_1 + k_2 + k_3 + w) \quad (8-10)$$

It is reasonable to assume that the initial concentration of the excited molecules in the conformations A and B is proportional to the concentration of the corresponding ensemble, i.e., $[B]_0/[A]_0 = K_{eq}$. One can therefore obtain Equations 8-11 and 8-12.

$$K_{eq} = \frac{C_1(k_1 + k_2 + k_3 + w) + C_2(k_1 + k_2 + k_3 + w)}{2k_2(C_1 + C_2)} \quad (8-11)$$

$$\frac{C_2}{C_1} = \frac{k_1 + k_2 + k_3 + w}{k_1 + k_2 + k_3 + w} \quad (8-12)$$

The combination of Equations 8-8 and 8-12 gives Equation 8-13 for the fluorescence intensity decay.

$$I = f \left[\frac{k_1 + k_2 + k_3 + w}{2k_2} e^{-k_1 t} + f \left[\frac{k_1 + k_2 + k_3 + w}{k_1 + k_2 + k_3 + w} \frac{k_1 + k_2 + k_3 + w}{2k_2} e^{-k_m t} \right] \right] \quad (8-13)$$

By measuring the circular dichroism (CD) spectrum at different temperatures and fitting the ellipticity values at 222 nm (See Figure 8-1) to Equation 8-14,⁸ we can get the equilibrium constant for the helix-coil transition experimentally.

$$\theta_{222} = \frac{f_H}{n} \left\{ (1 - s_{\square})(n - 2)([\theta]_{\square} + [\theta]_{\square T} [T - T_0]) + [\theta]_{\square WL} \right\} + \frac{1 - f_H}{n} \left\{ (n - 2)([\theta]_{\square} + [\theta]_{\square T} [T - T_0]) + [\theta]_{\square WL} \right\} \quad (8-14)$$

In Equation 8-14, f_H is the fractional population of helix state, $f_H = K_{eq}(T)/(1 + K_{eq}(T))$, n is the number of residues, $s_{\square} = 0.2$ accounts for the length-

dependence of the ellipticity, $([\theta]_H + [\theta]_{HT}[T - T_0])$ is the temperature-dependent ellipticity per residue in the helical conformation with $[\theta]_H = 4.3 \times 10^4 \text{ deg cm}^2 \text{ dm}^{-1}$, $[\theta]_{HT} = 145 \text{ deg cm}^2 \text{ dm}^{-1} \text{ K}^{-1}$ and $T_0 = 273 \text{ K}$, $[\theta]_R + [\theta]_{RT}[T - T_0]$ is the temperature-dependent ellipticity per residue in the random coil conformation with $[\theta]_R = 600 \text{ deg cm}^2 \text{ dm}^{-1}$ and $[\theta]_{RT} = 40 \text{ deg cm}^2 \text{ dm}^{-1} \text{ K}^{-1}$, and $[\theta]_{HWL}$ and $[\theta]_{RWL}$ are the contributions to the ellipticity by Trp in the helix and random coil conformations, respectively.⁸

Since k_0 can be independently obtained from the lifetime of the reference peptide, the peptide with identical sequence but without quencher, there remain only two variables, k_1 (or k_2) and k_3 , in Equation 8-13, which can be obtained by fitting the fluorescence decay trace.

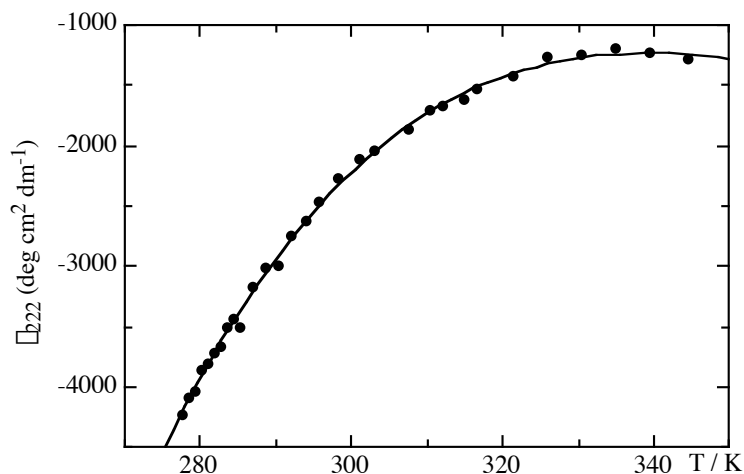


Figure 8-1. CD-temperature dependence plot. Dots are experimental data and the solid line is the fit according to Equation 8-14.

In this project we investigated an alanine-rich peptide (Trp-(Ala-Ala-Ala-Arg-Ala)₃-Ala-DBO). The early results are shown in Figure 8-1 and 8-2. Figure 8-1 shows good fitting for the CD data, which provides the equilibrium constant for coil-helix transition at different temperatures. The helix-coil transition equilibrium constant ranges from 0.12 (56 °C) to 0.52 (9.5°C) and suggests that the helix is similarly stable as the coil state for this peptide.

From Figure 8-2, it can be seen that the decay for the peptide without quencher is monoexponential, while the one for the peptide with quencher is clearly non-monoexponential, but instead can be fitted very well by a biexponential function. However, when the pre-exponential factors in Equation 8-13 are included into the fitting,

it is found that the decay traces cannot be fitted well. This indicates that the model we established is not perfect and that there is a step that was not considered in the helix-coil transition model. Furthermore, the fast process with a lifetime of 4-5 ns was not reported with the T-jump and transient absorption technique, which might suggest that there is a faster step in the helix-coil transition that could not be observed by T-jump and transient absorption due to the lower time resolution of ≥ 5 ns.^{8,9} In this project, some interesting points have appeared but a better model needs to be sought for.

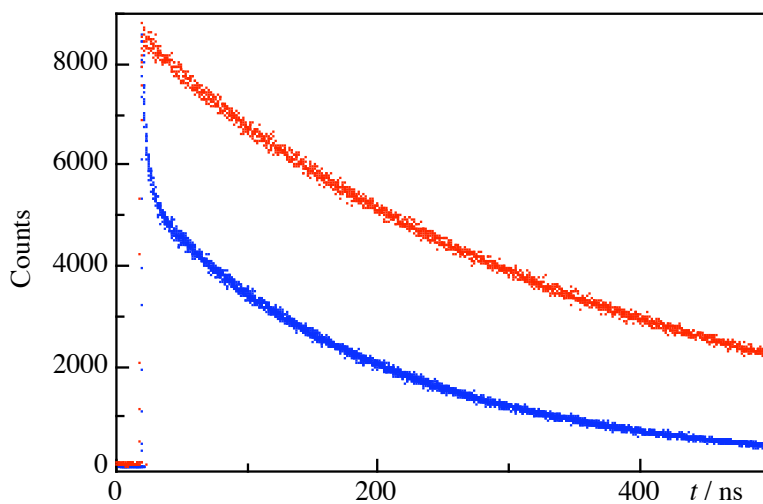


Figure 8-2. The time-resolved fluorescence decays for the helix peptides. The upper one is for the helix peptide without quencher and the lower one is for the helix peptide with quencher.

References:

- (1) Jas, G. S.; Eaton, W. A.; Hofrichter, J. *J. Phys. Chem. B* **2001**, *105*, 261-272.
- (2) Huang, C.-Y.; Klemke, J. W.; Getahun, Z.; DeGrado, W. F.; Gai, F. *J. Am. Chem. Soc.* **2001**, *123*, 9235-9238.
- (3) Munoz, V.; Thompson, P. A.; Hofrichter, J.; Eaton, W. A. *Nature* **1997**, *390*, 196-199.
- (4) Thompson, P. A.; Munoz, V.; Jas, G. S.; Henry, E. R.; Eaton, W. A.; Hofrichter, J. *J. Phys. Chem. B* **2000**, *104*, 378-389.
- (5) Hummer, G.; Garcia, A. E.; Garde, S. *Phys. Rev. Lett.* **2000**, *85*, 2637-2640.
- (6) Hudgins, R. R.; Huang, F.; Gramlich, G.; Nau, W. M. *J. Am. Chem. Soc.* **2002**, *124*, 556-564.
- (7) Lakowicz, J. R. *Principles of Fluorescence Spectroscopy*; 2nd ed.; Kluwer Academic/Plenum Publishers: New York, 1999.
- (8) Lapidus, L. J.; Eaton, W. A.; Hofrichter, J. *J. Mol. Biol.* **2002**, *319*, 19-25.
- (9) Thompson, P. A.; Eaton, W. A.; Hofrichter, J. *Biochemistry* **1997**, *36*, 9200-9210.

9. Summary

A fluorescence-based method, which takes the desirable properties of DBO, including small size, good solubility in water and long lifetime of the excited state, has been established for measuring submicrosecond dynamics of polypeptide chains. Combining this method with other techniques, such as UV absorption, NMR and CD spectroscopy, we have successfully investigated the length dependence of peptide end-to-end collision rates and reported a conformational flexibility scale for amino acids in peptides, which provides an absolute measure for the time-scale of conformational changes in a series of synthetic short peptides as a function of the amino acid type. In addition, by studying the kinetics of some elementary steps of protein folding, we also explored the folding mechanism of secondary structures of proteins, including the folding of the *N*-terminal β -hairpin in ubiquitin and the helix-coil transition in an alanine-rich peptide. As a complementary method, we have applied intramolecular fluorescence resonance energy transfer (FRET) to investigate the end-to-end distance distribution and the diffusion coefficient of random-coiled peptides, where donor/acceptor pairs with very short critical distance (~ 10 Å) were used. These results are invaluable for research on diffusion phenomena in polymers and biopolymers. In particular, they are pertinent for the understanding of protein folding and domain motions in proteins.

Furthermore, the success of this fluorescence-based method in peptide research has also stimulated the application of DBO to the structural and dynamic investigation of nucleic acids. At the same time, due to the strong dependence of intramolecular quenching on the properties of peptide backbone, DBO/Trp labeled peptides have the potential to be applied to test the activity of enzymes, which are expected to change the properties of the peptide backbones or cleave them.

10. A brief experimental description

Materials. All commercial materials were from Fluka or Aldrich. Fmoc-DBO was synthesized according to the reported procedure. The DBO-labeled peptides were commercially synthesized in > 95% purity (Affina, Berlin). Details on the synthesis of the probe and its suitability in solid-phase peptide synthesis can be obtained from Appendix I.

NMR and CD measurements. NMR experiments were carried out on a Bruker DRX 500 spectrometer in D₂O (with 10% H₂O) at 1 mM peptide concentration. Circular dichroism (CD) experiments of the peptides were performed on a Jasco 720 circular dichroism spectrometer at ambient temperature at peptide concentrations of 10–100 μ M.

Fluorescence and UV measurements. Fluorescence decays were recorded on a time-correlated single photon counting (TCSPC) fluorimeter (FLS920, Edinburgh Instruments, Edinburgh, Scotland) by using either a 1.5-ns pulse-width H₂ flash lamp or a Picoquant picosecond pulsed diode laser (λ_{exc} = 373 nm, ca. 50 ps pulse width) for excitation. The peptide concentrations were adjusted to 10–100 μ M, sufficiently low to exclude intermolecular quenching. The pH-dependent measurements were performed in phosphate buffer for pH 7, citrate/HCl/NaOH buffer for pH 2 and Na₂HPO₄/NaOH buffer for pH 12.

Solid-phase fluorescence experiments were carried out in trehalose glass with 1 mM naphthylalanine and 77 mM DBO. Trehalose glass was prepared by heating 5 g trehalose with a little water to ~130 °C to obtain a viscous solution with naphthylalanine and DBO dissolved in it, which was then quickly poured into a 1 cm cuvette and allowed to cool down to get a solid solution.

Absorption spectra were recorded on a Cary 4000 UV-Vis spectrophotometer (Varian) and steady-state fluorescence spectra on a Cary Eclipse fluorescence spectrometer (Varian).

11. Publications (contained in Appendix)

- I. Hudgins, R. R., Huang, F., Gramlich, G. & Nau, W. M. "A fluorescence-based method for direct measurement of submicrosecond intramolecular contact formation in biopolymers: An exploratory study with polypeptides" *J. Am. Chem. Soc.* **124**, 556-564 (2002).
- II. Huang, F. & Nau, W. M. "A conformational flexibility scale for amino acids in peptides" *Angew. Chem. Int. Ed.* **42**, 2269-2272 (2003).
- III. Nau, W. M., Huang, F., Wang, X., Bakirci, H., Gramlich, G. & Marquez, C. "Exploiting long-lived molecular fluorescence" *Chimia* **57**, 161-167 (2003).
- IV. Pischel, U., Huang, F. & Nau, W. M. "Intramolecular singlet-singlet energy transfer in antenna-substituted azoalkanes" *Photochem. Photobiol. Sci.* **3**, 305-310 (2004).
- V. Marquez, C., Huang, F. & Nau, W. M. "Cucurbiturils: Molecular nanocapsules for time-resolved fluorescence-based assays" *IEEE Trans. Nanobiosci.* **3**, 39-45 (2004).
- VI. Huang, F., Hudgins, R. R. & Nau, W. M. "Primary and secondary structure dependence of peptide flexibility assessed by fluorescence-based measurement of end-to-end collision rate" Submitted for publication (2004).
- VII. Huang, F. & Nau, W. M. "Photochemical techniques for studying the flexibility of polypeptides" *Res. Chem. Intermed.*, Submitted for publication (2004).
- VIII. Huang, F., Wang, X., Haas, E. & Nau, W. M. "Application of FRET donor/acceptor pairs with small critical radius to recover the structural and dynamic properties of short flexible peptides" In preparation (2004).

12. Presentations at conferences

Oral presentations:

- I. F. Huang and W. M. Nau, “*Dynamics of peptides measured with a long-lived fluorescent probe*”, July, 2003, 21th International Conference on Photochemistry, Nara, Japan
- II. F. Huang and W. M. Nau, “*Conformational change and flexibility of peptides monitored by fluorescence*”, April 2003, SGPP Graduate Student Symposium on Photochemistry, Photobiology and Photophysics, Fribourg

Poster presentations:

- I. F. Huang, X. Wang, G. Gramlich, A. Hennig, W. M. Nau “*Chain Flexibility of Biopolymers: An Example of Supramolecular Mechanics*”, NRP 47 “Supramolecular Functional Materials” Meeting, July 2003, Bern
- II. F. Huang, X. Wang, and W. M. Nau, “*Kinetics of Biopolymer Folding: Flexibility Scales for Polypeptides and Oligonucleotides*”, International Conference on Reactive Intermediates and Reaction Mechanisms, July 2002, Ascona
- III. F. Huang, Gabriela Gramlich and W. M. Nau, “*Fluorazophores as Tailored Probes for Biomolecule Dynamics*”, NRP 47 “Supramolecular Functional Materials” 1st progress report meeting, October 2001, Bern

13. Appendix

A Fluorescence-Based Method for Direct Measurement of Submicrosecond Intramolecular Contact Formation in Biopolymers: An Exploratory Study with Polypeptides

Robert R. Hudgins, Fang Huang, Gabriela Gramlich, and Werner M. Nau*

Contribution from the *Departement Chemie, Universität Basel, Klingelbergstrasse 80, CH-4056 Basel, Switzerland*

Received February 22, 2001. Revised Manuscript Received October 26, 2001

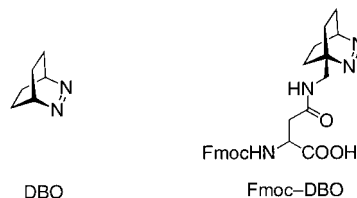
Abstract: A fluorescent amino acid derivative (Fmoc-DBO) has been synthesized, which contains 2,3-diazabicyclo[2.2.2]oct-2-ene (DBO) as a small, hydrophilic fluorophore with an extremely long fluorescence lifetime (325 ns in H₂O and 505 ns in D₂O under air). Polypeptides containing both the DBO residue and an efficient fluorescence quencher allow the measurement of rate constants for intramolecular end-to-end contact formation. Bimolecular quenching experiments indicated that Trp, Cys, Met, and Tyr are efficient quenchers of DBO ($k_q = 20, 5.1, 4.5,$ and $3.6 \times 10^8 \text{ M}^{-1} \text{ s}^{-1}$ in D₂O), while the other amino acids are inefficient. The quenching by Trp, which was selected as an intrinsic quencher, is presumed to involve exciplex-induced deactivation. Flexible, structureless polypeptides, Trp-(Gly-Ser)_n-DBO-NH₂, were prepared by standard solid-phase synthesis, and the rates of contact formation were measured through the intramolecular fluorescence quenching of DBO by Trp with time-correlated single-photon counting, laser flash photolysis, and steady-state fluorometry. Rate constants of 4.1, 6.8, 4.9, 3.1, 2.0, and $1.1 \times 10^7 \text{ s}^{-1}$ for $n = 0, 1, 2, 4, 6,$ and 10 were obtained. Noteworthy was the relatively slow quenching for the shortest peptide ($n = 0$). The kinetic data are in agreement with recent transient absorption studies of triplet probes for related peptides, but the rate constants are significantly larger. In contrast to the flexible structureless Gly-Ser polypeptides, the polyproline Trp-Pro₄-DBO-NH₂ showed insignificant fluorescence quenching, suggesting that a high polypeptide flexibility and the possibility of probe–quencher contact is essential to induce quenching. Advantages of the new fluorescence-based method for measuring contact formation rates in biopolymers include high accuracy, fast time range (100 ps–1 μs), and the possibility to perform measurements in water under air.

Introduction

There is great interest in “intelligent” fluorescent probes for biomolecules that can report information beyond mere detection, e.g., on the structure of polynucleotides and the dynamics of proteins.^{1–6} However, the fluorescence lifetimes of common fluorophores are typically in the range of several nanoseconds or less. This is too short to monitor nanosecond-to-microsecond processes as, for example, the intramolecular contact formation in polypeptides, which is important to understand the functions and folding dynamics of proteins.⁷ To bypass this limitation of fluorescent probes, long-lived triplet-state probes have recently been introduced for measuring the corresponding rates in

polypeptides in the nanosecond-to-microsecond time range by means of transient absorption techniques.^{7–10}

2,3-Diazabicyclo[2.2.2]oct-2-ene (DBO) is a fluorophore with an extremely long fluorescence lifetime (up to 1 μs). As a

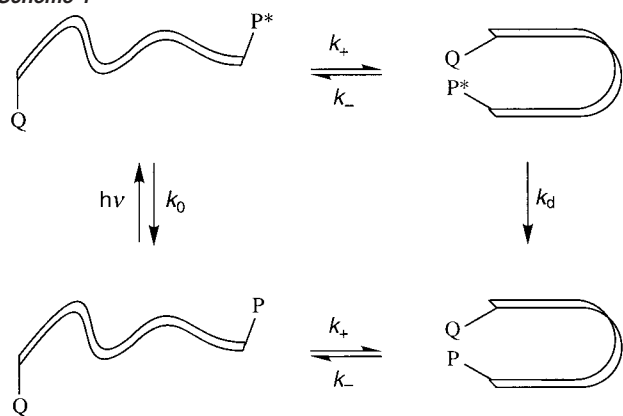


continuation of our efforts to exploit this unique property for uncommon fluorescence-based applications,^{11,12} we employ herein a DBO-labeled fluorescent amino acid, the asparagine derivative Fmoc-DBO, to introduce DBO into polypeptides and to monitor its intramolecular fluorescence quenching by tryptophan.

- (1) Haran, G.; Haas, E.; Szpikowska, B. K.; Mas, M. T. *Proc. Natl. Acad. Sci. U.S.A.* **1992**, *89*, 11764–11768.
- (2) Demchenko, A. P. *Biochim. Biophys. Acta* **1994**, *1209*, 149–164.
- (3) Seidel, C. A. M.; Schultz, A.; Sauer, M. H. M. *J. Phys. Chem.* **1996**, *100*, 5541–5553.
- (4) Muñoz, V.; Thompson, P. A.; Hofrichter, J.; Eaton, W. A. *Nature* **1997**, *390*, 196–199.
- (5) Deniz, A. A.; Dahan, M.; Grunwell, J. R.; Ha, T.; Faulhaber, A. E.; Chemla, D. S.; Weiss, S.; Schultz, P. G. *Proc. Natl. Acad. Sci. U.S.A.* **1999**, *96*, 3670–3675.
- (6) Lakowicz, J. R.; Nair, R.; Piszczek, G.; Gryczynski, I. *Photochem. Photobiol.* **2000**, *71*, 157–161.
- (7) Eaton, W. A.; Muñoz, V.; Hagen, S. J.; Jas, G. S.; Lapidus, L. J.; Henry, E. R.; Hofrichter, J. *Annu. Rev. Biophys. Biomol. Struct.* **2000**, *29*, 327–359.

- (8) McGimpsey, W. G.; Chen, L.; Carraway, R.; Samaniego, W. N. *J. Phys. Chem. A* **1999**, *103*, 6082–6090.
- (9) Bieri, O.; Wirz, J.; Hellrung, B.; Schutkowski, M.; Drewello, M.; Kiefhaber, T. *Proc. Natl. Acad. Sci. U.S.A.* **1999**, *96*, 9597–9601.
- (10) Lapidus, L. J.; Eaton, W. A.; Hofrichter, J. *Proc. Natl. Acad. Sci. U.S.A.* **2000**, *97*, 7220–7225.
- (11) Nau, W. M. *J. Am. Chem. Soc.* **1998**, *120*, 12614–12618.
- (12) Nau, W. M.; Zhang, X. *J. Am. Chem. Soc.* **1999**, *121*, 8022–8032.

Scheme 1

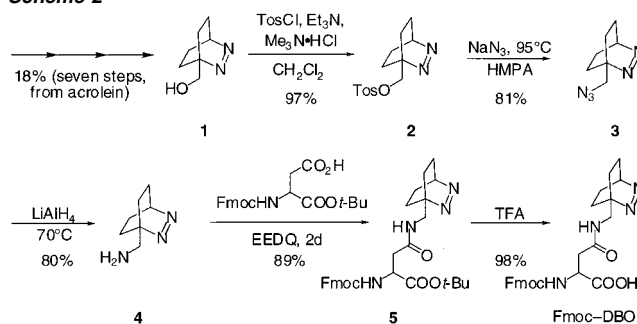


tophan (Trp). This has allowed the first direct measurements of submicrosecond contact formation kinetics in polypeptides by a fluorescence technique.^{13,14}

The general principle behind using photophysical probes to measure peptide dynamics is shown in Scheme 1. A photophysical probe (P) and a quencher (Q) are incorporated into a polypeptide (bottom-left structure). The backbone of the peptide is chosen to behave as a random coil, i.e., without preference for a particular conformation. An excited state of the peptide-bound probe (P*) is prepared with a short light pulse (top-left structure). The dynamics of the polypeptide will infrequently lead to conformations where P* and Q (top-right structure) or P and Q (bottom-right structure) come in contact, and it is this event that is of interest for the evaluation of polymer and biopolymer flexibility. The decay of P*, which can be followed through its characteristic emission or absorption, will reflect the rate of intrinsic excited-state decay (k_0) and the intramolecular quenching rate constant (k_q). Intermolecular quenching is excluded by working at sufficiently low concentrations. If the probe/quencher pair is designed in such a way that molecular contact formation between P* and Q (k_+) is followed by immediate quenching (k_d), k_q equals the pertinent rate of contact formation, k_+ . The condition of “immediate” quenching upon contact is fulfilled when $k_d \gg k_-$, the rate of dissociation of the encounter complex. This criterion is generally assumed to be met when the intermolecular quenching of free P* by free Q in solution occurs near the diffusion-controlled rate. In other cases, k_q will be a function of the three rate constants k_+ , k_- , and k_d , which requires a more involved analysis to extract k_+ , but, on the other hand, may also provide information on k_- .¹⁵

The methodology in Scheme 1 requires a probe with a sufficiently slow intrinsic decay rate, $k_0 \leq k_+$, to allow intramolecular quenching to compete with the natural decay and, thus, to report kinetic information on contact formation. DBO

Scheme 2



is a unique fluorophore due to its long intrinsic fluorescence lifetime (τ_0), which amounts to 325 ns in aerated H₂O, 420 ns in deaerated H₂O, 505 ns in aerated D₂O, and 730 ns in deaerated D₂O.^{12,16} Since $k_0 = 1/\tau_0 = 2.0 \times 10^6 \text{ s}^{-1}$ in aerated D₂O, diffusional processes in the submicrosecond range ($> 10^6 \text{ s}^{-1}$) become accessible.

Experimental Section

Materials. All commercial materials were from Fluka or Aldrich except for Fmoc-Asp-Ot-Bu (Bachem). They were used as received except for HMPA, which was dried (CaH₂) and freshly distilled prior to use, and Me₃N·HCl, which was sublimed in the presence of KOH (0.03 Torr, 100 °C). Column chromatography was performed with silica gel 60–200 μm . The synthetic sequence for Fmoc-DBO in 10% overall yield is shown in Scheme 2. 1-Hydroxymethyl-2,3-diazabicyclo[2.2.2]oct-2-ene (**1**) was synthesized according to a literature procedure¹⁷ and converted to the new 1-aminomethyl-2,3-diazabicyclo[2.2.2]oct-2-ene (**4**) by tosylation, azide substitution, and subsequent reduction with lithium aluminum hydride.

Synthesis of 1-(Aminomethyl)-2,3-diazabicyclo[2.2.2]oct-2-ene (4). For tosylation, the pyridine-free method of Tanabe was used.¹⁸ A solution of *p*-toluenesulfonyl chloride (12.4 g, 65 mmol) in 50 mL of dry CH₂Cl₂ was added to a stirred solution of 1-(hydroxymethyl)-2,3-diazabicyclo[2.2.2]oct-2-ene (5.29 g, 37.7 mmol), Et₃N (6.5 mL, 46.6 mmol), and dry Me₃N·HCl (4.35 mg, 45.5 mmol) in 150 mL of CH₂Cl₂, and the mixture was stirred under nitrogen for 18 h. The mixture was charged with 8.5 mL of *N,N*-dimethylethanolamine, stirred for 10 min, and, after addition of water, was extracted with ethyl acetate. The combined organic layers were washed with water and brine, dried over Na₂SO₄, and concentrated by rotary evaporation to give the sulfonate ester **2** as colorless crystals (10.8 g, 36.6 mmol, 97% yield). Recrystallization from ether afforded colorless needles with mp 119–121 °C: UV (*n*-hexane) λ_{max} 381 nm, ϵ 120 M⁻¹ cm⁻¹; ¹H NMR (400 MHz CDCl₃) δ 1.09–1.15 (2 H, m, CH₂), 1.29–1.35 (2 H, m, CH₂), 1.59–1.64 (4 H, m, CH₂), 2.46 (3 H, s, CH₃), 4.56 (2 H, s, CH₂O), 5.16 (1 H, s br, CH), 7.37 (2 H, d, $J = 8 \text{ Hz}$, CH) 7.86 (2 H, d, $J = 8 \text{ Hz}$, CH) ppm; ¹³C NMR (126 MHz CDCl₃) δ 21.2 (2 C, CH₂), 21.7 (CH₃), 23.2 (2 C, CH₂), 61.7 (CH), 65.6 (C_q), 74.2 (CH₂O), 128.1 (2 C, CH), 129.9 (2C, CH), 132.6 (C_q), 145.0 (C_q) ppm. Anal. Calcd for C₁₄H₁₈N₂O₃S: C, 57.12; H, 6.16; N, 9.52; O, 16.31. Found: C, 57.04; H, 6.21; N, 9.65; O, 16.42.

The sulfonate ester **2** (356 mg, 1.21 mmol) and 400 mg (6.15 mmol) of NaN₃ were dissolved in 10 mL of dry HMPA. The stirred mixture was heated under argon for 14 h at 90 °C (reflux condenser). After cooling, the mixture was diluted with 20 mL of water and extracted four times with ether. The combined extracts were rotary evaporated, redissolved in 25 mL of ether, and washed with 50 mL of water. Drying

(13) Lakowicz, J. R. *Principles of fluorescence spectroscopy*; Plenum Press: New York, 1983.

(14) Waggoner, A. S. In *Applications of fluorescence in the biomedical sciences*; Taylor, D. L., Waggoner, A. S., Lanni, F., Murphy, R. F., Birge, R. R., Eds.; Alan R. Liss, Inc.: New York, 1986; pp 3–28.

(15) It should be noted that the methodology in Scheme 1 is subject to two additional assumptions. First it is assumed that the diffusion rate constants in the excited-state resemble those in the ground state (top and bottom equilibria in Scheme 1). This assumption may be fulfilled for the association rate (k_+) but will not generally apply for the dissociation rate (k_-) due to the possibility of excited-state binding (exciplexes and excimers). Further, it is assumed that the rate constants are not governed by the diffusive behavior of the probe and the quencher (e.g., due to hydrophobe association) to allow an extrapolation to a characteristic dynamic property of the peptide backbone.

(16) Nau, W. M.; Greiner, G.; Rau, H.; Wall, J.; Olivucci, M.; Scaiano, J. C. *J. Phys. Chem. A* **1999**, *103*, 1579–1584.

(17) Engel, P. S.; Horsey, D. W.; Scholz, J. N.; Karatsu, T.; Kitamura, A. *J. Phys. Chem.* **1992**, *96*, 7524–7535.

(18) Yoshida, Y.; Sakakura, Y.; Aso, N.; Okada, S.; Tanabe, Y. *Tetrahedron* **1999**, *55*, 2183–2192.

over MgSO₄ and rotary evaporation gave the azide **3** (170 mg crude product, 81%) with ~5% HMPA. This intermediate was not purified for the next step due to its instability even at low temperature: ¹H NMR (400 MHz, CDCl₃) δ 1.15–1.25 (2 H, m, CH₂), 1.32–1.43 (2 H, m, CH₂), 1.51–1.68 (4 H, m, CH₂), 3.90 (2 H, s, CH₂–N₃), 5.17 (1 H, s br, CH); ¹³C NMR (101 MHz, CDCl₃) δ 21.7 (2 C, CH₂), 24.2 (2 C, CH₂), 58.3 (CH₂–N₃), 61.9 (CH), 67.0 (C_q) ppm.

A solution of azide **3** (164 mg, 0.99 mmol) in 10 mL of dry THF was added dropwise to a stirred slurry of lithium aluminum hydride (76 mg, 2 mmol) in THF (5 mL) under nitrogen. The mixture was stirred at 68 °C for 6 h, cooled to room temperature, diluted with 10 mL THF, and slowly treated with 15% NaOH until a white, granular precipitate was formed. The precipitate was removed by filtration and washed with THF, and the combined filtrates were evaporated. The residue was dissolved in CH₂Cl₂ and dried over KOH pellets. Concentration and flash column chromatography (CH₂Cl₂/methanol/NEt₃ 89:10:1) gave the amine **4** (111 mg, 80%) as a colorless, hygroscopic wax melting at room temperature: UV (D₂O) λ_{max} 369 nm, ε 43 M⁻¹ cm⁻¹ (D₂O); ¹H NMR (400 MHz, CDCl₃) δ 1.18–1.25 (2 H, m, CH₂), 1.31–1.48 (4 H, m, CH₂), 1.60–1.67 (2 H, m, CH₂), 1.78 (2H, br s, NH₂), 3.21 (2 H, br s, CH₂N), 5.14–5.17 (1 H, m, CH) ppm; ¹³C NMR (101 MHz, CDCl₃) δ 22.0 (2 C, CH₂), 24.0 (2 C, CH₂), 49.2 (1 C, CH₂N), 61.9 (1 C, CH), 67.2 (1 C, C_q) ppm. The hygroscopic nature of the pure amine prevented an accurate elemental analysis.

Synthesis of Fmoc-DBO. Amine **4** (80 mg, 0.575 mmol), Fmoc-Asp-*Or*-Bu (240 mg, 0.583 mmol) and 184 mg of EEDQ (0.75 mmol) were stirred in 15 mL of dry CH₂Cl₂ under argon for 2 days. The mixture was diluted to 50 mL, washed successively with 5% citric acid, water, saturated NaHCO₃, water, and brine, and dried over MgSO₄. Concentration and flash column chromatography (CH₂Cl₂ with 2% MeOH) gave the amide **5** (272 mg, 89%) as a colorless solid with mp 178–180 °C: ¹H NMR (CDCl₃, 500 MHz) δ 1.06–1.16 (2 H, m, CH₂), 1.24–1.35 (2 H, m, CH₂), 1.47 (9 H, s, CH₃), 1.45–1.66 (4 H, m, CH₂), 2.78 (1 H, dd, *J* = 16.0, 4.4 Hz, β-CH₂ Asp), 2.95 (1 H, dd, *J* = 16.0, 4.4 Hz, β-CH₂ Asp), 3.82 (2 H, d, *J* = 6.1 Hz, CH₂N), 4.21 (1 H, t, *J* = 7.4 Hz, CH Fmoc), 4.28 (1 H, dd, *J* = 10.4, 7.4 Hz, CH₂ Fmoc), 4.39 (1 H, dd, *J* = 10.4, 7.4 Hz, CH₂ Fmoc), 4.48–4.52 (1 H, m, α-CH Asp), 5.20 (1 H, br s, CH), 6.05 (1 H, br d, *J* = 8.5 Hz, urethane NH), 6.55 (1 H, br t, *J* = 6.1 Hz, NH), 7.30 (2 H, t, *J* = 7.4 Hz, CH Fmoc), 7.40 (2 H, t, *J* = 7.4 Hz, CH Fmoc), 7.58–7.62 (2 H, m, CH Fmoc), 7.76 (2 H, d, *J* = 7.4 Hz, CH Fmoc) ppm; ¹³C NMR (CDCl₃, 126 MHz) δ 21.7 (2 C, CH₂), 24.1 (2 C, CH₂), 27.9 (3 C, CH₃), 38.0 (CH₂ Asp), 45.3 (CH₂N), 47.1 (CH Fmoc), 51.3 (CH Asp), 62.0 (CH), 66.8 (C_q), 67.2 (CH₂ Fmoc), 82.3 (C_q), 119.9 (2 C, CH Fmoc), 125.2 (2 C, CH Fmoc), 127.0 (2 C, CH Fmoc), 127.7 (2 C, CH Fmoc), 141.3 (2 C, C_q Fmoc), 143.8 (C_q Fmoc), 143.9 (C_q Fmoc), 156.1 (C=O Fmoc), 170.0 (C=O), 170.3 (C=O); FAB⁺ MS (NBA) 533 (M + H⁺), 571 (M + K⁺). Anal. Calcd for C₃₀H₃₆N₄O₅·0.2CH₂Cl₂: C, 66.00; H, 6.68; N, 10.19; O, 14.55. Found: C, 65.81; H, 6.82; N, 10.10; O, 14.42.

Amide **5** (181 mg, 0.340 mmol) in 5 mL of dry CH₂Cl₂ was converted to the free carboxylic acid by adding 3 mL of TFA to the ice-cooled solution and subsequent stirring at room temperature for 3 h. Rotary evaporation of the mixture and coevaporation with toluene and acetonitrile gave Fmoc-DBO (160 mg, 98%) as a colorless solid, which was used directly for peptide synthesis: ¹H NMR (CDCl₃, 500 MHz) δ 1.07–1.19 (2 H, m, CH₂), 1.26–1.39 (2 H, m, CH₂), 1.50–1.57 (2 H, m, CH₂), 1.61–1.68 (2 H, m, CH₂), 2.81 (1 H, dd, *J* = 15.6, 8.1 Hz, β-CH₂ Asp), 3.03 (1 H, dd, *J* = 15.6, 2.7 Hz, β-CH₂ Asp), 3.74–3.88 (2 H, m, CH₂N), 4.20 (1 H, t, *J* = 7.2 Hz, CH Fmoc), 4.30–4.40 (2 H, m, CH₂ Fmoc), 4.52–4.57 (1 H, m, α-CH Asp), 5.20 (1 H, br s, CH), 6.23 (1 H, br d, *J* = 4.7 Hz, urethane NH), 7.30 (2 H, t, *J* = 7.5 Hz, CH Fmoc), 7.39 (2 H, t, *J* = 7.5 Hz, CH Fmoc), 7.44 (1 H, br t, *J* = 11 Hz, NH), 7.56–7.60 (2 H, m, CH Fmoc), 7.75 (2 H, d, *J* = 7.5 Hz, CH Fmoc); ¹³C NMR (CDCl₃, 126 MHz) δ 21.7 (2 C, CH₂), 24.2 (CH₂), 24.3 (CH₂), 37.8 (CH₂ Asp), 45.7 (CH₂N), 47.0 (CH

Fmoc), 50.6 (CH Asp), 62.2 (CH), 67.2 (C_q), 67.3 (CH₂ Fmoc), 120.0 (2 C, CH Fmoc), 125.2 (2 C, CH Fmoc), 127.1 (2 C, CH Fmoc), 127.7 (2 C, CH Fmoc), 141.3 (2 C, C_q Fmoc), 143.8 (2 C, C_q Fmoc), 156.0 (C=O Fmoc), 172.1 (C=O), 172.6 (COOH); FAB⁺ MS (NBA) 477 (M + H⁺); 515 (M + K⁺). HR-MS: calcd 477.2137 (M + H⁺); found (+ESI-TOF) 477.2120.

Peptide Synthesis. Polypeptides were made by Affina Immuntechnik GmbH (Berlin, Germany). The raw polypeptide was precipitated in diethyl ether and purified by semipreparative HPLC (LC-8A, Shimadzu) on an RP-18 column at 40 °C (VYDAC No. 218TP101522, 10 μL). Flow rates of 0.7 (250 × 4.5 column) or 8 mL min⁻¹ (250 × 22 column) with water containing 0.1% trifluoroacetic or phosphoric acid as eluent were adjusted to which a gradient of up to 50% acetonitrile containing 0.1% trifluoroacetic or phosphoric acid as coeluent was applied within 20 min. The retention times ranged between 10 and 22 min. The purity of the polypeptides was >95% as determined by MALDI-MS and HPLC. UV spectrophotometry confirmed also the presence of the characteristic chromophores (DBO, Trp). The extinction coefficients were the same, within error, as those reported for Trp (~5500 M⁻¹ cm⁻¹)¹⁹ and DBO (50 M⁻¹ cm⁻¹),^{12,20} which provides another purity and sample identity criterion.

The DBO probe and the Fmoc-DBO amino acid are fully compatible with standard Fmoc solid-phase peptide synthesis. No complications were found in coupling, and there was no apparent degradation of DBO during cleavage with 95% trifluoroacetic acid and HPLC purification. No special scavengers²¹ or protecting groups are required for the DBO residue during synthesis and cleavage.

Fluorescence Spectroscopy. All measurements were performed in aerated D₂O at ambient temperature. Fluorescence lifetimes were measured on a laser flash photolysis (LFP) setup (LP900, Edinburgh Instruments, Edinburgh, Scotland) with 7-mJ, 355-nm pulses of 4-ns width from a Nd:YAG laser (Minilite II, Continuum, Santa Clara, CA), and with a time-correlated single-photon counting (SPC) fluorometer (FLS900, Edinburgh Instruments) using a 1.5-ns pulse-width H₂ flash lamp at 370 nm. The FLS900 instrument was also used for the steady-state fluorescence (SSF) spectra (λ_{exc} = 365 nm). Fluorescence was detected at 430 nm on both time-resolved setups. The resulting data were analyzed with the Edinburgh software of the LP900 and FLS900 setup by means of monoexponential or biexponential decay functions and a reconvolution function for the excitation light pulse. Intermolecular quenching experiments were performed with 10 μM solutions of DBO and varying quencher concentrations up to 50% quenching effect or up to the solubility limit of the quencher (4–5 data points). Typical concentrations of polypeptides were 10 μM for LFP and 100 μM for SPC experiments. The polypeptides were measured over a concentration range of 1 μM–1 mM by LFP and 10 μM–1 mM by SPC. The fluorescence lifetimes remained constant within error within this concentration range. In the case of SSF measurements, a linear increase of the intensity with concentration (200 μM–1 mM, 5 data points) was found.

Results

Quenching by Amino Acids and Denaturing Agents. The photophysical methodology outlined in Scheme 1 required the selection of a quencher for the excited DBO with an efficient, preferably diffusion-controlled, quenching rate constant. It was appealing to select a natural amino acid as an intrinsic quencher.¹⁰ For this purpose, the quenching rate constants of the parent DBO by the 20 natural amino acids were measured in D₂O, H₂O, and pH 7.0 phosphate buffer. Table 1 reports the data for six amino acids that gave rise to significant quenching

(19) Luisi, P. L.; Rizzo, V.; Lorenzi, G. P.; Straub, B.; Suter, U.; Guarnaccia, R. *Biopolymers* **1975**, *14*, 2347–2362.

(20) Nau, W. M. *EPA Newsl.* **2000**, *70*, 6–29.

(21) Guy, C. A.; Fields, G. B. *Methods Enzymol.* **1997**, *289*, 67–83.

Table 1. Fluorescence Quenching Rate Constants for Natural Amino Acids

amino acid	$k_q/(10^9 \text{ M}^{-1} \text{ s}^{-1})^{a,b}$
tryptophan (Trp)	20
cysteine (Cys)	5.1 [1.5] ^b
methionine (Met)	4.5
tyrosine (Tyr)	3.6 [1.6] ^b
phenylalanine (Phe)	0.08
histidine (His)	0.06

^a Quenching rate constant measured for the parent DBO in D₂O; error in data is 5%. For the remaining 14 naturally occurring amino acids, k_q is less than $1 \times 10^6 \text{ M}^{-1} \text{ s}^{-1}$. ^b Deuterium isotope effects, i.e., $k_q(\text{H}_2\text{O})/k_q(\text{D}_2\text{O})$, are given in brackets for cases where significant effects were observed.

effects. The remaining 14 amino acids quenched at insignificant rates below $1 \times 10^6 \text{ M}^{-1} \text{ s}^{-1}$. The backbone of model polypeptides should be composed of such “inert” amino acids to avoid competitive intramolecular quenching in the actual kinetic measurements of peptide dynamics. The quenching experiments yielded identical results, within error, in buffered (pH 7.0) and unbuffered H₂O, except for quenching by histidine ($\text{p}K_a \sim 6-7$),²² for which the rate increased to $0.76 \times 10^8 \text{ M}^{-1} \text{ s}^{-1}$ in buffer. This indicates that the unprotonated imidazole group is a stronger quencher. Significant solvent isotope effects were observed for Tyr and Cys.

The fluorescence lifetimes of DBO in polypeptides consisting of the above-mentioned “inert” amino acids, i.e., without intramolecular quenchers, were measured for two representative sequences, Gln-Ile-Phe-Val-Lys-DBO-NH₂ and Thr-Leu-Thr-Gly-Lys-DBO-NH₂. The experimental lifetimes in aerated D₂O (510 and 490 ns) were the same, within error, as that of the parent chromophore (505 ns), which confirms the absence of intramolecular quenching by these amino acids in polypeptides.

Only for the four amino acids Trp, Cys, Tyr, and Met did the quenching approach the diffusion-controlled limit with values above $3 \times 10^8 \text{ M}^{-1} \text{ s}^{-1}$. Among these strongest quenchers, Trp and Tyr appear preferable for the design of intramolecular quenching experiments since the two sulfur-containing amino acids Cys and Met have a well-known lability during synthesis and photolysis. Presently, Trp was selected as the most efficient quencher.

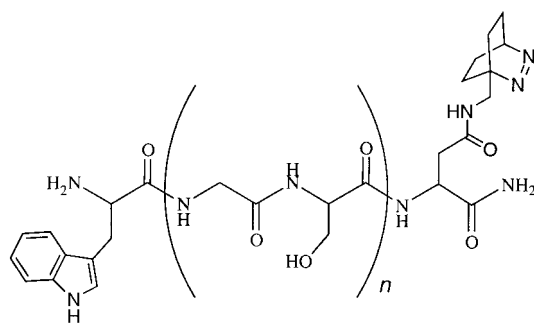
Fluorescence quenching by the denaturing agents urea and guanidinium chloride was found to be insignificant (<10%) up to 5.5 M concentration, with apparent quenching rate constants below $3 \times 10^4 \text{ M}^{-1} \text{ s}^{-1}$. This finding and the fact that the fluorescence lifetime of DBO is insensitive to pH between 2 and 12 should allow for a broad range of experimental conditions for studying peptide dynamics, albeit these have not been exploited in the present study.

Quenching Mechanism. Based on detailed investigations of the fluorescence quenching of the parent fluorophore,^{16,20,23-28}

two viable quenching mechanisms need to be taken into account: hydrogen abstraction^{16,24,25} and exciplex-induced quenching.²⁶⁻²⁸ Both mechanisms require a close probe/quencher contact. The deuterium isotope effect for Tyr and Cys (Table 1) provides evidence that a hydrogen atom abstraction (from the phenolic O–H or the S–H group) is indeed involved, which has in fact been previously observed in the quenching of DBO by the phenol group in α -tocopherol.¹¹ For cysteine, hydrogen abstraction is further supported by the quenching rate constants of methionine (Table 1) and cystine, i.e., the S–S oxidized cysteine dimer ($2 \times 10^8 \text{ M}^{-1} \text{ s}^{-1}$, in D₂O, this work). Although they are both better electron donors than cysteine, they are somewhat less efficient quenchers since they lack the reactive S–H bond.

For tryptophan, no deuterium isotope effect is observed. Moreover, we have evidence from quenching of DBO by dihydroxyindoles²⁹ that hydrogen abstraction from the labile N–H indole bond is inefficient. Hence, the quenching of DBO by Trp is likely to occur through an exciplex intermediate with close contact.²⁶⁻²⁸ This is corroborated by the observation that 1-methyl-Trp, which lacks the N–H bond, is quenched at a very similar rate ($1.6 \times 10^9 \text{ M}^{-1} \text{ s}^{-1}$, in D₂O, this work) as Trp itself ($2.0 \times 10^9 \text{ M}^{-1} \text{ s}^{-1}$). Since exciplexes of n,π^* -excited states, including ketones and azoalkanes, are nonemissive,^{26,30} only indirect evidence for their involvement has been obtained. For the interaction of n,π^* -excited states (which includes DBO) with aromatic donors, the structure of the exciplexes is presumed to involve a singly occupied lone pair orbital of the excited state to face the aromatic π system.³⁰ For amines as electron donors, exciplex formation with DBO is a diffusion-controlled reaction and radiationless deactivation of the exciplex is triggered by a close-lying conical intersection.²⁸ We presume a similar quenching mechanism for singlet-excited DBO by Trp.

Trp-(Gly-Ser)_n-DBO-NH₂ Polypeptides. To establish the overall suitability of the fluorescence-based method for measuring contact formation in biopolymers, we have performed an exploratory study on the length dependence of the intramolecular quenching rate constants between DBO and Trp in structureless peptides. Aerated D₂O was selected for the polypeptide studies, which presents a good tradeoff between the requirement of a long fluorescence lifetime (cf. Introduction), convenient measurement under air, and direct comparison with D₂O NMR data, which are employed in other cases to test for structural effects.



The sequences were chosen to be the (Gly-Ser)_n pairs introduced by Bieri et al., which are supposed to be “structure-

- (22) Abeles, R. H.; Frey, P. A.; Jencks, W. P. *Biochemistry*; Jones and Bartlett Publishers: Boston, 1992.
- (23) Nau, W. M.; Pischel, U. *Angew. Chem., Int. Ed. Engl.* **1999**, *38*, 2885–2888.
- (24) Nau, W. M.; Greiner, G.; Wall, J.; Rau, H.; Olivucci, M.; Robb, M. A. *Angew. Chem., Int. Ed. Engl.* **1998**, *37*, 98–101.
- (25) Nau, W. M.; Greiner, G.; Rau, H.; Olivucci, M.; Robb, M. A. *Ber. Bunsen-Ges. Phys. Chem.* **1998**, *102*, 486–492.
- (26) Pischel, U.; Zhang, X.; Hellrung, B.; Haselbach, E.; Muller, P.-A.; Nau, W. M. *J. Am. Chem. Soc.* **2000**, *122*, 2027–2034.
- (27) Pischel, U.; Allonas, X.; Nau, W. M. *J. Inf. Recording* **2000**, *25*, 311–321.
- (28) Sinicropi, A.; Pischel, U.; Basosi, R.; Nau, W. M.; Olivucci, M. *Angew. Chem., Int. Ed.* **2000**, *39*, 4582–4586.

- (29) Zhang, X.; Erb, C.; Flammer, J.; Nau, W. M. *Photochem. Photobiol.* **2000**, *71*, 524–533.
- (30) Wagner, P. J.; Truman, R. J.; Puchalski, A. E.; Wake, R. *J. Am. Chem. Soc.* **1986**, *108*, 7727–7738.

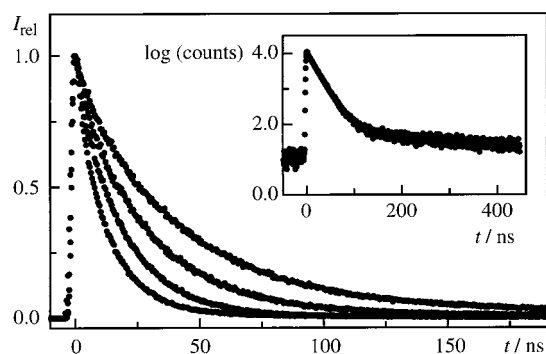


Figure 1. Fluorescence decays (SPC, normalized intensity) of 50 μM aerated D_2O solutions of $\text{Trp}-(\text{Gly-Ser})_n\text{-DBO-NH}_2$ polypeptides ($n = 1, 2, 4, 6$), linear scale. The lowest trace corresponds to $n = 1$, the uppermost one to $n = 6$. Shown in the inset is the decay for $n = 1$ on a semilogarithmic scale; note the long-lived component (1% preexponential factor contribution), which is assigned to a trace impurity.

less⁹. Shown in Figure 1 are the SPC results for the $\text{Trp}-(\text{Gly-Ser})_n\text{-DBO-NH}_2$ polypeptides with $n = 1, 2, 4$, and 6 (structure above). The shortest homologue of the series with $n = 0$, i.e., Trp-DBO-NH_2 , and a longer one with $n = 10$ were also measured. The Poissonian noise statistics of the digital SPC method allows an unsurpassed detection accuracy of minute deviations from monoexponential decay kinetics. As an example, the decay trace for $n = 1$ is shown on a semilogarithmic scale in the inset of Figure 1, which is the preferred SPC data representation mode. Clearly, a second longer lived exponential component is detected, which, however, contributes merely 1% to the total signal intensity (ratio of preexponential factors). This feature may well be due to an impurity. Within the purity specifications of the polypeptides (>95%), the SPC data (and also the LFP data) allow an assignment of monoexponential decay behavior (χ^2 values <1.1). This supports the findings by Bieri et al.⁹ and Lapidus et al.¹⁰ Multiexponential decays have been observed, for example, for fast electron transfer in polypeptides in the picosecond time regime.³¹ As suggested previously,⁹ end-to-end contact formation, which occurs in the nanosecond range, may be sufficiently slow to allow rapid interconversion between the various conformers and, thus, account for the observed monoexponential decay kinetics. A control experiment for a polypeptide with a more rigid, extended polyproline backbone, i.e., $\text{Trp}-(\text{Pro})_4\text{-DBO-NH}_2$, yielded a very long fluorescence lifetime of 460 ns. Monoexponential decay behavior was also observed in this case.

Note that the fluorescence lifetimes of the $\text{Trp}-(\text{Gly-Ser})_n\text{-DBO-NH}_2$ polypeptides range from 10 to 75 ns (Table 2). Fluorescence lifetimes in this region are readily and very accurately measurable by SPC or phase-modulation techniques.¹³ To extract intramolecular quenching rate constants (k_q , Table 2), a correction of the observed lifetimes (τ) for the inherent decay of the excited state (τ_0) according to eq 1 is recommended. The error introduced in k_q by a direct conversion ($k_q \sim 1/\tau$) is small for the present data set (<10%) due to the efficient quenching ($\tau \ll \tau_0$) but cannot generally be neglected. The inherent fluorescence lifetime of the DBO residue in aerated D_2O was taken as 500 ns, which is the average lifetime measured for peptide sequences lacking intramolecular quenchers and for

Table 2. Fluorescence Lifetimes and Intramolecular Quenching Rate Constants for DBO/Trp-Containing Polypeptides^a Obtained from Different Techniques

polypeptide	N^b	τ/ns^c			k_q^d (10^7 s^{-1}) SPC ^g
		SPC ^d	LFP ^e	SSF ^f	
$\text{Trp}-(\text{Gly-Ser})_n\text{-DBO-NH}_2$					
$n = 0$	2	23.3	24.5	20	4.1
$n = 1$	4	14.3	13.5	13	6.8
$n = 2$	6	19.5	18.5	18	4.9
$n = 4$	10	30.5	30	29	3.1
$n = 6$	14	45.6	45	[$\equiv 45.6$] ^h	2.0
$n = 10$	22	74.4	76	69	1.1
$\text{Trp-Pro}_4\text{-DBO-NH}_2$	6	460	460	470	<0.02

^a Lifetime of polypeptides not containing Trp or other amino acid quenchers is ~ 500 ns in aerated D_2O , e.g., 510 ns for $\text{Gln-Ile-Phe-Val-Lys-DBO-NH}_2$ and 490 ns for $\text{Thr-Leu-Thr-Gly-Lys-DBO-NH}_2$. ^b Number of peptide units between probe (DBO) and quencher (Trp). ^c Fluorescence lifetime in aerated D_2O at 23 $^\circ\text{C}$. ^d Measured by time-correlated single-photon counting; error in data is 0.3 ns except for $n = 10$ (1.0 ns). ^e Measured by laser flash photolysis; error in data is 5%. ^f Measured by steady-state fluorescence; the slope of the plot of the signal intensity vs the concentration was assumed to be proportional to the lifetime, using the SPC lifetime for $n = 6$ as reference; error in data is 5%. ^g Obtained from eq 1 by using the SPC lifetimes and $\tau_0 = 500$ ns. ^h Reference value.

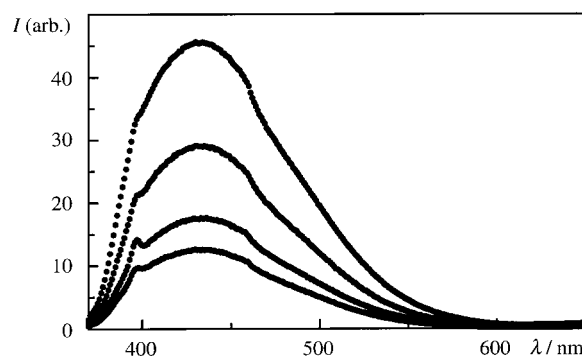


Figure 2. Steady-state fluorescence spectra of 500 μM $\text{Trp}-(\text{Gly-Ser})_n\text{-DBO-NH}_2$ polypeptides ($n = 1, 2, 4, 6$, from bottom to top spectrum) in aerated D_2O . The original intensity (in counts) of each spectrum was divided by the counts in the maximum (430 nm) and multiplied by 45.6, the reference lifetime (in ns) for the $n = 6$ polypeptide (Table 2).

the parent fluorophore. The experimental k_q values are taken as a direct measure of the rate constants for contact formation (k_+); cf. Introduction.

$$k_q = 1/\tau - 1/\tau_0 \approx k_+ \quad (1)$$

The availability of different experimental techniques is a unique advantage of fluorescence measurements^{13,14} and allows for a broad use of fluorescence-based methods in general. Three techniques for measuring fluorescence have been explored: SPC (Figure 1), LFP, and SSF (Figure 2). The mutual agreement that has been obtained by these three methods is excellent (Table 2). While SPC is preferred for high-accuracy results, SSF measurements are more commonly accessible and are well suited for relative lifetime measurements. Note that a reference with a known lifetime is required for the determination of absolute lifetimes by SSF.

Discussion

The purpose of this work is to establish a novel fluorescence-based method for measuring the kinetics of intramolecular contact formation in biopolymers. This requires beforehand a discussion of the advantageous properties of the new fluorophore

(31) G. Jones, I.; Lu, L. N.; Fu, H.; Farahat, C. W.; Oh, C.; Greenfield, S. R.; Gosztola, D. J.; Wasielewski, M. R. *J. Phys. Chem. B* **1999**, *103*, 572–581.

and a comparison with the previously employed techniques, followed by some principal suitability considerations, and, finally, an experimental test with polypeptides of different chain lengths.

Chromophore Characteristics. The distinct photophysical and chemical properties of the parent 2,3-diazabicyclo[2.2.2]-oct-2-ene fluorophore have been discussed previously.^{11,12} For use as a fluorescent label for biomolecules, in particular peptides, certain aspects are particularly noteworthy. First, DBO is small ($\sim 5\text{-\AA}$ diameter) and nearly spherical, which contrasts the established polyaromatic chromophores and luminescent transition metal complexes. Equally important is the high solubility of the neutral parent fluorophore in water, which is related to its high inherent dipole moment of 3.5 D.³² This minimizes the tendency for hydrophobic association^{33,34} and renders the possibility unlikely that the experiment reports on the rate of hydrophobe association³⁵ rather than on the pertinent biopolymer chain mobility.¹⁵ Also, the hydrophilic fluorophore promotes water solubility of the short polypeptides into the millimolar range. This allows standard measurements in water, and a direct comparison with NMR experiments, which are often performed in the same concentration range. The fluorophore has also a high chemical and photochemical stability with decomposition quantum yields of about 0.1% in H₂O³⁶ and 0.3% in D₂O.¹² No change in the fluorescence lifetime was observed even after extended measurements (> 1000 laser pulses) and several days storage in solution.

With respect to the photophysical behavior, the absorption maximum in the near-UV (364 nm)¹¹ and the high fluorescence quantum yield ($\sim 20\%$ in aerated water in the absence of quenchers) are appealing for various instrumental reasons. Common Nd:YAG, XeF excimer and N₂ near-UV laser excitation at 355, 351, and 337 nm can be selected, which by-passes Tyr and Trp excitation and complications due to peptide autofluorescence.¹⁴ The unique property of the parent chromophore, however, is its exceptionally long fluorescence lifetime ($\sim 1\ \mu\text{s}$ in gas phase, 505 ns in aerated D₂O),¹¹ which is the longest among organic chromophores in solution. It is this long fluorescence lifetime that allows the presently described novel kinetic applications and that differentiates this fluorescence-based method from others. It is important to note that the fluorescence of DBO can be monitored under air. This is possible due to the very slow oxygen quenching of DBO in water ($2.1 \times 10^9\ \text{M}^{-1}\ \text{s}^{-1}$) compared to other singlet-excited states.¹²

Techniques for Measuring Submicrosecond Biopolymer Kinetics. Many experiments using chromophore–quencher pairs to measure intramolecular kinetics in *polymers* have been discussed in the literature, including fluorescence quenching and triplet absorption experiments.^{37,38} Related photophysical approaches involve intramolecular excimer formation of pyrene,³³ phosphorescence decay from benzophenone,³⁹ and delayed

fluorescence from triplet–triplet annihilation between anthracene pairs.³⁸ However, few intramolecular quenching experiments have been applied to biomolecules such as peptides.⁷

In the present work, we have employed DBO as a fluorescent probe and Trp as a quencher to measure the rates of intramolecular contact formation in polypeptides. Previous studies on these rates have made use of similar photophysical methodologies but with a different technique (transient triplet absorption) and with different probe/quencher systems,^{8–10} which cannot exploit the advantages of fluorescence as a detection technique.^{13,14} McGimpsey et al. examined two systems with benzophenone as a probe and naphthalene as quencher (Bzp/Nap).⁸ Triplet benzophenone was obtained by a 355-nm laser flash (5-ns pulse width) in deaerated acetonitrile, but intramolecular energy transfer to naphthalene was too fast to allow measurement (< 10 ns). This Bzp/Nap system also offered the possibility of examining by 308-nm photolysis the (backward) Förster resonance energy transfer (FRET) from the singlet-excited Nap to Bzp. Bieri et al. used thioxanthone as probe and naphthalene as quencher (Thx/Nap).⁹ The fast kinetics of contact formation in short polypeptides was quantified for the first time in this study. The Thx triplet was produced by 351-nm laser excitation (20-ns pulse width) in degassed ethanol and in mixtures with water and glycerol. The triplet energy transfer, which in this case was rigorously established through the time-resolved rise of the Nap triplet, occurred near the diffusion-controlled limit, but was reversible and inefficient under some conditions, which precluded studies in water. Lapidus et al. used two natural amino acids, namely, tryptophan as probe and cysteine (and lipoate) as quencher (Trp/Cys).¹⁰ The Trp triplet was populated with 290-nm dye laser pulses (8 ns) in N₂O-saturated water. The quenching rate constant for Cys fell below the diffusion limit, and a correction was introduced by comparison with the more efficient intramolecular quenching by lipoate. It should be mentioned that the chemical and photochemical stability of the triplet probes Thx⁹ and Trp^{10,40} required attention during peptide synthesis and LFP experiments, respectively.

Each of the above-mentioned methods has its strengths and may be preferable to study a specific aspect of biopolymer kinetics. The advantages of the presently introduced fluorescence-based method (DBO/Trp) comprise, most importantly, the ease of experimental monitoring by fluorescence in water under air with high sensitivity and precision.⁴¹

The DBO-based fluorescence technique is particularly well suited to perform measurements in the fast time range (< 500 ns) and to analyze nonexponential decay behavior. Since recent experiments have demonstrated that the contact formation kinetics of the shortest polypeptides are significantly faster (< 10 and 20 ns, respectively)^{8,9} than previously presumed,⁴² and in fact fall into a critical time range,⁴³ it appears essential to have available techniques that allow accurate measurements of these

(32) Harmony, M. D.; Talkington, T. L.; Nandi, R. N. *J. Mol. Struct.* **1984**, *125*, 125–130.

(33) Lee, S.; Winnik, M. A. *Macromolecules* **1997**, *30*, 2633–2641.

(34) Daugherty, D. L.; Gellman, S. H. *J. Am. Chem. Soc.* **1999**, *121*, 4325–4333.

(35) Johnson, G. E. *J. Chem. Phys.* **1975**, *63*, 4047–4053.

(36) Pischel, U.; Nau, W. M. *J. Phys. Org. Chem.* **2000**, *13*, 640–647.

(37) Winnik, M. A. *Chem. Rev.* **1981**, *81*, 491–524.

(38) Horie, K.; Schnabel, W.; Mita, I.; Ushiki, H. *Macromolecules* **1981**, *14*, 1422–1428.

(39) Winnik, M. A. *Acc. Chem. Res.* **1977**, *10*, 173–179.

(40) Mialocq, J. C.; Amouyal, E.; Bernas, A.; Grand, D. *J. Phys. Chem.* **1982**, *86*, 3173–3177.

(41) Unfortunately, the absorbance of DBO is too low to reach the optimum sensitivity of fluorescence measurements (nM range). Nevertheless, the sensitivity of the DBO measurements compares favorably with that employed in the previous triplet transient absorption experiments with strong absorbers; cf. refs 9 and 10. The SPC detection limit could be significantly lowered by replacement of the hydrogen flash lamp by laser excitation.

(42) Hagen, S. J.; Hofrichter, J.; Szabo, A.; Eaton, W. A. *Proc. Natl. Acad. Sci. U.S.A.* **1996**, *93*, 11615–11617.

(43) Callender, R. H.; Dyer, R. B.; Gilmanshin, R.; Woodruff, W. H. *Annu. Rev. Phys. Chem.* **1998**, *49*, 173–202.

fast kinetic processes. Fluorescence detection opens a unique opportunity along this line since it allows measurement down to the picosecond range.¹³ Measurements with triplet probes are subject to instrumental limitations (typical laser pulse widths around 10 ns)^{8,9} and may also be limited by inefficient ($\sim 13\%$ for Trp)⁴⁴ and slow (~ 2.5 ns for both Trp and Thx)^{45,46} intersystem crossing from the initial singlet-excited state to the triplet, as well as concomitant fluorescence (about 10 and 7% for Trp and Thx, respectively),^{45,47} all of which limit the accessible time scale. Conversely, the triplet probes have lifetimes in the microsecond range due to their spin-forbidden decay ($\sim 30\text{--}40$ μs)^{9,10} and should also be applicable to slower kinetic processes. In contrast, the DBO method is restricted to the submicrosecond range as a consequence of the inherent fluorescence decay lifetime (< 1 μs).^{12,16} The different techniques are thus complementary and cover a large dynamic range.

Distance Dependence of Quenching. The methodology in Scheme 1 requires the quenching of the probe to occur (1) rapidly and (2) upon intimate contact with the quencher, resulting in a diffusion-controlled, contact-induced quenching process. With respect to the requirement of molecular contact, the fluorescence quenching of DBO is unique since its fluorescence quenching requires a close, structurally well-defined molecular approach within van der Waals contact ($2\text{--}3$ Å distance) with an efficient hydrogen^{16,24,25} or electron donor.^{26–28} The related quenching mechanisms, hydrogen abstraction and exciplex-induced quenching, are chemically inefficient and have been studied in experimental and theoretical detail.^{16,20,23–28} For comparison, it should be noted that the triplet–triplet energy transfer in the Thx/Nap probe/quencher pair proceeds supposedly through a Dexter mechanism.⁹ Dexter-type energy transfer does not strictly occur upon van der Waals radius contact but decreases exponentially with distance and orbital overlap, such that quenching events may occur within several nanoseconds at separations of $5\text{--}6$ Å.^{48–50} McGimpsey et al. further suggested for their Bzp/Nap polypeptides that superexchange (through-bond) triplet energy transfer may contribute as well.⁸ The quenching mechanism in the Trp/Cys probe/quencher pair has not been discussed in detail.¹⁰

Intramolecular quenching experiments based on FRET or electron transfer (ET) as the quenching mechanism may provide invaluable information on biomolecular structure and dynamics.^{4–6,31,51–53} However, FRET and ET do not require intimate molecular contact and may well occur over larger distances, e.g., through bond by a superexchange mechanism.⁵¹ Hence, the quenching rates may not directly reflect the rates of intrachain contact formation.^{9,54} For example, in the seminal

FRET work by Haas et al. with polypeptides⁵⁵ containing naphthalene as a probe ($\tau_0 \sim 60$ ns) and dansyl as quencher, energy transfer was found to occur over distances of $22\text{--}35$ Å and there is also substantial evidence for long-range electron transfer in polypeptides.^{31,51,56–58} For the DBO/Trp system, FRET is not possible since the singlet excitation energy of Trp ($E^* = 399$ kJ mol⁻¹)⁴⁵ is much higher than that of DBO ($E^* = 328$ kJ mol⁻¹ in water, calculated from $\lambda_{\text{max}} = 364$ nm).^{23,59}

ET as the fluorescence quenching mechanism of DBO by Trp requires more detailed attention, especially since Trp is known as a strong intrinsic electron donor in peptides with an oxidation potential of $\sim 0.80\text{--}0.85$ V vs SCE at neutral pH.^{53,60} However, the very low reduction potential of DBO ($E_{\text{p,red}} = -2.8$ V vs SCE)²³ results in an endergonic energetics for electron transfer ($\Delta G_{\text{ET}} > 20$ kJ mol⁻¹)⁶¹ which cannot account for the observed quenching rate constants in these polypeptides.⁵⁶ It has been proposed that electron-transfer-induced fluorescence quenching of end-labeled probes by a terminal Trp in polypeptides becomes important when the excited-state reduction potential ($E_{\text{red}} + E^*$) exceeds a value of 1.5 V.⁵³ This is by far not fulfilled for the fluorescent probe DBO, since $E_{\text{red}} + E^* \approx 0.6$ V, which points to another quenching mechanism. Moreover, we have recently ruled out ET for several tertiary amines as quenchers although they have even lower oxidation potentials than Trp.²⁶ The combined results are in line with exciplex-induced quenching but speak against ET. This is important for the interpretations since only the former mechanism requires contact between the probe and the quencher and can therefore be directly related to end-to-end intrachain contact formation.

Quenching Rate Constants. The intermolecular quenching rate constants for the probe/quencher pairs should ideally reflect the values that are commonly accepted for diffusion-controlled reactions of small solutes in a particular solvent.⁶² However, quenching rate constants that fall somewhat below the diffusion-controlled limit may well be acceptable, because the dissociation of an *intramolecular* probe/quencher encounter pair (k_- in Scheme 1) has been suggested¹⁰ to be slower than in the case of an *intermolecular* encounter, presumably due to the rigidity of the polypeptide backbone. This may allow a slower-than-diffusion-controlled quenching process to compete more favorably. This circumstance suggests that probe/quencher pairs whose quenching rate constants fall somewhat below the ideal value may still reliably reflect the rate constants for contact formation in a polypeptide. Even in cases where the quenching rate constants fall significantly below the desired limit, e.g.,

- (44) Chen, Y.; Liu, B.; Yu, H.-T.; Barkley, M. D. *J. Am. Chem. Soc.* **1996**, *118*, 9271–9278.
 (45) Murov, S. L.; Carmichael, I.; Hug, G. L. *Handbook of Photochemistry*; Marcel Dekker: New York, 1993.
 (46) Ley, C.; Morlet-Savary, F.; Jacques, P.; Fouassier, J. P. *Chem. Phys.* **2000**, *255*, 335–346.
 (47) Dalton, J. C.; Montgomery, F. C. *J. Am. Chem. Soc.* **1974**, *96*, 6230–6232.
 (48) Klán, P.; Wagner, P. J. *J. Am. Chem. Soc.* **1998**, *120*, 2198–2199.
 (49) Wagner, P. J.; Klán, P. *J. Am. Chem. Soc.* **1998**, *121*, 9626–9635.
 (50) Paddon-Row, M. N. In *Stimulating Concepts in Chemistry*; Vögtle, F.; Stoddart, J. F.; Shibasaki, M., Eds.; Wiley-VCH: Weinheim, 2000; pp 267–291.
 (51) Mishra, A. K.; Chandrasekar, R.; Faraggi, M.; Klapper, M. H. *J. Am. Chem. Soc.* **1994**, *116*, 1414–1422.
 (52) Williamson, D. A.; Bowler, B. E. *J. Am. Chem. Soc.* **1998**, *120*, 10902–10911.
 (53) G. Jones, I.; Lu, L. N.; Vullev, V.; Gosztola, D. J.; Greenfield, S. R.; Wasielewski, M. R. *Bioorg. Med. Chem. Lett.* **1995**, *5*, 2385–2390.

- (54) Thomas, D. D.; Carlsen, W. F.; Stryer, L. *Proc. Natl. Acad. Sci. U.S.A.* **1978**, *75*, 5746–5750.
 (55) Haas, E.; Katchalski-Katzir, E.; Steinberg, I. Z. *Biopolymers* **1978**, *17*, 11–31.
 (56) Faraggi, M.; DeFelippis, M. R.; Klapper, M. H. *J. Am. Chem. Soc.* **1989**, *111*, 5141–5145.
 (57) DeFelippis, M. R.; Faraggi, M.; Klapper, M. H. *J. Am. Chem. Soc.* **1991**, *112*, 5640–5642.
 (58) Lee, H.; Faraggi, M.; Klapper, M. H. *Biochim. Biophys. Acta* **1992**, *1159*, 286–294.
 (59) For DBO, FRET is generally unlikely due to the low oscillator strength ($f \approx 0.001$) of its lowest n, π^* transition.
 (60) DeFelippis, M. R.; Murthy, C. P.; Broitman, F.; Weinraub, D.; Faraggi, M.; Klapper, M. H. *J. Phys. Chem.* **1991**, *95*, 3416–3419.
 (61) According to Kikuchi, K.; Takahashi, Y.; Katagiri, T.; Niwa, T.; Hoshi, M.; Miyashi, T. *Chem. Phys. Lett.* **1991**, *180*, 403–408, exciplex formation dominates in this endergonic region over electron transfer, which is in line with our suggested quenching mechanism.
 (62) Becker, H. G. O.; Böttcher, H.; Dietz, F.; Rehorek, D.; Roewer, G.; Schiller, K.; Timpe, H.-J. *Einführung in die Photochemie*; Deutscher Verlag der Wissenschaften: Berlin, 1991.

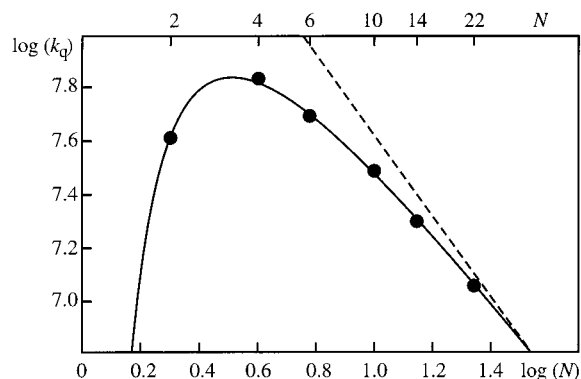


Figure 3. Double-logarithmic plot of the intramolecular quenching rate constant (k_q) of Trp-(Gly-Ser) $_n$ -DBO-NH $_2$ polypeptides vs the peptide length, taken as the number of intervening peptide units (N). The SPC values from Table 2 are used; the statistical errors obtained from this technique result in errors on the same order of magnitude as the size of the data points. A simple function of the type $y = a - 1.5x - b/x$ was fitted to the experimental data ($a = 9.37$ and $b = 0.392$) to reflect the theoretical slope of -1.5 at long chain lengths and the expected rapid falloff (b/x term) at short chain lengths; cf. ref 66. The dashed line has a slope of -1.5 and is shown to illustrate the deviation from the theoretical behavior.

$5.0 \times 10^8 \text{ M}^{-1} \text{ s}^{-1}$ for the Trp/Cys pair in water,^{63,64} the experimental rate data may serve to provide reliable *relative* kinetic data. The absolute rate constants for contact formation, as has been suggested, can be extrapolated.¹⁰

The quenching rate constant for the DBO/Trp pair ($2.0 \times 10^9 \text{ M}^{-1} \text{ s}^{-1}$), like that for the Trp/lipoate pair ($\sim 3 \times 10^9 \text{ M}^{-1} \text{ s}^{-1}$),^{10,63} is close to the diffusion-controlled limit in water ($6.5 \times 10^9 \text{ M}^{-1} \text{ s}^{-1}$),⁶² and the quenching rate of the Thx/Nap pair in ethanol ($4 \times 10^9 \text{ M}^{-1} \text{ s}^{-1}$)⁹ lies close to the diffusion rate constant in ethanol ($5.4 \times 10^9 \text{ M}^{-1} \text{ s}^{-1}$).⁶² These probe/quencher pairs should thus directly report on the rate of intramolecular end-to-end contact formation (k_+ in Scheme 1).

Length Dependence of Polypeptide Contact Formation Rates. To study the length dependence of polypeptide contact formation rates by the intramolecular quenching methodology (Scheme 1), the quencher is generally separated from the probe by a varying number of unreactive amino acids, and it is assumed that the experimental intramolecular quenching rate constants (k_q) are a direct measure of the rate for contact formation (k_+). Previous studies employed transient triplet absorption to study polypeptides with the structures Thx-(Gly-Ser) $_n$ -Nap-Ser-Gly ($n = 1-4$)⁹ and Cys-(Gln-Gly-Ala) $_n$ -Trp ($n = 1-6$).¹⁰ We have now examined the length dependence for Trp-(Gly-Ser) $_n$ -DBO-NH $_2$ polypeptides with $n = 0, 1, 2, 4, 6,$ and 10 . The DBO residue was attached at the C terminus and Trp was attached as a quencher to the N terminus. Tyrosine or artificial amino acids could be employed instead of tryptophan, but the latter was preferred in view of the fast quenching rate (Table 1) and natural relevance. The fluorescence lifetimes of the polypeptides are entered in Table 2.

The present data are entered in a $\log(k_q)$ - $\log(N)$ plot in Figure 3, where N denotes the number of -CO-NH- peptide units between probe and quencher, i.e., the peptide length.⁶⁵ According to the polymer theory by Flory, which treats the kinetics of

intrachain contact formation within a Gaussian chain approximation, such a plot should be linear with a slope of -1.50 at sufficiently long chain length.^{66,67} A comparison with the same plots provided in the previous studies^{9,10} reveals that the contact formation rates measured with the present fluorescence-based technique (taken as the intramolecular quenching rate constants in Table 2) are significantly and consistently faster at the same length than the previously measured values. The variance from the Thx/Nap data set appears to be quite constant around 40%, while that with the extrapolated Trp/Cys data ranges between 20 and 150%. For example, the rate constants for $N = 4$ and $N = 10$ in the DBO/Trp data set (6.8 and $2.0 \times 10^7 \text{ s}^{-1}$) exceed the results for $N = 3$ and 9 in the Thx/Nap series (5.0 and $1.4 \times 10^7 \text{ s}^{-1}$)⁹ as well as those extrapolated for $N = 4$ and $N = 10$ in the Trp/Cys study (2.7 and $1.7 \times 10^7 \text{ s}^{-1}$).¹⁰ Moreover, the rate constants for $N = 22$ in the DBO/Trp data set, which is the longest polypeptide among those yet studied, is significantly larger than that extrapolated for the shorter $N = 19$ peptide in the Trp/Cys study (11 vs $7.2 \times 10^6 \text{ s}^{-1}$).¹⁰ Whether these variances are due to the selection of different solvents and polypeptide sequences, assumptions related to diffusion-controlled quenching, or structural effects imposed by the probe/quencher pairs cannot be decided at present. However, with respect to the "speed limit"^{7,9,42} for intrachain contact formation in polypeptides, the present data suggest a value as short as 10 ns, which is similar to the upper limit (<10 ns) provided by McGimpsey et al.⁸

That the fluorescence quenching rate constants are indeed a measure of polypeptide chain contacts and not of differential rates of superexchange electron transfer (see above) is evident from the fluorescence lifetime of the shortest homologue of the series ($n = 0$), which is actually higher than those for the two next longer derivatives with $n = 1$ and 2 . In addition, the study of a derivative with a polyproline backbone, i.e., Trp-(Pro) $_4$ -DBO-NH $_2$, revealed a much longer fluorescence lifetimes of 460 ns in D $_2$ O, very close to that observed for polypeptides not containing Trp (500 ns). Polyprolines are presumed to have an extended, more rigid structure in solution,^{51,56} such that the longer fluorescence lifetimes can be interpreted in terms of a reduced flexibility of the polyproline backbone, which renders conformations with contact between the probe and the quencher less likely.⁶⁸

It is important to note that the $\log(k_q)$ - $\log(N)$ plot of our data (Figure 3) indicates a pronounced negative curvature with a sharp falloff near $N = 2$. In fact, this sharp falloff is theoretically expected at sufficiently short chain lengths due to the breakdown of the Gaussian chain approximation.⁶⁶ A first indication of a negative curvature for polypeptides was obtained from the Trp/Cys data set.¹⁰ Moreover, if a linear function is fitted through the data for the longer polypeptides with $n =$

(66) Suter, U. W.; Mutter, M.; Flory, P. J. *J. Am. Chem. Soc.* **1976**, *98*, 5740-5745.

(67) Mutter, M.; Suter, U. W.; Flory, P. J. *J. Am. Chem. Soc.* **1976**, *98*, 5745-5748.

(68) The control experiments with both polypeptides also provide additional evidence against superexchange electron transfer as the quenching mechanism (see above). The rate of the latter is expected to increase weakly, but exponentially with the number of peptide units.⁵⁶ If superexchange electron transfer were to play an important role, one would expect a similar quenching rate constant for the Pro and Gly-Ser peptides of the same length and one would expect the fastest rate constant for the shortest dipeptide ($n = 0$). Both are not observed experimentally. It should be noted that the kinetics of intramolecular chain diffusion has actually been an uncertainty in several studies of long-range electron transfer (e.g., refs 51 and 58). The present method should also be of interest in this context.

(63) Bent, D. V.; Hayon, E. *J. Am. Chem. Soc.* **1975**, *97*, 2612-2619.

(64) Gonnelli, M.; Strambini, G. B. *Biochemistry* **1995**, *34*, 13847-13857.

(65) The peptide unit in the asparagine chain (cf. structure) has been counted for the present polypeptides. If it is not counted ($N = 3, 5, 9, 13, 21$), the conclusions with respect to absolute rates, curvature, and slope (-0.91 ± 0.07) remain unchanged.

1–10 (Figure 3, $r^2 = 0.995$), the slope (-1.05 ± 0.06) falls below the theoretical value (-1.50) and the previously reported slope (-1.36 ± 0.26).⁹ While a smaller-than-theoretical slope can again be rationalized in terms of the pertinent approximations,⁶⁶ the contrast in slope between the two experimental studies is interesting in view of the identical polypeptide backbones.

Conclusions

The present fluorescence-based method for measuring sub-microsecond dynamics of polypeptide chain contact formation yields unsurpassed kinetic data with respect to accuracy, detection of nonexponentiality, and time range (100 ps–1 μ s). These features, along with the full compatibility with standard solid-phase peptide synthesis, the high photostability of the small, dipolar probe, and the use in aerated water, are advantageous for a wide range of biological applications. Attachment of the same fluorophore to other biological targets, including

other amino acids and nucleotides, should be viable, which renders the present fluorescence-based method an attractive alternative to assess the kinetics of intramolecular diffusion phenomena in polymers and biopolymers. In particular, this is pertinent for the understanding of protein folding and the domain motions in proteins.

Acknowledgment. R.R.H. thanks the National Science Foundation (U.S.A.) for an International Research Fellowship (grant INT-9901459). This work was generously supported through several grants of the Swiss National Science Foundation (MHV grant 2134-62567.00 for G.G., NF grant 620-58000.99 for W.M.N.). The study was performed within the Swiss National Research Program “Supramolecular Functional Materials” (grant 4047-057552 for W.M.N.). We acknowledge the help of C. Marquez with the Fmoc-DBO synthesis.

JA010493N

A Conformational Flexibility Scale for Amino Acids in Peptides**

Fang Huang and Werner M. Nau*

The molecular flexibility of proteins is a crucial factor in determining their biological activity,^[1] including binding affinity,^[2] antigenicity,^[3] and enzymatic activity.^[4] The identification of regions in proteins with the highest conformational flexibility and rigidity is essential for predicting the mechanism of protein folding,^[5,6] for understanding domain motions in proteins,^[1,7,8] and for predicting the rate of nonlocal interactions as well as intramolecular reactions, including electron and proton transfer^[9] and cyclizations.^[10] Consequently, there is considerable interest in predicting the flexibility or, conversely, the rigidity of peptides from their amino acid sequence.^[11–13] The prediction of peptide flexibility has additional implications for the de novo design of peptides^[14] and for the theoretical understanding of peptide dynamics.^[15]

We now report a novel scale for the flexibility of amino acids, which provides an absolute measure for the time scale of conformational changes in short structureless peptides as a function of the amino acid type. This experimental scale is derived from kinetic measurements of the collision frequency between the two ends of short random-coil polypeptides.

The present experiments provide the first application of our recently introduced fluorazophore method for measuring the kinetics of end-to-end collision in polypeptides.^[16,17] In essence, 2,3-diazabicyclo[2.2.2]oct-2-ene (DBO) is attached as a fluorescent probe at one end of the peptide and tryptophan is placed at the other end as an efficient quencher (Figure 1). The unique features of this probe/quencher pair are the exceedingly long fluorescence lifetime of the probe (several hundred nanoseconds) and the contact quenching

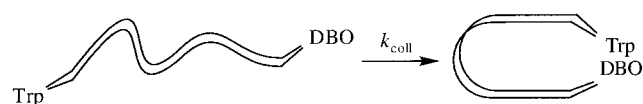


Figure 1. End-to-end collision in peptides labeled with DBO as a fluorescent probe at the C terminus and Trp as a fluorescence quencher at the N terminus.

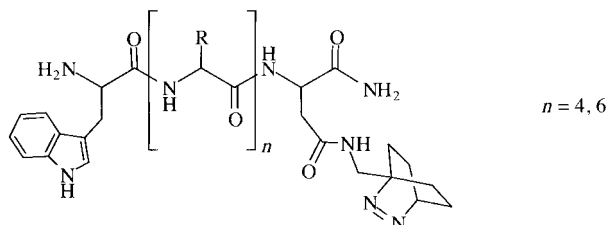
[*] Prof. Dr. W. M. Nau
 School of Engineering and Science
 International University Bremen
 Campus Ring 1, 28759 Bremen (Germany)
 Fax: (+49) 421-200-3229
 E-mail: w.nau@iu-bremen.de

Prof. Dr. W. M. Nau, Dipl.-Chem. F. Huang
 Departement Chemie
 Universität Basel
 Klingelbergstrasse 80, 4056 Basel (Switzerland)

[**] This work was supported by the Swiss National Science Foundation within the NFP 47 "Supramolecular Functional Materials".

mechanism, which differentiates it from conventional fluorescence resonance energy transfer (FRET) donor/acceptor pairs. The fluorescence lifetimes of DBO/Trp peptides provide the quenching rate constants (k_q), which measure the end-to-end collision frequency (k_{coll} in Figure 1).^[17] Such collisions occur on the ns– μ s time scale according to recent studies.^[17–20]

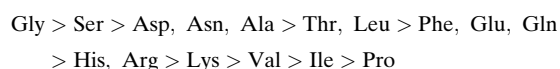
We reasoned that the collision frequency of peptides, in which Trp and DBO are separated by a sequence of identical amino acids (Scheme 1), should be an excellent measure of



Scheme 1. General structure of the peptides.

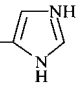
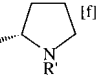
the conformational flexibility of the backbone.^[21] These peptides adopt random-coil conformations according to CD measurements.^[22] Since the conformational changes required for end-to-end contact derive from fast rotations about the N–C α and C α –C bonds,^[23] and since different α substituents are expected to hinder these bond rotations to a different degree, we expected different collision frequencies when the probe and the quencher are separated by different amino acids. This arrangement should allow us to correlate the collision frequency with the type of amino acid and thereby build up a flexibility scale (Table 1). It should be stated that this scale reflects the global or conformational flexibility of the amino acids in peptides. This scale is unrelated to previously introduced local or positional flexibility scales^[24] obtained from X-ray diffraction crystallographic data.^[11–13] The latter scales provide measures of the average displacements of atoms in amino acid residues from their equilibrium geometry, which are derived from vibrations on the femto-second time scale and reflect the shallowness of the potential centered around an energy minimum.

The quenching rate constants in Table 1, which were obtained from the fluorescence decays (Figure 2), show variations of 1–2 orders of magnitude for the various amino acids. Lower quenching rate constants correspond to lower end-to-end collision frequencies and indicate a lower flexibility (or higher rigidity). The following order of flexibility applies:

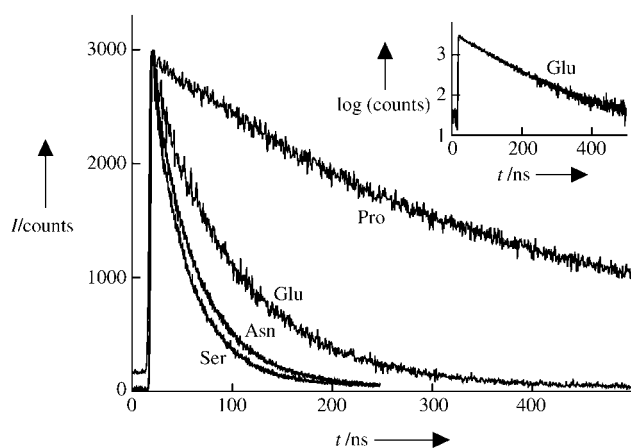


The above order was also preserved in the presence of 6 M guanidinium chloride, except that Leu appeared to give rise to a somewhat less flexible peptide. Guanidinium chloride is an efficient denaturant, which should destroy any remaining secondary structure as well as aggregation between hydro-

Table 1: Fluorescence quenching rate constants in Trp-X₆-DBO-NH₂ peptides.

X	Residue (R)	k_q [10^6 s^{-1}]	
		without additive ^[a]	with denaturant ^[b]
Gly	-H	39	23
Ser	-CH ₂ OH	25	19
Asp ^[c]	-CH ₂ CO ₂ H	21	
	-CH ₂ CO ₂ ⁻	19	12
Asn	-CH ₂ CONH ₂	20	14
Ala	-CH ₃	ca. 18 ^[d]	ca. 14 ^[d]
Thr	-CH(OH)CH ₃	11	9.3
Leu	-CH ₂ CH(CH ₃) ₂	ca. 10 ^[d]	ca. 5.1 ^[d]
Phe	-CH ₂ Ph	ca. 7.6 ^[d,e]	ca. 7.5 ^[d]
Glu ^[c]	-CH ₂ CH ₂ CO ₂ H	8.8	
	-CH ₂ CH ₂ CO ₂ ⁻	7.4	5.4
Gln	-CH ₂ CH ₂ CONH ₂	7.2	4.8
His ^[c]		4.8	4.0
Arg	-(CH ₂) ₃ NHCNH ₂ NH ₂ ⁺	4.6	2.6
Lys ^[c]	-(CH ₂) ₄ -NH ₂	4.0	
	-(CH ₂) ₄ -NH ₃ ⁺	2.8	1.9
Val	-CH(CH ₃) ₂	ca. 3.0 ^[d,e]	ca. 2.6 ^[d]
Ile	-CH(CH ₃)CH ₂ CH ₃	ca. 2.3 ^[d,e]	ca. 1.6 ^[d]
Pro		< 0.1	< 0.1

[a] Measured in D₂O. [b] Measured in H₂O with 6 M guanidinium chloride. [c] The unprotonated forms were studied at pD 12, the protonated ones at pD 2. [d] Extrapolated from the kinetics of the shorter peptide ($n=4$), see Experimental Section. [e] Measured with 30% acetonitrile. [f] Entire amino acid.


Figure 2. Fluorescence decays for selected Trp-X₆-DBO-NH₂ peptides in aerated D₂O measured by single photon counting. The inset shows a representative decay on a semi-logarithmic scale.

phobic peptides.^[25] The consistency of the results in the absence and presence of this denaturant provides strong evidence that the property which is being reflected by the kinetic measurements is indeed conformational flexibility. Note also that the rate of end-to-end collision in the presence of the salt is reduced throughout the entire series of peptides; this reflects the increased viscosity of the solution which limits the mutual diffusion of the chain ends.

According to the conformational flexibility scale, the introduction of Gly into the peptide increases the conformational flexibility, while Pro makes it more rigid. This is in line with expectations from conformational space,^[26] with Gly being the amino acid with the least limited rotational freedom and Pro being the one with a frozen N-C^α bond. The sequence found for the other amino acids cannot be predicted in a straightforward manner. There is a general trend between the residue size and the kinetics: larger residues lead to lower collision frequencies, which indicates a lower flexibility; for example, Gln < Asn; Thr < Ser; Phe, Leu < Ala < Gly; Ile < Val. This result is presumably related to the larger rotational barriers imposed by the larger residues and the decrease in the diffusion coefficient of the peptide chain with increasing residue size. The effect of residue charges was also examined; there appears to be a tendency for the neutral residues to allow a slightly greater flexibility, namely, unprotonated Lys > protonated Lys, protonated Glu > unprotonated Glu, and protonated Asp ≅ unprotonated Asp. The observed charge effect is not very large, but is in line with the intuitive expectation that Coulombic repulsions reduce the overall flexibility by limiting the conformational freedom.

β Branching is well known to increase the activation barriers for bond rotations of an amino acid and therefore decreases the accessible conformational space in a peptide significantly.^[27] Indeed, the peptides with β-substituted amino acids (Val and Ile) are amongst the least flexible ones on our scale. Particularly instructive is the comparison of the two constitutional isomers Leu and Ile, where the latter one imposes a higher rigidity. The β-branched Thr gives rise to more flexible peptides than Val and Ile. Nevertheless, the flexibility of the Thr peptides is slightly decreased compared to those composed of β-unsubstituted amino acids with even larger residues, for example, Thr < Asn, Asp. Evidently, the β-hydroxy group somewhat limits the flexibility, but much less severely than the β-methyl group in Val and Ile. The special effect of hydroxy substitution is also evident with Ser, which gives rise to a more flexible peptide than Ala, although it is larger as a result of the additional hydroxy group.

We did not observe a clear-cut relationship between the flexibility and the hydrophobicity of the residue. Val and Ile are very hydrophobic amino acids, but the high rigidity of the related peptides appears to be mainly a consequence of the β-substitution pattern, since there is a large differentiation from Leu, which is similarly hydrophobic. On the other hand, His and Arg are quite hydrophilic, but their peptides are less flexible than that based on the hydrophobic Phe. The hydrophobicity of the residues, therefore, does not emerge as a common denominator of peptide flexibility.

A long-standing question in peptide chemistry is which properties of an amino acid are decisive for the protein secondary structure. Statistical,^[28–30] theoretical,^[31] and experimental^[32,33] analyses have revealed relative abundances of particular amino acids in secondary protein structures such as α helices, β strands, and β turns. According to the statistical results,^[28] Met, Glu, Leu, Ala, Gln, Lys, His, and Cys are α-helix-forming amino acids, Val, Ile, Phe, Tyr, Thr, and Trp tend to form β-sheet structures, and Pro, Gly, Asp, Ser, and Asn favor β turns. A correlation between conformational

flexibility and the propensity of an amino acid to occur in a secondary structure emerges if one disregards the α -helix-forming amino acids and Pro (see below). Accordingly, the most flexible amino acids, including Gly, Ser, Asn, and Asp, are β -turn-forming amino acids, while the most rigid amino acids, namely Val and Ile, are β -sheet-forming amino acids. In addition, when comparing the β -branched amino acids, Thr is not only the most flexible one on our scale, but it also has a much higher tendency than Val and Ile to occur in β turns.^[28]

We consider that this agreement between the flexibility and the β -turn and β -sheet propensity is significant and suggest that both properties are the result of the same underlying reason: namely, the (energetically unfavorable) angular arrangements which are required in β turns may be the same as those which need to be reached for collision-induced quenching (Figure 1). In other words, the conformations required for quenching are turnlike. Large α substituents and in particular β branching do not favor β turns because of steric interactions,^[27] and this avoidance also manifests itself in the kinetic measurements where a similar conformation is required for quenching. It appears that flexible amino acids, in particular Gly and Ser, promote stable β turns, although one must keep in mind that the abundance of an amino acid also depends strongly on the specific position within a β turn.^[34] Rigid amino acids have a higher tendency to occur in β -sheet structures than in β turns, but they may also favor the formation of α helices. α -Helix formation is dominated by additional interactions between non-adjacent amino acids,^[35] which are unlikely to be related to chain flexibility. In fact, a relationship between α -helix propensity and flexibility cannot be recognized, although it is evident that the α -helix-forming amino acids adopt an intermediate position on the proposed flexibility scale.

A clear exception is Pro,^[22] which gives rise to the most rigid peptide, but which is also favored in β turns. The high rigidity is imposed by its cyclic structure, which prevents rotations about the N–C α bond. The high β -turn propensity, on the other hand, is related to the restricted -60° ϕ angle, which presents an ideal arrangement in the $i + 1$ position of β turns.^[36]

In summary, the following trends emerge for the conformational flexibility of amino acids in peptides as assessed by our method: 1) Large residues reduce the flexibility; 2) β -alkyl branching greatly reduces flexibility, while β -hydroxy substitution retains a high flexibility; 3) charge repulsions between residues decrease the flexibility slightly; 4) the conformationally frozen amino acid Pro is the least flexible while the simplest amino acid Gly is the most flexible; 5) a correlation with β -turn propensity applies, with the most flexible amino acids also being those with high β -turn propensity; 6) rigid amino acids appear to be favored in β sheets; and 7) there is no clear-cut relationship between flexibility and hydrophobicity or the α -helix propensity of amino acids. Finally, one must note that the present flexibility scale is based on a set of synthetic peptides with a backbone composed of identical amino acids. Whether the flexibility of native random-coil peptide sequences can be predicted from this scale in an incremental fashion or depends strongly on the specific sequence, will be the subject of future studies applying the same methodology.

Experimental Section

The peptides were commercially synthesized in >95% purity (Affina, Berlin). Details on the synthesis of the probe and its suitability in solid-phase peptide synthesis have been reported.^[17] The choice of the peptide length (number of amino acids as spacers of the probe and the quencher) is essential since the peptide should not be too long to enable measurement of significant quenching and to maintain water solubility, and neither should it be too short to maintain sufficiently long lifetimes for accurate measurement and to ensure that the measured rates reflect an intrinsic property of the backbone, namely, the amino acid. Six amino acids ($n = 6$) provided a good balance between these factors, but peptides of this chain length with the most hydrophobic amino acids (Ala, Leu, Phe, Val, and Ile) were poorly soluble in pure water, thus causing complications in both peptide synthesis as well as fluorescence measurement. For these cases, a shorter sequence of four amino acids ($n = 4$) was chosen, and the known length dependence of the kinetics of end-to-end collision^[17] allowed extrapolation of the rates to the value for $n = 6$.

Fluorescence decays were measured by single photon counting (FLS900, Edinburgh Instruments) under air, either in D₂O or in H₂O containing 6 M guanidinium chloride. All peptides were sufficiently soluble in the presence of guanidinium chloride, but peptides based on the hydrophobic amino acids Phe, Val, and Ile were not sufficiently soluble without this denaturant. In these three cases, 30% acetonitrile was added to D₂O to achieve the same working concentration (10 μ M) as for the other peptides and these solutions were deaerated. The co-solvent did not have a major effect on the measured rates, which could be demonstrated through control experiments in neat D₂O at lower peptide concentration (ca. 1 μ M).

The decay kinetics were monoexponential in all cases (Figure 2), such that it was possible to assign a characteristic fluorescence lifetime (τ) to each peptide and amino acid backbone.^[21] The quenching rate constants k_q were obtained from the experimental fluorescence lifetimes as $k_q = 1/\tau - 1/\tau_0$, where τ_0 corresponds to the intrinsic fluorescence lifetime of the probe in the absence of quenchers, for example, as measured for the free parent fluorophore as well as for peptides lacking a quencher. This value amounts to 500 ns in aerated D₂O and to 360 ns in H₂O containing 6 M guanidinium chloride. Subject to the assumption of a random coil conformation^[22] and subject to the assumption of diffusion-controlled intramolecular quenching,^[17,20] the quenching rate constant (k_q) can be directly interpreted as end-to-end collision frequency (k_{coll} in Figure 1).

Received: December 3, 2002 [Z50684]

Keywords: amino acids · fluorescence · peptides · protein folding · secondary structure

- [1] R. Huber, *Biochem. Soc. Trans.* **1987**, *15*, 1009–1020.
- [2] D. T. Braddock, J. M. Louis, J. L. Baber, D. Levens, G. M. Clore, *Nature* **2002**, *415*, 1051–1056.
- [3] N. Taschner, S. A. Müller, V. R. Alumella, K. N. Goldie, A. F. Drake, U. Aebi, T. Arvinte, *J. Mol. Biol.* **2001**, *310*, 169–179.
- [4] P. Závodszy, J. Kardos, A. Svingor, G. A. Petsko, *Proc. Natl. Acad. Sci. USA* **1998**, *95*, 7406–7411.
- [5] P. Hammarström, U. Carlsson, *Biochem. Biophys. Res. Commun.* **2000**, *276*, 393–398.
- [6] A. R. Fersht, *Curr. Opin. Struct. Biol.* **1997**, *7*, 3–9.
- [7] Y. Q. Qian, G. Otting, K. Furukubo-Tokunaga, M. Affolter, W. J. Gehring, K. Wüthrich, *Proc. Natl. Acad. Sci. USA* **1992**, *89*, 10738–10742.
- [8] S. Hayward, *Proteins* **1999**, *36*, 425–435.
- [9] D. Pogoćki, E. Ghezzi-Schöneich, C. Schöneich, *J. Phys. Chem. B* **2001**, *105*, 1250–1259.

- [10] M. Mutter, *J. Am. Chem. Soc.* **1977**, *99*, 8307–8314.
- [11] P. A. Karplus, G. E. Schulz, *Naturwissenschaften* **1985**, *72*, 212–213.
- [12] R. Bhaskaran, P. K. Ponnuswamy, *Int. J. Pept. Protein Res.* **1988**, *32*, 241–255.
- [13] M. Vihinen, E. Torkkila, P. Riikonen, *Proteins* **1994**, *19*, 141–149.
- [14] S. H. Gellman, *Acc. Chem. Res.* **1998**, *31*, 173–180.
- [15] W. F. van Gunsteren, R. Bürgi, C. Peter, X. Daura, *Angew. Chem.* **2001**, *113*, 363–367; *Angew. Chem. Int. Ed.* **2001**, *40*, 351–355.
- [16] W. M. Nau, X. Wang, *ChemPhysChem* **2002**, *3*, 393–398.
- [17] R. R. Hudgins, F. Huang, G. Gramlich, W. M. Nau, *J. Am. Chem. Soc.* **2002**, *124*, 556–564.
- [18] O. Bieri, J. Wirz, B. Hellrung, M. Schutkowski, M. Drewello, T. Kiefhaber, *Proc. Natl. Acad. Sci. USA* **1999**, *96*, 9597–9601.
- [19] L. J. Lapidus, P. J. Steinbach, W. A. Eaton, A. Szabo, J. Hofrichter, *J. Phys. Chem. B* **2002**, *106*, 11 628–11 640.
- [20] I.-C. Yeh, G. Hummer, *J. Am. Chem. Soc.* **2002**, *124*, 6563–6568.
- [21] Most amino acids have been shown not to act as quenchers. Only Trp, Tyr, Cys, and Met are themselves quenchers (ref. [17]) and these four amino acids could consequently not be included in the present study; the fluorescence lifetimes of peptides containing these amino acids in their backbone would be too short. Also His becomes a fairly strong quencher in its unprotonated form (above pH 6, ref. [17]), such that His could only be studied at low pH values in its protonated form.
- [22] CD measurements were performed for all peptides (including measurements at different pH values, for example, for protonated and unprotonated Lys and Glu). The CD patterns are characteristic of random-coil conformations, which excludes the occurrence of sizable amounts of secondary structures in any of the investigated short peptides, including the peptides composed of amino acids with known α -helix propensity. The only exception was the Pro-derived peptide since, according to the CD spectrum, it adopts its characteristic PPII helix.
- [23] D. V. Mikhailov, L. Washington, A. M. Voloshin, V. A. Daragan, K. H. Mayo, *Biopolymers* **1999**, *49*, 373–383.
- [24] J. Koca, *Prog. Biophys. Mol. Biol.* **1998**, *70*, 137–173.
- [25] D. Voet, J. G. Voet, C. W. Pratt, *Fundamentals of Biochemistry*, J. Wiley and Sons, New York, **1999**.
- [26] P. Chakrabarti, D. Pal, *Prog. Biophys. Mol. Biol.* **2001**, *76*, 1–102.
- [27] D. Pal, P. Chakrabarti, *Acta Crystallogr. D* **2000**, *56*, 589–594.
- [28] M. Levitt, *Biochemistry* **1978**, *17*, 4277–4285.
- [29] E. G. Hutchinson, J. M. Thornton, *Protein Sci.* **1994**, *3*, 2207–2216.
- [30] V. Muñoz, L. Serrano, *Proteins* **1994**, *20*, 301–311.
- [31] P. Koehl, M. Levitt, *Proc. Natl. Acad. Sci. USA* **1999**, *96*, 12 524–12 529.
- [32] C. N. Pace, J. M. Scholtz, *Biophys. J.* **1998**, *75*, 422–427.
- [33] M. Monné, M. Hermansson, G. von Heijne, *J. Mol. Biol.* **1999**, *288*, 141–145.
- [34] P. Y. Chou, G. D. Fasman, *Biophys. J.* **1979**, *26*, 367–383.
- [35] A. G. Street, S. L. Mayo, *Proc. Natl. Acad. Sci. USA* **1999**, *96*, 9074–9076.
- [36] A. Perczel, I. Jáklí, B. M. Foxman, G. D. Fasman, *Biopolymers* **1996**, *38*, 723–732.

Chimia 57 (2003) 161–167
© Schweizerische Chemische Gesellschaft
ISSN 0009–4293

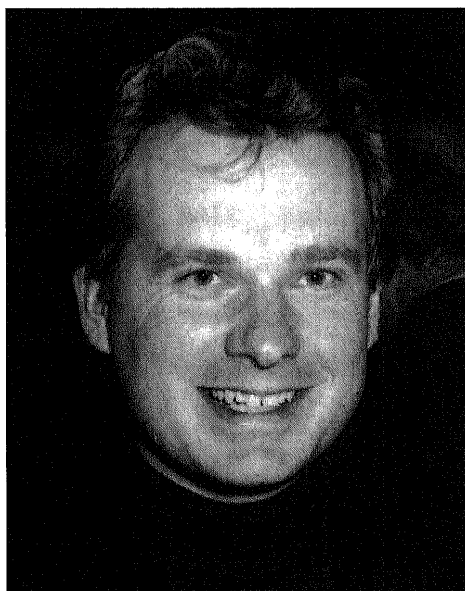
Exploiting Long-Lived Molecular Fluorescence

Werner M. Nau*, Fang Huang, Xiaojuan Wang, Huseyin Bakirci, Gabriela Gramlich, and Cesar Marquez

*Werner Prize Winner 2002

Abstract: Fluorophores based on the azo chromophore 2,3-diazabicyclo[2.2.2]oct-2-ene, referred to as fluorazophores, display an exceedingly long fluorescence lifetime. Besides the use in time-resolved screening assays, where the long-lived fluorescence can be time-gated, thereby improving the signal to background ratio, a distinct application of fluorazophores lies in the area of biopolymer dynamics. For this purpose, one chain end is labeled with a fluorazophore and the other one with an efficient fluorescence quencher. The fluorescence lifetime of the probe/quencher-labeled peptide then reflects the kinetics of intramolecular end-to-end collision. Applications to polypeptides are described and control experiments which establish the nature of the quenching mechanism as a diffusive process requiring intimate probe/quencher contact are described.

Keywords: Azoalkanes · Fluorescence · Kinetics · Photochemistry · Peptides



Werner Nau graduated with a M.Sc. in Chemistry 1992 from St. Francis Xavier University, Canada. His thesis was supervised by D. Klapstein and dealt with molecular spectroscopy (UV, IR, photoelectron) of acyl iso(thio)cyanates. He got his Ph.D. together with W. Adam in 1994 from the University of Würzburg on the EPR and transient absorption spectroscopy of 1,3-cyclopentadienyl diradicals. Thereafter, Werner Nau spent his post-doctoral studies with J.C. Scaiano at the University of Ottawa, where he worked on the mechanistic photochemistry of n,π^* -excited states. In 1996, he joined J. Wirz at the University of Basel, where he has started up with an independent research group and became a SNF assistant professor in 2000. In the same year he finished his habilitation. Since the fall semester 2002 he has been appointed as a professor of chemistry at the newly founded International University Bremen.

His research interests lie in the general area of physical organic chemistry and focus on photochemistry, radical chemistry, supramolecular chemistry, and biomolecular chemistry, including both synthetic-preparative, mechanistic, kinetic, and spectroscopic aspects. He has recently introduced a novel class of fluorescent probes, referred to as fluorazophores, which are based on the azo chromophore of 2,3-diazabicyclo[2.2.2]oct-2-ene. Fluorazophores are applied as sensors for antioxidants, versatile guest molecules in supramolecular chemistry, kinetic probes for biopolymer folding, and fluorophores for time-resolved screening assays.

Werner Nau has held numerous fellowships, among others a Kekulé and Liebig fellowship of the Fonds of the Chemical Industry, a NATO fellowship, a NSERC Interna-

tional fellowship, and a SNF Profil fellowship. His work has led to the award of several prizes, including the 1999 International Grammaticakis-Neumann prize for photochemistry, awarded by the Swiss Group for Photochemistry and Photobiology, and the 2000 ADUC-Prize, awarded for his habilitation thesis.

Fluorescent probes and sensors are well-established tools in analytical and biological chemistry, spanning such diverse applications as calcium ion detection, cell staining, and polarity sensing [1]. An interesting sub-class of fluorescent probes comprises chromophores with a particularly long fluorescence lifetime, *e.g.* more than 50 ns [2]. Perhaps the simplest yet very important application based on long-lived fluorescence (or generally luminescence) relies on the reliable differentiation of long fluorescence lifetimes from any shorter-lived luminescence components. This is of interest, in particular, for screening assays where fluorescent probes are employed to signal molecular events such as the inhibition of an enzyme by a library of potential drugs. Short-lived emission is ubiquitous and may stem from other additives, sample impurities, biological components, scattered light, the solvent, or sample container materials of cuvettes and microplates.

*Correspondence: Prof. Dr. W.M. Nau
School of Engineering and Science
International University Bremen
Campus Ring 1
D-28759 Bremen
Tel.: +49 421 200 3233
Fax: +49 421 200 3229
E-Mail: w.nau@iu-bremen.de
and
Department of Chemistry
University of Basel
Klingelbergstrasse 80
CH-4056 Basel

The shorter-lived components can be eliminated from detection through a time-gate, such that the emission from the long-lived fluorescent label (which serves as the signaling unit) can be selectively detected. This reduces the background during the measurement dramatically. An instructive example is depicted in Fig. 1, which compares the fluorescence decay of a long-lived fluorescent probe ($\tau = 500$ ns) with that of a shorter-lived fluorescing component ($\tau = 10$ ns), with the latter one, however, being much more intense (10^6 times larger preexponential factor). If as usual the integrated fluorescence intensity would be compared through steady-state methods, a 'signal-to-background' of 0.00005:1 would result, which would prevent any useful information to be obtained. If one carries out the experiment in lifetime mode with a time-gate between 200–1000 ns and integrates the areas under the curves, the 'signal-to-background' ratio becomes better than 10000:1, an impressive improvement by more than eight orders of magnitude, which has its underlying reason in the exponential decay kinetics of the fluorescence. This improvement renders the selective detection of long-lived fluorophores in so-called 'time-resolved' screening assays generally an entirely instrumental problem. In particular, the real background may be dominated by detector noise rather than contributions from short-lived emission.

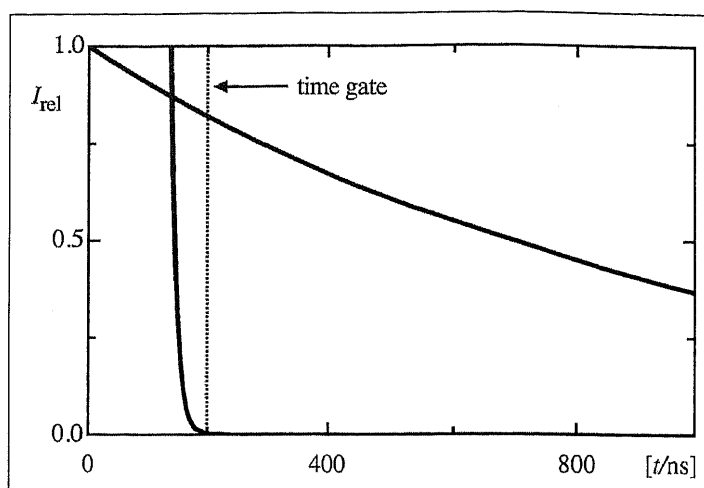
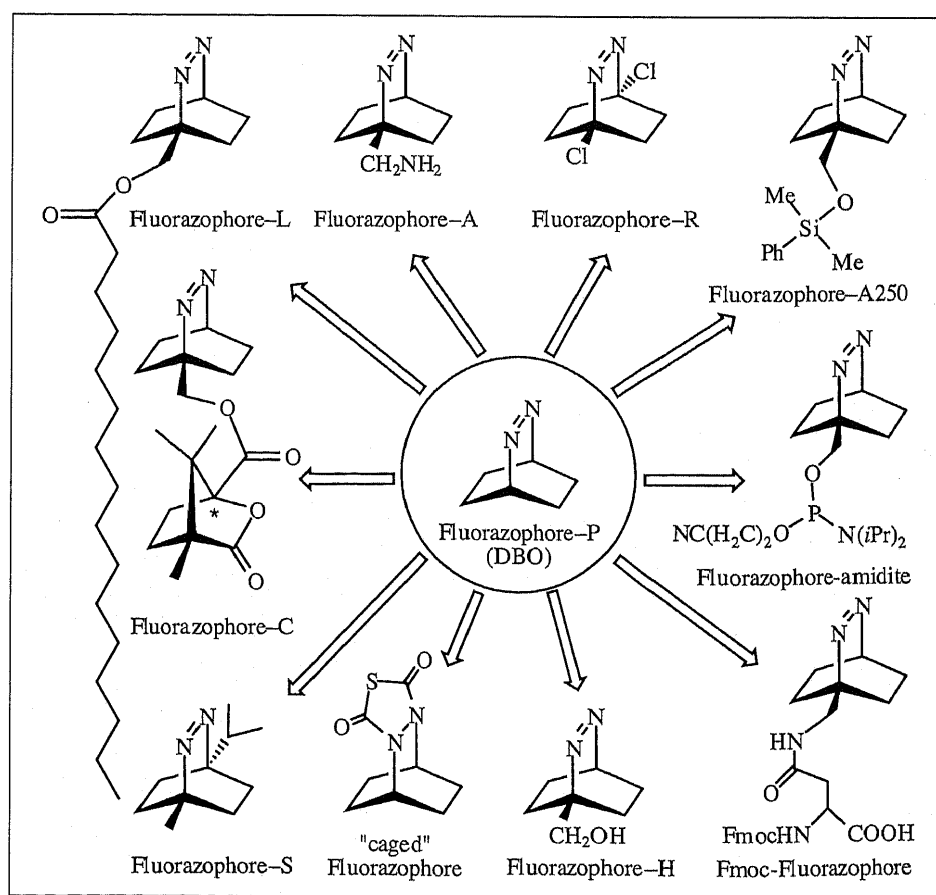
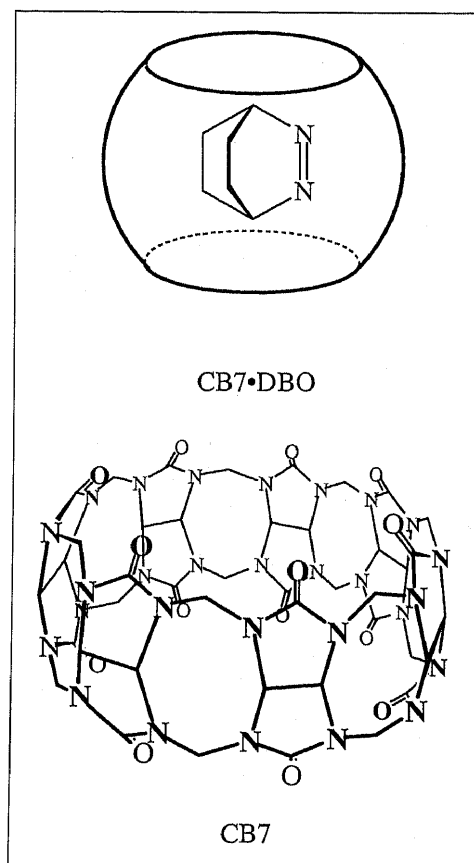


Fig. 1. Comparison of the fluorescence decay of a long-lived fluorescent probe ($\tau = 500$ ns) with that of a shorter-lived component ($\tau = 10$ ns); the shorter-lived component is 10^6 times more intense (relative preexponential factors). A suitable time gate for use in a time-resolved assay is shown at 200 ns.

Relatively few organic molecules display lifetimes in this long time regime, with azoalkanes derived from 2,3-diazabicyclo[2.2.2]oct-2-ene (DBO) displaying the longest fluorescence lifetime in solution [3]. The record for the longest fluorescence lifetime of an organic chromophore in solution lies currently at 1.03 μ s (in aerated H_2O) [4] and is held by the supramolecular complex (CB7•DBO) between the par-

ent azoalkane and cucurbit[7]uril (CB7), a barrel-like organic host molecule [5]. Over the past six years, we have investigated this interesting chromophore in great detail and have prepared several DBO derivatives, which we refer to as fluorazophores ('fluorescent azo chromophores'). Some of the investigated derivatives are shown in Scheme 1.



Scheme 1

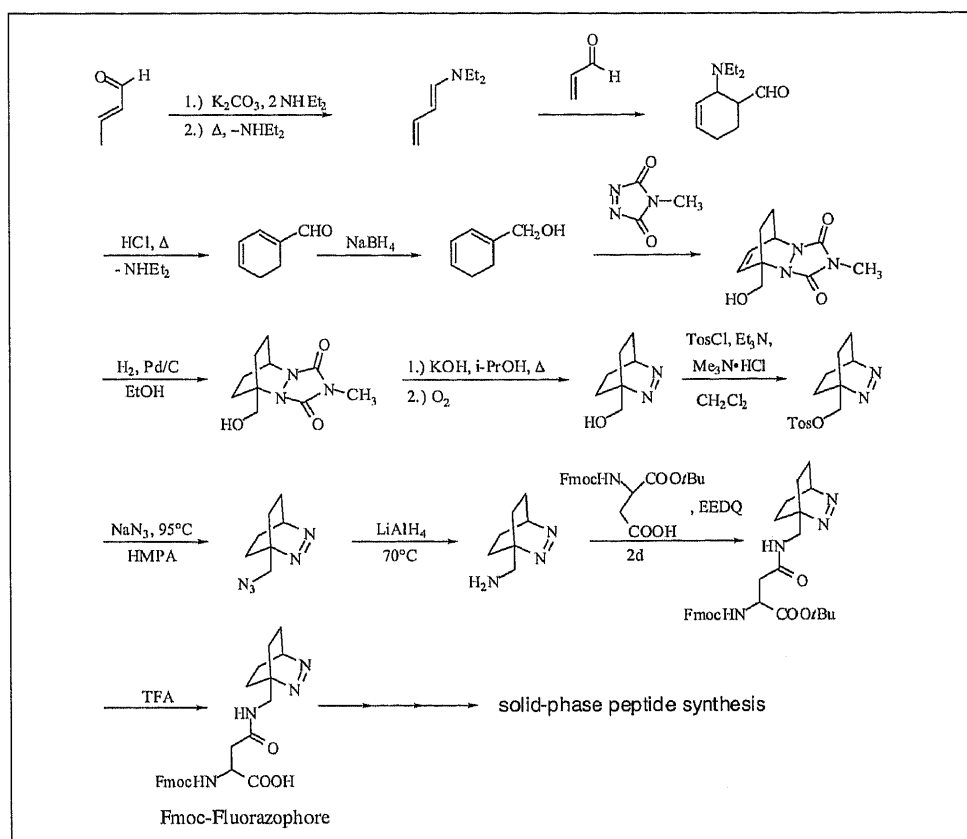
A representative synthetic sequence to obtain Fmoc-Fluorazophore is shown in Scheme 2, which has been scaled up to afford typically 3 g of Fmoc-DBO in an overall yield of 10%, sufficient for the commercial synthesis of up to 30 polypeptides (10 mg scale).

The intriguing photophysics of fluorazophores has been worked out in great detail [6–11] and the fascinating quenching pathways have been investigated through a combination of experimental and theoretical methods [12–14]. On the more applied side, fluorazophores have proven to be useful as sensors for antioxidant activity, both in solution [15][16] as well as in membrane-mimetic systems [17], as probes for measuring the kinetics of association with supramolecular systems [18][19], as tools to investigate the geometries of cyclodextrin inclusion complexes by means of circular dichroism [20][21], and as probes for the polarizability inside molecular container molecules [22].

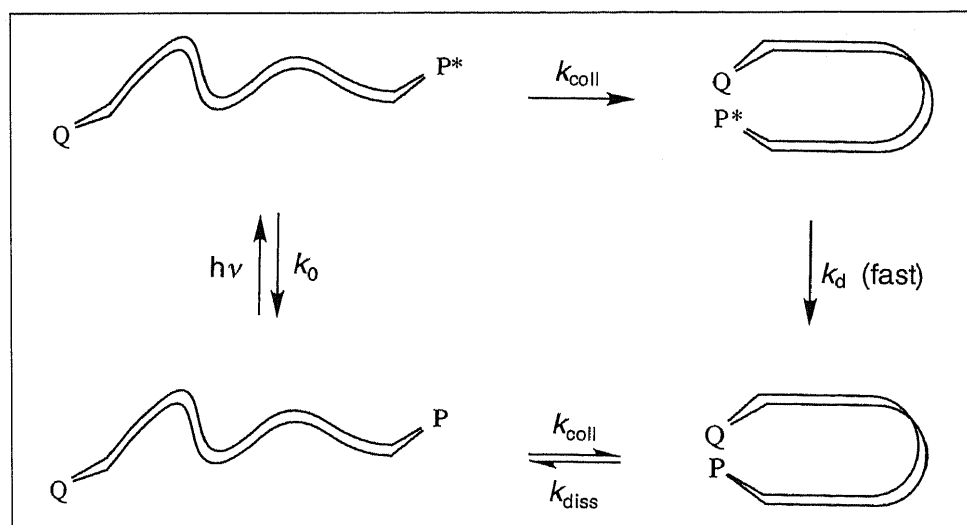
Most recently, we have employed fluorazophores to measure the kinetics of end-to-end collision in biopolymers (k_{coll} in Scheme 3), including peptides [23][24], and oligonucleotides [25]. For this purpose, the fluorazophore (P) is attached to one end of the biopolymer and an efficient (nearly diffusion-controlled) fluorescence quencher (Q) is attached to the other side; in peptides this quencher moiety is usually tryptophane and in oligonucleotides guanine. The kinetics of fluorescence quenching can then be equated to the rate of end-to-end collision, which has proven difficult to obtain accurately by alternative techniques.

Keeping in mind that alternative methods have other advantages [26][27], the fluorazophore approach presents, arguably, the most sensitive and most accurate tool for measuring end-to-end contact in biopolymers known to date. Note that this application is made possible by the exceedingly long fluorescence lifetime, which allows the fluorazophore to 'wait' sufficiently long until it is being approached (and immediately quenched) by the other end; this diffusive approach of the chain ends takes 10 ns to 1 μ s in aqueous solution. The lifetime of fluorazophores (ca. 505 ns in D₂O under air) is therefore ideally suited for investigations in this time regime.

Being able to measure the absolute rates for the motions within biopolymers or at least knowing the time scale for these processes is of fundamental importance for understanding the mechanism of protein folding [28], for predicting the kinetics of intramolecular reactions in biopolymers (formation of hydrogen bonds, cystine bridges, proton transfer, electron transfer)



Scheme 2



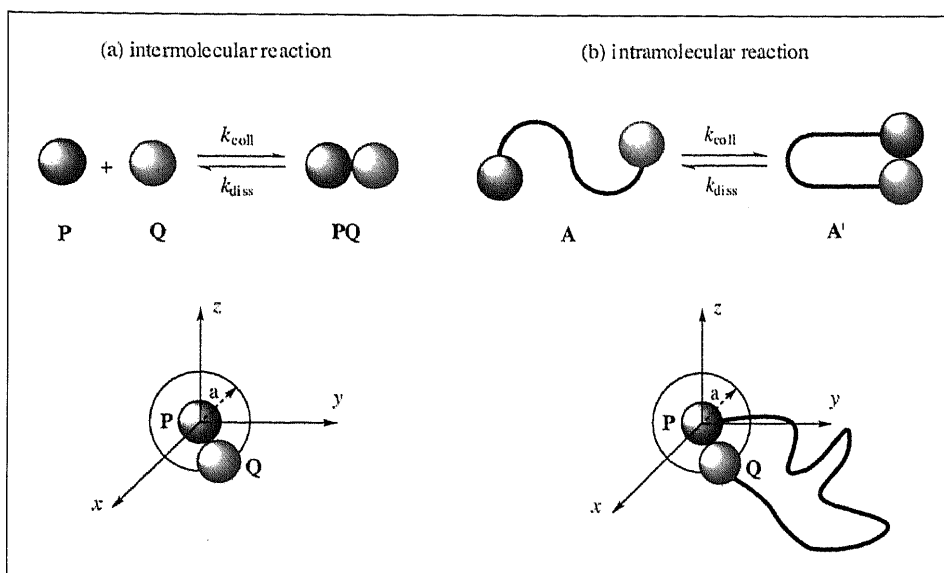
Scheme 3

[29], and for understanding protein domain motions [30]. The size of biopolymers and the effects of solvation, including salt effects, still present a major challenge to computational chemistry, which demands experimental data. The latter, in turn, may provide invaluable benchmark values for the calibration of theoretical models [31].

A simple problem already arises if one attempts to predict the time scale of diffusion-controlled end-to-end collision in (bio)polymers from the available rates for diffusion-controlled intermolecular reactions. To allow a comparison, it is useful to compare the probability for intramolecular

and intermolecular encounter complex formation between two fragments.

Consider Scheme 4a, the intermolecular case. We assume an ideal solution with no enthalpic interactions between the probe (P) and the quencher (Q) molecules. The concentration of the encounter complex, C_{PQ} , can be obtained according to Eqn. (1) with V_e being the volume of the encounter complex with radius a (spherical approximation). C_P^0 and C_Q^0 are the total concentrations of P and Q. The 'equilibrium constant' for encounter complex formation is then given by Eqn. (2), assuming that the concentration of molecules in contact is



Scheme 4

small (dilute solution, *i.e.* $C_P \approx C_P^0$ and $C_Q \approx C_Q^0$). It follows that the equilibrium constant for encounter complex formation (in units of $\text{m}^3\text{mol}^{-1}$) equals the volume of the encounter complex multiplied with the Avogadro constant (N_a). This in turn corresponds, due to the absence of enthalpic effects, to the loss of entropy associated with the formation of the encounter complex, *i.e.* $\Delta_{\text{coll}}S^0 = R\ln(1000K_{\text{inter}}C^0)$, where the factors 1000 and C^0 , the standard concentration in M , are added to give a dimensionless equilibrium constant.

$$C_{PQ} = C_P^0 N_a V_c C_Q^0 = C_P^0 C_Q^0 N_a \frac{4}{3} \pi a^3 \quad (1)$$

$$K_{\text{inter}} = \frac{C_{PQ}}{C_P C_Q} = \frac{C_{PQ}}{C_P^0 C_Q^0} = \frac{4}{3} \pi a^3 N_a \quad (2)$$

The intramolecular case, Scheme 4b, describes the pertinent situation for encounter complex formation within a biopolymer chain labeled with a probe (P) and a quencher (Q) at opposite ends. For simplicity, we assume that the chain does not introduce additional interactions between probe and quencher except to restrict the distance by which they can diffuse apart (ideal chain, Gaussian chain). Like for the intermolecular case, we assume no enthalpic interactions between the probe and the quencher residues. The fraction of chains with the two ends in contact, ($C_{A'}$), can be obtained in this case from the distribution function (g) in Eqn. (3), which has analytical solutions for a very long chain ($N \gg 1$, with N the number of chain segments) and for the shortest chain ($N = 2$). r is taken as the distance between the chain ends and b equals the length of an individual chain segment. The 'equilibrium constant' for end-to-end encounters is then given by Eqn. (4),

which assumes for the case of a very long chain ($N \gg 1$) that the concentration of molecules in contact is small ($C_{A'} \approx C_A + C_{A'}$). Again, this relates directly to the loss of entropy associated with the formation of an end-to-end encounter complex within an ideal chain, *i.e.* $\Delta_{\text{coll}}S^0 = R\ln K_{\text{intra}}$.

$$g(r) = \left(\frac{3}{2\pi \langle r^2 \rangle} \right)^{3/2} \exp\left(-\frac{3r^2}{2\langle r^2 \rangle} \right) \text{ with } \langle r^2 \rangle = Nb^2 \text{ for } N \gg 1 \quad (3)$$

$$g(r) = \frac{1}{8\pi b^2} \text{ for } N = 2$$

$$K_{\text{intra}} = \frac{C_{A'}}{C_A} = \frac{C_{A'}}{C_A + C_{A'}} = \int_0^a g(r) 4\pi r^2 dr \approx \frac{4}{3} \pi a^3 \left(\frac{3}{2\pi \langle r^2 \rangle} \right)^{3/2} = \frac{4}{3} \pi a^3 \left(\frac{3}{2\pi Nb^2} \right)^{3/2} \text{ for } N \gg 1 \quad (4)$$

$$K_{\text{intra}} = \frac{C_{A'}}{C_A} = \frac{\int_0^a g(r) 4\pi r^2 dr}{1 - \int_0^a g(r) 4\pi r^2 dr} = \frac{(a/b)^2}{4 - (a/b)^2} \text{ for } N = 2$$

The kinetics of end-to-end contact formation for the intramolecular reaction can be related to that of the intermolecular reaction (Eqn. (5)) if one reduces the equilibrium constants to ratios of microscopic rate constants and considers further that the elementary rate of dissociation of the encounter complex must be identical for both species within the approximations made ($k_{\text{diss}}^{\text{intra}} = k_{\text{diss}}^{\text{inter}}$). Recall, in particular that the on-

ly function of the chain for the intramolecular case is to limit the distance between probe and quencher.

$$\frac{K_{\text{intra}}}{K_{\text{inter}}} = \frac{k_{\text{coll}}^{\text{intra}} / k_{\text{diss}}^{\text{intra}}}{k_{\text{coll}}^{\text{inter}} / k_{\text{diss}}^{\text{inter}}} = \frac{k_{\text{coll}}^{\text{intra}}}{k_{\text{coll}}^{\text{inter}}} \quad (5)$$

Use of the respective expressions for the equilibrium constants for intermolecular and intramolecular encounter complex formation then affords Eqn. (6). If one further expresses the intermolecular collision rate constant through the relationship between the intermolecular diffusion rate constant and the diffusion coefficient ($k_{\text{coll}}^{\text{inter}} = 4D\pi a N_a$), one obtains Eqn. (7), with D being the mutual intermolecular diffusion coefficient.

Eqn. (7) provides the ideal relationship between the unknown rate constant for intramolecular end-to-end collision and the known (diffusion-controlled) rate constant for an intermolecular probe-quencher pair. Accordingly, the rate of end-to-end collision in a biopolymer increases linearly with the diffusion coefficient and size of the en-

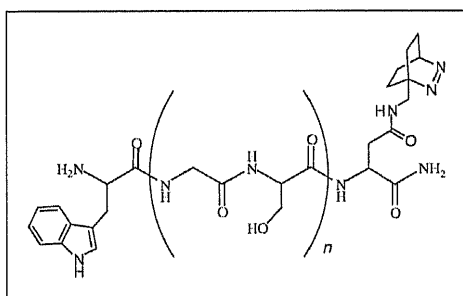
counter complex (radius a), it depends inversely on the cubed chain segment length (b), and it decreases with increasing chain length (N) with the characteristic exponent of $-3/2$. Eqn. (7) has been derived in a different context by Szabo, Schulten, and Schulten through an analysis of the first passage time of end-attached groups based on a modified Smoluchowski equation [32][33].

$$\frac{k_{\text{coll}}^{\text{intra}}}{k_{\text{coll}}^{\text{inter}}} = \frac{\frac{4}{3} \pi a^3 \left(\frac{3}{2\pi Nb^2} \right)^{3/2}}{\frac{4}{3} \pi a^3 N_a} = \frac{1}{N_a} \left(\frac{3}{2\pi Nb^2} \right)^{3/2} \text{ for } N \gg 1 \quad (6)$$

$$k_{\text{coll}}^{\text{intra}} = k_{\text{coll}}^{\text{inter}} \frac{1}{N_a b^3} \left(\frac{3}{2\pi} \right)^{3/2} N^{-3/2} = \frac{4D\pi a N_a}{N_a b^3} \left(\frac{3}{2\pi} \right)^{3/2} N^{-3/2} = \sqrt{\frac{54}{\pi}} \frac{Da}{b^3} N^{-3/2} \text{ for } N \gg 1 \quad (7)$$

To apply Eqn. (7), one may use commonly accepted intermolecular diffusion coefficients of $10^{-5} \text{ cm}^2\text{s}^{-1}$ in water (the mutual diffusion coefficient in Eqn. (7) corresponds to twice this value), a van-der-Waals reaction radius of 5 Å, and a chain segment length of 5 Å (typical for one peptide unit). The resulting estimates for the intramolecular collision times ($1/k_{\text{coll}}$) are 0.2 ns for $N = 4$ and 2.7 ns for $N = 20$. This means that end-to-end contact formation in biopolymers in solution may occur as fast as several ns according to the simplest theoretical framework. These theoretical rates can now be compared with the experimental results obtained from the fluorazophore probe/quencher technique in synthetic polypeptides.

Our initial experimental study focused on the length dependence of the end-to-end collision rates in peptides with the general structure $\text{Trp}-(\text{Gly-Ser})_n\text{-DBO-NH}_2$ (structure below); these peptides are water soluble and presumed to be 'structureless' according to a previous study [26]. This is an important requirement to apply theories based on Gaussian chain behavior [34][35].



The fluorescence decays of all peptides as recorded with the time-correlated single photon counting technique were strictly monoexponential (Fig. 2). The resulting fluorescence lifetimes (τ) for the peptides

with different length are listed in the Table and range from 10–75 ns. Subject to the assumption of diffusion-controlled quenching, the collision rates can be directly obtained through a correction for the inherent fluorescence lifetime (τ_0) according to Eqn. (8). The data for the collision rate constants demonstrate that end-to-end contact formation in short polypeptides may occur as fast as 10 ns in water, significantly faster than previous estimates of rates for peptides with the same length, but also substantially smaller than expected from the ideal-chain behavior according to Eqn. (7) (see above). Presumably, the diffusion coefficients of the peptide chain ends are much smaller than those of the free probe and quencher; the use of smaller diffusion coefficients in Eqn. (7) than the intermolecular ones would bring the theoretical data much closer to the experimental ones [36].

$$k_{\text{coll}} = 1/\tau - 1/\tau_0 \quad (8)$$

Table. Fluorescence lifetimes and end-to-end collision rate constants for $\text{Trp}-(\text{Gly-Ser})_n\text{-DBO-NH}_2$ polypeptides

n	N^a	τ / ns^b	$k_{\text{coll}} / 10^7 \text{ s}^{-1c}$
0	2	23.3	4.1
1	4	14.3	6.8
2	6	19.5	4.9
4	10	30.5	3.1
6	14	45.6	2.0
10	22	74.4	1.1

^aNumber of peptide units between probe and quencher. ^bFluorescence lifetime in aerated D_2O at 23 °C measured by time-correlated single photon counting. ^cObtained from Eqn. 8 with $\tau_0 = 500$ ns.

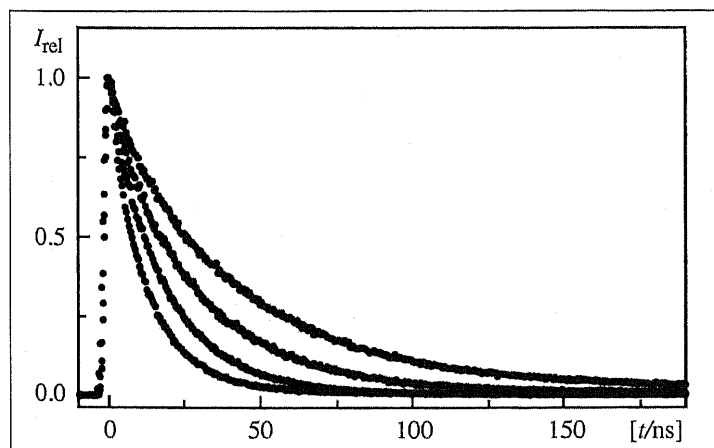


Fig. 2. Fluorescence decays (time-correlated single photon counting, normalized intensity) of $\text{Trp}-(\text{Gly-Ser})_n\text{-DBO-NH}_2$ polypeptides ($n = 1, 2, 4,$ and 6). The lowest trace corresponds to $n = 1$, the uppermost one to $n = 6$.

The dependence of the collision rates on the chain length as derived in Eqn. (7) predicts a linear increase of the logarithmic collision rates with the logarithm of the number of chain segments (N). The corresponding plot (Fig. 3) for the experimental data shows that this linear relationship is not observed. Instead, one obtains a plot with a strong negative curvature. Moreover, the theoretical slope [34][35] of $-3/2$ is only reached for the longer chains. These variances indicate deviations from the ideal behavior, which are presumably related to effects of chain stiffness, which impose an increased internal friction for end-to-end collision in the short chains [36].

The interpretation of the fluorescence lifetimes in terms of end-to-end collision rate constants requires a collision-induced fluorescence quenching, *i.e.* probe and quencher must come into van-der-Waals contact (2–3 Å distance) for quenching to occur. This is naturally fulfilled for quenching by hydrogen atom transfer or exciplex-induced quenching, which are the two prototypal quenching mechanisms of the DBO chromophore [3][6][8][13][14][37–39]. However, quenching by electron transfer, which presents an alternative quenching mechanism, could operate through bond (superexchange mechanism); it could also occur over a considerable distance through space or through the solvent (up to 5–8 Å) and must therefore be excluded [40]. The same applies for Dexter-type triplet energy transfer, which has been employed in other intramolecular probe/quencher pairs to assess end-to-end contact formation [26][41][42]. Quenching over larger distances than van-der-Waals contact would result in a continuum of distance-dependent rate constants, which could not be analyzed in terms of a diffusion-controlled collision

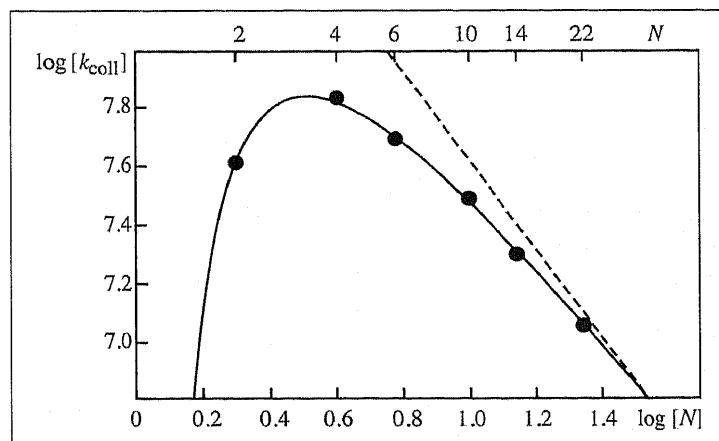


Fig. 3. Double-logarithmic plot of the end-to-end collision rate constants (k_{coll}) of $\text{Trp}-(\text{Gly-Ser})_n\text{-DBO-NH}_2$ polypeptides versus the peptide length, taken as the number of intervening peptide units (N). The dashed line has a slope of $-3/2$ and is shown to illustrate the deviation from the theoretical behavior (Eqn. 7).

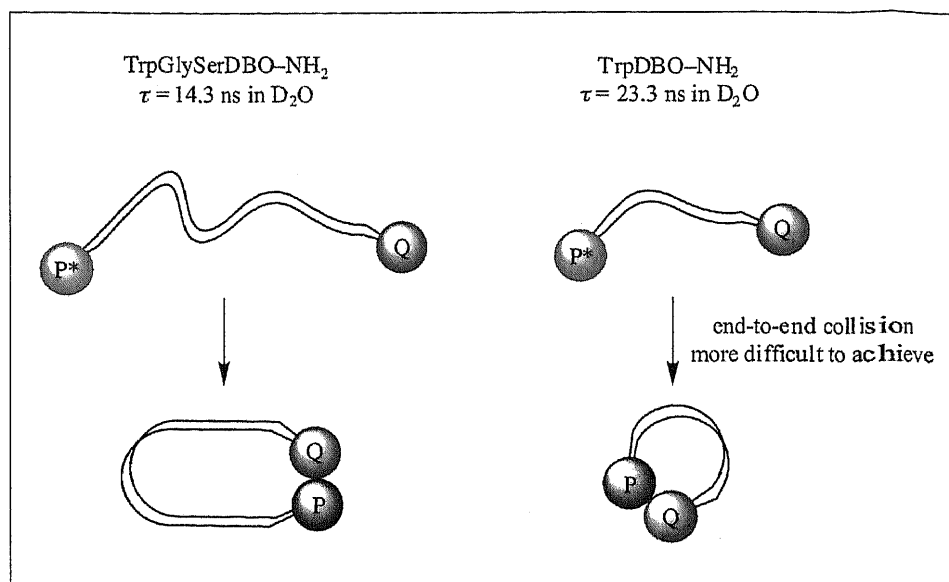
process. In this case, quenching presents no longer an elementary reaction to which a single rate constant can be assigned. In fact, fluorescence resonance energy transfer, which operates over even larger distances, has proven inapplicable to obtain the pertinent elementary rate constants [26][43].

In view of the possible complications due to distance-dependent quenching rates, it appeared compulsory to establish experimentally that quenching through bond or through the solvent do in fact not apply for the DBO/Trp probe/quencher pair. We have therefore performed a series of carefully designed control experiments (Schemes 5–7). Control experiments of this type are strongly recommended to establish alternative methods for assessing end-to-end contact formation, in particular if triplet energy transfer or electron transfer (both of which are candidates for distance-dependent quenching rates) are the postulated quenching mechanisms.

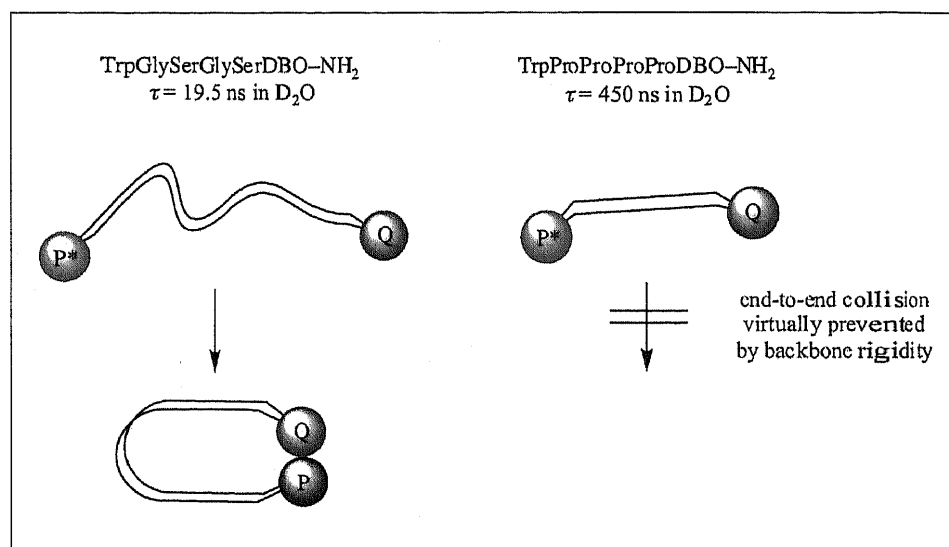
In the first experiment (Scheme 5), we have compared the fluorescence lifetime of the shortest peptide, in which probe and quencher are directly attached, with the longer ones. The lifetime of the shortest peptide is in fact longer than for the next longer one (Table), which speaks strongly against a through-bond quenching mechanism, but can be understood in terms of internal friction (steric hindrance effects) [36]. We encounter this effect in daily life: It is more difficult to make a knot in a very short rope than in a longer one.

In the second experiment (Scheme 6), we have exchanged the presumably flexible amino acids glycine and serine in the backbone of the peptide by rigid cyclic proline spacers. The proline peptide has a much longer lifetime than the glycine-serine one, close to the lifetime in the absence of quencher (505 ns in D_2O). This suggests that quenching through bond is unlikely since the number of bonds remains identical in both species. The effect of rigidifying the backbone provides also strong evidence that it is the diffusion between the chain ends which is decisive for the quenching process. Incidentally, it should also be mentioned that any increase in the solvent viscosity, as it can be achieved, for example, through the addition of denaturants like urea (5 M) or guanidinium chloride (6 M) also decreases the end-to-end collision rates of flexible DBO/Trp polypeptides, consistent with a diffusive process.

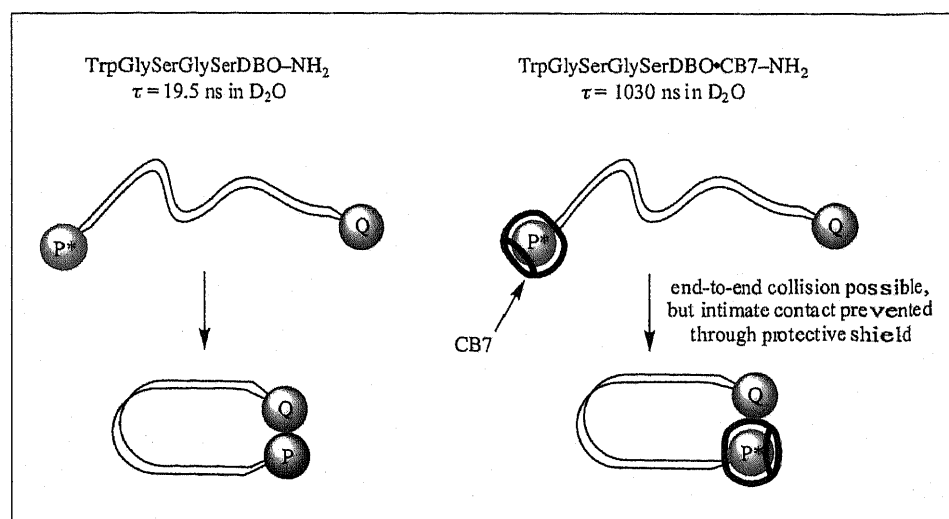
In the third experiment (Scheme 7), we have left the peptide backbone unchanged, but have added cucurbit[7]uril (CB7) to the aqueous solution of the peptide. As demonstrated by NMR experiments, CB7 complexes selectively and quantitatively the



Scheme 5



Scheme 6

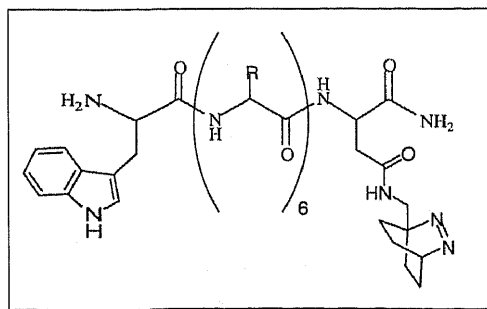


Scheme 7

DBO chromophore ($K = 4 \times 10^5 \text{ M}^{-1}$) and thereby provides a 'protective shield' around the chromophore.[22] This shield prevents van-der-Waals contact with the quencher, which is still free to diffuse since solvent and peptide backbone have remained unchanged. The resulting lifetime of the complexed peptide was found to be 1.03 μs , suggesting that the quencher is not able to quench the excited probe at all (the longer lifetime than in D_2O results from the exclusion of oxygen and the solvent from the cavity). This result provides strong evidence for the view that quenching requires intimate contact. If quenching would occur through space or through the solvent it should have also been mediated through the supramolecular wall.

It follows from the control experiment in Scheme 6, that the fluorescence lifetimes of DBO/Trp end-labeled peptides are a quantitative measure of the flexibility or rigidity of the peptide backbone. We have therefore most recently synthesized a series of random-coil peptides, in which Trp and DBO are separated by a sequence of identical amino acids (see structure below) [24]. Each peptide has a characteristic fluorescence lifetime, which can be interpreted in terms of the conformational flexibility, which a particular amino acid imposes on the backbone. This allows one to define a conformational flexibility scale for amino acids in peptides. The following order of flexibility applies, where glycine gives rise to the most flexible peptide and proline produces the most rigid one:

Gly > Ser > Asp, Asn, Ala > Thr, Leu > Phe, Glu, Gln > His, Arg > Lys > Val > Ile > Pro



In summary, the intramolecular fluorescence quenching of fluorazophores provides a distinct tool for investigations in the area of biopolymer dynamics. Future studies will involve oligonucleotides, larger, structured peptides, mutation effects, the determination of activation energies, and the transfer of the kinetic results to applications in high-throughput screening technology, where the long fluorescence lifetime provides the additional advantage of sup-

pressing background fluorescence through time-resolved detection (see Fig. 1).

Acknowledgements

This work was generously supported through the Swiss National Science Foundation (grant No. 620-58000). The studies were also performed within the Swiss National Research Program "Supramolecular Functional Materials" NFP 47 (grant No. 4047-057552).

Received: February 25, 2003

- [1] B. Valeur, 'Molecular Fluorescence', Wiley-VCH, Weinheim, 2002.
- [2] W.M. Nau, X. Wang, *ChemPhysChem* 2002, 3, 393-398.
- [3] W.M. Nau, *EPA Newsl.* 2000, 70, 6-29.
- [4] C. Marquez, W.M. Nau. Unpublished result.
- [5] a) W.L. Mock, in 'Comprehensive Supramolecular Chemistry', vol. 2, Ed.: F. Vögtle, Elsevier, Oxford, 1996, pp. 477-493; b) J. Kim, I.S. Jung, S.Y. Kim, E. Lee, J.K. Kang, S. Sakamoto, K. Yamaguchi, K. Kim, *J. Am. Chem. Soc.* 2000, 122, 540-541.
- [6] U. Pischel, X. Zhang, B. Hellrung, E. Haselbach, P.-A. Müller, W.M. Nau, *J. Am. Chem. Soc.* 2000, 122, 2027-2034.
- [7] U. Pischel, W.M. Nau, *J. Phys. Org. Chem.* 2000, 13, 640-647.
- [8] U. Pischel, X. Allonas, W.M. Nau, *J. Inf. Recording* 2000, 25, 311-321.
- [9] U. Pischel, W.M. Nau, *J. Am. Chem. Soc.* 2001, 123, 9727-9737.
- [10] U. Pischel, W.M. Nau, *Photochem. Photobiol. Sci.* 2002, 1, 141-147.
- [11] D. Klapstein, U. Pischel, W.M. Nau, *J. Am. Chem. Soc.* 2002, 124, 11349-11357.
- [12] W.M. Nau, G. Greiner, J. Wall, H. Rau, M. Olivucci, M.A. Robb, *Angew. Chem. Int. Ed.* 1998, 37, 98-101.
- [13] A. Sinicropi, U. Pischel, R. Basosi, W.M. Nau, M. Olivucci, *Angew. Chem. Int. Ed.* 2000, 39, 4582-4586.
- [14] A. Sinicropi, R. Pogni, R. Basosi, M.A. Robb, G. Gramlich, W.M. Nau, M. Olivucci, *Angew. Chem. Int. Ed.* 2001, 40, 4185-4189.
- [15] W.M. Nau, *J. Am. Chem. Soc.* 1998, 120, 12614-12618.
- [16] X. Zhang, C. Erb, J. Flammer, W.M. Nau, *Photochem. Photobiol.* 2000, 71, 524-533.
- [17] G. Gramlich, J. Zhang, W.M. Nau, *J. Am. Chem. Soc.* 2002, 124, 11252-11253.
- [18] W.M. Nau, X. Zhang, *J. Am. Chem. Soc.* 1999, 121, 8022-8032.
- [19] X. Zhang, G. Gramlich, X. Wang, W.M. Nau, *J. Am. Chem. Soc.* 2002, 124, 254-263.
- [20] X. Zhang, W.M. Nau, *Angew. Chem. Int. Ed.* 2000, 39, 544-547.
- [21] B. Mayer, X. Zhang, W.M. Nau, G. Marconi, *J. Am. Chem. Soc.* 2001, 123, 5240-5248.
- [22] C. Marquez, W.M. Nau, *Angew. Chem. Int. Ed.* 2001, 40, 4387-4390.
- [23] R.R. Hudgins, F. Huang, G. Gramlich, W.M. Nau, *J. Am. Chem. Soc.* 2002, 124, 556-564.
- [24] F. Huang, W.M. Nau, *Angew. Chem. Int. Ed.* 2003, 42, in press.
- [25] X. Wang, W.M. Nau. Unpublished results.
- [26] O. Bieri, J. Wirz, B. Hellrung, M. Schutkowski, M. Drewello, T. Kieflhaber, *Proc. Natl. Acad. Sci. USA* 1999, 96, 9597-9601.
- [27] L.J. Lapidus, W.A. Eaton, J. Hofrichter, *Proc. Natl. Acad. Sci. USA* 2000, 97, 7220-7225.
- [28] A.R. Fersht, *Curr. Opin. Struct. Biol.* 1997, 7, 3-9.
- [29] D. Pogoćki, E. Ghezzi-Schöneich, C. Schöneich, *J. Phys. Chem. B* 2001, 105, 1250-1259.
- [30] S. Hayward, *Proteins* 1999, 36, 425-435.
- [31] I.-C. Yeh, G. Hummer, *J. Am. Chem. Soc.* 2002, 124, 6563-6568.
- [32] A. Szabo, K. Schulten, Z. Schulten, *J. Chem. Phys.* 1980, 72, 4350-4357.
- [33] R.W. Pastor, R. Zwanzig, A. Szabo, *J. Chem. Phys.* 1996, 105, 3878-3882.
- [34] U.W. Suter, M. Mutter, P.J. Flory, *J. Am. Chem. Soc.* 1976, 98, 5740-5745.
- [35] M. Mutter, U.W. Suter, P.J. Flory, *J. Am. Chem. Soc.* 1976, 98, 5745-5748.
- [36] X. Wang, E.N. Bodunov, W.M. Nau, submitted for publication.
- [37] W.M. Nau, U. Pischel, *Angew. Chem. Int. Ed.* 1999, 38, 2885-2888.
- [38] W.M. Nau, G. Greiner, H. Rau, M. Olivucci, M.A. Robb, *Ber. Bunsen-Ges. Phys. Chem.* 1998, 102, 486-492.
- [39] W.M. Nau, G. Greiner, H. Rau, J. Wall, M. Olivucci, J.C. Scaiano, *J. Phys. Chem. A* 1999, 103, 1579-1584.
- [40] A.K. Mishra, R. Chandrasekar, M. Faraggi, M.H. Klapper, *J. Am. Chem. Soc.* 1994, 116, 1414-1422.
- [41] W.G. McGimpsey, L. Chen, R. Carraway, W.N. Samaniego, *J. Phys. Chem. A* 1999, 103, 6082-6090.
- [42] P.J. Wagner, P. Klán, *J. Am. Chem. Soc.* 1998, 121, 9626-9635.
- [43] E. Haas, E. Katchalski-Katzir, I.Z. Steinberg, *Biopolymers* 1978, 17, 11-31.

Intramolecular singlet–singlet energy transfer in antenna-substituted azoalkanes

Uwe Pischel,^a Fang Huang^b and Werner M. Nau^{*b,c}

^a REQUIMTE/Department of Chemistry, Faculty of Sciences, University of Porto, R. Campo Alegre, 4169-007 Porto, Portugal

^b Department of Chemistry, University of Basel, Klingelbergstrasse 80, CH-4056 Basel, Switzerland

^c School of Engineering and Science, International University Bremen, Campus Ring 1, D-28759 Bremen, Germany. E-mail: w.nau@iu-bremen.de

Received 18th September 2003, Accepted 3rd November 2003

First published as an Advance Article on the web 2nd December 2003

Two novel azoalkane bichromophores and related model compounds have been synthesised and photophysically characterised. Dimethylphenylsiloxy (DPSO) or dimethylnaphthylsiloxy (DNSO) serve as aromatic donor groups (antenna) and the azoalkane 2,3-diazabicyclo[2.2.2]oct-2-ene (DBO) as the acceptor. The UV spectral window of DBO (250–300 nm) allows selective excitation of the donor. Intramolecular singlet–singlet energy transfer to DBO is highly efficient and proceeds with quantum yields of 0.76 with DPSO and 0.99 with DNSO. The photophysical and spectral properties of the bichromophoric systems suggest that energy transfer occurs through diffusional approach of the donor and acceptor within a van der Waals contact at which the exchange mechanism is presumed to dominate. Furthermore, akin to the behaviour of electron-transfer systems in the Marcus inverted region, a rate of energy transfer 2.5 times slower was observed for the system with the more favourable energetics, *i.e.* singlet–singlet energy transfer from DPSO proceeded slower than from DNSO, although the process is more exergonic for DPSO (-142 kJ mol^{-1} for DPSO *versus* -67 kJ mol^{-1} for DNSO).

Introduction

2,3-Diazabicyclo[2.2.2]oct-2-ene (DBO) is a bicyclic azoalkane which has applications as a fluorescent probe for supramolecular assemblies, *e.g.* cyclodextrin- or cucurbituril-based host–guest systems,^{1,2} for the detection of antioxidants or nucleotides,^{3–5} and as a fluorescent label to study biopolymer dynamics.^{6–9} In particular, the exceptionally long fluorescence lifetime of DBO¹⁰ in solution (up to 1 μs), along with distinct novel quenching mechanisms, *i.e.* aborted hydrogen and electron transfer,^{11,12} open a wide dynamic range for the assessment of weak or remote interactions while maintaining a high selectivity towards the quencher. The low energy n, π^* transition of DBO allows selective excitation of the chromophore ($\lambda_{\text{max}} = 378 \text{ nm}$ hexane). However, the extinction coefficient of this transition is comparatively small ($\epsilon_{378} \approx 180 \text{ M}^{-1}\text{cm}^{-1}$ in alkanes),² due to poor spatial overlap between the n and π^* orbitals.

For many applications, it is essential to improve the absorption properties, while preserving the advantageous fluorescent properties, of the azoalkane. We have now investigated the feasibility of attaching an antenna for efficient light absorption and subsequent singlet energy transfer to the azoalkane. Numerous studies regarding intramolecular energy transfer involving singlet–^{13–17} as well as triplet–excited states have been reported.^{18,19} Variation of excited-state energies and spacer properties, *e.g.* flexibility and intra-chromophore distances, has provided valuable insights into the mechanistic details of this basic photophysical process.^{20,21} Although azoalkanes have been the subject of intermolecular energy-transfer studies,^{22–25} the only *intramolecular* study deals with triplet–triplet energy transfer from carbonyl chromophores to azoalkanes.²⁶

Morrison and co-workers have introduced the dimethylphenylsiloxy (DPSO) group as an antenna for singlet–singlet energy transfer (SSET) to keto functions in steroidal molecules.^{27–29} Owing to its high excitation energy, the DPSO antenna can undergo efficient, highly exergonic energy transfer

to an acceptor chromophore, and has a short excited-state lifetime, which reduces competitive intermolecular quenching reactions. Energy-transfer studies from DPSO to DBO appeared particularly promising, since DBO offers a UV spectral window between 250 and 300 nm, which should allow very selective excitation of the DPSO antenna. In addition to DPSO, we planned to study the dimethylnaphthylsiloxy (DNSO) group as a new antenna function. This was intended to allow the influence of the thermodynamics on the energy-transfer process to be investigated.

Two bichromophoric compounds with a phenyl or naphthyl moiety linked by a siloxy spacer to the bridgehead position of DBO (**1a** and **2a**) were also synthesised as part of this project (Chart 1). These molecules were photophysically characterised by UV absorption as well as steady-state and time-resolved fluorescence spectroscopy and compared with the antenna model compounds lacking the DBO acceptor (**1b** and **2b**).

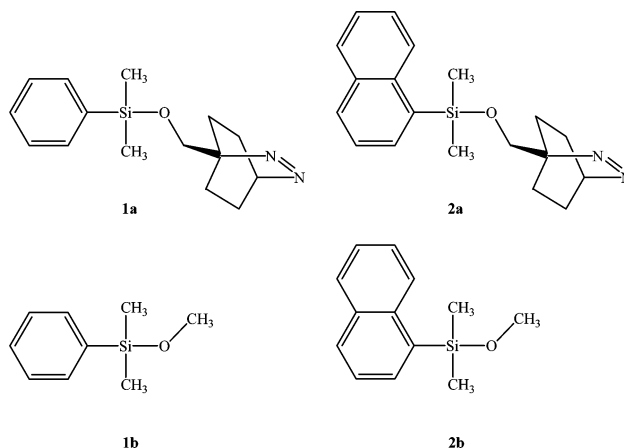


Chart 1 Structures of the bichromophoric azoalkanes (**1a** and **2a**) and antenna model compounds (**1b** and **2b**).

Experimental

Materials

1-(Hydroxymethyl)-2,3-diazabicyclo[2.2.2]oct-2-ene²⁶ and chlorodimethylnaphthylsilane³⁰ were synthesised according to literature procedures. All other chemicals and solvents for the synthesis were used as received from Aldrich. Column chromatography was performed with 70–230 μm silica gel from Merck. Cyclohexane was of spectroscopic quality from Fluka. Fluorescence grade benzene (Fluka) and naphthalene (National Bureau of Standards) were used as fluorescence standards.

Spectroscopic measurements

The absorption spectra were recorded using a Perkin-Elmer Lambda 19 spectrometer. All fluorescence measurements were performed in degassed solutions (3 freeze–pump–thaw cycles) at ambient temperature (24 °C). A home-made quartz cell with a high vacuum Teflon stopcock was used. Fluorescence spectra were recorded with a Glen Spectra Fluorolog Spex spectrometer. Fluorescence lifetimes were determined using an Edinburgh FLS900 single-photon counting setup operated by a 1.5 ns pulse width hydrogen flash lamp (nF900). The resulting data were analysed by means of monoexponential decay functions and a re-convolution function for the excitation light pulse. The concentration of bichromophoric compounds was kept low (10^{-5} – 10^{-4} M) to exclude competitive intermolecular quenching.

Synthesis of the antenna-substituted azoalkanes **1a** and **2a**

General procedure. A solution of 1 mmol 1-(hydroxymethyl)-2,3-diazabicyclo[2.2.2]oct-2-ene, 1.3 mmol triethylamine, and 1.5 mmol chlorodimethylarylsilane in 10 ml dry dichloromethane was stirred at room temperature under argon for 24 h. The resulting reaction mixture was extracted with 2×5 ml water and the resulting organic layer was dried over Na_2SO_4 . After filtration and solvent evaporation, a yellowish oil was obtained. Column chromatography with hexane–ethylacetate (1 : 1) yielded the product as colourless oil.

1-(Dimethylphenyl)siloxymethyl-2,3-diazabicyclo[2.2.2]oct-2-ene (1a**).** Yield 69%. UV/Vis (cyclohexane): λ 253 (log $\epsilon = 2.28$), 259 (2.44), 264 (2.44), 270 (2.30), 379 (2.22) nm. ¹H-NMR (400 MHz, CDCl_3): δ 0.44 [6 H, s, $(\text{CH}_3)_2\text{Si}$], 1.07–1.16 (2 H, m, CH_2), 1.28–1.38 (2 H, m, CH_2), 1.52–1.62 (4 H, m, CH_2), 4.17 (2 H, s, CH_2O), 5.12 (1 H, t, $J = 3.5$ Hz, CH), 7.37–7.41 (3 H, m, CH aryl), 7.60–7.64 (2 H, m, CH aryl) ppm. ¹³C-NMR (126 MHz, CDCl_3): δ -1.8 [2 C, $(\text{CH}_3)_2\text{Si}$], 21.6 (2 C, CH_2), 23.1 (2 C, CH_2), 61.9 (CH), 67.4 (C_q), 68.6 (CH_2O), 127.8 (2 C, CH aryl), 129.6 (2 C, CH aryl), 133.6 (CH aryl), 137.8 (C_q aryl) ppm. Elemental analysis calcd for $\text{C}_{15}\text{H}_{22}\text{SiN}_2\text{O}$: C, 65.65; H, 8.08; N, 10.21; found: C, 65.75; H, 8.02; N, 10.15%.

1-(Dimethylnaphth-1-yl)siloxymethyl-2,3-diazabicyclo[2.2.2]oct-2-ene (2a**).** Yield 19%. UV/Vis (cyclohexane): λ 262 (log $\epsilon = 3.58$), 273 (3.81), 283 (3.89), 294 (3.73), 379 (2.24) nm. ¹H-NMR (400 MHz, CDCl_3): δ 0.61 [6 H, s, $(\text{CH}_3)_2\text{Si}$], 1.11–1.16 (2 H, m, CH_2), 1.26–1.35 (2 H, m, CH_2), 1.54–1.61 (4 H, m, CH_2), 4.18 (2 H, s, CH_2O), 5.12 (1 H, t, $J = 3.5$ Hz, CH), 7.46–7.53 (3 H, m, CH aryl), 7.79 (1 H, dd, $J = 1.5$ and 5.8 Hz, CH aryl), 7.85–7.91 (2 H, m, CH aryl), 8.32–8.34 (1 H, m, CH aryl) ppm. ¹³C-NMR (126 MHz, CDCl_3): δ -0.6 [2 C, $(\text{CH}_3)_2\text{Si}$], 21.6 (2 C, CH_2), 23.2 (2 C, CH_2), 61.9 (CH), 67.4 (C_q), 68.7 (CH_2O), 125.0 (CH aryl), 125.5 (CH aryl), 126.0 (CH aryl), 128.3 (CH aryl), 128.9 (CH aryl), 130.4 (CH aryl), 133.3 (CH aryl), 133.9 (C_q aryl), 135.8 (C_q aryl), 136.9 (C_q aryl) ppm. Elemental analysis calcd for $\text{C}_{19}\text{H}_{24}\text{SiN}_2\text{O}$: C, 70.33; H, 7.46; N, 8.63; found: C, 70.32; H, 7.46; N, 8.70%.

Synthesis of the antenna model compounds **1b** and **2b**

General procedure. 2.3 mmol of sodium were dissolved in 3 ml methanol and 1.4 mmol of chlorodimethylarylsilane were added dropwise. The mixture was stirred for 2 h at room temperature. The solvent was evaporated and the residue was treated with 5 ml of freshly distilled diethyl ether. After filtration, the solvent was removed by evaporation and the resulting oil was purified by Kugelrohr microdistillation to yield a colourless product.

Methoxydimethylphenylsilane (1b**).** Yield 39%. UV/Vis (cyclohexane): λ 253 (log $\epsilon = 2.26$), 259 (2.43), 264 (2.42), 270 (2.29) nm. ¹H-NMR (400 MHz, CDCl_3): δ 0.39 [6 H, s, $(\text{CH}_3)_2\text{Si}$], 3.45 (3 H, s, CH_3O), 7.36–7.43 (3 H, m, CH aryl), 7.56–7.60 (2 H, m, CH aryl) ppm. ¹³C-NMR (126 MHz, CDCl_3): δ -2.4 [2 C, $(\text{CH}_3)_2\text{Si}$], 50.7 (CH_3O), 127.9 (2 C, CH aryl), 129.6 (2 C, CH aryl), 133.4 (CH aryl), 137.4 (C_q aryl) ppm. Elemental analysis calcd for $\text{C}_9\text{H}_{14}\text{SiO}$: C, 65.00; H, 8.49; found: C, 64.29; H, 8.04%.

Methoxydimethylnaphth-1-ylsilane (2b**).** Yield 30%. UV/Vis (cyclohexane): λ 262 (log $\epsilon = 3.59$), 273 (3.81), 283 (3.89), 294 (3.72) nm. ¹H-NMR (400 MHz, CDCl_3): δ 0.57 [6 H, s, $(\text{CH}_3)_2\text{Si}$], 3.48 (3 H, s, CH_3O), 7.47–7.57 (3 H, m, CH aryl), 7.76 (1 H, d, $J = 7.1$ Hz, CH aryl), 7.88–7.93 (2 H, m, CH aryl), 8.33 (1 H, d, $J = 8.1$ Hz, CH aryl) ppm. ¹³C-NMR (126 MHz, CDCl_3): δ -1.0 [2 C, $(\text{CH}_3)_2\text{Si}$], 50.6 (CH_3O), 125.0 (CH aryl), 125.5 (CH aryl), 126.1 (CH aryl), 128.0 (CH aryl), 128.9 (CH aryl), 130.4 (CH aryl), 133.3 (CH aryl), 133.9 (C_q aryl), 135.5 (C_q aryl), 136.9 (C_q aryl) ppm. Elemental analysis calcd for $\text{C}_{13}\text{H}_{16}\text{SiO}$: C, 72.17; H, 7.45; found: C, 72.04; H, 7.39%.

Results and discussion

Absorption properties

The UV spectra of the individual chromophores in cyclohexane are shown in Fig. 1. The aryl residues in the antenna model compounds show characteristic vibrationally structured π, π^* transitions, with a weaker band for the phenyl moiety in **1b** ($\lambda_{\text{max}} = 259$ nm, $\epsilon = 275$ $\text{M}^{-1} \text{cm}^{-1}$), due to its symmetry-forbidden nature, and a red-shifted absorption with a high transition probability ($\lambda_{\text{max}} = 283$ nm, $\epsilon = 7800$ $\text{M}^{-1} \text{cm}^{-1}$) for the naphthalene chromophore in **2b**. The symmetry-allowed but, due to poor spatial overlap of the participating n and π^* orbitals, orbital-forbidden transition³¹ of the azoalkane at 379 nm has an ϵ value of ca. 170 $\text{M}^{-1} \text{cm}^{-1}$ in hydrocarbon solvents.

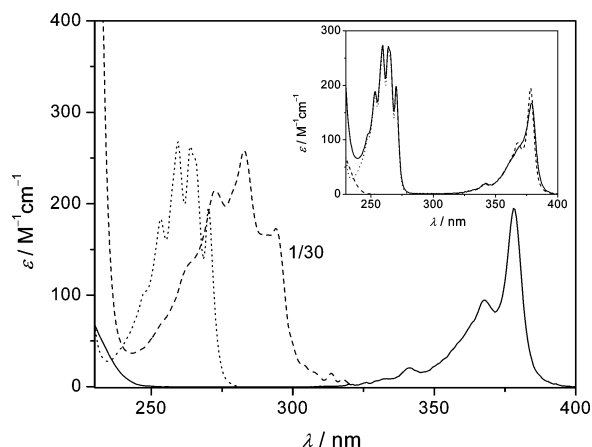


Fig. 1 Absorption spectra of the antenna model compounds **1b** (···) and **2b** (---; divided by 30) and the parent DBO (—). Note that the absorption of compounds **1b** and **2b** occurs in the spectral window of DBO, therefore allowing exclusive excitation of the antenna. The inset shows the absorption spectrum of the bichromophore **1a** (—) in comparison to the individual components, the antenna model **1b** (···) and the parent DBO (---), all in cyclohexane.

Table 1 Photophysical data for the investigated compounds (see Chart 1) in cyclohexane

	τ_f^a /ns	Φ_f^b	$\Phi_{\text{SSET}}^{c,d}$	$k_{\text{SSET}}^{e/s^{-1}}$	$J_{d-d}/\text{cm}^6 \text{ mol}^{-1}$	$J_{\text{ex}}^e/\text{cm}$	$k_{\text{inter}}^f/\text{M}^{-1} \text{ s}^{-1}$
1a	0.63	0.014	0.76	1.2×10^9	4.6×10^{-15}	1.3×10^{-5}	1.3×10^8
1b	2.61	0.040					
2a	0.33	0.008	0.99	3.0×10^9	4.8×10^{-14}	1.2×10^{-4}	1.5×10^{10}
2b	54.0	0.279					

^a Measured by single photon counting; 5% error. ^b Measured by steady-state fluorescence spectroscopy using benzene ($\Phi_f = 0.06$) or naphthalene ($\Phi_f = 0.19$) in cyclohexane as standards;³⁴ 10% error. ^c Equations for calculation are given in the text. ^d Quantum yields for energy transfer are based on time-resolved data. ^e Note that these values differ significantly from the Dexter spectral overlap integrals calculated by Engel *et al.*²⁴ for the intermolecular energy transfer between DBO and benzene ($J_{\text{ex}} = 2.0 \times 10^{-7} \text{ cm}$) or naphthalene ($J_{\text{ex}} = 6.8 \times 10^{-5} \text{ cm}$) in isoctane. ^f Intermolecular fluorescence quenching rate constants of benzene or naphthalene by DBO in isoctane taken from ref. 24.

The spectra of the bichromophoric systems are a superposition of the two separated chromophores, as shown in the inset of Fig. 1 for **1a** and the individual chromophores **1b** and DBO. Neither the spectral shapes nor the oscillator strengths are altered, which rules out a sizable electronic interaction between the two chromophores in the ground state. In fact, the only difference is that the spectra of the bichromophoric compounds reveal a marginal red shift (*ca.* 1 nm) of the maximum of the n, π^* transition of the azoalkane residue compared to the parent DBO. This effect may be indicative of the presence of the remote aryl groups, which should increase the apparent polarisability in the surroundings of the azo chromophore.³² Recent studies of DBO in various solvents have revealed a marked dependence of the absorption maximum on the polarisability of the environment: the higher the polarisability, the more red-shifted (and more intense) is the absorption.²

Note in particular the large UV window of DBO and the perfect spectral match of the antenna absorptions in the bichromophoric systems (Fig. 1), which render them quite unique. In photophysically related donor–acceptor combinations of dimethoxynaphthalene and bicyclic (di)ketones, selective excitation of the donor has only been achieved by exploiting the differences in molar absorption coefficients.³³

Fluorescence measurements

To investigate intramolecular singlet–singlet energy transfer in the antenna-substituted azoalkanes, steady-state as well as time-resolved fluorescence measurements were performed. Selective excitation of the antenna results, in both cases, in a weak residual fluorescence of the aromatic moiety ($\lambda_{\text{max}} = 295 \text{ nm}$ for **1a** and 345 nm for **2a**). The emission spectra are dominated by the characteristic broad band of DBO, with a maximum at 430 nm . In both cases, the excitation spectrum, with $\lambda_{\text{obs}} = 430 \text{ nm}$, matched the absorption spectrum of the bichromophore, which provides the signature of energy transfer from the aryl residue to the azoalkane chromophore. This is exemplified in Fig. 2, which shows the fluorescence emission and

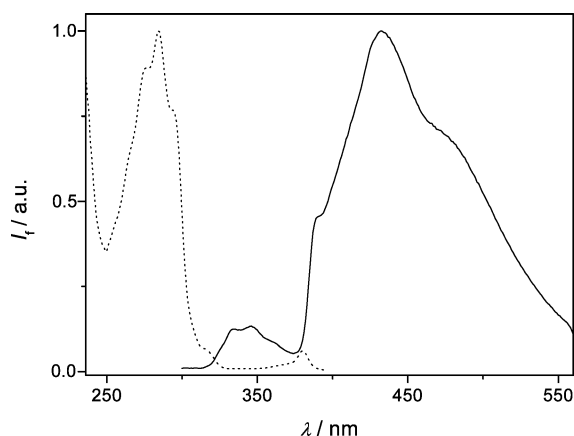


Fig. 2 Fluorescence emission (—; $\lambda_{\text{exc}} = 283 \text{ nm}$) and excitation (···; $\lambda_{\text{obs}} = 430 \text{ nm}$) spectra of **2a** in cyclohexane ($2.1 \times 10^{-5} \text{ M}$).

excitation spectra of the DNSO-substituted azoalkane **2a** in cyclohexane. In order to quantify the fluorescence properties, the emission quantum yields of the aryl residues in the antenna model compounds (**1b** and **2b**) and the bichromophoric systems (**1a** and **2a**) were determined (*cf.* Table 1). Benzene and naphthalene were used as reference standards ($\Phi_f = 0.06$ and 0.19 , respectively, in cyclohexane).³⁴

The shortened fluorescence lifetimes of the antenna in **1a** and **2a** compared to their respective model compounds, **1b** and **2b**, as obtained from single-photon counting-based measurements (*cf.* Table 1 and Fig. 3) are in line with the steady-state fluorescence quenching results. Deviations from monoexponential decay behaviour were not observed. The lifetimes are not dependent on the concentration of the bichromophoric system within the examined concentration range (10^{-5} – 10^{-4} M), which mitigates against intermolecular association and static quenching in the nonpolar solvent. As will be shown below, a contact-quenching mechanism is operative, for which deviations from monoexponential decay kinetics are only expected on a picosecond timescale.³⁵

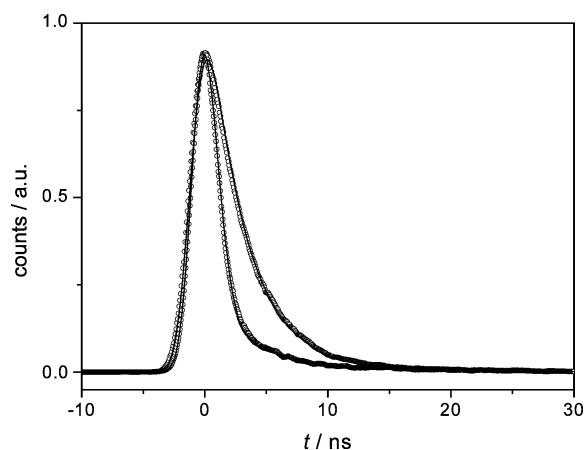


Fig. 3 Time-resolved fluorescence decay kinetics of **1a** (lower trace) and **1b** (upper trace) in cyclohexane ($[\mathbf{1a}] = 3.5 \times 10^{-4} \text{ M}$, $[\mathbf{1b}] = 1.9 \times 10^{-3} \text{ M}$; $\lambda_{\text{exc}} = 270 \text{ nm}$, $\lambda_{\text{obs}} = 295 \text{ nm}$). The solid lines represent reconvolution fits taking into account the lamp profile.

The assignment of the mechanism of intramolecular fluorescence quenching as singlet–singlet energy transfer from the arene to the azo chromophore requires attention. First, the fraction of naphthalene fluorescence which is lost due to intramolecular quenching is fully converted, within instrumental error, to DBO emission (*cf.* Fig. 2). Second, electron transfer, the most likely competitive quenching mechanism, is expected to be strongly endergonic in nonpolar cyclohexane for both phenyl and naphthyl. Even if the calculation is done for a polar solvent (acetonitrile),³⁶ only slightly exergonic thermodynamics applies for the oxidation of DBO ($\Delta G_{\text{et}} \approx -30 \text{ kJ mol}^{-1}$ for naphthalene and *ca.* -5 kJ mol^{-1} for benzene), while photo-reduction of DBO is already an uphill process ($\Delta G_{\text{et}} \approx +34 \text{ kJ mol}^{-1}$ for naphthalene and *ca.* $+33 \text{ kJ mol}^{-1}$ for benzene). Electron transfer is therefore not expected to compete with the

strongly exergonic singlet–singlet energy transfer (-142 kJ mol^{-1} for **1a** and -67 kJ mol^{-1} for **2a**).^{15,18,36,37}

Note that the fluorescence lifetime of the DBO chromophore remains unaffected for the phenyl derivative **1a** (270 versus 275 ns for the parent DBO in cyclohexane), but is shortened for the naphthyl derivative **2a** (106 ns). The weak quenching of DBO fluorescence by naphthalene is presumably induced by intramolecular exciplex formation, which is known for the quenching of n, π^* excited states by arenes.^{10,38,39} The naphthyl group is a stronger quencher than the phenyl group, as is also indicated by the *intermolecular* quenching rate constants of DBO, which are $1.0 \times 10^5 \text{ M}^{-1} \text{ s}^{-1}$ for benzene¹⁰ and $6.7 \times 10^6 \text{ M}^{-1} \text{ s}^{-1}$ for naphthalene.

Rate and efficiency of singlet–singlet energy transfer

The efficiency of singlet–singlet energy transfer (Φ_{SSET}) and the associated intramolecular rate constant (k_{SSET}) can be determined by using eqn. 1 and 2. The indices (a) and (b) refer to the compounds in Chart 1.

$$\Phi_{\text{SSET}} = 1 - \frac{\Phi_{\text{f(a)}}}{\Phi_{\text{f(b)}}} = 1 - \frac{\tau_{\text{f(a)}}}{\tau_{\text{f(b)}}} \quad (1)$$

$$k_{\text{SSET}} = \frac{\Phi_{\text{SSET}}}{\tau_{\text{f(a)}}} \quad (2)$$

The results are shown in Table 1. The quantum yields were calculated on the basis of the fluorescence lifetimes, which is made possible by the monoexponentiality of the decays. The use of steady-state fluorescence quantum yields leads, within error limits, to virtually the same values (0.66 for **1a** and 0.97 for **2a**). The intramolecular rate constant for SSET can be calculated from the lifetimes as $1.2 \times 10^9 \text{ s}^{-1}$ for the phenyl-substituted azo chromophore **1a** and as $3.0 \times 10^9 \text{ s}^{-1}$ for **2a**. These values are of the same order of magnitude as those observed for related bichromophoric systems with similar donor–acceptor spacing.⁴⁰

Strikingly, these rate constants seem to contradict the thermodynamic data for energy transfer (see above), *i.e.* the process is a factor of 2.5 *slower* for the thermodynamically favoured case **1a**, for which singlet–singlet energy transfer is 75 kJ mol^{-1} more exergonic than for **2a**. This inverted effect has previously been observed for *intermolecular* singlet–singlet energy transfer between aromatics and azoalkanes.^{22–24} In essence, we have reached the inverted region, where energy transfer is slowed down, regardless of favourable thermodynamics, due to decreased Franck–Condon overlap between the initial and final states, akin to the Marcus inverted region for electron transfer.⁴¹

The dominant quantities are the spectral overlap integrals (J) of the donor emission and the acceptor absorption, which enter directly the expressions (eqn. 3 and 4) for the rate constants of energy transfer according to the dipole–dipole (Förster, $k_{\text{d-d}}$) or the exchange (Dexter, k_{ex}) mechanisms.²¹ Note that the absorption band is normalised in Dexter theory such that a small absolute extinction coefficient of the acceptor (in this case, the azo chromophore) reduces the energy-transfer rate only for the dipole–dipole mechanism.

$$k_{\text{d-d}} = \frac{1}{\tau_{\text{D}}} \left(\frac{R_0}{R} \right)^6 \quad (3)$$

$$\text{where } R_0^6 = \frac{9000 \ln 10 (\kappa^2 \Phi_{\text{D}})}{128 \pi^5 n^4 N_{\text{A}}} J_{\text{d-d}}$$

$$k_{\text{ex}} = \frac{2\pi}{\hbar} K J_{\text{ex}} e^{(-2R/L)} \quad (4)$$

The spectral overlap integrals according to Förster ($J_{\text{d-d}}$) and Dexter (J_{ex}) theory¹⁴ were obtained by numerical integration and are presented in Table 1. Note that the absolute values for J are comparable to those obtained for similar intramolecular systems composed of 1,4-dimethoxynaphthalene and diketones.³³ For the phenyl case, **1a**, the excitation energy of the donor exceeds significantly that of the acceptor. This causes a mismatch of donor emission and acceptor absorption bands (*cf.* Fig. 4) and reduces J for both mechanisms. With the known fluorescence quantum yields and lifetimes in the absence of quencher (see values for **1b** and **2b** in Table 1), and by assuming a constant specific orbital interaction K (in eqn. 4, only for Dexter mechanism), the expectation factors by which energy transfer for **2a** should be faster than for **1a** can be calculated. Factors of 3.5 for the Förster mechanism and 9.2 for the Dexter mechanism are obtained, in qualitative agreement with experiment, but at variance with expectations based on the thermodynamics alone. The faster energy-transfer rates for **2a** are mainly due to the larger J values, while the differences in the radiative decay rates (which enter eqn. 3 as the ratio of Φ_{D} and τ_{D}) somewhat moderate the net effect in the dipole–dipole case.

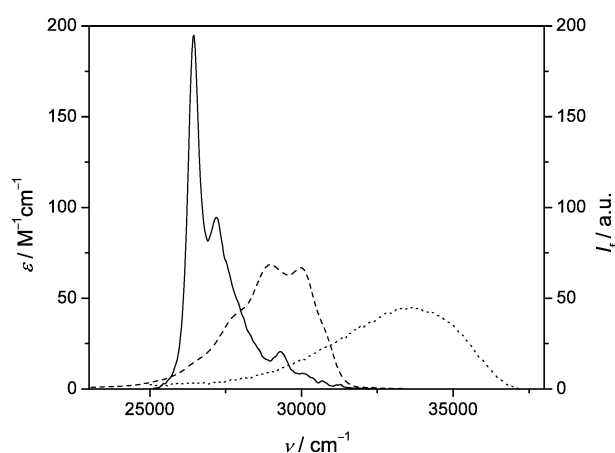


Fig. 4 Absorption spectrum of the parent DBO (—) and fluorescence spectra of the antenna model compounds **1b** (· · ·; $\lambda_{\text{exc}} = 249 \text{ nm}$) and **2b** (---; $\lambda_{\text{exc}} = 283 \text{ nm}$) in cyclohexane (fluorescence spectra normalised to same area as absorption spectrum). Note the very poor spectral overlap for the **1b**–DBO donor–acceptor pair.

Mechanism of energy transfer

Singlet–singlet energy transfer by the exchange mechanism requires orbital overlap, *i.e.* contact between probe and quencher. Fluorescence resonance energy transfer can occur over larger distances, as can be judged from the critical transfer distance, R_0 (eqn. 3).

With known spectral data and $\kappa^2 = 2/3$, the critical transfer radii for **1a** and **2a** can be calculated as $R_0 = 5.4$ and 11.1 \AA , respectively. These critical radii provide the distance at which energy transfer and the deactivation by other processes occur at the same rate. However, to account for the experimentally observed energy-transfer efficiencies, which are greater than 50% (Table 1), energy transfer must occur at a shorter mean distance (R), which can be derived from eqn. 5.

$$\Phi_{\text{SSET}} = \frac{1}{1 + \left(\frac{R}{R_0} \right)^6} \quad (5)$$

Mean distances of 4.5 and 5.2 \AA result for **1a** and for **2a**, respectively, which suggest that probe and quencher come effectively within van der Waals contact to undergo quenching (the sum of the radii of probe and quencher is *ca.* 5 \AA). This means that singlet–singlet energy transfer in the bichromophoric systems proceeds predominantly by the exchange

mechanism, which is generally anticipated when forbidden acceptor transitions are involved (in this case, the orbital-forbidden n, π^* transition of DBO).^{20,21} Previous studies on intermolecular energy transfer-induced fluorescence quenching of aromatics by azoalkanes have also led to the conclusion that an exchange mechanism operates.^{22–25,42} For example, steric hindrance effects were observed, which stress the requirement for orbital overlap between donor and acceptor orbitals.²⁵

The efficient quenching demonstrates that donor and acceptor must rapidly come into contact within the excited-state lifetime of the donor, *i.e.* within several nanoseconds. In fact, mutual diffusion of the two ends of a very short polymer chain is expected to occur on a timescale as fast as 1 ns.⁸ The observed timescale for energy transfer is, therefore, consistent with the idea that energy transfer is promoted by a diffusive intramolecular collision between the donor and acceptor.⁴⁰ Intramolecular diffusion should occur faster for the phenyl derivative **1a**, since the phenyl group has a higher diffusion coefficient. The fact that intramolecular quenching in **1a** is nevertheless slower reflects the less favourable electronic requirement for energy transfer (small overlap integral), *i.e.* not every collision between the phenyl and DBO residues may lead to quenching. In fact, the intermolecular fluorescence quenching rate constants of benzene and naphthalene by DBO (k_{inter} values in Table 1) demonstrate that the quenching of benzene, in contrast to naphthalene, is not diffusion controlled.²⁴

Comparison of the quenching rate constants for the intramolecular and the intermolecular reaction (Table 1) reveals also that the differentiation between the rate constants for the two aromatic chromophores is much less pronounced for the intramolecular case (the k_{SSET} values differ by a factor of 2–3) compared to the intermolecular case (the k_{inter} values differ by a factor of 100). This trend is in line with the idea that intrachain diffusion becomes an additional factor in determining the quenching rates. Note that the intramolecular diffusion coefficients of a chromophore in, for example, a polymer chain are typically 10 times smaller than the corresponding free intermolecular diffusion coefficients,^{35,43} such that the impact of electronic factors on the overall rate is less pronounced. In other words, the kinetics shifts from purely reaction controlled for the intermolecular case to partially diffusion controlled for the intramolecular case. In addition, any participation of fluorescence resonance energy transfer, which is likely to compete to an unknown extent for the intramolecular system, will tend to reduce the differential rates (see expectation factors above). The combined arguments account for the observation that the “inverted effect” on singlet–singlet energy transfer is less pronounced for the bichromophoric systems studied here than for the intermolecular reaction.

Conclusions

Two new bichromophoric DBO derivatives have been photo-physically characterised. Both perform very efficient singlet–singlet energy transfer by an exchange mechanism, which is induced by intramolecular diffusion to form van der Waals contact between donor and acceptor. An inverted effect of the intramolecular quenching rate constants on the thermodynamics of energy transfer was observed; however, this is less pronounced than for the intermolecular reaction. While the DPSO group in **1a** exhibits a weak absorption band like DBO, the DNSO group in **2a** shows an ϵ value which is *ca.* 50 times higher, which greatly improves the absorption features of DBO while performing an almost quantitative and irreversible singlet–singlet energy transfer. DNSO is therefore a suitable antenna for DBO. Unfortunately, the naphthyl group also causes some exciplex-induced quenching of the long-lived DBO chromophore, which certainly limits the scope of the antenna approach to remedy the weak absorption properties of DBO.

Acknowledgement

Financial support by the Schweizerischer Nationalfonds (NRP 47 “Supramolecular Functional Materials”) is gratefully acknowledged.

References and notes

- 1 W. M. Nau and X. Zhang, An exceedingly long-lived fluorescent state as a distinct structural and dynamic probe for supramolecular association: an exploratory study of host–guest complexation by cyclodextrins, *J. Am. Chem. Soc.*, 1999, **121**, 8022–8032.
- 2 C. Marquez and W. M. Nau, Polarizabilities inside molecular containers, *Angew. Chem., Int. Ed.*, 2001, **40**, 4387–4390.
- 3 W. M. Nau, A fluorescent probe for antioxidants, *J. Am. Chem. Soc.*, 1998, **120**, 12614–12618.
- 4 C. Marquez, U. Pischel and W. M. Nau, Selective fluorescence quenching of 2,3-diazabicyclo[2.2.2]oct-2-ene by nucleotides, *Org. Lett.*, 2003, **5**, 3911–3914.
- 5 G. Gramlich, J. Zhang and W. M. Nau, Increased antioxidant reactivity of vitamin C at low pH in model membranes, *J. Am. Chem. Soc.*, 2002, **124**, 11252–11253.
- 6 R. R. Hudgins, F. Huang, G. Gramlich and W. M. Nau, A fluorescence-based method for direct measurement of submicrosecond intramolecular contact formation in biopolymers: an exploratory study with polypeptides, *J. Am. Chem. Soc.*, 2002, **124**, 556–564.
- 7 W. M. Nau and X. Wang, Biomolecular and supramolecular kinetics in the submicrosecond time range: the fluorazophore approach, *ChemPhysChem*, 2002, **3**, 393–398.
- 8 W. M. Nau, F. Huang, X. Wang, H. Bakirci, G. Gramlich and C. Marquez, Exploiting long-lived molecular fluorescence, *Chimia*, 2003, **57**, 161–167.
- 9 F. Huang and W. M. Nau, A conformational flexibility scale for amino acids in peptides, *Angew. Chem., Int. Ed.*, 2003, **42**, 2269–2272.
- 10 W. M. Nau, G. Greiner, H. Rau, J. Wall, M. Olivucci and J. C. Scaiano, Fluorescence of 2,3-diazabicyclo[2.2.2]oct-2-ene revisited: solvent-induced quenching of the n, π^* -excited state by an aborted hydrogen atom transfer, *J. Phys. Chem. A*, 1999, **103**, 1579–1584.
- 11 W. M. Nau, G. Greiner, J. Wall, H. Rau, M. Olivucci and M. A. Robb, The mechanism for hydrogen abstraction by n, π^* excited singlet states: evidence for thermal activation and deactivation through a conical intersection, *Angew. Chem., Int. Ed.*, 1998, **37**, 98–101.
- 12 A. Sinicropi, U. Pischel, R. Basosi, W. M. Nau and M. Olivucci, Conical intersections in charge-transfer induced quenching, *Angew. Chem., Int. Ed.*, 2000, **39**, 4582–4586.
- 13 H. E. Zimmerman, T. D. Goldman, T. K. Hirzel and S. P. Schmidt, Rod-like organic molecules. Energy-transfer studies using single-photon counting, *J. Org. Chem.*, 1980, **45**, 3933–3951.
- 14 H. Oevering, J. W. Verhoeven, M. N. Paddon-Row, E. Cotsaris and N. S. Hush, Long-range exchange contribution to singlet–singlet energy transfer in a series of rigid bichromophoric molecules, *Chem. Phys. Lett.*, 1988, **143**, 488–495.
- 15 J. Kroon, A. M. Oliver, M. N. Paddon-Row and J. W. Verhoeven, Observation of a remarkable dependence of the rate of singlet–singlet energy transfer on the configuration of the hydrocarbon bridge in bichromophoric systems, *J. Am. Chem. Soc.*, 1990, **112**, 4868–4873.
- 16 F. Schael, M. B. Rubin and S. Speiser, Electronic energy transfer in solution in naphthalene-anthracene, naphthalene-acridine and benzene-DANS bichromophoric compounds, *J. Photochem. Photobiol., A*, 1998, **115**, 99–108.
- 17 S. Speiser and F. Schael, Molecular structure control of intramolecular electronic energy transfer, *J. Mol. Liq.*, 2000, **86**, 25–35.
- 18 G. L. Closs, M. D. Johnson, J. R. Miller and P. Piotrowiak, A connection between intramolecular long-range electron, hole, and triplet energy transfers, *J. Am. Chem. Soc.*, 1989, **111**, 3751–3753.
- 19 P. J. Wagner and P. Klán, Intramolecular triplet energy transfer in flexible molecules: electronic, dynamic, and structural aspects, *J. Am. Chem. Soc.*, 1999, **121**, 9626–9635.
- 20 N. J. Turro, Energy transfer processes, *Pure Appl. Chem.*, 1977, **49**, 405–429.
- 21 S. Speiser, Photophysics and mechanisms of intramolecular electronic energy transfer in bichromophoric molecular systems: solution and supersonic jet studies, *Chem. Rev.*, 1996, **96**, 1953–1976.
- 22 K. Razi Naqvi and C. Steel, Exchange-induced resonance energy transfer, *Chem. Phys. Lett.*, 1970, **6**, 29–32.

- 23 P. S. Engel and C. Steel, Photochemistry of aliphatic azo compounds in solution, *Acc. Chem. Res.*, 1973, **6**, 275–281.
- 24 P. S. Engel, L. D. Fogel and C. Steel, Singlet energy transfer to azoalkanes, *J. Am. Chem. Soc.*, 1974, **96**, 327–332.
- 25 C. C. Wamser, L. Lou, J. Mendoza and E. Olson, Singlet electronic energy transfer to azoalkanes: separation of collisional and long-range mechanisms by steric and solvent-viscosity effects, *J. Am. Chem. Soc.*, 1981, **103**, 7228–7232.
- 26 P. S. Engel, D. W. Horsey, J. N. Scholz, T. Karatsu and A. Kitamura, Intramolecular triplet energy transfer in ester-linked bichromophoric azoalkanes and naphthalenes, *J. Phys. Chem.*, 1992, **96**, 7524–7535.
- 27 Z.-Z. Wu, J. Nash and H. Morrison, Organic photochemistry. 97. Antenna-initiated photochemistry in polyfunctional steroids. Photoepimerization of 3 α -(dimethylphenylsiloxy)-5 α -androstane-6,17-dione and its 3 β isomer by through-bond exchange energy transfer, *J. Am. Chem. Soc.*, 1992, **114**, 6640–6648.
- 28 Z.-Z. Wu and H. Morrison, Organic photochemistry. 95. Antenna-initiated photochemistry of distal groups in polyfunctional steroids. Intramolecular singlet and triplet energy transfer in 3 α -(dimethylphenylsiloxy)-5 α -androstane-17-one and 3 α -(dimethylphenylsiloxy)-5 α -androstane-11,17-dione, *J. Am. Chem. Soc.*, 1992, **114**, 4119–4128.
- 29 J. K. Agyin, L. D. Timberlake and H. Morrison, Steroids as photonic wires. Z \rightarrow E olefin photoisomerization involving ketone singlet and triplet switches by through-bond energy transfer, *J. Am. Chem. Soc.*, 1997, **119**, 7945–7953.
- 30 T. R. van den Anker and C. L. Raston, Polymer- and metal-oxide-supported alkali metal naphthalenides: application in the generation of lithium and sodium reagents, *J. Organomet. Chem.*, 1998, **550**, 283–300.
- 31 W. M. Nau, n, π * Photochemistry beyond ketones, *EPA Newsl.*, 2000, **70**, 6–29.
- 32 K. A. Zachariasse, A. L. Maçanita and W. Kühnle, Chain length dependence of intramolecular excimer formation with 1,*n*-bis-(1-pyrenylcarboxy)alkanes for *n* = 1–16, 22, and 32, *J. Phys. Chem. B*, 1999, **103**, 9356–9365.
- 33 N. Lokan, M. N. Paddon-Row, T. A. Smith, M. La Rosa, K. P. Ghiggino and S. Speiser, Highly efficient through-bond-mediated electronic excitation energy transfer taking place over 12 Å, *J. Am. Chem. Soc.*, 1999, **121**, 2917–2918.
- 34 S. L. Murov, I. Carmichael and G. L. Hug, *Handbook of Photochemistry*, Marcel Dekker, Inc., New York, 2nd edn., 1993.
- 35 X. Wang, E. N. Bodunov and W. M. Nau, Fluorescence quenching kinetics in short polymer chains: dependence on chain length, *Opt. Spectrosc.*, 2003, **95**, 603–613.
- 36 To calculate the electron transfer energetics with the Rehm–Weller equation [ΔG_{et} (kJ mol⁻¹) = 96.5($E_{ox} - E_{red} - E^* + C$)], and for the energy-transfer energetics [$\Delta G_{SSET} = E^*(\text{Acceptor}) - E^*(\text{Donor})$], the following photophysical and electrochemical parameters (versus SCE in acetonitrile unless otherwise stated) were used: for DBO, $E^* = 3.30$ eV (318 kJ mol⁻¹),¹⁰ $E_{ox} = 1.45$ V (cf. W. M. Nau, W. Adam, D. Klapstein, C. Sahin and H. Walter, Correlation of oxidation and ionization potentials for azoalkanes, *J. Org. Chem.*, 1997, **62**, 5128–5132) and $E_{red} = -2.80$ V (cf. W. M. Nau and U. Pischel, “Inverted” solvent effect on charge transfer in the excited state, *Angew. Chem., Int. Ed.*, 1999, **38**, 2885–2888); for naphthalene, $E^* = 3.99$ eV (385 kJ mol⁻¹),³⁴ $E_{ox} = 1.60$ V⁴¹ and $E_{red} = -2.29$ V⁴¹; for benzene $E^* = 4.75$ eV (460 kJ mol⁻¹),³⁴ $E_{ox} = 2.35$ V (cf. S. Fukuzumi, K. Ohkubo, T. Suenobu, K. Kato, M. Fujitsuka and O. Ito, Photoalkylation of 10-allylacridinium ion via a charge-shift type of photoinduced electron transfer controlled by solvent polarity, *J. Am. Chem. Soc.*, 2001, **123**, 8459–8467) and $E_{red} = -3.31$ V versus SCE in 1,2-dimethoxyethane (cf. F. Gerson, H. Ohya-Nishiguchi and C. Wydler, Indirect determination of the half-wave reduction potential of benzene and of [2.2]paracyclophane, *Angew. Chem., Int. Ed. Engl.*, 1976, **15**, 552–553). The Coulomb term (*C*) was taken as -0.06 eV.
- 37 G. L. Closs, P. Piotrowiak, J. M. MacInnis and G. R. Fleming, Determination of long distance intramolecular triplet energy transfer rates. A quantitative comparison with electron transfer, *J. Am. Chem. Soc.*, 1988, **110**, 2652–2653.
- 38 P. J. Wagner, R. J. Truman, A. E. Puchalski and R. Wake, Extent of charge transfer in the photoreduction of phenyl ketones by alkylbenzenes, *J. Am. Chem. Soc.*, 1986, **108**, 7727–7738.
- 39 C. Coenjarts and J. C. Scaiano, Reaction pathways involved in the quenching of the photoactivated aromatic ketones xanthone and 1-azaxanthone by polyalkylbenzenes, *J. Am. Chem. Soc.*, 2000, **122**, 3635–3641.
- 40 An interaction of both chromophores mediated by the spacer orbitals, *i.e.* a superexchange mechanism, was also considered. Its participation in the overall mechanism is presumably negligible, since considerable flexibility of the spacer chain reduces the probability of a favourable arrangement of σ orbitals.^{15,17} For triplet energy transfer in bichromophoric ω -aryloxyalkanophenones with flexible tethers, it was found that through-space energy transfer by the exchange mechanism is overwhelmingly predominant¹⁹.
- 41 G. J. Kavarnos and N. J. Turro, Photosensitization by reversible electron transfer: theories, experimental evidence, and examples, *Chem. Rev.*, 1986, **86**, 401–449.
- 42 M. Gisin and J. Wirz, Photolysis of the azo precursors of 2,3- and 1,8-naphthoquinodimethane, *Helv. Chim. Acta*, 1976, **59**, 2273–2277.
- 43 S. J. Hagen, J. Hofrichter and W. A. Eaton, Rate of intrachain diffusion of unfolded cytochrome *c*, *J. Phys. Chem. B*, 1997, **101**, 2352–2365.

Cucurbiturils: Molecular Nanocapsules for Time-Resolved Fluorescence-Based Assays

Cesar Marquez, Fang Huang, and Werner M. Nau*

Abstract—A new fluorescent host–guest system based on the inclusion of the fluorophore 2,3-diazabicyclo[2.2.2]oct-2-ene (DBO) into the cavity of the molecular container compound cucurbit[7]uril (CB7) has been designed which possesses an exceedingly long-lived emission (690 ns in aerated water). The large binding constant of $(4 \pm 1) \times 10^5 M^{-1}$ along with the resistance of the CB7·DBO complex toward external fluorescence quenchers allow the use of CB7 as an enhancer in time-resolved fluorescence-based assays, e.g., to screen enzyme activity or inhibition by using DBO-labeled peptides as substrates. The response of CB7·DBO to different environmental conditions and possible quenchers are described.

Index Terms—Assays, fluorescence, molecular containers, nanocapsules, peptides, sensors.

I. INTRODUCTION

ALL life processes are based on intermolecular recognition and interactions; whether it is the transport of ions, such as sodium and potassium, enzymatic catalysis, or antigen–antibody complexation, etc. They depend on weak and delicate forces requiring minute energies far below those required for forming a covalent bond [1]. These intermolecular forces involve binding energies smaller than the values required for covalent bonds (50–100 kcal mol⁻¹). Consequently, simultaneous binding at multiples sites is generally required to accumulate a sizable binding energy of 2–20 kcal mol⁻¹ in solution [2]. The chemical field concerned with such weak interactions is the area of supramolecular chemistry [3].

One of the most fascinating supramolecular assemblies are host–guest complexes [4]. Since Pedersen demonstrated the potential of a new class of host systems, namely, crown ethers, which are able to form strong complexes with alkali metal ions [5], host–guest chemistry has grown to an area of intensive chemical research, mostly due to the potential of host–guest systems to serve as mimics for enzyme–substrate complexes. Most host systems have a concave interior, which is reminiscent

of the hydrophobic pocket of many enzymes. When a guest can be deeply immersed in a sufficiently large concave host molecule, the host serves as a molecular container. Molecular containers are unique structures in that they can lead to a virtually perfect chemical isolation of the guest. In addition, with an outer diameter of 1–3 nm, they present the smallest discrete examples of nanocapsules.

The weak interactions between the molecular container and the encapsulated guest may include hydrogen bonding, ion pairing, π – π dispersion interactions, van der Waals attractions, metal ion ligation, or solvophobic effects. A major challenge has been to understand these weak interactions in an effort to reproduce particular properties and selectivities observed in natural processes, as well as to transfer the knowledge to practical applications such as sensors, catalysis, information technology, removal of contaminants, nuclear waste treatment, etc.

Different types of molecular containers have been described, e.g., podands, corands, clathrochelates, cryptands, speleands, spherands, cavitands, carcerands, hemicarcerands, calixarenes, cyclophanes, and cryptophanes (see Scheme 1 for selected molecular structures). The size and shape of their binding cavity, their rigidity or flexibility, as well as their overall appearance distinguish them from each other and render them useful for special types of applications [6]. The size of some oligomeric host systems, including α -, β -, and γ -cyclodextrins (CDs) composed of six, seven, or eight α -D-glucose units (Scheme 2), can be adjusted to match the guests.

Molecular container compounds, and in particular CDs, have already been widely employed in nanobiotechnological areas of interest, e.g., in the selective removal of heavy metals [7], [8], radioactive waste [9]–[11], organic compounds [12], [13], or other contaminants from polluted waters, in metal switching and sensing [14]–[16], in the controlled release of drugs, perfumes, and flavors [17], in catalysis [18]–[20], and metal ion transport [21].

A general objective of our group has been to explore the intrinsic properties and the potential use of a family of nanocapsules known as cucurbit[n]urils (CBn) [22]–[24]. Like CDs, they can be designed in different sizes, which allows a fine-tuning of their host–guest complexation properties. The most common ones are CB5, CB6, and CB7 (Scheme 3), of which only the last one is sufficiently large to encapsulate larger organic guests or residues with more than seven heavy atoms. We have studied the effects governing the thermodynamics and kinetics of host–guest complex formation of CB6 [25] and the influence of the CB7 cavity on the physical properties of the guest moieties [26].

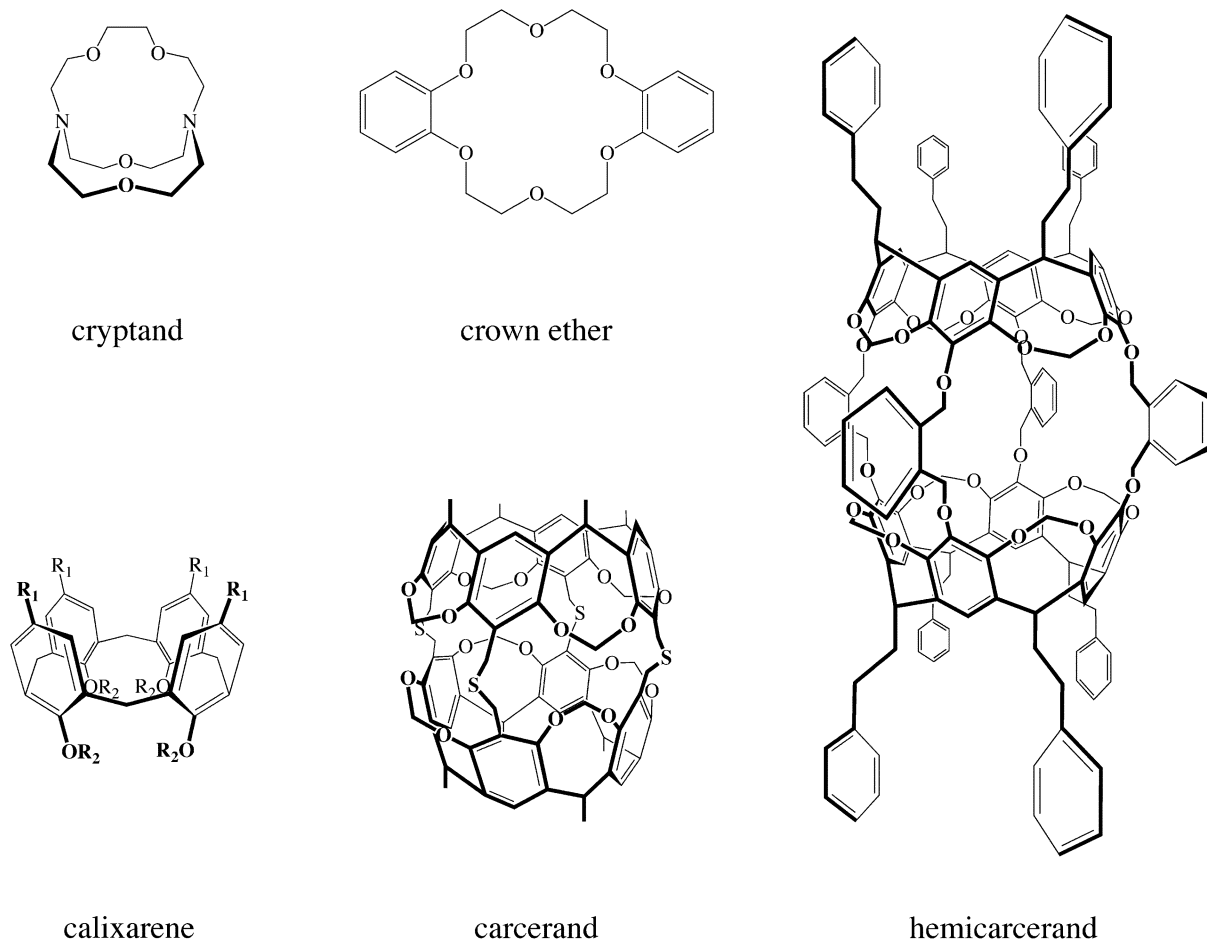
Manuscript received September 12, 2003; revised October 30, 2003. This work was supported by the Swiss National Science Foundation under Projects 620-58000.99 and 4047-0575552 within Program NRP 47. Asterisk indicates corresponding author.

C. Marquez is with the School of Engineering and Science, International University Bremen, Bremen D-28759, Germany (e-mail: c.marquez@iu-bremen.de).

F. Huang is with the Department of Chemistry, University of Basel, Basel CH-4056, Switzerland (e-mail: fang.huang@unibas.ch).

*W. M. Nau is with the School of Engineering and Science, International University Bremen, Bremen D-28759, Germany, and also with the Department of Chemistry, University of Basel, Basel CH-4056, Switzerland (e-mail: w.nau@iu-bremen.de).

Digital Object Identifier 10.1109/TNB.2004.824269



Scheme 1.

To explore new applications of the potentially most useful CB7, we have encapsulated as a fluorescent guest the azoalkane 2,3-diazabicyclo[2.2.2]oct-2-ene (DBO), a chromophore possessing a weak n, π^* absorption in the near UV ($\lambda_{\max} = 365$ nm in water) [26]–[31]. Different advantages of DBO (marketed as Fluorazophore-P, derived from FLUORescent AZOalkane chromoPHORE-Parent) make it an ideal probe for host–guest studies. DBO has a small volume, spherical shape, and good solubility in water as well as in organic media. In addition, the fluorescence lifetime of DBO is exceptionally long, for example, $1.03 \mu\text{s}$ in the gas phase [30] and 325 ns in aerated water [28]. It fluoresces with a high quantum yield (approximately 20% in water) over a broad spectral range ($\lambda_{\max} = 430$ nm), and its spectroscopic properties respond strongly to the chemical environment [26].

The resulting fluorescent host–guest complex CB7·DBO (Scheme 4) can serve as a water-soluble fluorescent probe or sensor for biochemical applications. The complex presents, in particular, an appealing fluorophore for application in time-resolved fluorescence assays, which allow an efficient removal of autofluorescence by application of an electronic time gate. This application is made possible by the exceedingly long lifetime (up to 690 ns in aerated H₂O) of the complex. CB7 protects the fluorescent probe from the outside environment, improving its application potential for optical signaling. In this

sense, the CB7·DBO complex serves as a true nanomolecular device, since it can be used as a “nano flashlamp” in biological environments due to its exceedingly long-lived emission.

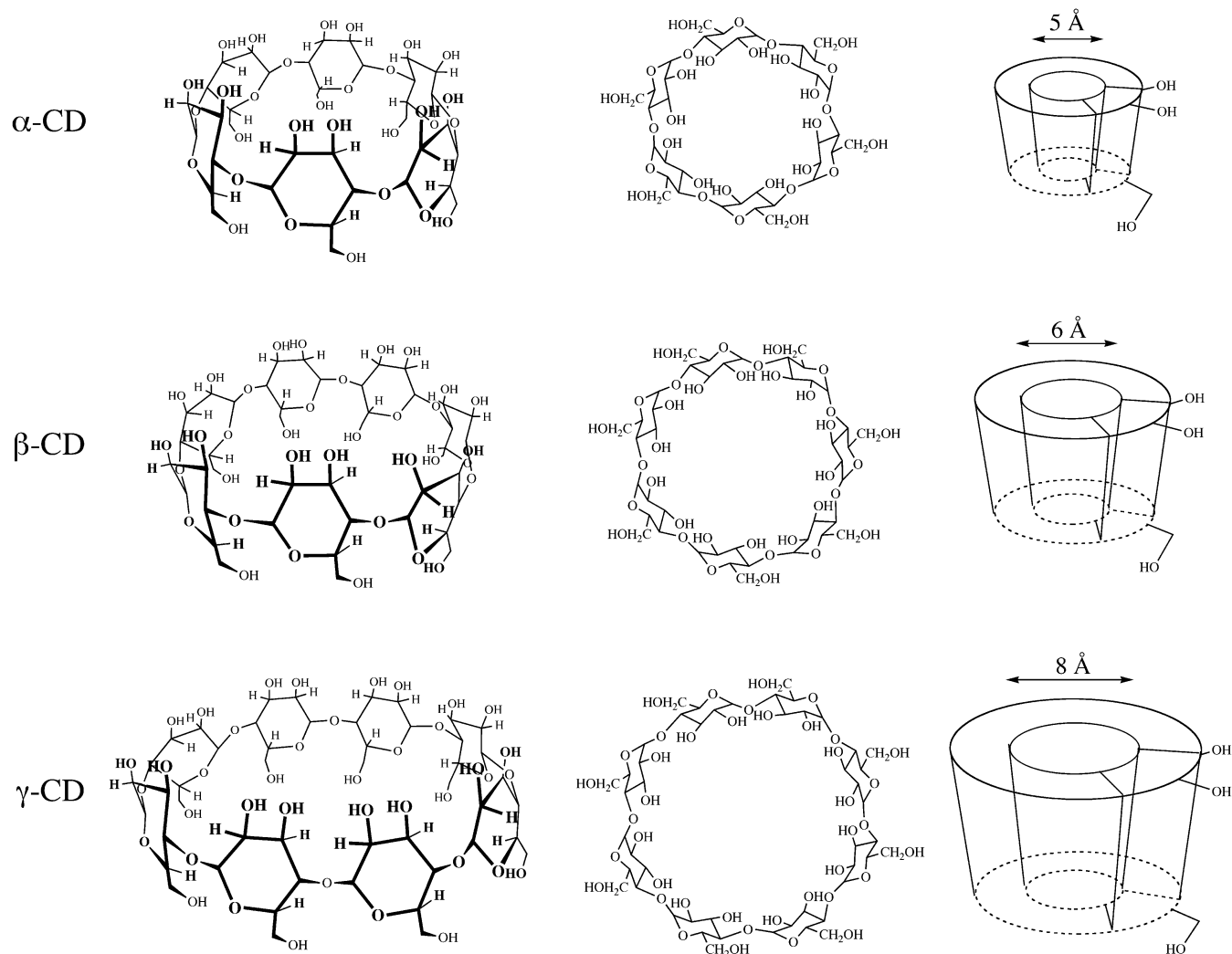
II. MATERIALS AND METHODS

A. Synthesis of CB7

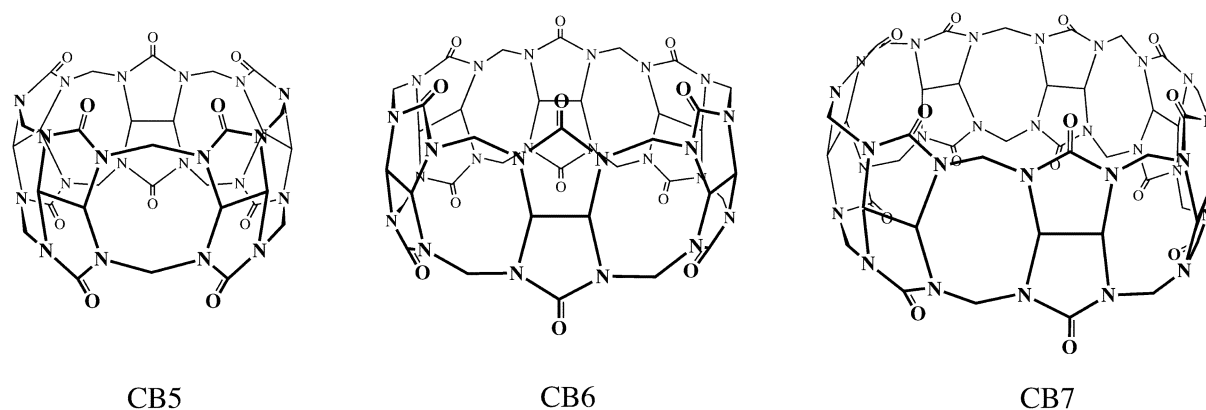
Since the reported synthetic procedure for CB7 is quite tedious and proceeds in very low yield [31], it was essential to develop an improved synthetic method, which exploited some recent mechanistic insights into the oligomerization of glycoluril [32], [33].

Formaldehyde (14 mL of a 37% aqueous solution, 182 mM) was mixed with sulfuric acid (60 mL of a 9-M aqueous solution) and the magnetically stirred mixture was cooled down to 5 °C. Glycoluril (11.4 g, 80 mM) was added, which dissolved slowly to produce a thick transparent gel. After approximately 30 min the gel became too viscous to allow further stirring, and at this point the temperature was elevated to 100 °C, which resulted in a redissolution of the gel. After heating for 72 h, no precipitate, which would be indicative of an excess of undesirable CB6, was observed.

The reaction mixture was then poured into 200 mL of bidistilled water, and 800 mL of acetone was added, thereby inducing precipitation of all CB_n oligo- and polymers. Filtration



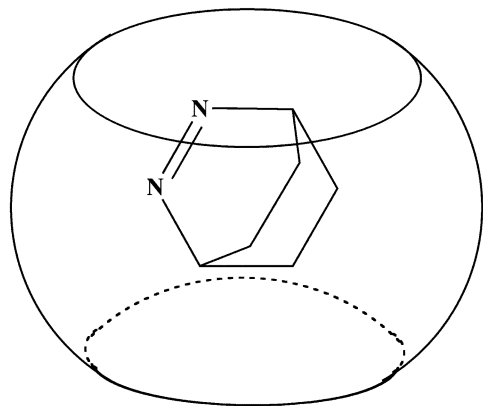
Scheme 2.



Scheme 3.

and subsequent washing with 1.5 L of a mixture of cold acetone/water (8 : 2 v/v) to remove the acid produced a mixture of CBn as a white powder. Addition of 400 mL of bidistilled water dissolved all CBn but CB6 (6.8 g) which is, therefore, easily separated (the solubility of CB6 in water is $< 50 \mu\text{M}$) [34]. When the remaining solution was treated with 300 mL of acetone, a new precipitate (8.5 g) appeared, which contained

mainly CB7. The precipitate was purified by dissolving the crude material in 200 mL of bidistilled water. Addition of 20 mL of acetone caused the precipitation of a mixture of CB7 with other unidentified homologues, which was disregarded. The further addition of acetone (100 mL) led to the precipitation of the major fraction of CB7. Washing of the latter fraction with acetone and diethyl ether and subsequent drying under vacuum



CB7·DBO

Scheme 4.

at 140 °C for 72 h gave 6.5 g of CB7 (> 95% purity, 49% yield with respect to glycoluril). The product was characterized by proton nuclear magnetic resonance and electrospray ionization mass spectrometry based on known literature data [31].

B. Preparation of the CB7·DBO Host–Guest Complex

When CB7 (approximately 3 mM) was added to an aqueous solution of DBO (approximately 2 mM), complexation took place almost instantaneously as monitored by ^1H NMR. At these concentrations, >99% of DBO are included inside the CB7 cavity (the binding constant is $(4 \pm 1) \times 10^5 \text{ M}^{-1}$ [26]). The solubility of the CB7·DBO complex in pure water is approximately 5 mM, which can be increased by addition of salts (metal ions).

C. Fluorescence Spectroscopy

All measurements were performed in H_2O or D_2O at ambient temperature. Fluorescence lifetimes were measured on a laser flash photolysis (LFP) setup (LP900, Edinburgh Instruments, Edinburgh, U.K.) with 7 mJ, 355-nm pulses of 4 ns width from a Nd:YAG laser (Minilite II, Continuum, Santa Clara, CA), and with a time-correlated single-photon counting (SPC) fluorimeter (FLS920, Edinburgh Instruments, Edinburgh, U.K.) using 50-ps laser pulses at 373 nm for excitation (Picoquant PDL 800-B pulse generator with LDH-P-C-375 laser head). The FLS920 instrument was also used for the steady-state fluorescence spectra ($\lambda_{\text{exc}} = 365 \text{ nm}$). Fluorescence was detected at 450 nm on both time-resolved setups. The resulting data were analyzed with the instrument software by means of monoexponential decay functions with a reconvolution fit for the excitation pulse. Intermolecular quenching experiments were performed with 0.1 mM solutions of DBO and varying quencher concentrations up to 50% quenching effect or up to the solubility limit of the quencher (4–5 data points). The DBO-labeled peptide concentration was adjusted to approximately 0.1 mM (SPC measurement).

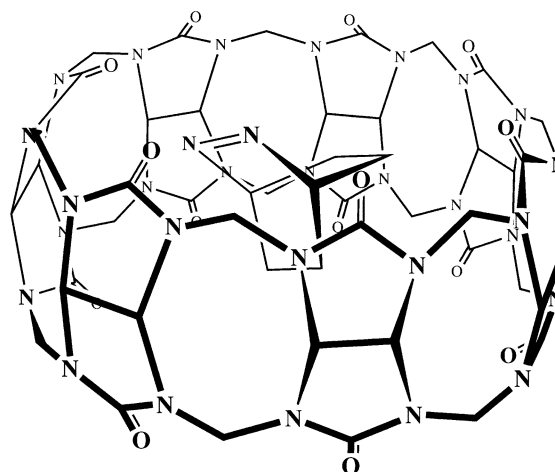


TABLE I
FLUORESCENCE LIFETIMES

Conditions	$\tau_{\text{DBO}} / \mu\text{s}$	$\tau_{\text{CB7-DBO}} / \mu\text{s}$
gas phase	1.03	
H_2O , aerated	0.33	0.69
H_2O , deaerated	0.42	0.69
D_2O , aerated	0.51	0.97
D_2O , deaerated	0.73	0.97
H_2O , Na_2SO_4 , aerated	0.33	0.95
D_2O , Na_2SO_4 , aerated	0.51	1.03

Fluorescence lifetimes (τ) of DBO in water and encapsulated in the CB7 complex, measured under conditions of nearly quantitative complexation (>99 %, $[\text{DBO}] = 2 \text{ mM}$, $[\text{CB7}] = 3 \text{ mM}$).

III. RESULTS

A. Fluorescence Lifetimes and Quenching

The inclusion of DBO inside CB7 provokes an increase in its fluorescence lifetime from 325 ns in aerated aqueous solution to 690 ns (Table I). The lifetime does not change when the solution is degassed, suggesting that oxygen is incapable of quenching the encapsulated chromophore. However, when deuterated water is used, a further increase in lifetime is observed due to the less efficient quenching by O–D bonds [29], reaching a value of 970 ns. This is the longest fluorescence lifetime measured for an organic chromophore in solution. For biochemical applications, it is noteworthy that the fluorescence is detected in water under air.

The goodness of fit between host and guest is corroborated by molecular dynamics calculations [26], which suggest that even a water or oxygen molecule cannot be coincluded together with DBO. The cavity of CB7 is, thus, completely filled out by DBO without leaving a larger “empty” space.

The protection effect operates also for potential quenchers of DBO fluorescence (see Table II). The encapsulation of DBO into CB7 prevents contact between the quencher and the guest, which efficiently suppresses collision-induced quenching. In this way, potential “contact” quenchers such as ascorbic acid

TABLE II
FLUORESCENCE QUENCHING RATE CONSTANTS

Quencher	DBO $k_q/10^9 \text{ M}^{-1}\text{s}^{-1}$	CB7•DBO $k_q/10^9 \text{ M}^{-1}\text{s}^{-1}$
oxygen	2.1	< 0.04
biacetyl	6.1	< 0.05
sodium iodide	1.6	< 0.005
sodium nitrite	2.5	< 0.1
ascorbic acid	2.1	< 0.006
tryptophan	2.1	< 0.1
dGMP ^{a)}	0.5	< 0.005

Fluorescence quenching rate constants (k_q) of DBO in H₂O and encapsulated in the CB7 complex, measured under conditions of nearly quantitative complexation (>99 %, [DBO] = 2 mM, [CB7] = 3 mM). ^{a)} 2'-deoxyguanosine-5'-monophosphate disodium salt.

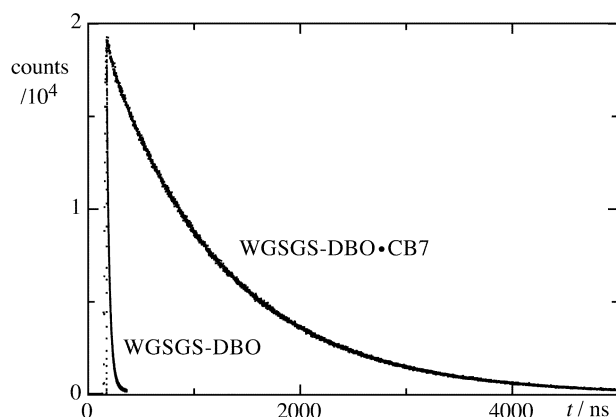


Fig. 1. Fluorescence decays for the uncomplexed peptide WGS GS-DBO and the complexed peptide WGS GS-DBO•CB7 in aerated D₂O measured by SPC.

[28], tryptophan [35], or 2'-deoxyguanosine-5'-monophosphate disodium salt (dGMP), which are efficient quenchers of DBO fluorescence in the absence of CB7, are inefficient in quenching the fluorescent complex. Only few additives, e.g., biacetyl, iodide, or nitrite, are able to cause a minor fluorescence quenching of the complex (two orders of magnitude lower quenching rate constant). In these cases, quenching is presumed to occur by either energy transfer (biacetyl) or electron transfer (iodide, nitrite), i.e., by quenching mechanisms which are well known to operate through space or through the solvent over medium to large distances.

B. Complexation of DBO-Labeled Biomolecules

The fluorophore DBO can be covalently attached to biomolecules like peptides and oligonucleotides [35]–[39]. Subsequent addition of CB7 allows one to selectively complex the fluorophore and thereby lengthen its lifetime to approximately 0.7 μs in H₂O and 1.0 μs in D₂O. A specific example of the enhancement of lifetime is shown in Fig. 1 (experimental data) and Scheme 5 (where F represents DBO as fluorophore and Q tryptophan as quencher) for a peptide with the structure WGS GS-DBO (80 μM in aerated D₂O). The fluorophore is attached through a labeled asparagine [35]. Before complexation, the fluorescence lifetime of the peptide is very short (19.5 ns) because the peptide contains an *N*-terminal tryptophan as an internal quencher, which can cause quenching through exciplex formation by end-to-end collision [35]. The addition of CB7

(0.8 mM) leads to an increase in fluorescence lifetime by a factor of 50, resulting in a lifetime of 1030 ns. This can be accounted for by a selective and nearly quantitative (> 99%) complexation of the DBO chromophore by CB7, which is corroborated by the shielding effect upon the guest in NMR experiments. This chromophore complexation suppresses quenching by excluding the possibility of end-to-end collision of DBO with the internal tryptophan, which is required to induce quenching.

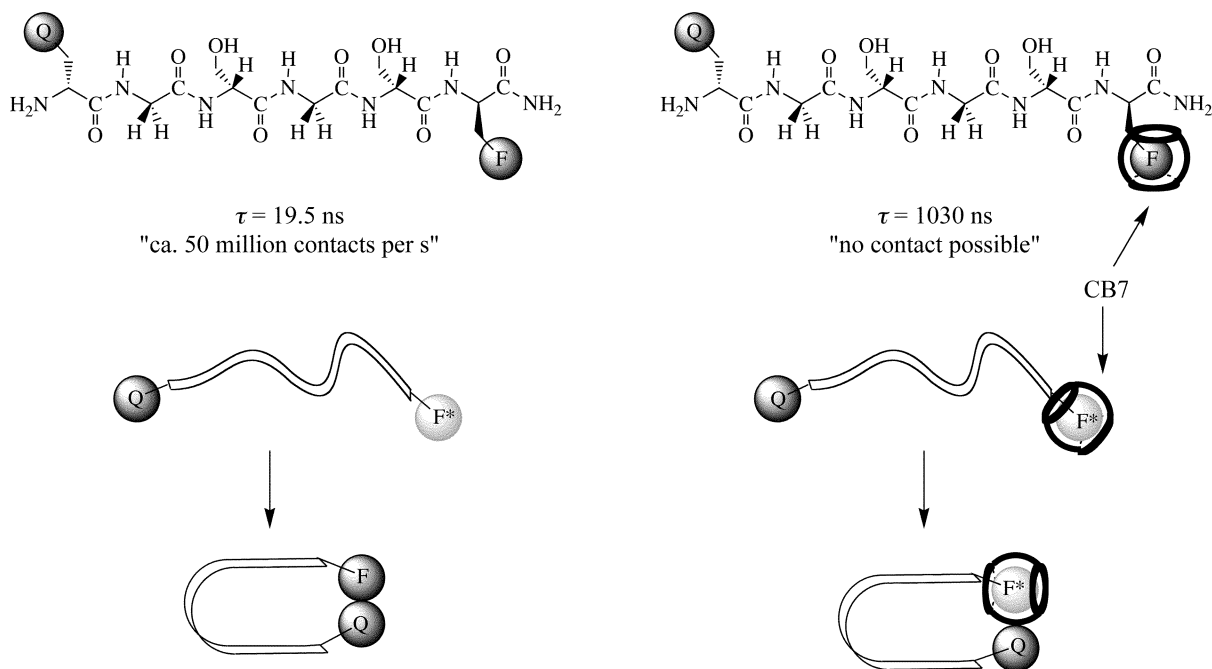
IV. DISCUSSION

Fluorescent labels are invaluable tools in numerous areas of biological chemistry, e.g., for the purpose of calcium ion detection, cell staining, and polarity sensing [40]. An appealing subclass of fluorescent probes comprises chromophores with a particularly long fluorescence lifetime (> 50 ns) [35]. One powerful application, which exploits long-lived fluorescence (or generally luminescence), relies on the reliable differentiation of long fluorescence lifetimes from any shorter-lived luminescence components. This is of interest, in particular, for screening assays, where fluorescent probes are employed to signal molecular events such as the inhibition of an enzyme by a library of potential drugs.

CB7 is an interesting molecular container compound. It is able to both encapsulate and release guest molecules, which characterizes it as a true nanocapsule. As demonstrated herein, the addition of CB7 to a DBO-labeled peptide results in the formation of a supramolecular fluorescent complex (CB7•DBO). This complex displays the longest fluorescence lifetime amongst purely organic chromophores in solution, amounting up to 1 μs , even in water under air. In fact, the lifetime inside the complex can reach the value measured for the gas phase (Table I), implying a virtually perfect shielding from the outside environment. This is also confirmed by the inefficient quenching by a series of known fluorescence quenchers (Table II). Quenching is completely suppressed for quenchers requiring intimate probe–quencher contact, while in the case of other quenching mechanisms (electron and energy transfer) the quenching rate constant decreases by two orders of magnitude.

We suggest that the long lifetime of this complex can be exploited for the sensitive detection of biomolecules in assays. Short-lived emission is ubiquitous and may stem from other additives, sample impurities, biological components, scattered light, the solvent, or sample container materials of cuvettes and microplates. The shorter lived components can be relatively easily eliminated, however, from the detection by applying a time gate, such that the emission from the long-lived fluorescent label (which serves as signaling unit—in this case, CB7•DBO) can be selectively detected. This reduces the background during the measurement dramatically.

An instructive hypothetical example is depicted in Fig. 2 [41], which compares the fluorescence decay of a long-lived fluorescent probe ($\tau = 1.0 \mu\text{s}$) with that of a shorter-lived fluorescing component ($\tau = 10 \text{ ns}$), with the latter one, however, being much more intense (10^6 times larger pre-exponential factor). If as usual the integrated fluorescence



Scheme 5.

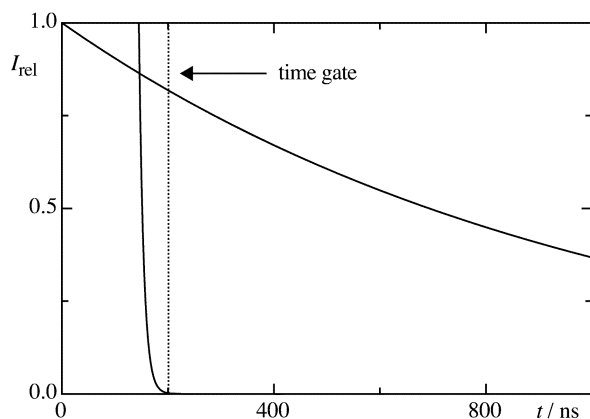


Fig. 2. Comparison of the fluorescence decay of a long-lived fluorescent probe ($\tau = 1.0 \mu\text{s}$) with that of a shorter-lived component ($\tau = 10 \text{ ns}$); the shorter lived component is 10^6 times more intense (relative preexponential factors). A suitable time gate for use in a time-resolved assay is shown at 200 ns.

intensity would be compared through steady-state methods, a “signal-to-background” of 0.0001 : 1 would result, which would exclude one from obtaining any useful information. If one carries out the experiment in lifetime mode with a time gate between 200 and 1000 ns and integrates the areas under the curves, the “signal-to-background” ratio becomes better than 20 000 : 1, an impressive improvement by more than eight orders of magnitude, which has its underlying reason in the exponential decay kinetics of the fluorescence. This improvement renders the selective detection of long-lived fluorophores in so-called time-resolved screening assays generally an entirely instrumental problem. In particular, the real background may be dominated by detector noise rather than contributions from short-lived emission.

Note that the effect observed upon complexation of CB7 and DBO-labeled peptides (Fig. 1) resembles closely the situation

described in Fig. 2, which underscores the potential of this complex for time-gated fluorescence detection. In essence, the addition of CB7 serves as an “enhancer” which could be exploited in assays to detect the formation or consumption, for example of a DBO-labeled peptide substrate, with high accuracy by employing time-gated detection of fluorescence. A similar principle of measuring time-gated fluorescence, albeit on a slower time scale ($> 10 \mu\text{s}$), is already commercially applicable in so-called time-resolved fluorescence (TRF) assays. Examples are the DELFIA and LANCE assays [42], which exploit long-lived micellized europium clathrates as luminescent labels. In the case of the europium assays, the addition of micelles serves as an “enhancement solution,” which greatly reduces the quenching of the lanthanide ion by the surrounding water. The application of the CB7·DBO complex could provide a purely organic equivalent and true fluorescence-based method to the established inorganic luminescence-based techniques.

V. CONCLUSION

Addition of the molecular container compound CB7 to DBO-labeled biomolecules greatly enhances the fluorescence lifetime of DBO through the formation of a host-guest complex. The resulting fluorescence lifetime of approximately $1 \mu\text{s}$ is sufficiently long-lived to discriminate it reliably from shorter-lived autofluorescence. This allows for a sensitive detection, which could be useful, among others, for high-throughput screening technology.

REFERENCES

- [1] S. Gronowitz. (1987) *Nobel Prize in Chemistry: Presentation Speech* [Online]. Available: <http://www.nobel.de/chemistry/laureates/1987/presentation-speech.html>
- [2] D. J. Cram, “Molecular container compounds,” *Nature*, vol. 356, pp. 29–36, 1992.

- [3] J.-M. Lehn, "Supramolecular chemistry. Scope and perspectives molecules, supermolecules, and molecular devices (nobel lecture)," *Angew. Chem. Int. Ed.*, vol. 27, pp. 89–112, 1988.
- [4] D. J. Cram, "The design of molecular hosts, guests, and their complexes," *Angew. Chem. Int. Ed.*, vol. 27, pp. 1009–1020, 1988.
- [5] C. J. Pedersen, "The discovery of crown ethers," *Angew. Chem. Int. Ed.*, vol. 27, pp. 1021–1027, 1988.
- [6] J.-M. Lehn, *Supramolecular Chemistry*. Heidelberg, Germany: Wiley-VCH, 1995.
- [7] H.-J. Buschmann and E. Schollmeyer, "Verringerung der Konzentration von Schwermetallen in Abwässern von Textilveredlungsbetrieben," *Textilveredlung*, vol. 28, pp. 182–184, 1993.
- [8] R. Ludwig and N. T. K. Dzung, "Heavy metal extraction and absorption by calixarenes—A brief overview," *Biologische Abwasserreinigung*, vol. 14, pp. 49–65, 2000.
- [9] G. R. Choppin, "Overview of chemical separation methods and technologies," in *Chemical Separation Technologies and Related Methods of Nuclear Waste Management*, ser. NATO Science Series, Subseries 2. Dordrecht, The Netherlands: Kluwer, 1999, vol. 53, pp. 1–16.
- [10] M. T. Blanda, D. B. Farmer, J. S. Brodbelt, and B. J. Goosby, "Synthesis and alkali metal ion binding properties of two rigid stereochemical isomers of calix[6]arene bis-crown-4," *J. Amer. Chem. Soc.*, vol. 122, pp. 1486–1491, 2000.
- [11] V. Lamare, J.-F. Dozol, S. Fuangswasdi, F. Arnaud-Neu, P. Thuery, M. Nierlich, Z. Asfari, and J. Vicens, "A new calix[4]arene-bis (crown ether) derivative displaying an improved caesium over sodium selectivity: Molecular dynamics and experimental investigation of alkali-metal ion complexation," *J. Chem. Soc. Perkin Trans.*, vol. 2, pp. 271–284, 1999.
- [12] H.-J. Buschmann, K. Jansen, and E. Schollmeyer, "Cucurbituril and α - and β -cyclodextrins as ligands for the complexation of nonionic surfactants and polyethyleneglycols in aqueous solutions," *J. Includ. Phenom. Macrocyclic Chem.*, vol. 37, pp. 231–236, 2000.
- [13] H.-J. Buschmann and E. Schollmeyer, "Stabilization of dyes against hydrolytic decomposition by the formation of inclusion compounds," *J. Includ. Phenom. Mol. Recognit. Chem.*, vol. 14, pp. 91–99, 1992.
- [14] L. Fabbri and A. Poggi, "Sensors and switches from supramolecular chemistry," *Chem. Soc. Rev.*, pp. 197–202, 1995.
- [15] A. P. de Silva, H. Q. N. Gunaratne, T. Gunnlaugsson, A. J. M. Huxley, C. P. McCoy, J. T. Rademacher, and T. E. Rice, "Signaling recognition events with fluorescence sensors and switches," *Chem. Rev.*, vol. 97, pp. 1515–1566, 1997.
- [16] L. Fabbri, M. Licchelli, P. Pallavicini, L. Parodi, and A. Taglietti, "Fluorescent sensors for and with transition metals," in *Transition Metals in Supramolecular Chemistry*, J.-P. Sauvage, Ed. Chichester, U.K.: Wiley, 1999, vol. 5, pp. 93–134.
- [17] J. Szejtli, "Introduction and general overview of cyclodextrin chemistry," *Chem. Rev.*, vol. 98, pp. 1743–1753, 1998.
- [18] A. McCurdy, L. Jimenez, D. A. Stauffer, and D. A. Dougherty, "Biomimetic catalysis of S_N2 reactions through cation- π interactions. The role of polarizability in catalysis," *J. Amer. Chem. Soc.*, vol. 114, pp. 10314–10321, 1992.
- [19] W. L. Mock and N. Y. Shih, "Cycloaddition induced by cucurbituril. A case of pauling principle catalysis," *J. Org. Chem.*, vol. 48, pp. 3619–3620, 1983.
- [20] R. van Heerbeek, P. C. J. Kamer, P. W. N. M. van Leeuwen, and J. N. H. Reek, "Dentrimers as support for recoverable catalysis and reagents," *Chem. Rev.*, vol. 102, pp. 3717–3756, 2002.
- [21] V. S. Talanov, G. G. Talanova, M. G. Gorbunova, and R. A. Bartsch, "Novel caesium-selective, 1, 3-alternate calix[4]arene-bis(crown-6-ethers) with proton-ionizable groups for enhanced extraction efficiency," *J. Chem. Soc. Perkin Trans.*, vol. 2, pp. 209–215, 2002.
- [22] R. Behrend, E. Meyer, and F. Rusche, "Ueber condensationsproducte aus glycoluril und formaldehyd," *Liebigs Ann. Chem.*, vol. 339, pp. 1–40, 1905.
- [23] W. L. Mock, "Cucurbituril," in *Comprehensive Supramolecular Chemistry*, F. Vögtle, Ed. New York: Elsevier, 1996, vol. 2, pp. 477–493.
- [24] P. Cintas, "Cucurbituril: Supramolecular perspectives for an old ligand," *J. Includ. Phenom. Mol. Recognit. Chem.*, vol. 17, pp. 205–220, 1994.
- [25] C. Marquez and W. M. Nau, "Two mechanisms of slow host-guest complexation between cucurbit[6]uril and cyclohexylmethylamine: pH-responsive supramolecular kinetics," *Angew. Chem. Int. Ed.*, vol. 40, pp. 3155–3160, 2001.
- [26] —, "Polarizabilities inside molecular containers," *Angew. Chem. Int. Ed.*, vol. 40, pp. 4387–4390, 2001.
- [27] W. M. Nau, G. Greiner, J. Wall, H. Rau, M. Olivucci, and M. A. Robb, "The mechanism for hydrogen abstraction by n, π^* excited singlet states: Evidence for thermal activation and deactivation through a conical intersection," *Angew. Chem. Int. Ed.*, vol. 37, pp. 98–101, 1998.
- [28] W. M. Nau, "A fluorescent probe for antioxidants," *J. Amer. Chem. Soc.*, vol. 120, pp. 12614–12618, 1998.
- [29] W. M. Nau, G. Greiner, H. Rau, J. Wall, M. Olivucci, and J. C. Scaiano, "Fluorescence of 2,3-diazabicyclo[2,2,2]oct-2-ene revisited: Solvent-induced quenching of the n, π^* -excited state by an aborted hydrogen atom transfer," *J. Phys. Chem. A*, vol. 103, pp. 1579–1584, 1999.
- [30] D. Klapstein, U. Pischel, and W. M. Nau, "Quenching of n, π^* -excited states in the gas phase: Variations in absolute reactivity and selectivity," *J. Amer. Chem. Soc.*, vol. 124, pp. 11349–11357, 2002.
- [31] J. Kim, I. S. Jung, S. Y. Kim, E. Lee, J. K. Kang, S. Sakamoto, K. Yamaguchi, and K. Kim, "New cucurbituril homologues: Syntheses, isolation, characterization, and X-ray crystal structures of cucurbit[n]uril ($n = 5, 7, \text{ and } 8$)," *J. Amer. Chem. Soc.*, vol. 122, pp. 540–541, 2000.
- [32] K. S. Oh, J. Yoon, and K. S. Kim, "Structural stabilities and self-assembly of cucurbit[n]uril ($n = 4-7$) and decamethylcucurbit[n]uril ($n = 4-6$): A theoretical study," *J. Phys. Chem. B*, vol. 105, pp. 9726–9731, 2001.
- [33] A. Day, A. P. Arnold, R. J. Blanch, and B. Snushall, "Controlling factors in the synthesis of cucurbituril and its homologues," *J. Org. Chem.*, vol. 66, pp. 8094–8100, 2001.
- [34] H.-J. Buschmann, K. Jansen, C. Meschke, and E. Schollmeyer, "Thermodynamic data for complex formation between cucurbituril and alkali and alkaline earth cations in aqueous formic acid solution," *J. Solution Chem.*, vol. 27, pp. 135–140, 1998.
- [35] R. R. Hudgins, F. Huang, G. Gramlich, and W. M. Nau, "A fluorescence-based method for direct measurement of submicrosecond intramolecular contact formation in biopolymers: An exploratory study with polypeptides," *J. Amer. Chem. Soc.*, vol. 124, pp. 556–564, 2002.
- [36] F. Huang and W. M. Nau, "A conformational flexibility scale for amino acids in peptides," *Angew. Chem. Int. Ed.*, vol. 42, pp. 2269–2272, 2003.
- [37] W. M. Nau and X. Wang, "Biomolecular and supramolecular kinetics in the submicrosecond time range: The fluorazophore approach," *Chem. Phys. Chem.*, vol. 3, pp. 393–398, 2002.
- [38] C. Marquez, U. Pischel, and W. M. Nau, "Selective fluorescence quenching of 2,3-diazabicyclo[2.2.2]oct-2-ene by nucleotides," *Org. Lett.*, vol. 5, pp. 3911–3914, 2003.
- [39] X. Wang and W. M. Nau, "Kinetics of end-to-end collision in short single-stranded nucleic acids," *J. Amer. Chem. Soc.*, vol. 126, pp. 808–813, 2004.
- [40] B. Valeur, *Molecular Fluorescence*. Heidelberg, Germany: Wiley-VCH, 2002.
- [41] W. M. Nau, F. Huang, X. Wang, H. Bakirci, G. Gramlich, and C. Marquez, "Exploiting long-lived molecular fluorescence," *Chimia*, vol. 57, pp. 161–167, 2003.
- [42] PerkinElmer Life Sciences, Wellesley, MA. [Online]. Available: <http://www.perkinelmer.com/>

Cesar Marquez, photograph and biography not available at the time of publication.

Fang Huang, photograph and biography not available at the time of publication.

Werner M. Nau, photograph and biography not available at the time of publication.

**Primary and Secondary Structure Dependence of Peptide Flexibility Assessed by
Fluorescence-Based Measurement of End-to-End Collision Rates**

Fang Huang,[†] Robert R. Hudgins,^{†,‡} and Werner M. Nau^{†,§,*}

*A contribution from the Department of Chemistry, University of Basel, Klingelbergstrasse 80, CH-4056
Basel, Switzerland, and the School of Engineering and Science, International University Bremen,
Campus Ring 1, D-28717 Bremen, Germany*

Abstract

The intrachain fluorescence quenching of the fluorophore 2,3-diazabicyclo[2.2.2]oct-2-ene (DBO) is measured in short peptide fragments relevant to the protein folding of ubiquitin, namely the two strand parts and the turn fragment of the *N*-terminal β -hairpin. The investigated peptides adopt a random-coil conformation in aqueous solution according to CD and NMR experiments. The combination of quenchers with different quenching efficiency, namely tryptophan and tyrosine, allows the extrapolation of the rate constants for end-to-end collision rates as well as the dissociation of the end-to-end encounter complex. The measured activation energies for fluorescence quenching demonstrate that the end-to-end collision process in peptides is partially controlled by internal friction within the backbone, while measurements in solvents of different viscosity (H_2O , D_2O , and 7.0 M guanidinium chloride) suggest that solvent friction is an additional important factor in determining the collision rate. The extrapolated end-to-end collision rates, which are only slightly larger than the experimental rates for the DBO/Trp probe/quencher system, provide a measure of the conformational flexibility of the peptide backbone. The chain flexibility is found to be strongly dependent on the type of secondary structure that the peptides represent. The collision rates for peptides derived from the β -strand motifs (ca. $1 \times 10^7 \text{ s}^{-1}$) are ca. 4 times slower than that derived from the β -turn. The results provide further support for the hypothesis that chain flexibility is an important factor in the preorganization of protein fragments during protein folding. Mutations to the β -turn peptide show that subtle sequence changes strongly affect the flexibility of peptides as well. The protonation and charge status of the peptides, however, is shown to have no significant effect on the flexibility of the investigated peptides. The meaning and definition of end-to-end collision rates in the context of protein folding is critically discussed.

Introduction

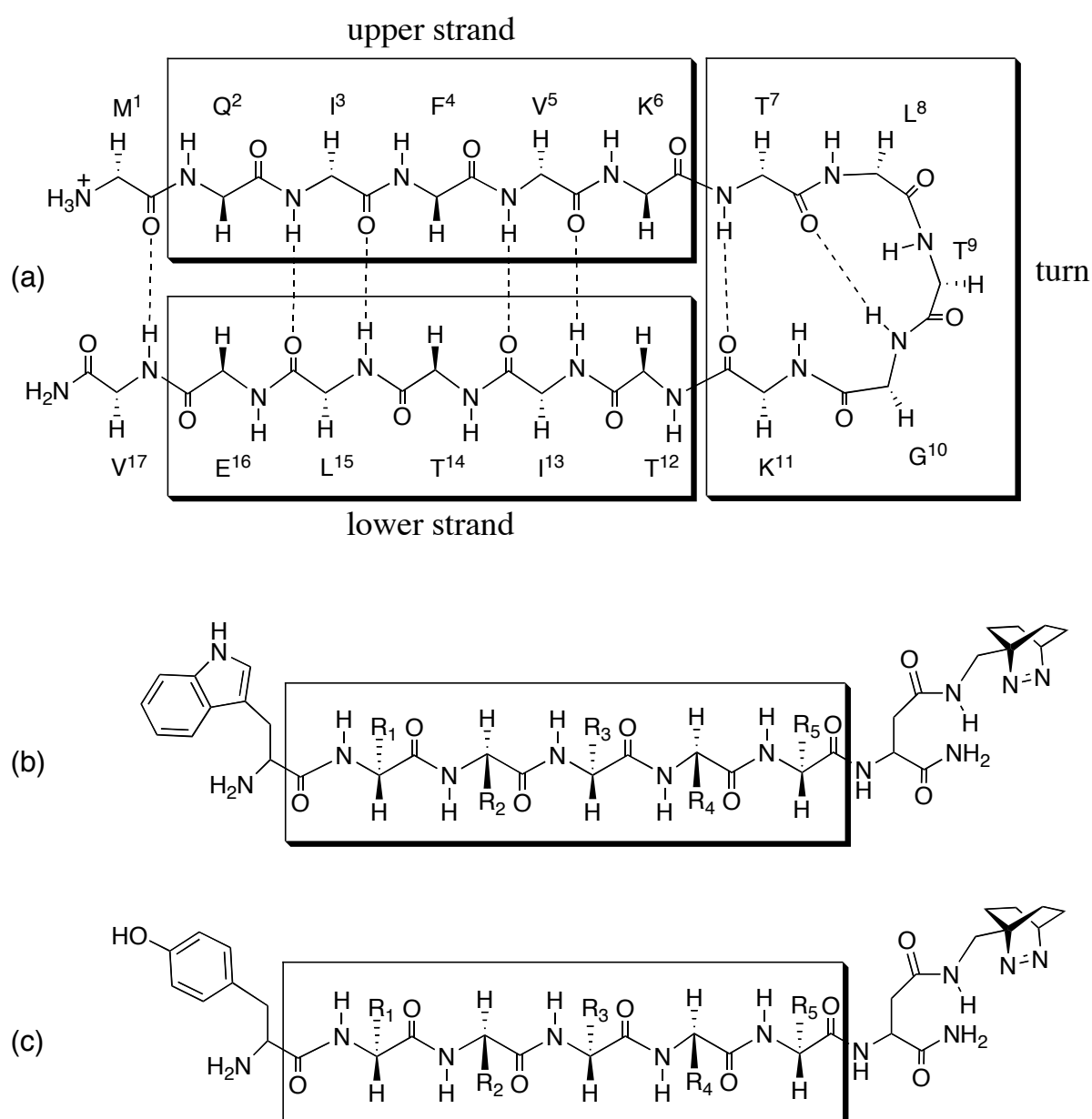
Protein folding is one of the “holy grails” of the physical and life sciences.¹⁻⁵ While several general folding mechanisms, such as the framework model, the hydrophobic collapse model, and the nucleation-condensation model, have been proposed,^{1,4,6} the long-standing controversy on whether protein folding is kinetically or thermodynamically controlled has remained.⁷⁻⁹ Studies of the elementary steps in protein folding, such as the formation of β -hairpins, β -helices, and loops, and in particular on the kinetics of the formation of these secondary structures are necessary to validate the various proposed folding mechanisms.^{2,6} To better understand how the domains of a protein move, in which sequence a protein folds, and which secondary structures emerge first, it is essential to investigate peptide dynamics, to measure the kinetics of nonlocal intrachain interactions, and to predict the flexibility of peptide sequences.^{2,10,11} For example, it may be anticipated that nucleation may occur near the conformationally most flexible (or most “dynamic”) portions of a protein.

Recent studies show that the timescale of the elementary protein folding steps ranges from several nanoseconds to tens of microseconds. Such studies have included indirect dynamic NMR experiments,^{12,13} and direct photophysical intrastrand quenching experiments.¹⁴⁻²³ A critical parameter for protein folding is the rate of intrachain collision, which imposes a rate limit for the formation of a loop or β -turn.^{2,19,24} Recently, we have established a fluorescence-based method, with 2,3-diazabicyclo[2.2.2]oct-2-ene (DBO) as a probe and Trp as quencher, for measuring end-to-end collision in biopolymers occurring on the submicrosecond time scale. Intramolecular fluorescence quenching of DBO by Trp has already proven useful to assess the rate and length dependence of intrachain collisions,^{23,25} and to establish a conformational flexibility scale of amino acids in model peptide sequences.²⁴ The extremely long fluorescence lifetime of DBO, even in water under air, and its efficient contact quenching by Trp form the basis for its application to biopolymer dynamics. In addition, DBO is small, hydrophilic, and very versatile during peptide synthesis.^{23,24}

To contribute to the area of protein folding, it is essential to apply the established DBO quenching method to the properties of native proteins. In the present work, we investigate the flexibility of some important fragments of ubiquitin with the fluorescence-based method. Ubiquitin is a small protein with 76 amino acids. The structure, stability and folding of ubiquitin as well as its peptide fragments have been previously studied.²⁶⁻³¹ Shown in Scheme 1a is the 17-residue *N*-terminal β -hairpin of ubiquitin, which is composed of two β -strands connected by a β -turn.²⁹ This β -hairpin is

believed to play a key role in the early events of ubiquitin folding.^{28,29} To compare the sequence dependence of end-to-end collision rates and thereby assess the flexibility, we synthesized DBO/Trp or DBO/Tyr end-labeled peptides (Scheme 1b,c) derived from the “upper strand” (Q²IFVK⁶), the “lower strand” (T¹²ITLE¹⁶), and the “turn” (T⁷LTGK¹¹). These sequences are of interest because although they show random-coil behavior in solution, they represent structurally well-defined and distinct parts of the protein in the native, intact state.

Scheme 1. Structure of the *N*-terminal β -hairpin (1–17) of ubiquitin (a) and general structure of the peptides labeled with DBO/Trp (b) or DBO/Tyr (c).



The individual sequences should possess a different intrinsic flexibility and propensity for folding, which is reflected in the rate by which the two ends of the peptide collide. These intrinsic dynamic parameters of primary peptide sequences can be investigated in short sequences without the complications imposed by secondary structures, i.e., in the absence of any preferred, thermodynamically stable conformation. Since fast-folding turns are implicated as the initiators of the folding of β -hairpins, measuring the end-to-end collision rates of the turn and strand fragments of the β -hairpin may help to clarify β -hairpin folding kinetics and mechanism.^{16,32,33} These rates can be directly related to the intramolecular fluorescence quenching of DBO by either Trp or Tyr in the labeled sequences. The combination of these two quenchers with different quenching efficiency allows the extrapolation of the microscopic rate constants for formation and dissociation of the end-to-end encounter complex, which itself present a new methodology and extension of our fluorescence technique.²³ In addition, to the best of our knowledge, we report the first activation energies for end-to-end collision in short polypeptides obtained by direct photophysical experiments.

Experimental Section

Materials. The synthesis of the Fmoc-protected and DBO-labeled asparagine derivative has been described previously.²³ Polypeptides (all amidated at the C-terminus) were made by Affina Immuntechnik (Berlin, Germany) in > 95% purity (determined by MALDI-MS and HPLC). Water was bi-distilled. D₂O (> 99.9% D) was from Glaser AG, Basel. Other commercial analytical-grade materials were from Fluka or Aldrich.

NMR and CD measurements. NMR experiments were carried out on a Bruker DRX 500 spectrometer in D₂O (with 10% H₂O) at 1 mM peptide concentration. Circular dichroism (CD) experiments of the peptides were performed on a Jasco 720 circular dichroism spectrometer at ambient temperature at peptide concentrations of 10–100 μ M.

Fluorescence lifetime measurements. Fluorescence lifetimes were measured on a laser flash photolysis setup (LP900, Edinburgh Instruments, Edinburgh, Scotland) with 7 mJ, 355-nm pulses of 4-ns width from a Nd:YAG laser (Minilite II, Continuum, Santa Clara, CA), and with a time-correlated single-photon counting fluorimeter (FLS920, Edinburgh Instruments) using a 1.5-ns pulse-width H₂ flash lamp at 365 nm. Fluorescence was detected at 430 nm.

Peptides were measured in H₂O and D₂O at ambient temperature unless stated differently. Typical concentrations of polypeptides were 10 μ M for flash photolysis and 100 μ M for single-photon

counting experiments. The temperature-dependent experiments were carried out from 20–50°C. The pH-dependent measurements were performed in phosphate buffer for pH 7, citrate/HCl/NaOH buffer for pH 2 and Na₂HPO₄/NaOH buffer for pH 12. The concentration of guanidinium chloride was adjusted by measuring the refractive index.

Results

NMR and CD Experiments. NMR and CD spectroscopy were carried out to corroborate that the investigated peptides adopt the random-coil conformation expected for such short sequences.^{24,34} Assignments were based on a combination of 1D-NMR, 2D-COSY, and 2D-TOCSY spectra. The chemical shifts are very sensitive to the secondary structure,³⁵ which allows one to differentiate the random-coil structures from defined secondary structures. The chemical shifts obtained for all labeled peptides were compared with those reported for folded²⁷ as well as denatured³⁶ ubiquitin, see Table 1 for example. The chemical shifts of those residues which possess identical neighboring residues in the synthetic peptide fragments as in ubiquitin were not significantly different (± 0.02 ppm) from those measured for denatured ubiquitin, i.e., in agreement with a random-coil conformation. Slight variances in chemical shift were expectedly observed for the residues *directly adjacent* to the probe or quencher, which experience an environment different from that in the denatured protein (upper and lower entry in Table 1).³⁴

CD measurements were also performed for all peptides at different pH values.³⁷ All CD spectra show the characteristic pattern for a random coil.^{38,39} It is the combination of NMR and CD experiments, which allows us to exclude the existence of sizable amounts of secondary structure in the investigated peptides. All interpretations are therefore based on the assignment of random-coil behavior to the labeled peptide fragments.

Kinetics of end-to-end collision in the turn and strand peptides. The fluorescence-based method for measuring the end-to-end collision rate constants in peptides has been discussed in detail.²³ The intramolecular quenching rate constant in a probe/quencher-labeled peptide is first obtained according to eq. 1 from the experimental fluorescence lifetimes of the probe-labeled peptides with (τ) and without (τ_0) attached quencher.

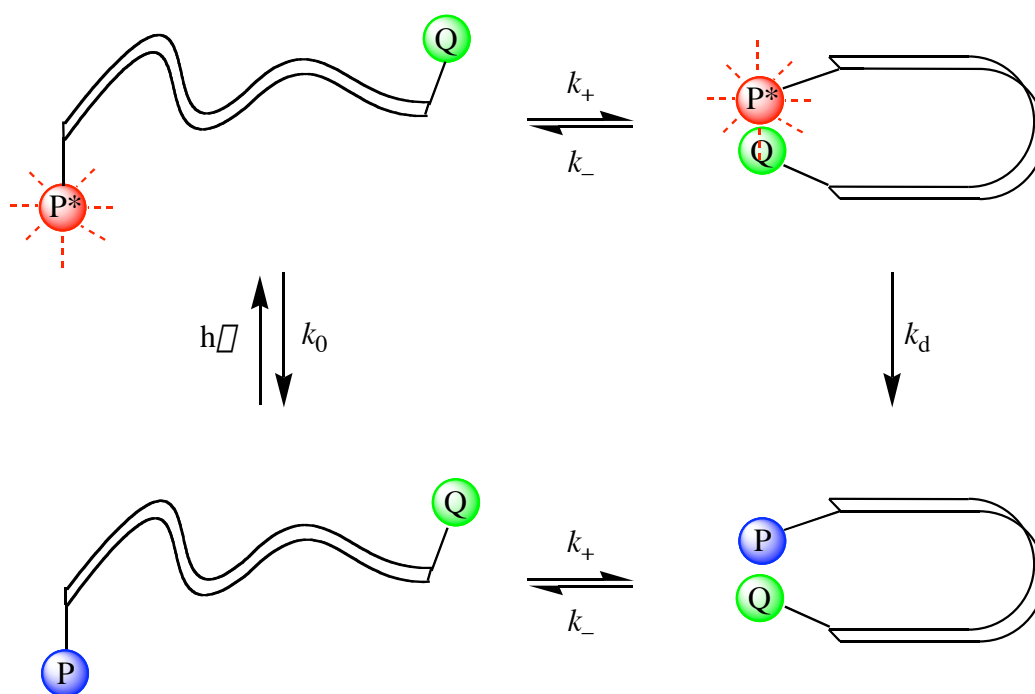
$$k_q = \frac{1}{\tau} - \frac{1}{\tau_0} \quad (1)$$

$$k_q = \frac{k_+ \cdot k_d}{k_- + k_d} \quad (2)$$

$$k_q \approx k_+ \text{ for } k_d \gg k_- \quad (3)$$

The quenching rate constant is a composite of the microscopic rate constants in Scheme 2 and can be expressed by eq. 2, which employs the common steady-state approximation for the formation of the end-to-end encounter complex. k_+ is the end-to-end collision rate constant to form the probe/quencher encounter complex and k_- and k_d are the rate constants for its dissociation and deactivation, respectively. For a diffusion-controlled reaction $k_d \gg k_-$ applies and the simplified eq. 3 results, i.e., for a diffusion-controlled probe/quencher pair the end-to-end collision rate constant equals directly the experimental quenching rate constant. For a non-diffusion-controlled system, interpretations must be based on eq. 2. In the present work Trp was employed as an essentially diffusion-controlled quencher of DBO, and Tyr as a non-diffusion-controlled quencher.

Scheme 2. Kinetic scheme for intramolecular fluorescence quenching.



The three peptide fragments without quencher, TLTGK–DBO, QIFVK–DBO and TITL–DBO, displayed fluorescence lifetimes of 480, 510 and 540 ns in D_2O , respectively. These fluorescence lifetimes are similar to that of parent DBO (505 ns), indicating that a peptide composed of inert amino acids does not significantly quench DBO.²³ The attachment of Trp or Tyr as quencher reduced the lifetimes substantially. From the quenching effects the intramolecular quenching rate

constants were obtained according to eq. 1 (Table 2). When Tyr is used as quencher, the peptide corresponding to the β -turn (YTLTGK–DBO) gives the fastest fluorescence quenching rate, the one corresponding to the upper strand (YQIFVK–DBO) displays approximately a 4 times slower quenching rate, and the rate for the lower strand peptide (YTITL–DBO) lies in between.⁴⁰ Substitution of Tyr by Trp (Table 2) results in much shorter fluorescence lifetimes and accordingly higher quenching rate constants, around 3–5 fold higher. In contrast, measurements in more viscous⁴¹ guanidinium chloride solutions (Table 3) lead to decrease in rate constants by a factor of 2–3 (Table 3). However, regardless of the variation in the absolute rate constants, the order of the quenching efficiency remains the same for both quenchers, i.e., β -turn < lower strand < upper strand. Shown in Figure 1 are representative fluorescence decay traces.

The intramolecular fluorescence quenching is induced by a collision between probe and quencher, which occurs with a different frequency depending on the flexibility of the peptide backbone. The quenching rate constants can therefore be interpreted in terms of the peptide flexibility,^{23,24} i.e., the turn sequence of ubiquitin is more flexible than the two strand sequences.⁴²

Activation energy of end-to-end collision. The activation energies for intramolecular end-to-end collision in probe/quencher-labeled peptides were obtained by plotting the temperature dependence of the quenching rate constants. For this purpose, the fluorescence lifetimes were measured for each peptide with and without quencher at different temperatures and the quenching rate constants were then individually determined for each temperature according to eq. 1. In the absence of quenchers, the fluorescence lifetime of DBO shows a very weak temperature dependence.⁴³ The variation in the fluorescence lifetime of the DBO-labeled peptides without quencher was therefore much weaker than that of the peptides with quencher attached, which indicated a sizable activation barrier for the quenching process. All Arrhenius plots were linear, see Figure 2 for example.

Notably, the experimental activation energies for intramolecular quenching in aqueous solution (17–25 kJ mol⁻¹, Table 3) are similar to or larger than the apparent activation energy of solvent viscous flow in the same temperature range (298–328 K), which amounts to 15.5 kJ mol⁻¹ for H₂O and 16.6 kJ mol⁻¹ for D₂O.⁴⁴ Activation energies in the same range have been reported for intrachain collision in a larger unfolded protein.⁴⁵ For comparison, the activation energies for the bimolecular quenching of a DBO-labeled peptide (QIFVK–DBO) by the free quenchers, Trp and Tyr, fell in the range of 15 ± 3 kJ mol⁻¹ in deaerated H₂O and D₂O. The intermolecular values have a larger error due to the fractional

quenching even at the solubility limit of Tyr and Trp. Note also that the difference in the activation energy of viscous flow between D₂O or H₂O (ca. 1 kJ mol⁻¹) is too small to result in experimentally significant effects on the activation barriers. In contrast, the selection of 7.0 M guanidinium chloride solution as a substantially more viscous solvent causes a pronounced increase in the activation energies for intramolecular quenching (Table 3).

The order of the activation energies follows the order of the end-to-end collision rates, i.e., the most flexible α -turn peptide (TLTGK) displays the lowest activation energy, and the upper, most rigid β -strand peptide shows the highest activation barrier. Accordingly, end-to-end collision is energetically facilitated in the α -turn peptide compared to the β -strand peptides. The fact that some activation barriers exceed the value expected for viscous flow in water immediately indicates that the end-to-end collision process is not only slowed down by “solvent friction”, but also by an “internal friction” (to employ the terminology of polymer models). In other words, some residues impose sizable barriers for those conformational rearrangements of the peptide backbone, which are required to bring the chain ends into contact.

Importantly, the values of the activation energies in the different peptides are the same, within error, for both Trp (Table 3) and Tyr (data not shown) as quencher. This result is consistent with the notion that the experimental activation energies result from an interplay of the effects of internal friction (flexibility of the peptide backbone) and solvent friction (viscosity-dependent diffusional motion) on the collision rate k_+ in Figure 2, but not from a potential activation energy of the rapid deactivation step (k_d). The lower intramolecular quenching efficiency of Tyr (Table 2) is therefore mainly manifested in a reduced preexponential A factor, as expected from the very different transition states for quenching (see below).

The trend of the preexponential A factors with the type of peptide fragment (Table 3) is less intuitively understood. However it can at least be demonstrated that the *order of magnitude* is reasonable for an intramolecular reaction by comparison with the theoretical relationship for an ideal (Gaussian) chain and an ideal intermolecular collision in eq. 4, which assumes the same activation barrier for both processes.⁴⁶

$$\frac{A^{\text{intra}}}{A^{\text{inter}}} = \frac{3}{2\sqrt{N}b^2N_a} \left(\frac{3}{2}\right)^{\frac{3}{2}} \quad (\text{ideal behavior}) \quad (4)$$

N represents the number of chain segments, N_a the Avogadro number, and b the length of one segment. For a heptapeptide ($N = 7$) with a length of 3.8 Å for each peptide bond,¹⁵ A^{intra} , the preexponential factor of an intramolecular reaction, should then amount to approximately 50% of the value for the corresponding intermolecular reaction, A^{inter} . One therefore expects the preexponential factors for the intramolecular reactions to fall below those for the intermolecular processes ($\ln A \approx 26$ for quenching of QIFVK–DBO by Trp or Tyr). The experimental results in Table 3 are in agreement with this notion, although the decrease is quite pronounced for some peptides, which points to strong deviations from ideal-chain behavior.

Charge effects. The effects of charge on the end-to-end collision process in the peptides derived from ubiquitin were also investigated through pH control as well as positional mutation in the peptides. Shown in Table 4 is the pH dependence of the lifetimes for free DBO and the peptides without quencher. The lifetime of DBO remains constant from pH 2–12. Peptides without quencher also have the same lifetime within error at pH 2 and pH 7, but their fluorescence lifetimes decreased at pH 12, especially for QIFVK–DBO and TLGK–DBO. This decrease is related to the deprotonation of the photochemically inert aminium groups at the N -terminus and in particular in lysine to reactive amino groups; amines are well-known quenchers of DBO fluorescence (through exciplex formation),⁴⁷ which accounts for the decrease in fluorescence lifetime, most pronounced in peptides containing lysine, at very alkaline pH. For comparison, the intermolecular quenching rate constant for DBO by lysine increases from $\leq 1 \times 10^6 \text{ M}^{-1}\text{s}^{-1}$ at acidic and neutral pH²³ to $1.45 \times 10^7 \text{ M}^{-1}\text{s}^{-1}$ at pH 12 (this work). Note that the intrachain quenching by other amino acids but Tyr and Trp is explicitly corrected for in eq. 1 by the proper choice of β .

The charge effects on the quenching rate constants for the peptides with quencher are contained in Table 5. Strikingly, quenching for all Tyr peptides increases significantly at high pH. This increase, however, is not indicative for an effect on the chain dynamics but due to the deprotonation of tyrosine itself, which produces the phenoxyl anion, a stronger quencher of DBO fluorescence. Note that while the *intermolecular* quenching rate constant of DBO by Trp is independent of pH, that by Tyr increases by a factor of 4 between pH 7 and 12 (Table 2). There appears to be a change in quenching mechanism by tyrosine from hydrogen abstraction²³ for the phenol form at pH 7 to exciplex formation for the phenolate ion at pH 12. This is reflected in the decrease in solvent isotope effect from 1.6 at pH 7 to 1.2 at pH 12 (Table 2); the isotope effect at pH 7 is related to a partially reaction-controlled abstraction of

the solvent-exchangable phenolic hydrogen atom, while the minor isotope effect at pH 12 can be accounted for in terms of the viscosity-related solvent isotope effect on a close to diffusion-controlled reaction, akin to the minor solvent isotope effect observed for Trp (Table 2).

Due to the variation of the quenching rate constants, the tyrosine peptides studied at pH 12 should be treated separately. Note, however, that Tyr at pH 12 has (incidentally) the same quenching rate constant as Trp. Since the intramolecular quenching of DBO by Trp is presumed to be essentially diffusion-controlled, the same should apply for tyrosine at pH 12. In fact, the rate constants for all Tyr-labeled peptides at pH 12 are equal, within error, to the corresponding Trp-labeled sequences (Table 5).

Mutation effects. Numerous studies in the area of protein engineering have demonstrated that specific amino acids can have a substantial effect on the folding, structure, stability, and function of proteins.⁴⁸⁻⁵¹ We have therefore investigated mutation effects of a *single* amino acid on the flexibility of the β -turn peptide derived from ubiquitin (Table 6). The different mutants show very different quenching rate constants, which confirms the importance of individual amino acids in determining peptide chain flexibility.

Discussion

We have investigated the end-to-end collision rates of equally long peptides derived from the *N*-terminal β -hairpin of ubiquitin, which report on the flexibility in dependence on primary structure and secondary structure propensity of the peptides.⁴² The intrachain dynamics was studied by measuring the intramolecular fluorescence quenching rate constants between DBO, attached as fluorophore to the *C*-terminus, and either Trp or Tyr, attached as quenchers to the *N*-terminus (Scheme 1b,c). Due to the nearly diffusion-controlled quenching of excited DBO by Trp, the corresponding quenching rate constants have been proposed to be approximately equal to the end-to-end collision rate constants.^{23,25} Tyr presents also a good, albeit not diffusion-controlled quencher among the 20 amino acids.²³ Tyr was selected as a complementary quencher to investigate the quantitative effect of non-diffusion-controlled *intermolecular* quenching on the *intramolecular* quenching rate,²³ to extrapolate to the fully diffusion-controlled end-to-end collision rates (k_+), and to estimate the dissociation rates of the end-to-end encounter complex (k_- in Scheme 2).

Primary and secondary structure dependence of peptide flexibility. The quenching rate constants for the three peptide fragments derived from the ubiquitin β -hairpin have been determined for both the DBO/Trp and the DBO/Tyr probe/quencher pair. All investigated peptides adopt a random-

coil conformation as established by NMR and CD, which allows one to relate the efficiency of intramolecular quenching to the dynamics of the intrachain motion rather than to a structural preference or spatial proximity between probe and quencher.⁴² Both sets of data (for Trp and Tyr as quencher) reveal the same order of quenching rates and therefore flexibility of the peptide sequence: turn > lower strand > upper strand. For example, the quenching rate constant for the turn peptide (TLTGK) is 2–4 times faster than that of the peptides corresponding to the upper and lower strand (QIFVK and ELTIT). The spectroscopic measurements suggest that the β -turn region of ubiquitin is “more flexible” than the β -strand regions. This notion is also supported by the activation energy for end-to-end collision, which is significantly (up to 8 kJ mol⁻¹) lower for the β -turn than for both β -strand parts (Table 3). Indeed, the TLTGK turn has been suggested to be highly flexible even in the structure of native ubiquitin.²⁶ The fact that TLTGK is more flexible and can form a turn much faster than the other examined peptides may play an important role in the early events of ubiquitin folding. In other words, a flexible region in a protein is more likely to serve as nucleus for the formation of the secondary structure.

Note that the investigated peptide fragments are equally long, such that the known distance dependence of the end-to-end collision rate²³ can be neglected in the interpretation of the kinetic data. In addition, FRET experiments⁴² indicate that the average end-to-end distance is comparable in the three peptide fragments. The strong variation in the end-to-end collision rates of the peptides must therefore have its underlying reasons in the chain dynamics, i.e., the flexibility of the backbone as imposed by the specific amino acid sequence. As shown in a preliminary communication, individual amino acids affect the flexibility of peptides to a different extent with the flexibility order being as follows:²⁴ Gly > Ser > Asp, Asn, Ala > Thr, Leu > Phe, Glu, Gln > His, Arg > Lys > Val > Ile > Pro. This scale was established for peptide backbones composed of six identical amino acids, such that a direct comparison with the mixed ubiquitin sequences is difficult. However, it is reasonable to assume that the high flexibility of the TLTGK turn region is mainly due to the presence of the most flexible Gly unit, while the high rigidity of the ELTIT and, more pronounced, the QIFVK strand parts is mainly imposed by the presence of one or two very rigid β -branched valine and isoleucine segments, respectively. To verify this intuition, the effect of mutations on the β -turn region was investigated.

In a first set of experiments, Gly in the TLTGK β -turn, was mutated to Ala, Phe, Thr and Val to demonstrate its importance in determining the flexibility of this fragment. Indeed, the quenching rate constants (studied for the DBO/Tyr probe quencher pair, Table 6) decreased significantly in the order

Gly > Ala, Phe, Thr > Val, suggesting an increase in rigidity. This increase is in line with expectations from the flexibility scale (see above), yet somewhat less pronounced than in the preliminary study²⁴ since only a single amino acid was exchanged. Note again that variations in hydrophobicity of the residues have no systematic effect on the flexibility of the peptide mutants, in agreement with our previous study on peptide homopolymers.²⁴

The rate constants for the Ala, Phe, and Thr mutants resemble those observed for the lower strand while the rate constant for the Val mutant even approaches the rate measured for the upper strand (Table 2 and Table 6). This result demonstrates that the Gly in the turn sequence is indispensable for the high flexibility, while the β -alkyl-branched residues substantially increase the rigidity in the strand parts. The latter have, in fact, also a high propensity to occur in β -strands, while Gly is a prominent amino acid in β -turn regions.⁵²⁻⁵⁵ The β -alkyl-branched residues may predispose these sequences to be relatively extended and rigid, which does, along with the high flexibility of the β -turn region, essentially predefine the formation of a β -hairpin. The β -hydroxyl-branched Thr appears more flexible than the β -alkyl-branched amino acids Val and Ile.²⁴ In contrast to Val and Ile, Thr has also a high propensity to occur in β -turns, in addition to β -sheets.⁵²⁻⁵⁵ The higher flexibility of Thr is reflected in the larger quenching rate constant of the G β T mutant compared to the G β V mutant (Table 6).

The mutation of an additional amino acid adjacent to the presumably most flexible Gly linkage, namely of T β G to give TLGGK, causes an additional increase in chain flexibility (Table 6), which is in line with expectations based on the individual flexibility of the amino acids.²⁴ However, it appears unlikely that effects related to chain flexibility are simply additive or predictable in an incremental fashion. Rather, specific amino acids and specific positions as well as the particular sequence are all expected to affect the internal friction in a peptide and they may be vital to produce a flexible peptide, which requires more detailed follow-up work.⁴⁰ For example, we have designed an inverse sequence of the lower strand peptide in which the amino acid composition is the same, but in which the sequence is inverted from TITL (original) to ELTIT (inverted). The results (Table 2) revealed a significant sequence effect (ca. 20–30%) on the fluorescence quenching rate constant, which demonstrates the limitations of predicting chain flexibility in an incremental fashion.

The experimental data for the two β -strand parts suggest a somewhat higher flexibility of the lower strand (Table 2), which is presumably related to the presence of an additional β -alkyl branched amino acid in the upper strand. However, in the actual β -hairpin of ubiquitin both strands could display

a comparable rigidity. Note that the present studies were limited to pentameric β -strand sections of the β -hairpin (Q²IFVK⁶ and T¹²ITLE¹⁶) in order to allow a direct comparison to the intervening pentameric β -turn fragment (T⁷LTGK¹¹). The inclusion of the additional residues of the β -strands, i.e., the comparison of the hexamers M¹QIFVK⁶ and T¹²ITLEV¹⁷ (see Scheme 1), should give rise to similarly rigid strand fragments since a stiffening β -branched Val residue is added to the lower strand.

We also questioned to which degree a variation in the charge status of the different peptide fragments could be responsible for the observed variations in end-to-end collision rates. Much effort has therefore been devoted to the design of pH-dependent experiments (Table 5) to scrutinize the existence of charge effects on the end-to-end collision rates. In addition, we used a peptide sequence with a Glu \rightarrow Lys mutation to invert the charge status within the same sequence through the exchange of an acidic for a basic site (YTITLLE–DBO and YTITLTK–DBO in Table 5). However, the combined experiments did not yield a systematic dependence on the charge status.

We conclude from Table 5 that any effects related to the repulsion or attraction of two charges are too minute to result in experimentally significant effects on the end-to-end collision rates (< 10 %). In fact, in our preliminary communication only a small charge effect on the end-to-end collision rates (ca. 10%) became observable even with six charged residues.²⁴ The important conclusion in regard to end-to-end collision rate constants for the three ubiquitin-derived peptide fragments is that charge effects *cannot* be responsible for the observed variations, i.e., the faster kinetics of the β -turn (TLTGK). The failure to observe a salt effect (up to 0.1 M NaCl, data not shown), which is expected to reduce electrostatic interactions by screening the charges, also supports the finding that charge effects on the end-to-end collision rate (k_+) are not well developed in our peptide sequences.

Microscopic rate constants for end-to-end collision and dissociation. We reasoned that the study of two different quenchers with varying quenching efficiency can be used to extrapolate the end-to-end collision rates and, in addition, to obtain estimates of the dissociation rates (k_{\square} in Scheme 2) for the different peptide sequences. For fluorescence quenching of DBO, one can employ Trp as a quencher with high efficiency and Tyr as a quencher with a lower efficiency. The same results could be obtained with deprotonated Tyr (at pH 12), which is an equally efficient quencher as Trp. The end-to-end collision rates are proposed to be determined by the peptide backbone such that the rate constants for both formation as well as dissociation of the encounter complex should be the same for the

DBO/Trp and DBO/Tyr pairs, i.e., $k_+^Y \square k_+^W \equiv k_+$ and $k_-^Y \square k_-^W \equiv k_-$. Eqs 5a,b then apply for the Trp and Tyr cases as specific expressions of eq. 2.

$$(a) k_q^W = \frac{k_+ \cdot k_d^W}{k_- + k_d^W} \quad \text{and} \quad (b) k_q^Y = \frac{k_+ \cdot k_d^Y}{k_- + k_d^Y} \quad (5)$$

To solve this system of coupled equations for the respective formation and dissociation rate constants, one must specify the unimolecular rate constants for deactivation of the excited encounter complexes (k_d) for both Trp and Tyr. These rate constants should only be dependent on the quencher and therefore be independent of the chain, i.e., the same for the intramolecular and intermolecular reactions. The values for k_d are obtained according to eqs 6a,b from the intermolecular quenching rate constants (k_q^{inter}) by assuming quenching in an ideal solution without enthalpic interactions between probe and quencher.^{46,56,57} The diffusion-limited rate for the intermolecular reaction ($k_{\text{diff}}^{\text{inter}}$) was taken as $3.0 \square 10^9 \text{ M}^{-1}\text{s}^{-1}$ in H_2O ,⁵⁸ assuming a collision radius (a) of 4 Å.⁵⁹ The values for k_d , obtained from eqs 6, amount then to $2.1 \square 10^{10} \text{ s}^{-1}$ for Trp and $1.5 \square 10^9 \text{ s}^{-1}$ for Tyr in H_2O . In accordance with the proposed quenching mechanism, the estimated k_d values display a significant isotope effect for Tyr (1.8, hydrogen atom abstraction), but not for Trp.

$$(a) k_d^Y = \frac{3k_{\text{diff}}^{\text{inter}} k_q^{\text{inter},Y}}{4000 \square a^3 N_a (k_{\text{diff}}^{\text{inter}} \square k_q^{\text{inter},Y})} \quad \text{and} \quad (b) k_d^W = \frac{3k_{\text{diff}}^{\text{inter}} k_q^{\text{inter},W}}{4000 \square a^3 N_a (k_{\text{diff}}^{\text{inter}} \square k_q^{\text{inter},W})} \quad (6)$$

The resulting values for k_+ and k_- , obtained by solving the system of coupled eqs 5, are entered in Table 7. While the rate constant for *intermolecular* quenching of the QIFVK–DBO peptide by Trp ($1.6 \square 10^9 \text{ M}^{-1}\text{s}^{-1}$) falls about a factor of 2 below the expected diffusion-limited rate ($3.0 \square 10^9 \text{ M}^{-1}\text{s}^{-1}$), the extrapolated end-to-end collision rate constants (Table 7) turn out to be only slightly larger than the *intramolecular* quenching rate constants for the DBO/Trp system (Table 2). The DBO/Trp probe/quencher pair is therefore well suited to assess end-to-end collision kinetics in peptides, as already projected in previous studies.^{23,24} The results in Table 7 therefore support the suggestion that a reaction which is somewhat slower than diffusion-controlled in the *intermolecular* case, can become close to diffusion-controlled in the corresponding *intramolecular* system.^{21,23} This is due to the decrease of the diffusion coefficient of probe and quencher when attached to the chain, which may amount to one order of magnitude.^{21,60} The internal friction of the chain limits free diffusion, which resembles the effect of an increased viscosity in a diffusion-controlled intermolecular reaction. This diffusive effect should operate both on the formation of the encounter complex and its dissociation, since both the forward and the reverse reactions require the same conformational changes. The peptide chain will

therefore not only reduce the rate of end-to-end collision (k_+), but it should, in a first approximation, also increase the lifetime of the encounter complex. This accounts for the observation that the k_{\square} value decreases from $1.9 \times 10^{10} \text{ s}^{-1}$ for the intermolecular reaction to $2.0\text{--}4.6 \times 10^9 \text{ s}^{-1}$ for the intramolecular cases (Table 7). Note that this decrease in k_{\square} improves the condition for diffusion-controlled quenching in Scheme 2 ($k_d \gg k_{\square}$), since the deactivation rate (k_d) should be independent of the attachment of the chain.

The significant variances in the rate constants for the various peptides reveal the biopolymer chains as being far from ideal, since an ideal chain would be characterized by constant values of k_+ and k_{\square} .⁴⁶ In addition, the equilibrium constants for intramolecular encounter complex formation ($K_{\text{intra}} = k_+/k_{\square}$, Table 7) are not constant for the different peptides. They range from $3\text{--}9 \times 10^{-3}$ and fall one order of magnitude below the ideal expectation value⁴⁶ (ca. 0.09 for an ideal chain with 7 segments, a reaction radius of 4.0 \AA ⁵⁹ and a segment length of 3.8 \AA ¹⁵). This is indicative of a slight steric repulsion between the chain ends and speaks certainly against a hydrophobic attraction and association between probe and quencher. The latter should give rise to larger values of K_{intra} than for an ideal chain. For example, in a recent study employing time-resolved confocal fluorescence spectroscopy,⁶¹ K_{intra} values in the range of 2.2–4.9 have been obtained for oxazine/Trp labeled peptides, in which probe and quencher are separated by 8–9 amino acids. These are one order of magnitude *larger* than the ideal-chain values expected for peptides of this length (ca. 0.2 for reaction radius of 5.5 \AA ⁶²). Indeed, a strong hydrophobic association between oxazine as probe and Trp as quencher is observed in the ground state (static quenching) and provides also a prerequisite for applying the confocal fluorescence technique, which is based on an equilibrium between two states with different fluorescence properties. In contrast, steady-state fluorescence experiments for the intramolecular and intermolecular quenching of DBO by Trp did not reveal significant static quenching,⁵⁷ which once more corroborates the absence of significant hydrophobic probe/quencher association and is in line with the very small calculated K_{intra} values (Table 7).²³

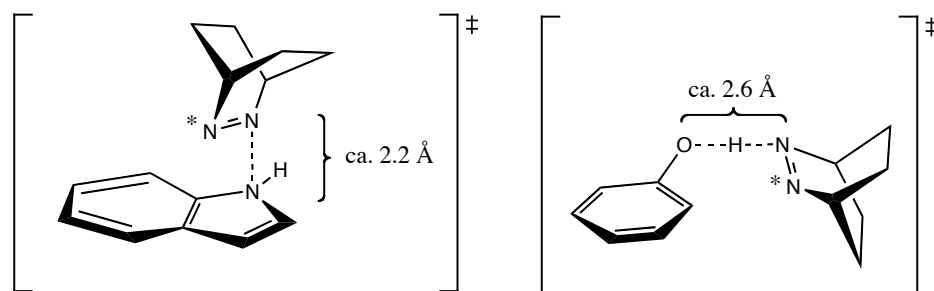
Factors determining end-to-end collision rates. For peptides with Trp as quencher, the isotope effect (Table 2) on the quenching rate constants ranges from 1.1–1.2, which comes close to the ratio of the viscosities of D₂O and H₂O at 25 °C [$\eta(\text{D}_2\text{O})/\eta(\text{H}_2\text{O}) = (1.1 \text{ cP})/(0.89 \text{ cP}) = 1.23$]. More significantly, there is a factor of 2–3 decrease for the end-to-end collision rates in 7.0 M guanidinium chloride solution (Table 3), which can also be accounted for in terms of the higher viscosity effect in

this medium ($\eta = 1.71$ cP). In fact, the decrease is somewhat larger than expected on the basis of viscosity alone, which has been observed previously and attributed to some association of the additive to the peptide.⁴⁵ The latter is expected to cause an additional decrease of the diffusion coefficient of the chain ends.

The viscosity effects demonstrate that solvent friction is an important factor in determining the end-to-end collision rates. On the other hand, we have also evidence derived from the activation barriers (Table 3) and the large variations in end-to-end collision rate constants for different sequences (Table 2 and 7) that the internal friction of the peptide backbone is *another* important factor. Consequently, the end-to-end collision rates in short peptides are determined by a subtle interplay between internal friction and solvent friction. The activation barriers in Table 3 suggest that end-to-end collision in the most flexible turn is mainly controlled by solvent friction; internal friction becomes sizable in the more rigid strand fragments.

Interpretation of end-to-end collision rates. It should be mentioned that the end-to-end collision rate in a peptide depends on the definition of what an end-to-end collision (or contact formation) actually is. The choice of the proper reaction or collision radius is particularly critical.⁵⁸ We have used a value of 4 Å for the present DBO/Trp and DBO/Tyr probe/quencher systems and the data in Table 7.⁵⁹ It can be shown that the choice of a larger radius is expected to lead to substantially higher end-to-end collision rates. It is therefore less surprising that probe/quencher systems with larger reaction radius, like those performing exergonic triplet-triplet⁶³ or singlet-singlet energy transfer,^{64,65} may display intramolecular quenching rate constants which are larger than those obtained from the DBO/Trp and DBO/Tyr probe/quencher pairs. Exchange energy transfer is expected to occur as soon as orbital overlap between probe and quencher is established within distances as large as 8 Å⁶⁶⁻⁶⁸ while quenching of DBO by Trp is subject to the stringent and proximate (≤ 4 Å)⁵⁹ transition state geometries for exciplex formation and hydrogen abstraction (see Scheme 3). The latter have been calculated at a very high level of theory for alcohols⁶⁹ and amines^{47,70} as quenchers.

Scheme 3. Presumed structures for the transition states for fluorescence quenching of DBO by an indole as a model for Trp and by a phenol as a model for Tyr.



As can be seen, the quenching of DBO by Trp and Tyr requires a more intimate and better defined end-to-end contact (“a specific atom-to-atom contact”) than quenching by exchange energy transfer (“a chromophore-to-chromophore orbital overlap”). Systems with a larger effective quenching radius may yield faster quenching rate constants^{63,65} and therefore imply apparently faster end-to-end collision rates, which, however, are then due to a different definition of what the “end” represents, namely an increased size of the ends. The more stringent geometric selection rules for fluorescence quenching of DBO are also reflected in the unique observation that the rates go through a maximum when the chain length is altered, i.e., the shortest homologue is *not* the fastest one.²³ While this characteristic “inversion” behavior is expected for bonding interactions in peptides,^{71,72} as well as polymers,^{73,74} it has not yet been reported in the related studies on polypeptides for alternative probe/quencher pairs with looser quenching geometries.^{19,21,63,65}

With the important insight that there is no universal rate constant of end-to-end collision, we can return to the original motivation for measuring this quantity, which was the prediction of the rates of the elementary steps of protein folding. Clearly, the formation of initial secondary structures, whether β -turn or β -helix, requires the crucial formation of at least a single “correct” hydrogen bond, which may then lead to a zipping of the remaining parts. Hydrogen bonding presents a specific, proximate, and geometrically well-defined atom-to-atom contact, which leads us to suggest that the presently reported end-to-end collision rates present excellent estimates for the maximum rates for formation of peptide hydrogen bonds. In this context, it may or may not be important to emphasize that the atomic arrangement responsible for quenching of DBO by tyrosine with a collinear N---H---O

transition state (see Scheme 3) presents an excellent mimic of the N---H---O hydrogen bond in peptides.

The present rate data suggest that the formation of the first hydrogen bond in the β -turn region can occur as fast as 25 ns ($1/k_+$). The actual rate of formation of the entire β -hairpin cannot be directly predicted from this value alone, but it can be used as the basis to estimate the time scale. If one assumes as one extreme scenario (i) that each of the 6–7 important hydrogen bonds in the ubiquitin hairpin (Scheme 1a) is formed with the same rate of 25 ns (which neglects the known length dependence of end-to-end collision rates),^{19,21,23} (ii) that exclusively correct hydrogen bonds are formed and (iii) that each formation of a correct hydrogen bond leads to a rapid zipping of the two strand parts, one obtains a rate as fast as 4 ns for the formation of the entire β -hairpin. If, however, one makes the reasonable assumption that mismatched hydrogen bonds are also formed and that the hairpin sequence can be transiently trapped in incorrect structures, the overall process can be slowed down by as much as 1–2 order of magnitudes, similar to the situation for ssDNA hairpin structures.⁷⁵ It is therefore likely that the overall rates of β -hairpin formation lie in the range of several tens to hundreds of ns, thereby approaching some early estimates.^{14,16}

Conclusions

In conclusion, we have used a combination of two intramolecular probe/quencher pairs of varying efficiency, namely DBO/Trp and DBO/Tyr, to extrapolate the end-to-end collision rates in polypeptides derived from the two strand and the single turn regions of a natural β -hairpin secondary structure. The extrapolated collision rates lie close to the rates determined for the DBO/Trp pair, thereby supporting the conjectures from previous studies and confirming the notion that reactions between probe and quencher tend to become “more diffusion-controlled” upon attachment to a peptide chain as a consequence of the reduced diffusion coefficients when attached as ends to a chain. Fluorescence quenching of DBO mimics an elementary step of peptide folding, namely the formation of initial hydrogen bonds to initiate secondary structure formation, in that it involves a specific “atom-to-atom” type of collision, which is characterized by a specific transition state geometry with an intimate approach in reach of covalent bonding. The present study has also revealed that the end-to-end collision rates and thereby flexibility of peptides is highly dependent on the peptide sequence. Peptides derived from the β -turn of ubiquitin were found to be much more flexible than those of the β -strands. Varying flexibility of peptide sequences may therefore impose a strong kinetic bias in the early stages

of protein folding. The collision rate for the turn allowed an estimated rate of ca. 25 ns for the formation of a single hydrogen bond in the β -turn region. The prediction of the formation rate of an entire β -hairpin, however, does critically depend on the formation of mismatched structures, which could slow down the overall process, akin to the situation for ssDNA hairpins.⁷⁵ In addition, individual amino acids were shown to have a dramatic effect on peptide flexibility through peptide “mutation” experiments, while charge repulsions or attractions between the chain ends have an insignificant effect on the end-to-end collision rates. The end-to-end collision rate constants, activation energies, and isotope effects demonstrate finally that it is a combination of internal friction in the peptide backbone (conformational changes) and solvent friction (viscosity-limited diffusion), which determines the rates of end-to-end collision in equally long peptides. Variations of the end-to-end distance distribution functions are also expected, but do not need to be invoked to account for the observed effects on the end-to-end collision dynamics.

Acknowledgments. R.R.H. thanks the National Science Foundation (U.S.A.) for an International Research Fellowship (grant INT-9901459). The study was performed within the Swiss National Research Program "Supramolecular Functional Materials" (grant No. 4047–57552 for W.M.N.) and supported by the Schweizerischer Nationalfonds (grant No. 620–58000 for W.M.N.). We thank Dr. K. Kulicke and G. Gramlich for assistance with the NMR measurements and Prof. J. Seelig and his group (Biozentrum, University of Basel) for help with the CD experiments.

References and Notes

† University of Basel

‡ Present address: Department of Chemistry, York University, 4700 Keele Street, Toronto, ON, M3J 1P3 Canada

¶ International University Bremen

* To whom correspondence should be addressed: Tel. +49 421 200 3233, Fax: +49 421 200 3229, e-mail: w.nau@iu-bremen.de

- (1) Pain, R. H., Ed. *Mechanisms of Protein Folding*; 2nd ed.; Oxford University Press: Oxford, 2000.
- (2) Eaton, W. A. et al. *Annu. Rev. Biophys. Biomol. Struct.* **2000**, *29*, 327-359.
- (3) Brooks, C. L., III *Acc. Chem. Res.* **2002**, *35*, 447-454.
- (4) Daggett, V.; Fersht, A. R. *Trends Biochem. Sci.* **2003**, *28*, 18-25.
- (5) Zhuang, X.; Rief, M. *Curr. Opin. Struct. Biol.* **2003**, *13*, 88-97.
- (6) Volk, M. *Eur. J. Org. Chem.* **2001**, *2001*, 2605-2621.
- (7) Baker, D.; Agard, D. A. *Biochemistry* **1994**, *33*, 7505-7509.
- (8) Baskakov, I. V.; Legname, G.; Prusiner, S. B.; Cohen, F. E. *J. Biol. Chem.* **2001**, *276*, 19687-19690.
- (9) Cruzeiro-Hansson, L.; Silva, P. A. S. *J. Biol. Phys.* **2001**, *27*, S6-S9.
- (10) Callender, R. H.; Dyer, R. B.; Gilmanshin, R.; Woodruff, W. H. *Annu. Rev. Phys. Chem.* **1998**, *49*, 173-202.
- (11) Mayor, U. et al. *Nature* **2003**, *421*, 863-867.
- (12) Wang, M.; Tang, Y.; Sato, S.; Vugmeyster, L.; McKnight, C. J.; Raleigh, D. P. *J. Am. Chem. Soc.* **2003**, *125*, 6032-6033.
- (13) Huang, G. S.; Oas, T. G. *Proc. Natl. Acad. Sci. USA* **1995**, *92*, 6878-6882.
- (14) Hagen, S. J.; Hofrichter, J.; Szabo, A.; Eaton, W. A. *Proc. Natl. Acad. Sci. USA* **1996**, *93*, 11615-11617.
- (15) Hagen, S. J.; Hofrichter, J.; Eaton, W. A. *J. Phys. Chem. B* **1997**, *101*, 2352-2365.
- (16) Munoz, V.; Thompson, P. A.; Hofrichter, J.; Eaton, W. A. *Nature* **1997**, *390*, 196-199.
- (17) Thompson, P. A.; Eaton, W. A.; Hofrichter, J. *Biochemistry* **1997**, *36*, 9200-9210.
- (18) Shastry, M. C. R.; Roder, H. *Nat. Struct. Biol.* **1998**, *5*, 385-392.
- (19) Bieri, O.; Wirz, J.; Hellrung, B.; Schutkowski, M.; Drewello, M.; Kiefhaber, T. *Proc. Natl. Acad. Sci. USA* **1999**, *96*, 9597-9601.
- (20) Lednev, I. K.; Karnoup, A. S.; Sparrow, M. C.; Asher, S. A. *J. Am. Chem. Soc.* **1999**, *121*, 4076-4077.
- (21) Lapidus, L. J.; Eaton, W. A.; Hofrichter, J. *Proc. Natl. Acad. Sci. USA* **2000**, *97*, 7220-7225.
- (22) Jas, G. S.; Eaton, W. A.; Hofrichter, J. *J. Phys. Chem. B* **2001**, *105*, 261-272.
- (23) Hudgins, R. R.; Huang, F.; Gramlich, G.; Nau, W. M. *J. Am. Chem. Soc.* **2002**, *124*, 556-564.

- (24) Huang, F.; Nau, W. M. *Angew. Chem. Int. Ed.* **2003**, *42*, 2269-2272.
- (25) Yeh, I.-C.; Hummer, G. *J. Am. Chem. Soc.* **2002**, *124*, 6563-6568.
- (26) Vijaykumar, S.; Bugg, C. E.; Cook, W. J. *J. Mol. Biol.* **1987**, *194*, 531-544.
- (27) Weber, P. L.; Brown, S. C.; Mueller, L. *Biochemistry* **1987**, *26*, 7282-7290.
- (28) Cox, J. P. L.; Evans, P. A.; Packman, L. C.; Williams, D. H.; Woolfson, D. N. *J. Mol. Biol.* **1993**, *234*, 483-492.
- (29) Zerella, R. et al. *Protein Sci.* **1999**, *8*, 1320-1331.
- (30) Bolton, D.; Evans, P. A.; Stott, K.; Broadhurst, R. W. *J. Mol. Biol.* **2001**, *314*, 773-787.
- (31) Kitahara, R.; Akasaka, K. *Proc. Natl. Acad. Sci. USA* **2003**, *100*, 3167-3172.
- (32) Klimov, D. K.; Thirumalai, D. *Proc. Natl. Acad. Sci. USA* **2000**, *97*, 2544-2549.
- (33) Wang, H.; Sung, S.-S. *J. Am. Chem. Soc.* **2000**, *122*, 1999-2009.
- (34) Schwarzsinger, S.; Kroon, G. J. A.; Foss, T. R.; Chung, J.; Wright, P. E.; Dyson, H. J. *J. Am. Chem. Soc.* **2001**, *123*, 2970-2978.
- (35) Wishart, D. S.; Sykes, B. D.; Richards, F. M. *J. Mol. Biol.* **1991**, *222*, 311-333.
- (36) Peti, W.; Smith, L. J.; Redfield, C.; Schwalbe, H. *J. Biomol. NMR* **2001**, *19*, 153-165.
- (37) The application of CD as an alternative technique to NMR was warranted since Maynard et al. have suggested that the relevant chemical shifts only occur when the full β -hairpin of ubiquitin is present, while the β -strand alone may give almost random-coil-like values for the ^1H chemical shifts, cf. Maynard, A. J.; Sharman, G. J.; Searle, M. S. *J. Am. Chem. Soc.* **1998**, *120*, 1996-2007. The authors further suggested that the $^3J_{\text{DN}}$ coupling constants may be a better indicator for secondary structure, which were not determined in the present work.
- (38) Woody, R. W. *Adv. Biophys. Chem.* **1992**, *2*, 37-79.
- (39) Greenfield, N. J. *Anal. Biochem.* **1996**, *235*, 1-10.
- (40) For consistency, all peptides were labeled with DBO at the C terminus. A control experiment with the turn-derived peptide DBO-TLTGKY, where the terminal positions of probe and quencher are exchanged but where the peptide backbone remains the same, yielded the same quenching rate constant within error as the YTLTGK-DBO peptide (Table 2), which supports the idea that the measured quenching rates reflect an intrinsic dynamic property of the peptide backbone, namely its flexibility.
- (41) Kawahara, K.; Tanford, C. *J. Biol. Chem.* **1966**, *241*, 3228-3232.
- (42) Variations in the distribution functions also have an effect on the kinetics of end-to-end collision, which was demonstrated in previous peptide length-dependence studies.(ref. 19, 21, 23) Differences in the distribution functions of the ubiquitin-derived peptide fragments, although equally long, are expected as well. To obtain information on the average end-to-end distance between probe and quencher, fluorescence resonance energy transfer (FRET) experiments in the same peptides were performed, in which Trp serves as singlet energy donor and DBO as acceptor (F. Huang, W. M. Nau, unpublished results). The Trp/DBO system, akin to related Phenyl/DBO

and Naphthyl/DBO systems,(ref. 64) constitutes a unique FRET system which allows selective excitation of the donor and the study of short donor/acceptor separations owing to the short Förster critical radius ($R_0 = 9.9 \text{ \AA}$ for Trp/DBO in H_2O). Since the fluorescence lifetime of Trp is short (3.1 ns) (Lakowicz, J. R. *Principles of Fluorescence Spectroscopy*; 2nd ed.; Kluwer Academic/Plenum Publishers: New York, 1999.) in relation to the time scale of end-to-end collision ($>25 \text{ ns}$, see below), the Trp/DBO FRET system reports on the average distance between Trp and DBO, i.e., on the chain equilibrium rather than on the chain dynamics. The efficiency of energy transfer determined by both steady-state and time-resolved experiments amounted to 60–70%, corresponding to an effective transfer distance of 9.5 \AA for upper strand, 8.8 \AA for the lower strand, and 9.2 \AA for the turn peptide, within an error limit of $\pm 0.5 \text{ \AA}$. These experiments are in line with the assumption that the three equally long peptide fragments have comparable distribution functions. More importantly, the data do not point to a substantially shorter average end-to-end distance for the turn fragment, which could be an alternative explanation for its observed faster end-to-end collision rate.

- (43) Nau, W. M.; Greiner, G.; Rau, H.; Wall, J.; Olivucci, M.; Scaiano, J. C. *J. Phys. Chem. A* **1999**, *103*, 1579-1584.
- (44) Cho, C. H.; Urquidi, J.; Singh, S.; Robinson, G. W. *J. Phys. Chem. B* **1999**, *103*, 1991-1994.
- (45) Hagen, S. J.; Carswell, C. W.; Sjolander, E. M. *J. Mol. Biol.* **2001**, *305*, 1161-1171.
- (46) Nau, W. M.; Huang, F.; Wang, X.; Bakirci, H.; Gramlich, G.; Marquez, C. *Chimia* **2003**, *57*, 161-167.
- (47) Pischel, U.; Zhang, X.; Hellrung, B.; Haselbach, E.; Muller, P.-A.; Nau, W. M. *J. Am. Chem. Soc.* **2000**, *122*, 2027-2034.
- (48) Vendruscolo, M.; Pacl, E.; Dobson, C. M.; Karplus, M. *Nature* **2001**, *409*, 641-645.
- (49) Brannigan, J. A.; Wilkinson, A. J. *Nat. Rev. Mol. Cell Biol.* **2002**, *3*, 964-970.
- (50) Goldenberg, D. P. *Annu. Rev. Biophys. Biophys. Chem.* **1988**, *17*, 481-507.
- (51) Waldburger, C. D.; Jonsson, T.; Sauer, R. T. *Proc. Natl. Acad. Sci. USA* **1996**, *93*, 2629-2634.
- (52) Levitt, M. *Biochemistry* **1978**, *17*, 4277-4285.
- (53) Hutchinson, E. G.; Thornton, J. M. *Protein Sci.* **1994**, *3*, 2207-2216.
- (54) Muñoz, V.; Serrano, L. *Proteins* **1994**, *20*, 301-311.
- (55) Koehl, P.; Levitt, M. *Proc. Natl. Acad. Sci. USA* **1999**, *96*, 12524-12529.
- (56) The absence of a significant enthalpic driving force for a hydrophobic association between probe and quencher in the ground state, in particular, is in line with steady-state fluorescence quenching experiments (see below).
- (57) Wang, X.; Bodunov, E. N.; Nau, W. M. *Opt. Spectrosc.* **2003**, *95*, 560-570.
- (58) We used an empirical formula ($D = 10^{17} \exp(-\frac{m}{m_0}) \text{ nm}^2$) with m the molecular weight) suggested for amino acids, peptides and proteins to estimate the diffusion coefficients of QIFVK-DBO and Trp, cf. ref. 21 and Creighton, T. E. *Proteins: Structures and Molecular Properties*; 2nd ed.; W. H.

Freeman and Company: New York, 1993. The diffusion coefficients were then used in the Smoluchowski equation ($k_D = 4\pi N_A (r_B + r_C)(D_B + D_C)$) along with an effective reaction radius (a) of 4 Å between the reactive sites, cf. ref. 59. In contrast to the use of the simple Debye-Smoluchowski equation to estimate diffusion rates ($k_{\text{diff}} = 8RT/3\eta$), this sequential treatment allows one to explicitly consider the fact that the attachment of a peptide chain to a probe or quencher will necessarily reduce its diffusion coefficient, but not enhance the reaction rate since the true reaction radius remains confined to the volume around the reactive sites of the probe and quencher itself.

- (59) The collision radius (a) of 4 Å corresponds approximately to the sum of the van-der-Waals radii of probe (DBO) and quencher (Trp/Tyr) and is the average distance of van-der-Waals complexes produced by molecular dynamics simulations (M. Zacharias, D. Roccatano, unpublished results). In addition, the distance between the reactive atoms in the transition states for quenching (see Scheme 3 below) lies within this range.
- (60) Liu, G.; Guillet, J. E. *Macromolecules* **1990**, *23*, 4292-4298.
- (61) Neuweiler, H.; Schulz, A.; Boehmer, M.; Enderlein, J.; Sauer, M. *J. Am. Chem. Soc.* **2003**, *125*, 5324-5330.
- (62) Vaiana, A. C.; Neuweiler, H.; Schulz, A.; Wolfrum, J.; Sauer, M.; Smith, J. C. *J. Am. Chem. Soc.* **2003**, *125*, 14564-14572.
- (63) Krieger, F.; Fierz, B.; Bieri, O.; Drewello, M.; Kiefhaber, T. *J. Mol. Biol.* **2003**, *332*, 265-274.
- (64) Pischel, U.; Huang, F.; Nau, W. M. *Photochem. Photobiol. Sci.* **2004**, *3*, 305-310.
- (65) Huang, F.; Nau, W. M., unpublished results.
- (66) Nau, W. M.; Wang, X. *ChemPhysChem* **2002**, *3*, 393-398.
- (67) Wagner, P. J.; Klán, P. *J. Am. Chem. Soc.* **1998**, *121*, 9626-9635.
- (68) Paddon-Row, M. N. In *Stimulating Concepts in Chemistry*; Vögtle, F., Stoddart, J. F., Shibasaki, M., Eds.; Wiley-VCH: Weinheim, 2000, pp 267-291.
- (69) Nau, W. M.; Greiner, G.; Rau, H.; Olivucci, M.; Robb, M. A. *Ber. Bunsenges. Phys. Chem.* **1998**, *102*, 486-492.
- (70) Sinicropi, A.; Pischel, U.; Basosi, R.; Nau, W. M.; Olivucci, M. *Angew. Chem. Int. Ed.* **2000**, *39*, 4582-4586.
- (71) Mutter, M. *J. Am. Chem. Soc.* **1977**, *99*, 8307-8314.
- (72) Camacho, C. J.; Thirumalai, D. *Proc. Natl. Acad. Sci. USA* **1995**, *92*, 1277-1281.
- (73) Zachariasse, K. A.; Macanita, A. L.; Kuehnle, W. *J. Phys. Chem. B* **1999**, *103*, 9356-9365.
- (74) Mar, A.; Fraser, S.; Winnik, M. A. *J. Am. Chem. Soc.* **1981**, *103*, 4941-4943.
- (75) Wang, X.; Nau, W. M. *J. Am. Chem. Soc.* **2004**, *126*, 808-813.
- (76) Mathews, C. K.; van Holde, K. E.; Ahern, K. G. *Biochemistry*; 3rd ed.; Benjamin/Cummings: San Francisco, 2000.

Table 1. ¹H NMR chemical shifts of the labeled turn fragment (DBO-TLTGKY) in comparison to those in denatured and folded ubiquitin

position	ϕ(NH)			ϕ(ϕH)		
	labeled	denatured	folded	labeled	denatured	folded
	peptide ^a	ubiquitin ^b	ubiquitin ^c	peptide ^a	ubiquitin ^b	ubiquitin ^c
[T-7] ^d	8.66	8.34	8.69	4.37	4.41	5.00
L-8	8.50	8.51	8.91	4.44	4.44	4.33
T-9	8.09	8.09	7.59	4.36	4.37	4.41
G-10	8.34	8.32	7.78	3.94	3.94	3.62/4.36 ^e
[K-11] ^d	8.17	8.10	7.25	4.18	4.09	4.37

^a This work in D₂O with 10% H₂O. ^b At 8 M urea and pH 2, taken from ref. ³⁶. ^c At 50 °C in 25 mM acetic acid at pH 4.7, taken from ref. ²⁷. ^d Amino acid has a different direct neighbor in the labeled peptide and in ubiquitin. ^e Separate peaks for glycine ϕ-protons.

Table 2. Fluorescence lifetimes, quenching rate constants, and solvent deuterium isotope effects for the intramolecular and intermolecular quenching of DBO-labeled peptides and DBO by tryptophan and tyrosine

fragment	sequence	in H ₂ O		in D ₂ O		$k_q(\text{H}_2\text{O})/$ $k_q(\text{D}_2\text{O})$
		τ /ns	$k_q/(10^6 \text{ s}^{-1})^a$	τ /ns	$k_q/(10^6 \text{ s}^{-1})^a$	
upper strand	WQIFVK–DBO	90	8.2	110	7.1	1.2
	YQIFVK–DBO	172	3.0	266	1.8	1.7
lower strand	WTITLE–DBO	63	13.0	74	12.0	1.1
	YTITLE–DBO	110	6.1	175	3.9	1.6
	[YELTIT–DBO] ^b	126	5.0	215	2.8	1.8
turn	WTLTGK–DBO	27	34.0	33	28.0	1.2
	YTLTGK–DBO	74	10.2	130	5.6	1.8
	[DBO–TLTGKY] ^c	76	9.9	135	5.3	2.0
intermolecular	W + QIFVK–DBO		1600 M ⁻¹		1400 M ⁻¹	1.1
	Y + QIFVK–DBO		230 M ⁻¹		130 M ⁻¹	1.8
	W + DBO		2100 M ⁻¹		2000 M ⁻¹	1.1
	Y + DBO (pH 7)		560 M ⁻¹		360 M ⁻¹	1.6
	Y + DBO (pH 12)		2100 M ⁻¹		1800 M ⁻¹	1.2

^a Unless stated differently, lifetimes of corresponding peptides without quencher were taken as τ in the calculation of intramolecular quenching rate constants according to eq. 1. ^b Inverted lower strand; lifetime of TITLE–DBO taken as τ . ^c Probe/quencher-exchanged turn; lifetime of TLTGK–DBO taken as τ .

Table 3. End-to-end collision rates and activation energies of DBO/Trp-labeled peptides in different solvents^a

fragment	sequence	solvent ^b	$k_q/(10^6 \text{ s}^{-1})$	$\ln(A/\text{s}^{-1})$	$E_a/(\text{kJmol}^{-1})$
upper strand	WQIFVK–DBO	H ₂ O	8.2	25.5	23
		D ₂ O	7.1	25.5	25
		4.4 M Gdn.HCl	6.7		
		7.0 M Gdn.HCl	3.8	26.8	29
lower stand	WTITLE–DBO	H ₂ O	13.0	25.0	21
		D ₂ O	12.0	24.5	20
		4.4 M Gdn.HCl	9.5		
		7.0 M Gdn.HCl	4.6	27.4	28
turn	WTLTGK–DBO	H ₂ O	34.0	24.0	17
		D ₂ O	28.0	24.0	17
		4.4 M Gdn.HCl	22.0		
		7.0 M Gdn.HCl	12.2	25.8	23

^a To obtain the intramolecular quenching rate constant at different temperatures (298–328 K), the lifetime of the corresponding peptide without quencher was measured at the same temperature and taken as τ . Error in k_q is 5% and in $E_a \pm 1 \text{ kJ mol}^{-1}$.

^b The viscosities of the solvents at 25 °C are 0.89 cP in H₂O, 1.10 cP in D₂O, 1.18 cP in 4.4 M Gdn.HCl, and 1.71 cP in 7.0 M Gdn.HCl.

Table 4. Intrinsic fluorescence lifetimes of the DBO-labeled reference peptides and DBO in the absence of tryptophan and tyrosine as quenchers at different pH in H₂O

fragment	sequence	τ / ns		
		pH 2	pH 7	pH 12
upper strand	QIFVK-DBO	355	355	240
lower strand	TITLE-DBO	350	340	320
turn	TLTGK-DBO	315	305	205
intermolecular	DBO	315	320	315

Table 5. Charge effects on the rate constants for the intramolecular and intermolecular fluorescence quenching of DBO-labeled peptides and DBO in dependence on pH in H₂O

fragment	sequence	$k_q/(10^6 \text{ s}^{-1})^a$		
		charge status ^b		
		pH 2	pH 7	pH 12
upper strand	WQIFVK-DBO	7.2 + + WQIFVK-DBO	8.2 + + WQIFVK-DBO	7.1 WQIFVK-DBO
	YQIFVK-DBO	2.8 + + YQIFVK-DBO	3.0 + + YQIFVK-DBO	6.7 - YQIFVK-DBO
lower strand	WTITLE-DBO	11.0 + WTITLE-DBO	13.0 + - WTITLE-DBO	15.0 - WTITLE-DBO
	YTITLE-DBO	5.8 + YTITLE-DBO	6.1 + - YTITLE-DBO	16.0 - - YTITLE-DBO
	[YTITLK-DBO] ^c	4.5 + + YTITLK-DBO	4.4 + + YTITLK-DBO	13.0 - YTITLK-DBO
	[YELTIT-DBO] ^d	4.6 + YELTIT-DBO	5.0 + - YELTIT-DBO	16.0 - - YELTIT-DBO
turn	WTLTGK-DBO	30.0 + + WTLTGK-DBO	34.0 + + WTLTGK-DBO	35.0 WTLTGK-DBO
	YTLTGK-DBO	9.8 + + YTLTGK-DBO	10.2 + + YTLTGK-DBO	31.0 - YTLTGK-DBO
	[DBO-TLTGKY] ^c	10.0 + + DBO-TLTGKY	9.9 + + DBO-TLTGKY	34.0 DBO-TLTGKY ^u
intermolecular	W + DBO	1800 M⁻¹ + DBO + W	2000 M⁻¹ DBO + W	2300 M⁻¹ DBO + W ⁻
	Y + DBO	600 M⁻¹ + DBO + Y	560 M⁻¹ DBO + Y	2100 M⁻¹ DBO + Y ^{- -}
	K + DBO	≤ 1 M⁻¹ ++ DBO + K	≤ 1 M⁻¹ + DBO + K	14.3 M⁻¹ - DBO + K

^a Reference values (k_q) were individually determined for corresponding peptide without quencher. ^b

Charge status based on the pK_a values reported in ref. ⁷⁶. ^c Mutated lower strand; lifetime of

TLTGK-DBO taken as τ_0 . ^dInverted lower strand; lifetime of TITLE-DBO taken as τ_0 .

^eProbe/quencher-exchanged turn; lifetime of TLTGK-DBO taken as τ_0 .

Table 6. Mutation effects on the rate constants for intramolecular fluorescence quenching of the DBO-labeled turn peptide by tyrosine as *N*-terminal quencher

mutation	sequence	in H ₂ O		in D ₂ O	
		τ /ns	$k_q/(10^6 \text{ s}^{-1})^a$	τ /ns	$k_q/(10^6 \text{ s}^{-1})^a$
none	YTLTGK-DBO	74	10.2	130	5.6
G → A	YTLT <u>A</u> K-DBO	108	6.1	164	4.1
G → F	YTLT <u>F</u> K-DBO	110	6.0	168	4.0
G → T	YTLT <u>T</u> K-DBO	112	5.8	185	3.4
G → V	YTLT <u>V</u> K-DBO	138	4.1	220	2.5
T → G	YTL <u>G</u> GK-DBO	68	11.6	120	6.3

^a τ was taken as 325 ns in H₂O and 500 ns in D₂O.

Table 7. Extrapolated microscopic rate constants^a for the intramolecular and intermolecular quenching of DBO-labeled peptides and DBO according to Scheme 2 in H₂O [kinetic solvent deuterium isotope effects, i.e., $k(\text{H}_2\text{O})/k(\text{D}_2\text{O})$, given in square brackets]

fragment	sequence	$k_+/10^6 \text{ s}^{-1}$	$k_-/10^9 \text{ s}^{-1}$	$K/10^{-3}$
upper strand	W/Y-QIFVK-DBO	9.5 [1.2]	3.2 [1.1]	3.0
lower strand	W/Y-TITLE-DBO	14.2 [1.1]	2.0 [1.0]	7.1
turn	W/Y-TLTGK-DBO	41.4 [1.2]	4.6 [1.1]	9.0
intermolecular	W/Y + QIFVK-DBO	$\cong 3000 \text{ M}^{-1}$ [$\cong 1.23$]	18.6 [1.23]	160 M^{-1}

^a The values were extrapolated by assuming an ideal intermolecular diffusion, *cf.* text and ref.⁵⁸.

Captions for Figures

Figure 1. Fluorescence decays (measured by single-photon counting) of ubiquitin-derived peptides (100 μ M in D₂O). The traces derive from the upper strand (WQIFVK-DBO, upper trace), lower strand (WTITLE-DBO, middle trace), and the turn (WTLTGK-DBO, lower trace). Shown in the inset is the decay for WQIFVK-DBO on a semilogarithmic scale.

Figure 2. Representative Arrhenius plots for the intramolecular fluorescence quenching in DBO-labeled peptides by Trp.

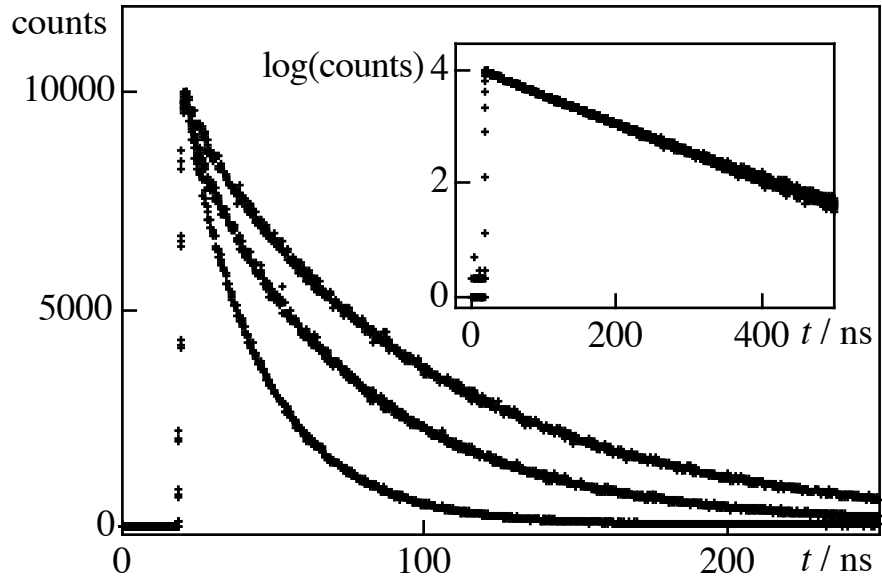


Figure 1

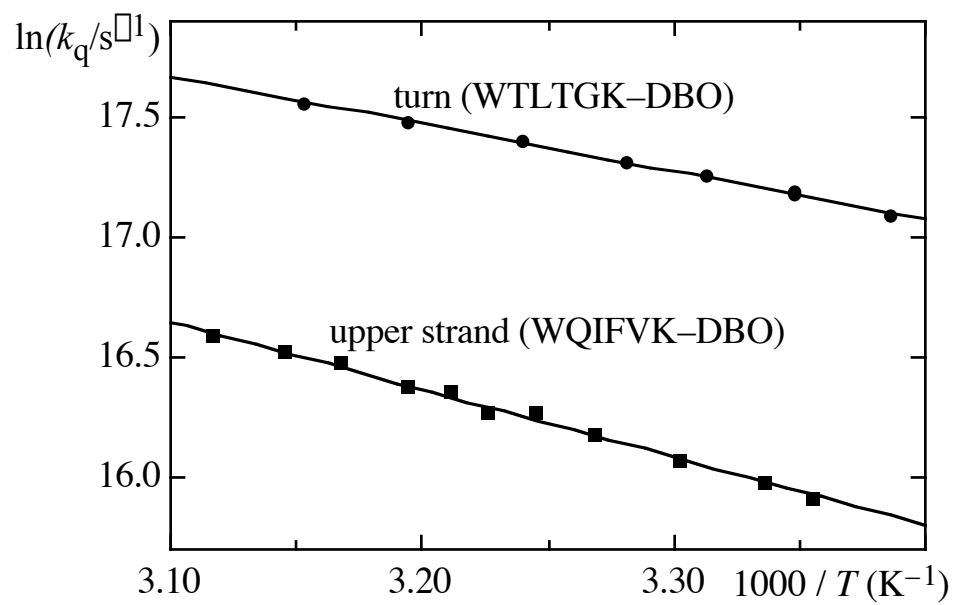
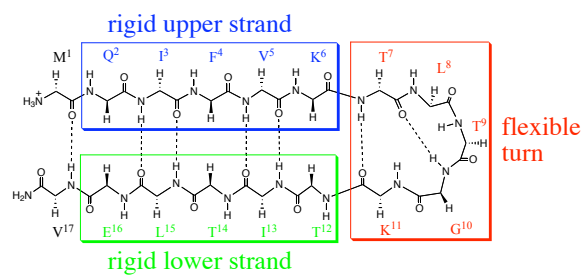


Figure 2

TOC graphics



Photochemical Techniques for Studying the Flexibility of Polypeptides

Fang Huang¹ and Werner M. Nau^{2,*}

¹ Department of Chemistry, University of Basel, Klingelbergstrasse 80, CH-4056 Basel, Switzerland

² School of Engineering and Science, International University Bremen, Campus Ring 1, D-28759 Bremen, Germany

* To whom correspondence should be addressed. E-mail: w.nau@iu-bremen.de

Abstract

Knowledge of peptide dynamics and flexibility is of importance for understanding and predicting the folding mechanisms of proteins and their functions. The present work gives an overview and applies a fluorescence-based technique to investigate the dynamics and flexibility of peptides with different length and different sequences. This new technique takes full advantages of fluorescence for detection as compared to the previously employed transient absorption. The length dependence of end-to-end collision rates suggests that the behavior of peptides is far from that of an ideal chain, and the strong sequence dependence of peptides flexibility allows one to extract a flexibility scale for amino acids in peptides. The rigidifying character of a polyproline backbone, the effect of charges on the end-to-end collision frequency, and the flexibility of α -peptides in comparison to their β homologues are also studied.

Introduction

A common approach to measure intrachain dynamics in polymers is based on the use of a photophysical probe and a quencher attached to the ends of a polymer chain [1-5]. Following excitation of the probe, there is a certain possibility that the quencher diffuses to the excited probe to induce, upon collision, excited-state deactivation. In the case of efficient quenching, the intramolecular quenching rate constant is directly related to the rate of end-to-end collision, which is an important parameter since it reports on the conformational flexibility of the backbone and allows the comparison of the dynamic properties of different polymers. In addition, it allows experimental tests of theoretical models for polymer motions and polymer reactions [6], in particular the cyclization propensity [5, 7]. An important requirement of the probe/quencher methodology is that long-lived excited states need to be employed, since the lifetimes have to be sufficiently long to allow intrachain diffusion to compete efficiently with the intrinsic excited-state decay. Triplet-excited states (monitored by transient absorption) and some long-lived fluorescent states (mostly pyrene) have been employed in the respective measurements with polymers [1-5]. Another requirement is that quenching must take place strictly upon contact of the probe/quencher pair but not through a longer distance as is often the case for fluorescence resonance energy transfer (FRET) or highly exergonic electron transfer. Otherwise, the quenching process does not directly report on the elementary process of end-to-end collision but reflects the distance distribution and the diffusion coefficients of the chain ends [8], which is of primary interest in a different context. The preferred probe/quencher pairs for addressing end-to-end collision kinetics are therefore based on quenching by either hydrogen atom transfer and exciplex or excimer formation. Quenching by triplet-triplet energy transfer [9, 10] and electron transfer [11, 12] may be applicable in limiting cases and in combination with careful control experiments [13], while fluorescence energy transfer (FRET) needs to be avoided unless donor/acceptor pairs with a very small Förster critical radius (ca. 10 Å) are employed [14].

The principle for measurement of end-to-end collision kinetics by the probe/quencher methodology and the relationship of the quenching rate constant to the microscopic rate constants for formation (k_+), dissociation (k_-), and deactivation of the excited-state encounter complex (top right structure) are shown in Figure 1 [15, 16]. Note that the quenching rate constant equals the

end-to-end collision rate constant whenever quenching is efficient, i.e., $k_d \gg k_-$. It is then said that quenching is determined by intrachain diffusion, which is restricted by two factors: internal friction within the backbone and solvent friction by the surrounding medium.

The transfer of the probe/quencher methodology from polymers to biopolymers has proven to be the opposite of straightforward, since there are a number of additional constraints in polypeptides and oligonucleotides. For example, polar probes and quenchers should be used to reduce hydrophobic effects and the probe/quencher system must allow measurement in aqueous solution. These are not fulfilled for the traditional chromophores like pyrene and anthracene [1-4], which has led to a quest of suitable probe/quencher systems for biopolymers [9-12].

In this context, we have introduced the use of 2,3-diazabicyclo[2.2.2]oct-2-ene (DBO) as a long-lived fluorescent probe [15, 16], and either tryptophan (for polypeptides) [17, 18] or guanine (for oligonucleotides) [19, 20] as intrinsic fluorescence quenchers. In the case of polypeptides, tyrosine can be used as an alternative, although somewhat less efficient, quencher [21]. The condition $k_d \gg k_-$ in Figure 1 is fulfilled when the corresponding intermolecular reaction between probe and quencher is diffusion-controlled, but this is no necessary criterion. In biopolymers, quenching may be determined by intrachain diffusion even if the intermolecular quenching of the probe falls up to one order of magnitude below the diffusion-controlled limit. This is due to the reduced diffusion coefficient of the chain ends, which results in a slower k_- rate (Figure 1) than for the intermolecular ones [11, 21].

The DBO chromophore is unique due to its long lifetime (e.g., 325 ns in H₂O), which can be further increased to about 1 μ s by addition of an enhancement solution containing the supramolecular host cucurbit[7]uril and sodium sulfate [22]; this value is the same as that measured in the gas phase [23]. In addition, the DBO chromophore has a very small size, it is uncharged yet polar, does not tend to form ground-state complexes or excimers, is compatible with solid-phase synthesis, as well as thermally and photochemically stable. All these features are advantageous for use as a fluorescent probe for biomolecules, even if the extinction coefficient is very low [15, 24].

Experimental Section

The fluorescence lifetimes of the water-soluble peptides ($\leq 100 \mu$ M) were measured in D₂O at 25°C by time-correlated single photon counting (FLS920, Edinburgh Instruments) with a

Picoquant picosecond pulsed diode laser ($\lambda = 373$ nm, ca. 50 ps pulse width) for excitation. Fmoc-DBO, which is a labeled asparagine, was synthesized as previously described [17], which allows the attachment of the DBO chromophore to a polypeptide by standard solid-phase synthesis techniques. Peptides were made by Biosyntan (Berlin) in a purity better than 95%. The three α -peptides were supplied by the group of Prof. Samuel H. Gellman, University of Wisconsin-Madison.

Results and Discussion

The end-to-end collision rates reported in the present study have been obtained by analyzing fluorescence quenching in DBO/Trp end-labeled peptides according to our previously established methodology [17, 18, 21]. The DBO/Trp probe/quencher method has been established as an accurate and broadly applicable tool to assess end-to-end collision rates, which has received independent support by the most recent theoretical studies [6, 25] as well as single-molecule experiments employing time-resolved confocal fluorescence microscopy [26]. For example, the end-to-end collision rate for the peptide structure X-SQETFSDLWKLLPEN is 9.8×10^6 s⁻¹ for the ensemble measurement with X = DBO and 8.3×10^6 s⁻¹ for the single molecule measurement with X = oxazine, where the small deviation can be attributed to a slower diffusion of the larger oxazine probe.

The measured intramolecular quenching rate constants for different polypeptides are entered in Table 1. The results show that the intramolecular quenching rate constants are strongly dependent on chain length and chain sequence and vary by 1–2 orders of magnitude. The first section in Table 1 shows the length dependence of the quenching efficiency for the Gly-Ser series with the characteristic inversion at very short separation (“no backbone”) [17]. A double logarithmic plot of the quenching rate constants *versus* peptide length gives rise to an evident negative curvature and a much smaller slope than the theoretical prediction for an ideal chain (Figure 2), which suggests a significant deviation of the behavior of the peptides from ideal chain behavior. The inversion may either come from the breakdown of the Gaussian approximation, i.e., distribution deviation from ideal chain, or the significant decrease of end-to-end diffusion coefficient since the end-to-end collision rate is determined by both the end-to-end distribution and the diffusion coefficient. Further theoretical and experimental studies have revealed that the

distribution function is not the dominant factor inducing the inversion [6], but that a significant decrease of the end-to-end diffusion coefficient is expected for the shortest peptides.

On the other hand, the observed inversion immediately speaks against the remote possibility of a through space quenching mechanism for the DBO/Trp probe/quencher pair, which would be expected, for example, if electron transfer through bond or energy transfer, but supports the exciplex quenching mechanism. This characteristic “inversion” behavior is expected for bonding interactions in peptides [7] as well as polymers [1], because specific steric effects in very short backbones hinder cyclization and therefore end-to-end contact. However, the inversion has not been reported in related studies on polypeptides with alternative probe/quencher pairs [9, 11], which is presumably due to looser and less well-defined quenching geometries.

Listed in the second section in Table 1 is the length dependence and rigidifying character in polyprolines. A comparison with the equally long Gly-Ser peptides shows a significant decrease of the quenching rate constant for polyproline peptides. This is due to the high rigidity of proline, i.e., the large internal friction in polyproline, which stems from its frozen N-C α bond. Polyproline peptides also show a much more significant length dependence, i.e. the quenching rate decreases much more steeply with increasing peptide length than it is the case for the Gly-Ser peptides or an ideal Gaussian chain (Figure 2). This is presumably a consequence of the PPII-helix formation in polyprolines [18], which becomes more stable for longer sequences, as evidenced by CD measurements. The increased internal friction and PPII-helix propensity both slow end-to-end collision by decreasing the rotation rate of the backbone and changing the conformational equilibrium, respectively. Note that for the remaining equally long peptides, no sizable secondary structure formation was indicated by CD and/or ^1H NMR spectra, such that we assign a random-coil conformation to all tetrameric and hexameric peptides except for the polyprolines. Changes in conformational equilibrium are not held responsible for the differences in end-to-end collision rates in these cases [21], but rather variations in internal flexibility as imposed by the amino acid type and sequence.

α -Peptides, composed of α -amino acids, are considered to be good scaffolds for creating biologically active molecules due to their characteristics over β -peptides [27, 28]. It is very interesting to compare the flexibility of α -peptides and β -peptides with similar structure, which may

reveal some important underlying reasons for the different properties of these two related biopolymers. A slightly higher flexibility of β -peptides as compared to their α -homologues has been suggested theoretically [29]. To provide direct experimental evidence, the end-to-end collision rate of β -peptides and its length dependence were also investigated [30], which are shown in the third section in Table 1. Shown in Figure 3 are the structures of the β -peptides used in present work, the amino acid of which has very similar structure to Gly, but with an “additional” methylene group. A comparison of the data with those for α -peptides with similar structure, e.g. Gly or Gly-Ser peptides, and the same number of peptide bonds shows similar quenching rate constants. This is surprising if one considers that the contour length of a β -peptide is extended by an additional $-\text{CH}_2-$ bond in each monomeric unit, and if one recalls that longer peptides should give rise to slower quenching according to the known length dependence (see above). Making use of the rough approximation that the length of a β -peptide is $4/3$ that of an α -peptide due to the additional β -bond in each monomeric unit, and transferring the known length dependence for α -peptides, where $\log k_{\mu} \propto b \log l$ with l the contour length of a peptide and $b = 1-1.5$ [9, 11, 17], one expects the rates of end-to-end collision in β -peptides to be 30–40% slower than for equally long α -peptides. Experimentally, the rate constants for end-to-end collision are very similar, e.g., $3.9 \times 10^6 \text{ s}^{-1}$ for the β -hexaglycine and $3.5 \times 10^6 \text{ s}^{-1}$ for the β -hexaglycine derivative. This demonstrates that the effect related to the increased chain length (expectation value ca. $2.5 \times 10^6 \text{ s}^{-1}$) is at least partially offset by an extra element of chain flexibility in the β -peptide. We assign this tentatively to the rotation about the additional CH_2-CH_2 bond which should increase the conformational space accessible to the β -peptide [27]. The latter may facilitate end-to-end collision, which is being probed by the present experimental technique. For comparison, it should be mentioned that the activation energies for the end-to-end collision process of both α - and β -peptides are comparable and lie close to the activation energy of solvent viscous flow [21].

Another very important aspect in peptide dynamics is to know whether or not charges impose significant effect on the end-to-end collision rates or peptide flexibility. To test electrostatic effect on peptide intramolecular collision, experiments were also carried out at different pH to control the charge status of the peptides. Shown in the fourth section in Table 1 are the quenching rate constants of some typical peptides, the residues of which can be protonated and deprotonated, and

the charges can be changed by adjusting the pH. A slight charge effect was observed in the 6-mer peptides, in which all of the residues can be charged [18]. In another set of experiment carried out with peptides containing only two chargeable residues, the end-to-end collision rate did not show a systematic effect [21], which suggests that any effects related to the repulsion or attraction of two charges are too minute to result in experimentally significant effects on the end-to-end collision rates (< 10 %). Both of the experiments strongly suggest that charge does not impose significant effect on the end-to-end collision rate although it is well known to affect the thermodynamic parameters of peptides and proteins.

The reason for the very weak charge effect has not been clearly demonstrated yet. In addition to the efficient screening of charges by water, one must take into account that the actual position of the charged residues is quite remote from the backbone. The results for the amino acid type have demonstrated that end-to-end collision rates are mainly governed by the atoms or groups in close proximity to the backbone [18]. For example (see also below), the β -branched amino acid Ile was found to reduce peptide end-to-end collision rate significantly, while the β -branched isomeric amino acid Leu gives rise to peptides with much faster collision rate, demonstrating that a β -methyl group imposes much less hindrance on the rotation of the peptide back bone than a α -methyl group. In line with these observations, the more remote charged residues have also a significantly decreased effect on the internal friction; they are quite remote from the backbone, which offers them a larger conformational space such that they can better “avoid” friction.

The end-to-end collision rates for peptides composed of a sequence of identical amino acids are also investigated. With the assumption that the end-to-end distances are similar for all of the equally long peptides, we reasoned that the end-to-end collision rates can be directly related to the flexibility of peptides. The end-to-end collision rate as a function of amino acid type gives a flexibility scale of amino acids in peptides with the order: Gly > Ser > Asp, Asn, Ala > Thr, Leu > Phe, Glu, Gln > His, Arg > Lys > Val > Ile > Pro [18]. The quenching rate constants in section five of Table 1 show variations by 1–2 orders of magnitude for the various amino acids. Such large variations indicate that the individual amino acid type can impose hindrance to the rotation of peptide backbone in very different degree, which are hardly possible to come from the variation of conformational equilibrium. Recent fluorescence resonance energy transfer (FRET) investigations

on peptides derived from the first β -hairpin at the *N*-terminus of ubiquitin supports our assumption that equally long peptides have similar end-to-end distance and that variations in the distribution functions are not the dominant factor in determining the difference of end-to-end collision rate [21]. The interpretation of the end-to-end collision rate constants in terms of internal friction or dynamic flexibility as imposed by the amino acid type and sequence remains therefore valid.

Finally, we also addressed the effect of the solvent on the end-to-end collision rates for peptides. The collision rates of peptides in H₂O and D₂O have already been investigated in our previous work and the results suggest a viscosity-dependence of the end-to-end collision rate [21]. The effect of urea on the collision rates was presently investigated and the results are shown in the first and the sixth sections in Table 1, where values in the parenthesis were obtained in 4.8 M urea-D₂O solution. One of the important features of DBO is that it is not efficiently quenched by the common denaturants, urea and guanidinium chloride, i.e., the quenching rate constant are $< 3 \times 10^4 \text{ M}^{-1}\text{s}^{-1}$ [17]. This allows experiments to be performed in concentrated urea or guanidinium chloride solution without losing the crucial property of long-lived fluorescence. As shown in Table 1, the quenching rate constants decrease in urea solution. The decrease of the quenching rate constant, ranging from 1.2–1.4, is similar as or larger than that expected on the basis of viscosity increase ($\eta/\eta_0 = 1.28$ for urea/H₂O solution [31]), which is similar, although less pronounced, as the results from measurements in 7.0 M guanidinium chloride solution for other peptides [21]. On the contrary, experiments on Gly-Ser peptides carried out in acetonitrile give similar quenching rate constant as in D₂O (data not shown). This cannot be accounted for in terms of a viscosity effect, because the viscosity of acetonitrile is approximately 3 times lower than in water, and demonstrates that other factors but viscosity, e.g., variations in distribution functions, may become important when the reaction medium is substantially altered, e.g., by the use of organic solvents or co-solvents.

Conclusion

We have established a fluorescence-based method for measuring the end-to-end collision rates of polypeptides, where DBO is used as long-lived fluorescent probe, and Trp or Tyr as efficient quencher. Length dependence and sequence dependence on the end-to-end collision rates

of peptides were investigated in detail, which shows real peptides are significantly different from ideal chains. A conformational flexibility scale for amino acids in peptides was reported, depending on the variation of end-to-end collision rate on peptide sequence. Charges have weak effect on the end-to-end collision rates of peptides and viscosity effect for significantly different solvent cannot be simply predicted.

Acknowledgements:

This study was performed within the Swiss National Research Program NRP 47 "Supramolecular Functional Materials" (grant No. 4047-57552) and supported by the Schweizerischer Nationalfonds (grant No. 620-58000).

References:

1. K. A. Zachariasse, A. L. Macanita and W. Kuehnle. *J. Phys. Chem. B* **103**, 9356 (1999).
2. M. A. Winnik. *Acc. Chem. Res.* **10**, 173 (1977).
3. M. A. Winnik. *Chem. Rev.* **81**, 491 (1981).
4. K. Horie, W. Schnabel, I. Mita and H. Ushiki. *Macromolecules* **14**, 1422 (1981).
5. A. Mar, S. Fraser and M. A. Winnik. *J. Am. Chem. Soc.* **103**, 4941 (1981).
6. X. Wang, E. N. Bodunov and W. M. Nau. *Opt. Spectrosc.* **95**, 560 (2003).
7. M. Mutter. *J. Am. Chem. Soc.* **99**, 8307 (1977).
8. E. Haas, E. Katchalski-Katzir and I. Z. Steinberg. *Biopolymers* **17**, 11 (1978).
9. O. Bieri, J. Wirz, B. Hellrung, M. Schutkowski, M. Drewello and T. Kiefhaber. *Proc. Natl. Acad. Sci. USA* **96**, 9597 (1999).
10. F. Krieger, B. Fierz, O. Bieri, M. Drewello and T. Kiefhaber. *J. Mol. Biol.* **332**, 265 (2003).
11. L. J. Lapidus, W. A. Eaton and J. Hofrichter. *Proc. Natl. Acad. Sci. USA* **97**, 7220 (2000).
12. M. Buscaglia, B. Schuler, L. J. Lapidus, W. A. Eaton and J. Hofrichter. *J. Mol. Biol.* **332**, 9 (2003).
13. L. J. Lapidus, W. A. Eaton and J. Hofrichter. *Phys. Rev. Lett.* **87**, 258101/1 (2001).
14. U. Pischel, F. Huang and W. M. Nau. *Photochem. Photobiol. Sci.* **3**, 305 (2004).
15. W. M. Nau and X. Wang. *ChemPhysChem* **3**, 393 (2002).
16. W. M. Nau, F. Huang, X. Wang, H. Bakirci, G. Gramlich and C. Marquez. *Chimia* **57**, 161 (2003).
17. R. R. Hudgins, F. Huang, G. Gramlich and W. M. Nau. *J. Am. Chem. Soc.* **124**, 556 (2002).
18. F. Huang and W. M. Nau. *Angew. Chem. Int. Ed.* **42**, 2269 (2003).
19. X. Wang and W. M. Nau. *J. Am. Chem. Soc.* **126**, 808 (2004).
20. C. Marquez, U. Pischel and W. M. Nau. *Org. Lett.* **5**, 3911 (2003).
21. F. Huang, R. R. Hudgins and W. M. Nau. submitted for publication (2004).
22. C. Marquez, F. Huang and W. M. Nau. *IEEE Trans. NanoBioSci.* **3**, 39 (2004).
23. D. Klapstein, U. Pischel and W. M. Nau. *J. Am. Chem. Soc.* **124**, 11349 (2002).
24. C. Marquez and W. M. Nau. *Angew. Chem., Int. Ed.* **40**, 4387 (2001).
25. I.-C. Yeh and G. Hummer. *J. Am. Chem. Soc.* **124**, 6563 (2002).
26. H. Neuweiler, A. Schulz, M. Boehmer, J. Enderlein and M. Sauer. *J. Am. Chem. Soc.* **125**, 5324 (2003).
27. R. P. Cheng, S. H. Gellman and W. F. DeGrado. *Chem. Rev.* **101**, 3219 (2001).
28. T. L. Raguse, J. R. Lai and S. H. Gellman. *J. Am. Chem. Soc.* **125**, 5592 (2003).
29. T. Beke, I. G. Csizmadia and A. Perczel. *J. Comput. Chem.* **25**, 285 (2003).
30. F. Huang, S. H. Gellman, J. Langenhan and W. M. Nau.
31. K. Kawahara and C. Tanford. *J. Biol. Chem.* **241**, 3228 (1966).

Captions for Figures

Figure 1. Scheme for intramolecular excited-state quenching and pertinent kinetic equations.

Figure 2. Double logarithmic plot of the intramolecular quenching rate constant (k_q) vs peptide length of peptides with the general structure Trp-(Gly-Ser)_n-DBO (n = 0, 1, 2, 4, 6, 10; ●) and Trp-(Pro)_n-DBO (n = 0, 2, 4,6; ■). The solid line is a fit of data for the Gly-Ser peptides to the function $y = a - 1.5x - b/x$ ($a = 9.37$ and $b = 0.392$). The dotted line has a slope of -1.5 and is shown to illustrate the deviation from the theoretical behaviour for an ideal Gaussian chain. The dashed line is a fit of data for the Pro peptides to the function $y = a + bx$, which gives a slope of -4.4 .

Figure 3. Structure of Trp-/DBO-labeled α -peptides.

Table 1. Intrachain quenching rate constants in peptides.^a

Backbone	$k_q / (10^6 \text{ s}^{-1})$	Backbone	$k_q / (10^6 \text{ s}^{-1})$
1) Length dependence for Gly-Ser series		5) Dependence on amino acid type	
Trp-DBO	41	Trp-Gly ₆ -DBO	39
Trp-Gly-Ser-DBO	68 (59) ^b	Trp-Ser ₆ -DBO	25
Trp-(Gly-Ser) ₂ -DBO	49 (40) ^b	Trp-Asp ₆ -DBO	21
Trp-(Gly-Ser) ₄ -DBO	31 (24) ^b	Trp-Asn ₆ -DBO	20
Trp-(Gly-Ser) ₆ -DBO	20 (14) ^b	Trp-Ala ₆ -DBO	≈ 18
Trp-(Gly-Ser) ₁₀ -DBO	11	Trp-Thr ₆ -DBO	11
2) Length dependence for Pro series		Trp-Leu ₆ -DBO	≈ 10
Trp-Pro ₂ -DBO	1.1	Trp-Phe ₆ -DBO	≈ 7.6
Trp-Pro ₄ -DBO	0.2	Trp-Glu ₆ -DBO	8.8
Trp-Pro ₆ -DBO	< 0.1	Trp-Gln ₆ -DBO	7.2
3) Length dependence for □-peptides		Trp-His ₆ -DBO	4.8
n = 2 (see Figure 3)	68	Trp-Arg ₆ -DBO	4.6
n = 4 (see Figure 3)	49	Trp-Lys ₆ -DBO	4.0
n = 6 (see Figure 3)	35	Trp-Val ₆ -DBO	≈ 3.0
4) Dependence on residue charges		Trp-Ile ₆ -DBO	≈ 2.3
Trp-Asp ₆ -DBO (pD 2)	21	Trp-Pro ₆ -DBO	< 0.1
Trp-Asp ₆ -DBO (pD 12)	19	6) Secondary structure dependence	
Trp-Glu ₆ -DBO (pD 2)	8.8	YQIFVK-DBO	1.8 (1.2) ^b
Trp-Glu ₆ -DBO (pD 12)	7.4	YELTIT-DBO	2.8 (1.7) ^b
Trp-Lys ₆ -DBO (pD 2)	2.8	YTLTGK-DBO	5.6 (4.0) ^b
Trp-Lys ₆ -DBO (pD 12)	4.0		

^a Values obtained in D₂O.^b Values in parenthesis obtained in 4.8 M urea-D₂O solution.

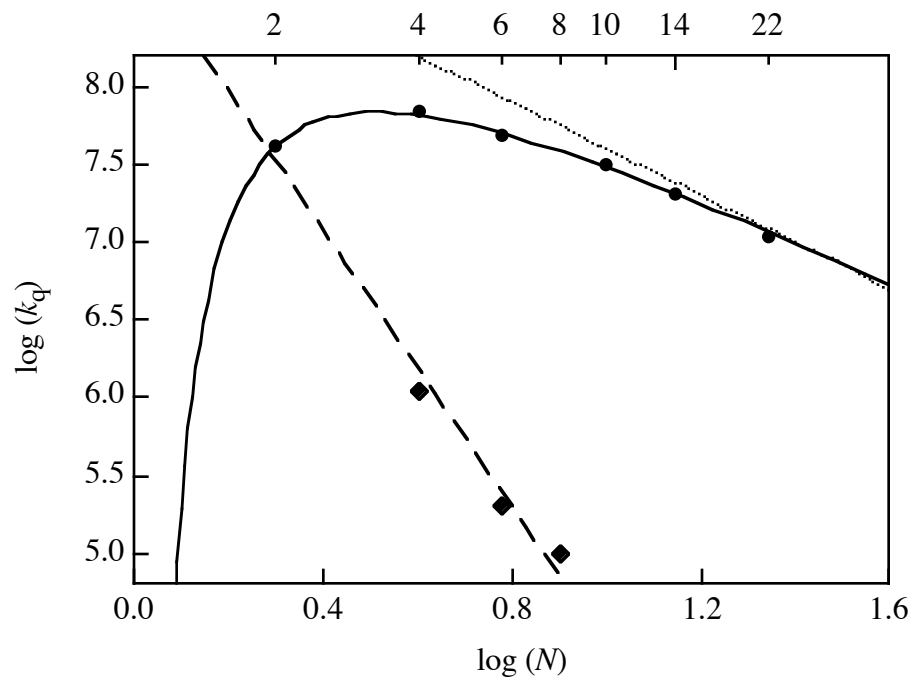


Figure 2

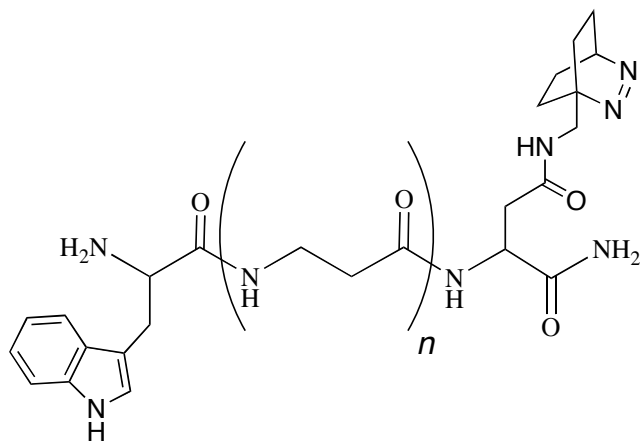


Figure 3

Corresponding author:

Prof. Dr. Werner M. Nau

School of Engineering and Science

International University Bremen

Campus Ring 1

D-28759 Bremen

Germany

**Application of FRET donor/acceptor pairs with small critical radius to
recover structural and dynamic properties of short flexible peptides**

Fang Huang,^a Xiaojuan Wang,^a Elisha Haas,^b and Werner M. Nau^{*, a, c}

^a Departement Chemie, Universität Basel, Klingelbergstrasse 80, CH-4056 Basel, Switzerland

^b Department of Life Sciences, Bar-Ilan University, Ramat-Gan 52900, Israel

^c School of Engineering and Science, International University Bremen, Campus Ring 1, D-28759 Bremen, Germany

w.nau@iu-bremen.de

Abstract

Intramolecular fluorescence resonance energy transfer (FRET) has been measured to recover detailed structural and dynamic properties in flexible Gly-Ser peptides. Two fluorescence energy donor/acceptor pairs with very small Förster critical radius ($< 10\text{\AA}$) are introduced, where either naphthalene or tryptophan serves as energy donor and 2,3-diazabicyclo[2.2.2]oct-2-ene (DBO) as acceptor. The fluorescence decays of the donor (naphthalene) and acceptor (DBO) in the presence and absence of FRET have been measured and subjected to global data analysis. The recovered intramolecular diffusion coefficients ($0.78 - 20 \times 10^{-7} \text{ cm}^2/\text{s}$) were found to be much smaller than those of free amino acids ($10^{-5} \text{ cm}^2/\text{s}$), which provides experimental evidence that the diffusion of the chain ends of these biopolymers is considerably slowed down. The slowest diffusion coefficients were obtained for the shortest peptides, which is consistent with expectations from theoretical studies. Shorter chains are proposed to exhibit a larger internal friction, which limits chain flexibility. Additionally, the intramolecular energy transfer efficiency has been measured for both donor/acceptor pairs and the effective average end-to-end distances were calculated, which are compared with independently determined end-to-end collision rates in the same set of peptides.

Introduction

How proteins fold and how proteins function remain to be two of the most important and fundamental questions in protein science. The kinetics and dynamics of peptide chain motions presents an indispensable element in this context. The sequence and rate of the formation of the individual secondary structures will be critical for the correct folding to the functional native conformation of a protein,¹ while the rates of hinge or shear domain motions in a protein will be decisive for substrate binding.^{2,3} Peptide motion, as an essential step for conformational changes of peptides and proteins, is therefore indispensable in protein folding and protein functions.

To explore the mechanism, predict the rate limit in protein folding, and to disclose the relationship between the function and flexibility of different regions in a protein, several photophysical methods for monitoring intramolecular collisions in peptides have been established. For this purpose, a probe and quencher are introduced at the two ends or in two positions of a peptide,^{4,6} and the intramolecular collision rates are then extracted from the kinetics of quenching of the excited probe, either a triplet state monitored by transient absorption, or a fluorescent singlet state. All of these methods are based on an assumption that the excited probe is quenched by the quencher through contact, which has been experimentally established for the fluorescence-based method.⁷ Any quenching that can occur over a longer distance, including super electron transfer and fluorescence resonance energy transfer (FRET), should therefore be avoided.⁶ While the use of FRET as spectroscopic ruler⁸ to estimate average distances in static, large proteins is well-established, its application to short flexible peptides as more dynamic systems has been less frequently explored.^{9,10} The latter can be used to recover the end-to-end distribution function and diffusion coefficients of the chain ends as additional key parameters.⁹

The short peptides, for which the end-to-end collision rates have been determined in previous studies, have typical lengths between 2–20 amino acid residues, suggesting average

end-to-end distance on the order of 10 Å. In order to investigate such short peptides by FRET, and thereby obtain complementary information on the dynamics, it is essential to design FRET donor/acceptor pairs with Förster critical radii (R_0) on the same order of magnitude, i.e., 10 Å.^{11,12} This is because the determination of distances by FRET is most accurate when the donor/acceptor distance lies within a range of $0.5R_0$ – $2.0R_0$. This limitation restricts the choice of donor/acceptor pairs dramatically, since in addition to a very low oscillator strength of the acceptor, both donor and acceptor must ideally be small organic chromophores and in addition, the acceptor should have no absorption at the excitation wavelength of the donor.

The previously investigated peptides were of the type Trp–backbone–DBO, where the backbone represents the characteristic amino acid sequence and where DBO presents 2,3-diazabicyclo[2.2.2]oct-2-ene, a fluorescent azo chromophore with an exceedingly long lifetime, which is efficiently quenched intramolecularly by forming an intimate contact with Trp to allow the accurate determination of the end-to-end collision rate constants between the chain ends represented by the *C*-terminal probe (DBO) and the *N*-terminal quencher.^{6,13,14}

We reckoned that the identical peptides, i.e., Trp–backbone–DBO could be employed as FRET systems, by exciting Trp as donor and monitoring the singlet energy transfer to DBO as acceptor. Luckily, it turned out further that the Förster critical radius for this pair is exactly the 10 Å required to apply FRET for reliable distance measurements in the identical set of peptides, and therefore to allow an excellent and self-consistent comparison of experimental data, namely the previously determined end-to-end collision rates. In a second step, it turned out that substitution of Trp by the very closely related naphthylalanine (Nal) provides an additional insight and some advantages due to the longer donor lifetime while preserving the very short Förster critical radius at the same value.

The results of this FRET study are described in this paper for peptides of different chain length, Nal-(Gly-Ser)_{*n*}-DBO and Trp-(Gly-Ser)_{*n*}-DBO⁶ ($n = 0, 1, 2, 4, 6$ and 10, cf. Scheme

1), for which we expected substantial variations in the end-to-end distribution functions and diffusion coefficients.¹⁵

Experimental Section

Materials. All commercial materials were from Fluka or Aldrich. The DBO-labeled peptides were commercially synthesized in > 95% purity (Affina, Berlin). Details on the synthesis of the probe and its suitability in solid-phase peptide synthesis can be obtained from our previous study.⁶

Fluorescence measurements. Fluorescence decays were recorded on a time-correlated single photon counting (TCSPC) fluorometer (FLS920, Edinburgh Instruments, Edinburgh, Scotland) by using a 1.5-ns pulse-width H₂ flash lamp or a Picoquant picosecond pulsed diode laser ($\lambda_{\text{ex}} = 373$ nm, ca. 50 ps pulse width) for excitation. The peptide concentrations were adjusted to 10-100 μM , sufficiently low to exclude intermolecular interactions. Experiments were carried out in D₂O under air to keep the experimental conditions consistent with previous study, where the end-to-end collision rates for peptides with the same backbone have been measured.⁶ For each peptide, Nal-(Gly-Ser)_n-DBO, three independent fluorescence decay traces were collected. Upon excitation of the naphthalene chromophore ($\lambda_{\text{ex}} = 285$ nm), the temporal evolution of the fluorescence of both the donor (naphthalene $\lambda_{\text{em}} = 335$ nm) and the acceptor (DBO $\lambda_{\text{em}} = 450$ nm) were monitored. In an independent set of experiments the fluorescence decay of acceptor (DBO) was also measured for direct excitation ($\lambda_{\text{ex}} = 373\text{nm}$). To obtain the donor decay in the absence of FRET, a reference peptide, Nal-(Gly-Ser)₆, was synthesized, in which only the donor moiety, naphthalene, is present, i.e., without acceptor.

Solid-phase fluorescence experiments were carried out in trehalose glass with 1 mM naphthylalanine and 77 mM DBO. Trehalose glass was prepared by heating 5 g trehalose with ca. 0.5 mL water to ~130 °C to obtain a viscous solution with dissolved naphthylalanine and DBO, which was then quickly poured into a 1 cm cuvette and allowed to cool down to get a transparent glassy matrix.

Absorption spectra were recorded on a Cary 4000 UV-Vis spectrometer (Varian) and steady-state fluorescence spectra on a Cary Eclipse fluorometer (Varian)

Data analysis. There are two factors which affect the efficiency of FRET: (1) the end-to-end distance distribution, i.e., the donor/acceptor distance, which is dependent on the sequence and the length of the peptides, and (2) the conformational flexibility, since the peptide chains undergo conformational changes during the excited state lifetime. The latter leads to diffusional fluctuations of donor acceptor distance during the probe lifetime, which enhances the FRET efficiency by a varying degree. In principle, the time-resolved decay of the surviving excited donor sites is described by the following distribution function:^{10,15,16}

$$\frac{\partial}{\partial t} g_N^*(r, t) = -\frac{1}{\tau_0} g_N^*(r, t) + D \frac{1}{r^2} \frac{\partial}{\partial r} r^2 \frac{\partial}{\partial r} g_N^*(r, t) + D \frac{1}{r^2} \frac{\partial}{\partial r} r^2 g_N^*(r, t) \frac{\partial}{\partial r} \beta U(r) \quad (1)$$

D is the mutual intramolecular end-to-end diffusion constant, which is the sum of the individual diffusion coefficients of the two chain ends. β^{-1} is the product of the Boltzman constant and temperature ($\beta = 1/k_B T$), and $U(r)$ is the potential energy of the chain possessing an end-to-end distance r . If the ground-state equilibrium distribution $g_N(r)$ is known, the potential energy can be obtained according to Equation 2, assuming no perturbation of the distribution function upon excitation of the donor.^{10,17}

$$\beta U(r) = -\ln g_N(r) \quad (2)$$

Equation 1 can be used to calculate the survival probability density of an excited state at distance r subject to the boundary condition

$$\left. \frac{\partial}{\partial r} g_N^*(r, t) + g_N^*(r, t) \frac{\partial}{\partial r} \beta U(r) \right|_{r=a} = 0 \quad (3)$$

FRET experiments can in principle yield both, the end-to-end distance distribution and the intrachain diffusion coefficient. However, since these parameters are tightly correlated, the recovery of both distribution and diffusion coefficient from the donor fluorescence decay becomes very difficult. According to Haas and coworkers this problem is overcome by global

analysis of both the donor and acceptor fluorescence decays and growth curves.⁹ This approach of “over-determination” has been adapted in this paper.

Results

Intramolecular energy transfer from naphthalene to DBO. In a previous work, efficient singlet-singlet energy transfer from naphthalene to DBO has been observed,¹⁸ where naphthalene and DBO were directly connected through a short dimethylsiloxy tether. The experimental results (for *n*-hexane as solvent) suggested that the effective average end-to-end distance between naphthalene and DBO is as short as 5.2 Å, which means that naphthalene and DBO come essentially in contact (orbital overlap) such that exchange energy transfer mechanism was expected to be dominant. In the present set of experiments with peptides, FRET was expected to become dominant due to the longer and more rigid tether and due to the more viscous aqueous solution which both favor FRET over exchange- energy transfer due to (1) a larger average end-to-end distances and (2) slower diffusion.

In order to corroborate the participation of FRET in the case of the Nal/DBO doubly labeled peptides, a control experiment was performed, in which a host molecule, cucurbit[7]uril (CB7), was added to solutions of Nal-(Gly-Ser)₆-DBO and Nal-(Gly-Ser)₆, respectively. It has been demonstrated that DBO can be included into the cavity of CB7 to form a supramolecular host-guest complex, where CB7 can serve as a protective shield to exclude the contact between DBO and naphthalene.^{7,19} Independent control experiment revealed that naphthalene is also included into CB7. At the selected concentrations of peptide (3.8×10^{-5} M) and CB7 (7.5×10^{-4} M) less than 1% of peptide is uncomplexed, owing to the high binding constants, $(5 \pm 1) \times 10^4$ M⁻¹ for Nal•CB7 and $(4 \pm 1) \times 10^5$ M⁻¹ for DBO•CB7. The salient feature of this control experiment is that the complexed chromophores cannot undergo exchange energy transfer due to the separation imposed by the supramolecular host, but only FRET, which is free to operate through space. Indeed, under such conditions the resonance energy transfer between naphthalene and DBO is still observed in both steady-state

and time-resolved measurements. The emission spectrum of the doubly labeled peptide Nal-(Gly-Ser)₆-DBO in the presence of CB7 is shown in Figure 4, where the emission of DBO above 400 nm was observed with excitation of naphthalene at 285 nm. When time-resolved measurements were performed, the fluorescence decay of the naphthalene residue in both Nal-(Gly-Ser)₆ and Nal-(Gly-Ser)₆-DBO could be roughly fitted with a monoexponential decay function, lifetimes of 73 ns and 62 ns were observed. The significantly longer lifetime than that of free naphthalene under the same condition without CB7 (37 ns) was also an evidence that the naphthalene residue in both peptides has been efficiently protected by CB7 from the quenching of oxygen. However, the obviously shorter naphthalene lifetime in the doubly labeled peptide Nal-(Gly-Ser)₆-DBO suggested that the excited naphthalene can still be quenched by DBO even in the cavity of CB7. Recall that the inclusion of DBO by CB7 in peptide Trp-(Gly-Ser)₂-DBO excludes completely the quenching by tryptophan (increasing the lifetime of DBO from 20 ns to 1030 ns), where a contact quenching mechanism applies.⁷ This control experiment suggests that a close contact is not necessary for the quenching of naphthalene by DBO and that a through-space electron or energy transfer process, which can occur through the walls of the supramolecular cages, dominates at long distances. The possibility of an electron transfer mechanism, however, has been excluded in a previous work on the basis of the endergonic thermodynamics.¹⁸ The energy transfer efficiency for peptide Nal-(Gly-Ser)₆-DBO in the presence of CB7, calculated from fluorescence lifetime, is 15.1%, suggesting an effective distance of energy transfer of 13.1 Å, which corresponds to the average end-to-end distance of this peptide. This average end-to-end distance is a little longer than the corresponding one in the absence of the CB7 (See Table 2 and 3), because that the donor and acceptor are prevented to approach closer than the cucurbituril diameter when they are included by CB7 (Scheme 2). Admittedly, this experiment does not provide compulsory evidence that FRET dominates in the uncomplexed peptide as well, but it is an appealing experiment to address the question by means of supramolecular technology.

The quenching rate constants of naphthalene by DBO in the intermolecular case were also measured in D₂O ($\eta = 1.1$ cP), H₂O ($\eta = 0.89$ cP) and acetonitrile ($\eta = 0.345$ cP), which are $5.7 \times 10^9 \text{ M}^{-1}\text{s}^{-1}$, $6.3 \times 10^9 \text{ M}^{-1}\text{s}^{-1}$, and $9.5 \times 10^9 \text{ M}^{-1}\text{s}^{-1}$ at 25°C, respectively, demonstrating diffusion-controlled quenching.

Characterization of FRET donor/acceptor pair. The critical Förster radius (R_0) for resonance energy transfer from naphthalene to DBO in D₂O was calculated according to Förster theory from the overlap (J) of the absorption spectrum of DBO and the fluorescence emission spectrum of naphthalene. The R_0 value of the Nal/DBO energy donor/acceptor pair in D₂O is $9.8 \pm 0.2 \text{ \AA}$ ($J = 3.05 \times 10^{11} \text{ M}^{-1}\text{cm}^{-1}\text{nm}^4$). Note that the critical radius in H₂O is the same as in D₂O within error due to the very similar spectra, quantum yield (this work) and refractive index.²⁰ Naphthalene has a fluorescence lifetime of 37 ns in both H₂O and D₂O. Peptide-attached naphthalene and DBO, Nal-(Gly-Ser)₆ and (Gly-Ser)₆-DBO, were also applied to measure R_0 . Results show that the attachment to peptides does not affect J and R_0 values.

Alternatively, R_0 was obtained by measuring the fluorescence decay in the absence of diffusion and energy migration among donor molecules, which can be described by Equations 4 and 5.²¹

$$I = I_0 \exp\left[-t/\tau - 2(C_A/C_{0A})(t/\tau)^{1/2}\right] \quad (4)$$

$$C_{0A} = 3000/2\tau^{3/2}NR_0^3 \quad (5)$$

Here, τ is the lifetime in the absence of quencher, C_A is the concentration of the acceptor and C_{0A} is the critical acceptor concentration for energy transfer.

The pertinent measurements were done in solid trehalose, where diffusion could be neglected.²² Additionally, the concentration of the acceptor DBO (77 mM) was controlled to be much higher than that of the naphthylalanine donor (1 mM) such that the energy migration between donor molecules (homo-FRET) could be neglected. Note that naphthylalanine was

used instead of naphthalene in the solid phase experiments because the preparation of the solid sample needs enhanced temperatures, where naphthalene itself sublimates. The fluorescence decay was recorded and then applied to Equations 4 and 5 to calculate R_0 . The result is $9.4 \pm 0.4 \text{ \AA}$, consistent within error with the value calculated from the spectral overlap. The slightly smaller value may come from the difference of the medium, e.g., a larger refractive index in trehalose than in water.

Time-resolved fluorescence measurements. The time-resolved fluorescence decay of naphthalene residue ($\lambda_{em} = 335 \text{ nm}$) was recorded in the donor-only-labeled peptide and the donor/acceptor doubly-labeled peptides by donor excitation ($\lambda_{ex} = 285 \text{ nm}$) (representative decay traces are shown in Figure 1). The decay trace of the donor-only-labeled peptide can be fitted with a mono-exponential function with a lifetime of 36 ns, similar to the decay of free naphthalene. However, a multi-exponential function is required in the case of the doubly-labeled peptides due to the continuum of energy transfer rates. The fitting results are summarized in Table 1; for simplicity and ease of comparison, “average” fluorescence lifetimes are provided also for the multiexponential decays by a weighing procedure. Expectedly, the average fluorescence lifetimes of the naphthalene donor residue are consistently shorter than that of free naphthalene as a result of energy transfer. The lifetimes increase with increasing peptide length, indicating a reduced FRET efficiency in the longer peptides.

The time-resolved fluorescence decay traces of the DBO acceptor residue ($\lambda_{em} = 450 \text{ nm}$) was measured by exciting the naphthalene donor residue ($\lambda_{ex} = 285 \text{ nm}$, Figure 2) as well as by directly exciting DBO ($\lambda_{ex} = 373 \text{ nm}$). The direct excitation of the DBO acceptor residue resulted in a monoexponential decay, with the lifetimes increase with peptide chain length as well, from 135 ns for Nal-DBO to 270 ns for Nal-(Gly-Ser)₁₀-DBO. These lifetimes fall shorter than the fluorescence lifetimes of the DBO-only-labeled peptide (e.g., 403 ns for (Gly-Ser)₆-DBO) as a consequence of some intramolecular exciplex-induced quenching of the

excited DBO by the ground-state naphthalene residue; this quenching channel becomes less efficient as the distance between probe and quencher increases. The fluorescence response of the DBO acceptor residue upon excitation of naphthalene as donor is characterized by a rapid growth and slower decay, which can be understood in terms of the initial population of the excited DBO by FRET and its subsequent deactivation. The time constant characterizing the decay component found for DBO populated by FRET was identical, within error, to the time constant measured upon direct excitation. This is not necessarily expected since the FRET experiment populates a subpopulation of peptide conformations in which the DBO and naphthalene chromophores are within distances and geometries suitable for FRET, while the direct excitation samples the conformational ensemble average.

End-to-end distance distribution and intramolecular diffusion coefficient. The time-resolved fluorescence data for each peptide were analyzed according to Equation 1 by employing the Globals software package (Experimental section).⁹ The mean end-to-end distance and the intramolecular diffusion coefficient were calculated for all peptides. The results are summarized in Table 2.

Firstly, the fluorescence data were directly employed in fitting. The representative end-to-end distance distributions recovered from direct global analysis are shown in Figure 3. From the parameters in Table 2 we can see that the mean end-to-end distance is significantly shorter than the contour length (sum of length of the individual segments), and increases only slowly with increasing backbone length. For example, while the contour length increases from 22.8 Å for Nal-(Gly-Ser)₂-DBO to 53.2 Å for Nal-(Gly-Ser)₆-DBO the extracted mean end-to-end distances increase merely from 7.96 Å to 10.91 Å. This suggests that the Gly-Ser peptide chains are highly flexible and form more random-coil-type than extended conformations. On the other hand, the obtained intramolecular diffusion coefficients are all on the order of 10⁻⁷ cm²/s and increase with chain length for the shorter peptides ($N \leq 10$) to reach an upper limit for the longer ones ($N \geq 10$).

Due to the high correlation of the parameters the errors remained large even in the over-determined global analysis, which required a model-assisted data analysis to better expose the salient features of the trends of the diffusion coefficients. For this purpose, we calculated a set of approximate root mean square end-to-end distances as $\langle R^2 \rangle = Ll$, where L is the contour length and l is the Kuhn length of Gly-Ser peptides, both obtained by assuming a length of one peptide unit as 3.8 Å.²³ It was found that the calculated means (R_{mean}) are close to the fitted ones but change in a more systematic way. Re-analysis of the kinetic data by constraining the R_{mean} values provided an improved set of distributions and diffusion coefficients. The recovered intramolecular diffusion coefficients were also found to lie in the range of $10^{-7}\text{cm}^2/\text{s}$ to $10^{-6}\text{cm}^2/\text{s}$, which are in the same order of magnitude as values for similar peptides obtained experimentally^{5,24} and theoretically,²⁵ and one to two orders of magnitude slower than those of free amino acids.²⁶ For the available values ($N \leq 10$), the coefficients increase with contour length.

Energy transfer efficiency. Average energy transfer efficiency in the system can be calculated through time-resolved or steady-state fluorescence measurements according to the following equations:

$$\eta_{ET} = 1 - \frac{I}{I_0} \quad (6a)$$

$$\eta_{ET} = 1 - \frac{\tau}{\tau_0} \quad (6b)$$

I and I_0 as well as τ and τ_0 are the fluorescence intensity and average lifetime of the donor residue in the presence and absence of the acceptor residue, respectively. Equation 6b is only valid if the fluorescence decay can be fitted monoexponentially. This is not the case for the present FRET systems, such that the fluorescence intensity was preferred in the calculation of the energy transfer efficiency.

Figure 4 shows the fluorescence emission spectra (donor excitation) of the doubly-labeled peptides with different contour lengths and the naphthalene donor-only-labeled peptide. In the absence of the DBO acceptor, a strong emission of the naphthalene donor was observed from 300–400 nm. In the Nal/DBO doubly-labeled peptides, the emission of naphthalene was significantly reduced and the typical emission of DBO appeared at longer wavelength as a consequence of singlet-singlet energy transfer. With increasing peptide length, the intensity of naphthalene fluorescence recovers again partially as a result of a reduced energy transfer efficiency. As a peculiarity, it has to be noted that the DBO fluorescence intensity remains surprisingly constant regardless of the large variations in donor fluorescence; this is due to the delicate balance of two factors since the shorter peptides show more efficient energy transfer, but also shorter DBO fluorescence lifetimes due to more efficient intramolecular quenching of the excited acceptor by the ground state donor.

The steady-state fluorescence results are summarized in Table 3. The average energy transfer efficiency calculated according to the changes of naphthalene emission is strongly dependent on the contour length of the peptides. It decreases from 94% for the shortest Nal-DBO peptide to 60% of the longest one, Nal-(Gly-Ser)₁₀-DBO. There are two parameters that can principally reduce the energy transfer efficiency: longer average distances or slower conformational fluctuation rates. The recovered intramolecular diffusion coefficients actually increase for the longer peptides, which demonstrates that the reduced energy transfer efficiency derives from a larger end-to-end distance in the longer peptides.

The effective average end-to-end distance at which energy transfer occurs, R'_{mean} , can be calculated from the energy transfer efficiency according to Equation 7.

$$\eta_{\text{ET}} = \frac{R_0^6}{R_0^6 + R'_{\text{mean}}{}^6} \quad (7)$$

In case that the conformations of the peptides are fixed, i.e, no fluctuations occur during the lifetime of excited donor, R'_{mean} will be equal to the equilibrium average end-to-end distances

(R'_{mean}), returned from the global analysis. However, in the case of Gly-Ser peptides, the high flexibility of the backbone facilitates rapid conformational changes, such that the R'_{mean} values reflects the average distances at which energy transfer occurs, which will be naturally shorter than the equilibrium average end-to-end distance, R_{mean} , as a consequence of the vastly more efficient transfer rates at shorter distance (R^6 dependence). Additionally, the difference between R'_{mean} and R_{mean} should be larger for the longer peptides because the reduced energy transfer efficiency in the longer peptides results in a longer lifetime of the donor residue, which makes it possible that even peptides with remote donor/acceptor separation have sufficient time for diffusion to explore conformations with suitable energy transfer distanced.

The R'_{mean} values obtained from steady-state measurements in Table 3 with the R_{mean} values recovered by global analysis in Table 2 are generally consistent with the above expectations: for the shorter peptides, the R'_{mean} value are quite similar to R_{mean} due to the high energy transfer efficiency, but with increasing contour length, the R_{mean} values become significantly larger than the corresponding R'_{mean} values. However it is also noticed that the assumed R_{mean} value for the shortest Nal-DBO peptide, 5.4 Å, is shorter than the calculated R'_{mean} value, 6.2 Å. This suggested that the model used for predicting the root mean square end-to-end distance has some shortcoming for the very short chain with only two peptide bonds. In fact, both numerical simulations,¹⁵ molecular dynamics simulations,²⁷ as well as end-to-end collision rate measurements⁶ have demonstrated that the very short peptide is an outlier due to its apparently higher rigidity, which is now also borne out by a higher-than-expected effective average distance of energy transfer, again suggesting a more extended conformation.

FRET from tryptophan donor to DBO acceptor residue. The fluorescence and triplet-triplet absorption of tryptophan has been intensively employed to study the structural and dynamic properties of protein and peptides.²⁸⁻³⁰ The emission of tryptophan in water is very broad with a maximum at 350 nm. The large overlap with the absorption of DBO makes FRET possible. The critical radius, R_0 , for the Trp/DBO energy donor/acceptor pair was also

calculated from the spectra overlap ($J = 3.97 \times 10^{11} \text{ M}^{-1}\text{cm}^{-1}\text{nm}^4$, being the same for peptide-linked tryptophan and DBO, Trp-(GlySer)₆ and (GlySer)₆-DBO), and a value of $9.9 \pm 0.2 \text{ \AA}$, virtually the same as for the Nal/DBO pair, which allows one to conduct closely related experiment.

In this paper, we also employed the steady-state fluorescence intensity of tryptophan (donor) to calculate the energy transfer efficiency and the effective average end-to-end distance. The chemical structure of Nal and Trp is very similar (Scheme 1); it is therefore a very good approximation that the structural and dynamic properties of these two series of peptides such as the equilibrium end-to-end distance distribution and the intramolecular diffusion coefficient are very similar. There is, however, an important photophysical difference between the two probes, which should have a direct and predictable effect on the energy transfer efficiencies. Namely, the fluorescence lifetime of Trp is shorter than that of Nal by one full order of magnitude, which limits the probability that FRET is induced through diffusional fluctuation and conformational changes, but favor a static energy transfer. In other words, the contribution of the diffusion-enhanced FRET, and therefore the overall FRET efficiency is reduced in the Trp-based peptides (Table 3). An additional manifestation of this notion is that the Trp peptides should give rise to systematically larger R'_{mean} value (closer to the equilibrium R_{mean}), which is supported by the experimental data in Table 3.

Participation of intermolecular energy transfer. It should be noted that the global analysis is based on the assumption that the FRET process only occurs between naphthalene and DBO attached in the same peptide, i.e., that the change of the fluorescent property of the naphthalene residue is only caused by an *intramolecular* energy transfer process. To exclude *intermolecular* energy transfer or other quenching processes, control experiments were performed. For this purpose, the donor-only labeled peptide, 100 μM Nal-(Gly-Ser)₆ D₂O solution was excited at 285 nm. The emission spectrum between 290-550 nm showed a typical naphthalene fluorescent peak at 335 nm. After the addition of the acceptor-only

labeled peptide, 100 μ M (Gly-Ser)₆-DBO, 285-nm excitation did not lead to DBO emission. Additionally, time-resolved measurement demonstrated that before and after addition of acceptor-only labeled peptide, the lifetime of naphthalene in the donor-only peptide remained unchanged, indicating the absence of quenching. These control experiments suggested that at 100 μ M, the upper limit of peptide concentration applied in the fluorescence measurements in this paper, no intermolecular energy transfer happens, i.e., any FRET observed in the doubly-labeled peptides must occur intramolecularly.

In addition, this experiment provides conclusive evidence that association between the peptides does not occur at typical experimental concentrations, since aggregation would situate probe and quencher in sufficiently close proximity to allow FRET. In addition, aggregation should be further disfavored by the lower concentration employed in most experiments.

Discussion

FRET is widely employed, besides its application in supramolecular photonic devices,³¹ to measure molecular conformational changes and probe-quencher distances, mostly intramolecularly in biopolymers.^{9,10,32,33} One of the key problems in the application of FRET is the selection of suitable donor/acceptor pairs with the appropriate Förster critical radii, which is due to the very strong distance dependence of the energy transfer rate and therefore transfer efficiency (Figure 5).

Note that most conventional FRET probe/quencher pairs have critical radii ranging from 20–100 Å.³⁴ The resonance energy donor/acceptor pairs employed in this paper, Trp/DBO and Nal/DBO, have similar, very small critical radii of 9.9 Å and 9.8 Å respectively, and should therefore be suitable to probe chromophore separations at such short distances. Since FRET measurements are most sensitive in the range where the distance between probe and quencher lies between $0.5 R_0$ and $2 R_0$, the present probe/quencher pairs should excel when probe/quencher separation between 5–20 Å are to be investigated. For average energy transfer

distance below 5 Å energy transfer would be too fast and efficient ($> 98\%$, $k_{ET} > 64k_0$), while above 20 Å it is too inefficient ($< 2\%$, $k_{ET} > 1/64k_0$), compare Figure 5. The average end-to-end distances in the short flexible Gly-Ser peptides studied in this work range from a few angstrom to less than 20 Å, and are therefore ideally suited for the present FRET pairs.

An additional motivation for using donors and acceptors with small molecular size as well as small Förster critical radii comes from theoretical work and molecular dynamic simulations. These have shown that the survival probability of energy donor/acceptor pairs in doubly-labeled polymer chains can be most accurately recovered from the approximate theories, such as WF theory or the SSS model, if the Förster critical radius and chromophore sizes are smaller or similar to the chain length.^{11,12} Evidently, this theoretical condition cannot be fulfilled by most established FRET donor/acceptor pairs when the end-to-end distances become very short. In comparison, the energy donors used in the present work (tryptophan or naphthalene) and in particular the acceptor (DBO) are very small compared with conventional fluorescent probes.³⁵ This specific advantage together with the small Förster critical radius around 10 Å make it possible to recover the structural and dynamic properties of short peptides from the fluorescence decays, based on the modified Smoluchowski equation and global analysis.³⁶

Singlet-singlet energy transfer may occur through an exchange (Dexter) or a resonance (FRET) mechanism, or both.^{18,34,37} Transfer due to exchange interaction become more important at very small donor/acceptor separation, while FRET dominates at longer distance. In our previous work, where naphthalene and DBO were separated by a dimethylsiloxy tether and measured in *n*-hexane, energy transfer from naphthalene to DBO was considered to occur mainly through Dexter mechanism due to the very short and flexible tether and very lower solvent viscosity.¹⁸ In the current work on a more rigid peptide chain and more viscous solvent, we expect FRET to become dominant. Actually, the ratio of energy transfer through

Dexter and FRET can be estimated roughly. At the rapid-diffusion limit of fluorescence resonance energy transfer, the upper limit of energy transfer rate can be estimated by eq. 8.^{34,38}

$$k_{\text{FRET}} = \frac{2.523R_0^6}{\tau_D r^3} \quad (8)$$

τ_D is the lifetime (in s) of the donor in the absence of the energy transfer and r is the distance of closest approach of the donor and acceptor (in nm), which is taken as 0.4 from the reaction distance for Trp/DBO.²⁷ The calculated FRET rate constant is found to be $1.1 \times 10^9 \text{ M}^{-1}\text{s}^{-1}$, much smaller than the experimental intermolecular quenching rate constant of naphthalene by DBO (ca. $6 \times 10^9 \text{ M}^{-1}\text{s}^{-1}$ in water, see Results), indicating that a Dexter mechanism dominates in the intermolecular case with less than 20% of energy transfer through FRET. However, this does not mean that Dexter is also dominant in the case of intramolecular energy transfer, which is due to a slower intramolecular diffusion, which puts the exchange mechanism at a disadvantage since it requires a close donor/acceptor approach. Both current work and previous work have shown that intramolecular diffusion coefficients fall at least one order of magnitude below the respective intermolecular ones,^{5,24-26} which suggests the energy transfer rate by Dexter will decrease by at least 10 times in the intramolecular case. On the other hand, the intrinsic distance dependence of the energy transfer rates by FRET remains almost unchanged. It is therefore reasonable to assume that FRET becomes dominant in the peptides investigated.

Experimentally, time-resolved fluorescence decay traces of donor and acceptor were recorded for each peptide in the presence and absence of FRET. The fluorescence decay traces of naphthalene in the presence of FRET cannot be satisfactorily fitted monoexponentially. Nevertheless, a biexponential fit is sufficient to describe the decay traces and even in this case the contribution of the longer-lived component is small (< 10%). It is possible to define an “average” lifetime (Table 1) and employ it to calculate an apparent intramolecular quenching rate constant by energy transfer, which can be compared with the

end-to-end collision rate constants previously determined for the same Gly-Ser peptide backbone (k_q values in Table 1).⁶ The results entered in Table 1 as k_{qET} values and plotted in Figure 6 as the logarithmic rate constants versus $\log N$, with N taken as number of peptide units. Such plots are common in polymer and biopolymer kinetics^{4,6} in order to evaluate deviations from ideal-chain behavior. As can be seen, the apparent quenching rate constants from FRET fall far above the end-to-end collision rates, which suggests that the quenching of the donor by the acceptor does not occur through a well-defined and intimate contact, but through a longer-range interaction characteristic for FRET. In addition, the inversion at very short donor/acceptor, which is found for the end-to-end collision rates disappears, although a negative curvature remains, which reflects steric hindrance effects prominent in very short chain. This discriminating feature also points to a quenching mechanism with looser geometrical constraints, namely FRET, which depends primarily on the distance.

The fluorescence decay traces were accordingly subjected to global analysis according to the pertinent FRET model (eq. 1). This analysis yielded the equilibrium end-to-end distance distributions (for example see Figure 3) and the intrachain diffusion coefficient (Table 2). The recovered intramolecular diffusion coefficients lie in the reasonable range of $10^{-7} \text{cm}^2/\text{s}$, at least one order of magnitude smaller than the diffusion of free amino acid molecules (ca. $10^{-5} \text{cm}^2/\text{s}$ in H_2O).²³ Most importantly, a decrease of the diffusion constants for the shorter peptides is observed. In a previous study,¹⁵ we have numerically simulated the dynamics of the short Gly-Ser peptides and suggested that a slower diffusion coefficient of shorter peptides would be the underlying reason for the negative curvature and the weaker length-dependent end-to-end collision rates (Figure 6) compared with theoretical prediction for the ideal chain model. The results in the present paper now verify this suggestion experimentally. The lower diffusion coefficients in the shorter peptides can be most intuitively in terms of steric hindrance effects, since a short backbone restricts motion of the chain ends more than a longer one does. In addition, the lower diffusion coefficients can be interpreted in terms of a

higher “internal friction”, which is yet another conceptual approach to chain stiffness in polymers and biopolymers.^{14,39}

The time-resolved fluorescence measurements in the Trp/DBO doubly-labeled peptides, which are exactly those for which the end-to-end collision rates have been measured, were less conclusive and not amenable for more detailed global analysis. This is because the time-resolved fluorescence decay of tryptophan is complex and non-monoexponential even in the absence of acceptors.³⁴ Even free tryptophan shows a bi-exponential trace in neutral aqueous solution. In Trp/DBO-labeled peptides, the decay pattern becomes more complex. As a second complication, the very broad emission of tryptophan overlaps with that of DBO, which would require a ratiometric method to discriminate the fluorescence of the DBO acceptor upon excitation of tryptophan as donor. Nevertheless, the integrated energy transfer efficiency can be determined from steady-state fluorescence measurements, which allows at least estimates of the effective average end-to-end distances.

The directly observable properties of fluorescent labeled biopolymer chain, such as the end-to-end collision rates and the intramolecular energy transfer efficiency in peptides and oligonucleotides, are dependent on two factors: the equilibrium end-to-end distance distribution and the flexibility of the backbone. The Trp/DBO probe/quencher pair has been proven to provide a measure of the end-to-end collision rates in peptides, where DBO serves as a long-lived probe and Trp as a selectively collision-induced quencher.^{6,7,13} By changing the role of tryptophan from the contact quencher to that of an energy donor with DBO acting as acceptor, or by exchanging tryptophan by the closely related naphthalene as donor, it is now possible to obtain approximate distributions. The results are shown for naphthalene in Figure 3, obtained by global analysis. The data for tryptophan allow a more direct estimate on the average end-to-end distances and therefore distributions because the singlet lifetime of tryptophan is very short (< 3 ns), such that the Brownian motion during its excited state lifetime cannot result in a large displacement, especially because of the relatively small

diffusion coefficients of the chain ends. The effective average energy transfer distance, R'_{mean} , recovered from the Trp/DBO FRET system should therefore fall only slightly below the actual average distance under equilibrium conditions, R_{mean} . In a first approximation, the average energy transfer distances obtained from (steady-state) FRET in Trp/DBO peptides can be taken as measure of the average end-to-end distance. This approximation should hold particularly well for rigid peptides or in very viscous media where the motion of the chain on a 3-ns time scale can be neglected.¹⁴ Even in the case of the presently investigated flexible Gly-Ser peptides, the agreement between the energy transfer distance obtained from Trp/DBO FRET (Table 3) are in satisfactory agreement with the experimental values by global fitting of the Nal/DBO FRET data, as well as the theoretical values for an ideal chain model (Table 2).

Conclusions

Two energy donor/acceptor pairs (naphthalene/DBO and tryptophan/DBO) with very small Förster radius ($R_0 \sim 10 \text{ \AA}$) have been applied to recover structural and dynamic properties of short flexible peptides through intramolecular FRET. These donor/acceptor pairs with very small critical radius have proven very suitable for investigating these very short biopolymers. In addition, FRET efficiencies in the tryptophan/DBO donor/acceptor pair allowed direct estimates the average end-to-end distance of peptides, which is made possible by the short fluorescence lifetime of tryptophan. Global analysis of the time-resolved fluorescence decay traces and end-to-end distances obtained from the ideal chain model were also employed to improve the accuracy of the results. The results confirmed that the intramolecular diffusion coefficients are one to two orders of magnitude smaller than the intermolecular diffusion coefficients. The smallest diffusion coefficients were observed in the shorter peptides, in line with previous numerical simulations result.

Acknowledgement

This work was supported by the Swiss National Science Foundation and by the NRP 47 "Supramolecular Functional Materials". We would like to acknowledge the experimental help of R. Meyer in this project.

References:

- 1 C. M. Dobson, Protein folding and misfolding, *Nature*, 2003, **426**, 884-890.
- 2 G. E. Schulz, Domain motions in proteins, *Curr. Opin. Struct. Biol.*, 1991, **1**, 883-888.
- 3 F. G. Parak, Proteins in action: the physics of structural fluctuations and conformational changes, *Curr. Opin. Struct. Biol.*, 2003, **13**, 552-557.
- 4 O. Bieri, J. Wirz, B. Hellrung, M. Schutkowski, M. Drewello and T. Kiefhaber, The speed limit for protein folding measured by triplet-triplet energy transfer, *Proc. Natl. Acad. Sci. USA*, 1999, **96**, 9597-9601.
- 5 L. J. Lapidus, W. A. Eaton and J. Hofrichter, Measuring the rate of intramolecular contact formation in polypeptides, *Proc. Natl. Acad. Sci. USA*, 2000, **97**, 7220-7225.
- 6 R. R. Hudgins, F. Huang, G. Gramlich and W. M. Nau, A fluorescence-based method for direct measurement of submicrosecond intramolecular contact formation in biopolymers: An exploratory study with polypeptides, *J. Am. Chem. Soc.*, 2002, **124**, 556-564.
- 7 W. M. Nau, F. Huang, X. Wang, H. Bakirci, G. Gramlich and C. Marquez, Exploiting long-lived molecular fluorescence, *Chimia*, 2003, **57**, 161-167.
- 8 L. Stryer and R. P. Haugland, Energy transfer: A spectroscopic ruler, *Proc. Natl. Acad. Sci. USA*, 1967, **58**, 719-726.
- 9 J. M. Beechem and E. Haas, Simultaneous determination of intramolecular distance distributions and conformational dynamics by global analysis of energy transfer measurements, *Biophys. J.*, 1989, **55**, 1225-1236.
- 10 E. Haas, E. Katchalski-Katzir and I. Z. Steinberg, Brownian motion of the ends of oligopeptide chains in solution as estimated by energy transfer between the chain ends, *Biopolymers*, 1978, **17**, 11-31.
- 11 G. Srinivas, A. Yethiraj and B. Bagchi, Nonexponentiality of time dependent survival probability and the fractional viscosity dependence of the rate in diffusion controlled reactions in a polymer chain, *J. Chem. Phys.*, 2001, **114**, 9170-9178.
- 12 G. Srinivas, A. Yethiraj and B. Bagchi, FRET by FET and dynamics of polymer folding, *J. Phys. Chem. B*, 2001, **105**, 2475-2478.
- 13 F. Huang and W. M. Nau, A conformational flexibility scale for amino acids in peptides, *Angew. Chem. Int. Ed. Engl.*, 2003, **42**, 2269-2272.

- 14 F. Huang, R. R. Hudgins and W. M. Nau, Primary and secondary structure dependence of peptide flexibility assessed by fluorescence-based measurement of end-to-end collision rates, 2004, submitted for publication.
- 15 X. Wang, E. N. Bodunov and W. M. Nau, Fluorescence quenching kinetics in short polymer chains: Dependence on chain length, *Opt. Spectrosc.*, 2003, **95**, 560-570.
- 16 J. R. Lakowicz, J. Kusba, I. Gryczynski, W. Wiczk, H. Szmanski and M. L. Johnson, End-to-end diffusion and distance distributions of flexible donor-acceptor systems observed by energy transfer and frequency-domain fluorometry; Enhanced resolution by global analysis of externally quenched and nonquenched samples, *J. Phys. Chem.*, 1991, **95**, 9654-9660.
- 17 A. Szabo, K. Schulten and Z. Schulten, First passage time approach to diffusion controlled reactions, *J. Chem. Phys.*, 1980, **72**, 4350-4357.
- 18 U. Pischel, F. Huang and W. M. Nau, Intramolecular singlet-singlet energy transfer in antenna-substituted azoalkanes, *Photochem. Photobiol. Sci.*, 2004, **3**, 305-310.
- 19 C. Marquez, U. Pischel and W. M. Nau, Selective fluorescence quenching of 2,3-diazabicyclo[2.2.2]oct-2-ene by nucleotides, *Org. Lett.*, 2003, **5**, 3911-3914.
- 20 H. A. H. Billiet, J. P. J. Van Dalen, P. J. Schoenmaker and L. De Galan, Measurement of deuterium oxide elution data in reversed-phase liquid chromatography with a microwave induced plasma detection, *Anal. Chem.*, 1983, **55**, 847-851.
- 21 K. K. Pandey, H. C. Joshi and T. C. Pant, Migration effects on excitation energy transfer by decay analysis using a nanosecond fluorimeter, *Chem. Phys. Lett.*, 1988, **148**, 472-478.
- 22 L. J. Lapidus, W. A. Eaton and J. Hofrichter, Dynamics of intramolecular contact formation in polypeptides: Distance dependence of quenching rates in a room-temperature glass, *Phys. Rev. Lett.*, 2001, **87**, 258101/258101-258101/258104.
- 23 S. J. Hagen, J. Hofrichter and W. A. Eaton, Rate of intrachain diffusion of unfolded cytochrome c, *J. Phys. Chem. B*, 1997, **101**, 2352-2365.
- 24 D. R. Buckler, E. Haas and H. A. Scheraga, Analysis of the structure of ribonuclease A in native and partially denatured states by time-resolved nonradiative dynamic excitation energy transfer between site-specific extrinsic probes, *Biochemistry*, 1995, **34**, 15965-15978.
- 25 I.-C. Yeh and G. Hummer, Peptide loop-closure kinetics from microsecond molecular dynamics simulations in explicit solvent, *J. Am. Chem. Soc.*, 2002, **124**, 6563-6568.
- 26 T. E. Creighton, *Proteins: Structures and Molecular Properties*. 2nd ed. New York, W. H. Freeman and Company, 1993.
- 27 M. Zacharias, D. Roccatano, unpublished results.

- 28 Dynamics of intramolecular contact formation in polypeptides: Distance dependence of quenching rates in a room-temperature glass. *Phys. Rev. Lett.*, 2001:258101/258101-258101/258104.
- 29 V. Gopalan, R. Golbik, G. Scheriber, A. R. Fersht and S. Altman, Fluorescence properties of a tryptophan residue in an aromatic core of the protein subunit of ribonuclease P from *Escherichia coli*, *J. Mol. Biol.*, 1997, **267**, 765-769.
- 30 D. P. Millar, Time-resolved fluorescence spectroscopy, *Curr. Opin. Struct. Biol.*, 1996, **6**, 637-642.
- 31 M. A. Hossain, H. Mihara and A. Ueno, Novel peptides bearing pyrene and coumarin units with or without β -cyclodextrin in their side chains exhibit intramolecular fluorescence resonance energy transfer, *J. Am. Chem. Soc.*, 2003, **125**, 11178-11179.
- 32 A. A. Deniz, et al., Single-molecule protein folding: Diffusion fluorescence resonance energy transfer studies of the denaturation of chymotrypsin inhibitor 2, *Proc. Natl. Acad. Sci. U. S. A.*, 2000, **97**, 5179-5184.
- 33 B. Schuler, E. A. Lipman and W. A. Eaton, Probing the free-energy surface for protein folding with single-molecule fluorescence spectroscopy, *Nature*, 2002, **419**, 743-747.
- 34 J. R. Lakowicz, *Principles of Fluorescence Spectroscopy*. 2nd ed. New York, Kluwer Academic/Plenum Publishers, 1999.
- 35 W. M. Nau and X. Wang, Biomolecular and supramolecular kinetics in the submicrosecond time range: The fluorazophore approach, *ChemPhysChem*, 2002, **3**, 393-398.
- 36 T. Bandyopadhyay and S. K. Ghosh, Diffusion influenced end-to-end reaction of a flexible polymer chain: the memory effect, *J. Chem. Phys.*, 2002, **116**, 4366-4369.
- 37 S. Faure, C. Stern, R. Guilard and P. D. Harvey, Role of the spacer in the singlet-singlet energy transfer mechanism (Forster vs Dexter) in cofacial bisporphyrins, *J. Am. Chem. Soc.*, 2004, **126**, 1253-1261.
- 38 C. F. Meares, S. M. Yeh and L. Stryer, Exchange interaction contribution to energy-transfer between ions in the rapid-diffusion limit, *J. Am. Chem. Soc.*, 1981, **103**, 1607-1609.
- 39 X. Wang and W. M. Nau, Kinetics of end-to-end collision in short single-stranded nucleic acids, *J. Am. Chem. Soc.*, 2004, **126**, 808-813.

Captions for schemes and figures

Scheme 1. Structure of doubly labeled peptides: a) Nal/DBO labeled peptides, Nal-(Gly-Ser)_n-DBO and b) Trp/DBO labeled peptides, Trp-(Gly-Ser)_n-DBO.

Scheme 2. Structure of CB7 combined peptides Nal-(Gly-Ser)₆-DBO.

Figure 1. Time-resolved fluorescence decay of naphthalene donor in doubly labeled peptides a) Nal-DBO, b) Nal-(Gly-Ser)₂-DBO, c) Nal-(Gly-Ser)₆-DBO, d) Nal-(Gly-Ser)₁₀-DBO, and in the donor-only peptide e) Nal-(Gly-Ser)₆. $\lambda_{\text{ex}} = 285\text{nm}$, $\lambda_{\text{em}} = 335\text{nm}$.

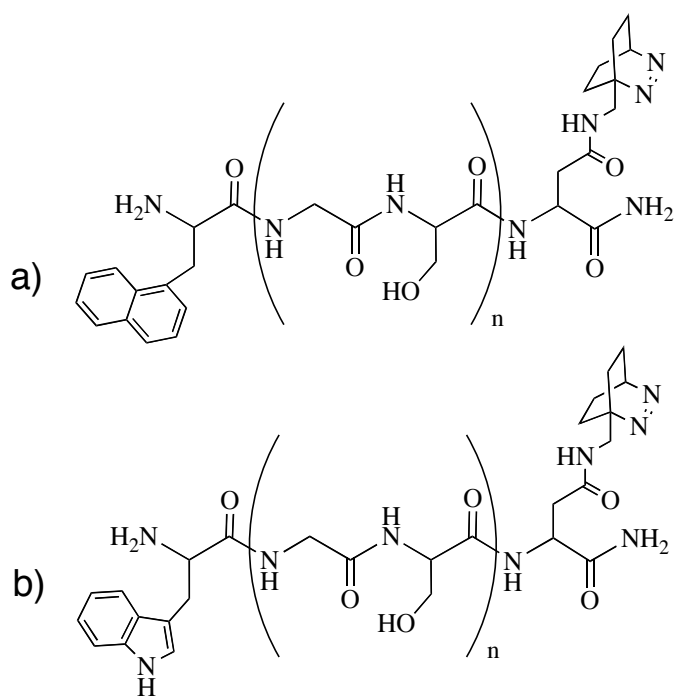
Figure 2. Time-resolved fluorescence decay of DBO acceptor in doubly labeled peptides a) Nal-DBO, b) Nal-(Gly-Ser)₂-DBO, c) Nal-(Gly-Ser)₆-DBO, and d) Nal-(Gly-Ser)₁₀-DBO. $\lambda_{\text{ex}} = 285\text{nm}$, $\lambda_{\text{em}} = 450\text{nm}$.

Figure 3. Representative end-to-end distance distribution in Nal/DBO doubly labeled peptides recovered from direct global analysis: Nal-DBO (—), Nal-(Gly-Ser)₂-DBO (----), and Nal-(Gly-Ser)₆-DBO (- - - -).

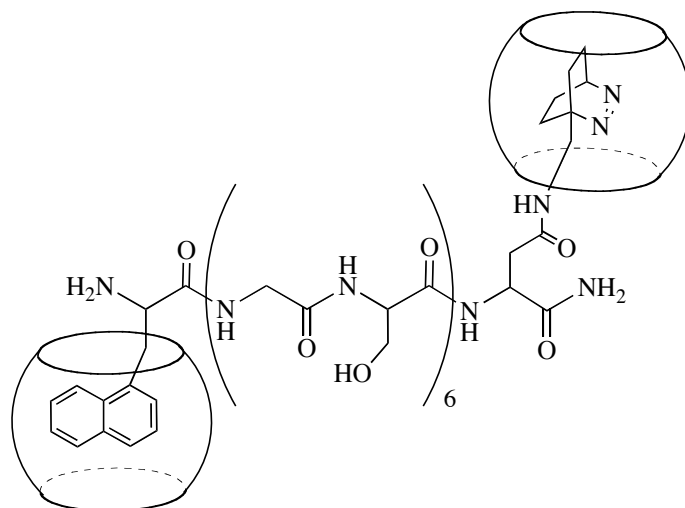
Figure 4. Fluorescence emission spectra of doubly labeled peptides Nal-(Gly-Ser)_n-DBO (solid line, from lower to the upper ones, $n = 0, 1, 2, 4, 6,$ and $10,$ respectively) and naphthalene donor-only peptide (dashed line, Nal-(Gly-Ser)₆), as well as the emission spectrum of peptide Nal-(Gly-Ser)₆-DBO (3.8×10^{15} M) in the presence of CB7 (7.5×10^{14} M) (dotted line). $\lambda_{\text{ex}} = 285$ nm.

Figure 5. FRET efficiency dependent on the donor/acceptor distance.

Figure 6. Double logarithmic plot of $k_{\text{q,ET}}$ (open cycle) and k_{q} (solid cycle) versus peptide length (data taken from Table 1). A function of the type $y = a - 1.5x - b/x$ was fitted to the experimental data ($a = 9.37, b = 0.392$ for data obtained from collision-based experiments,⁶ and $a = 9.57, b = 0.229$ for data obtained from experiments based on singlet-singlet energy transfer from current work). The dash-dot-dash line has a slope of -1.5 and is shown to illustrate the deviation from the theoretical behavior.



Scheme 1



Scheme 2

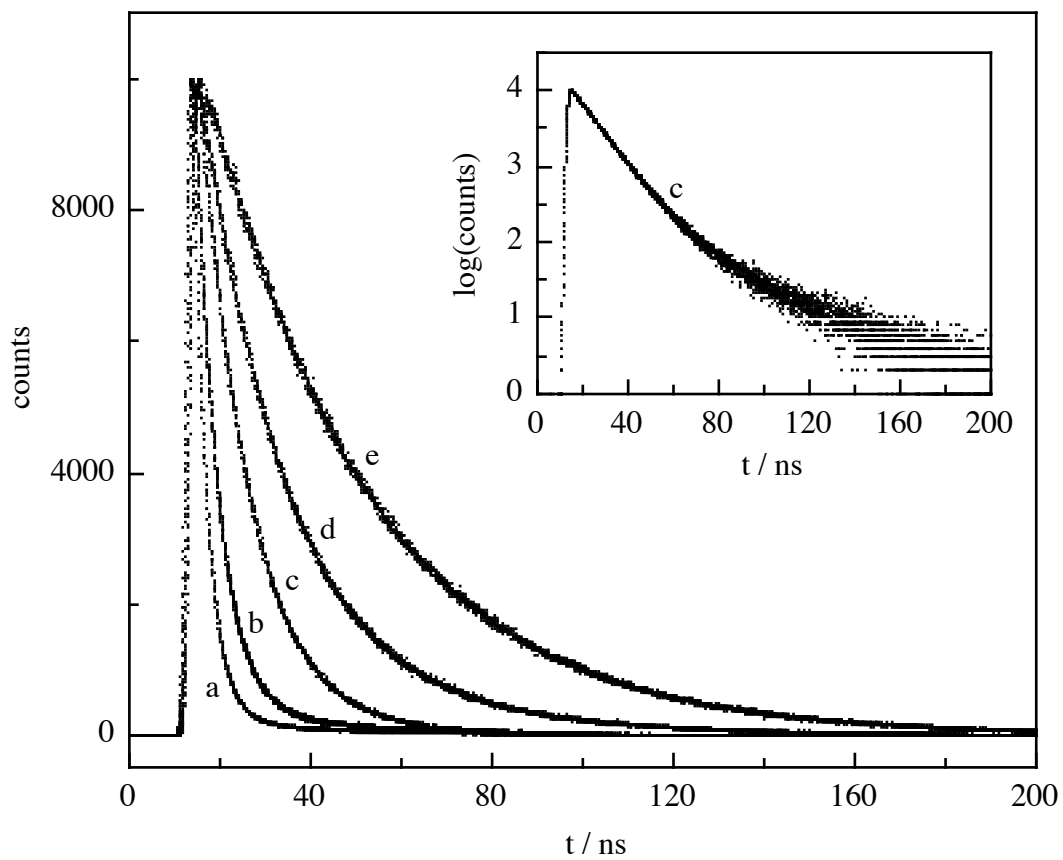


Figure 1

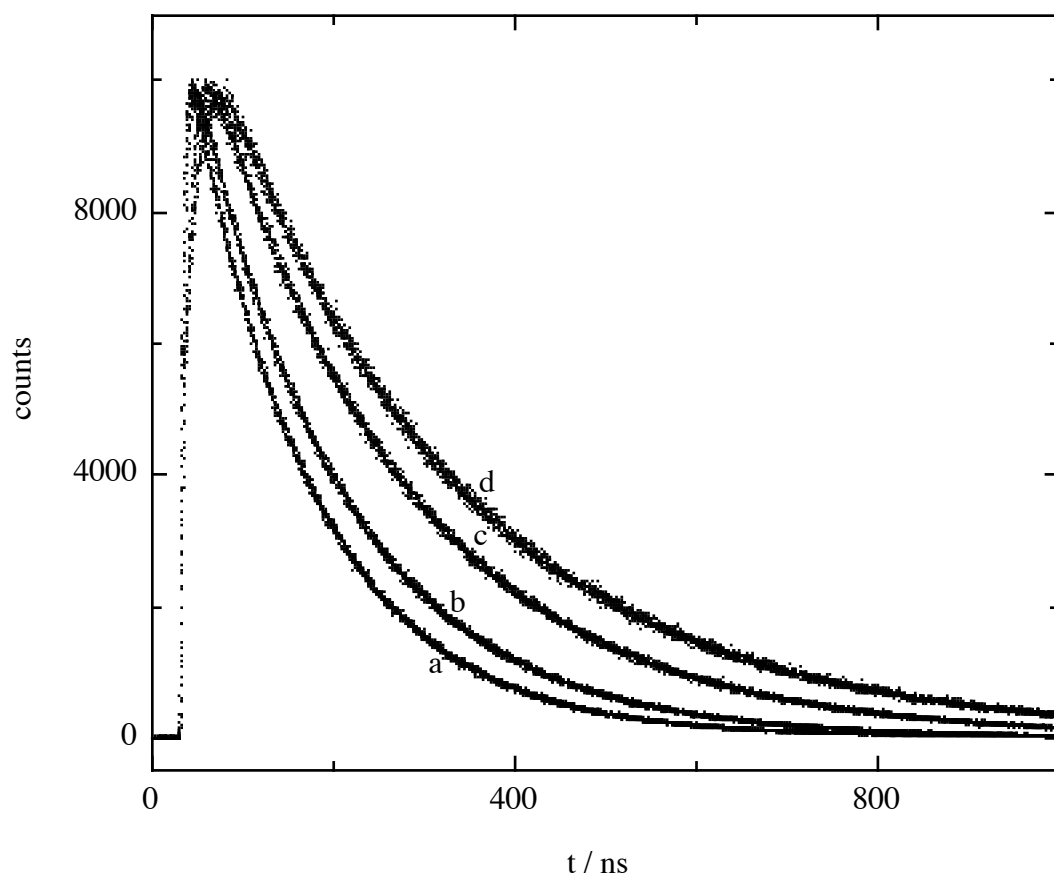


Figure 2

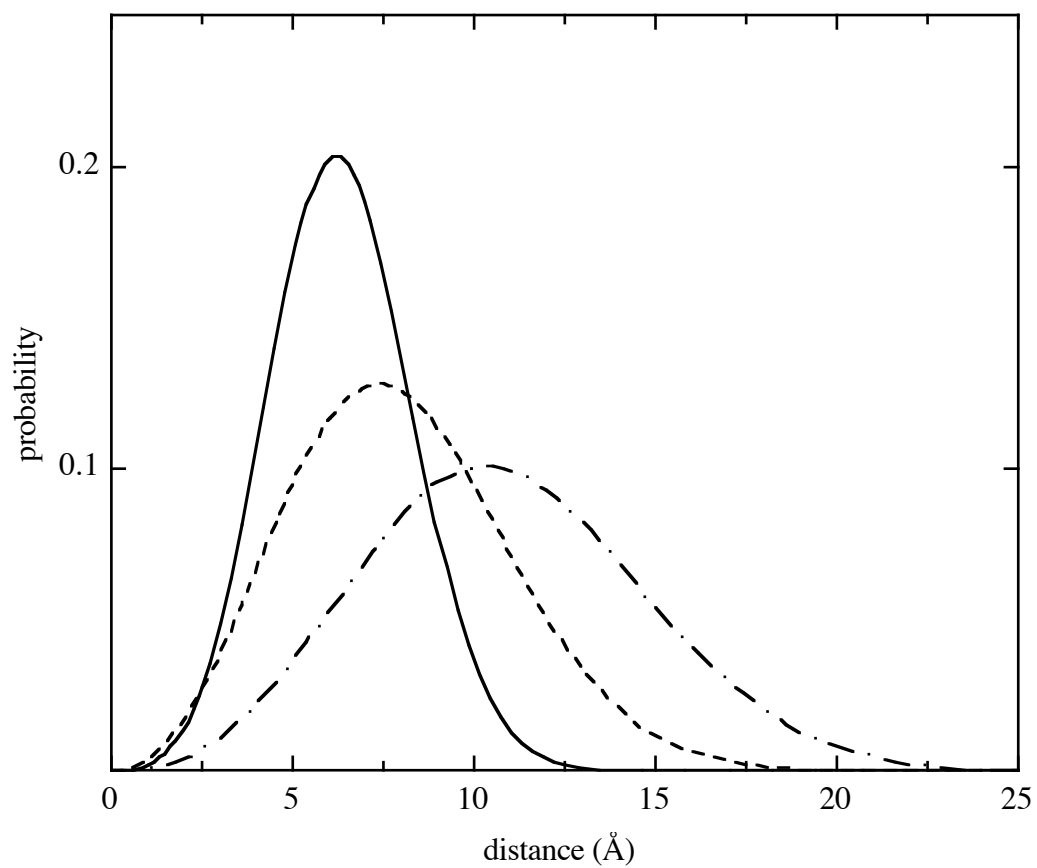


Figure 3

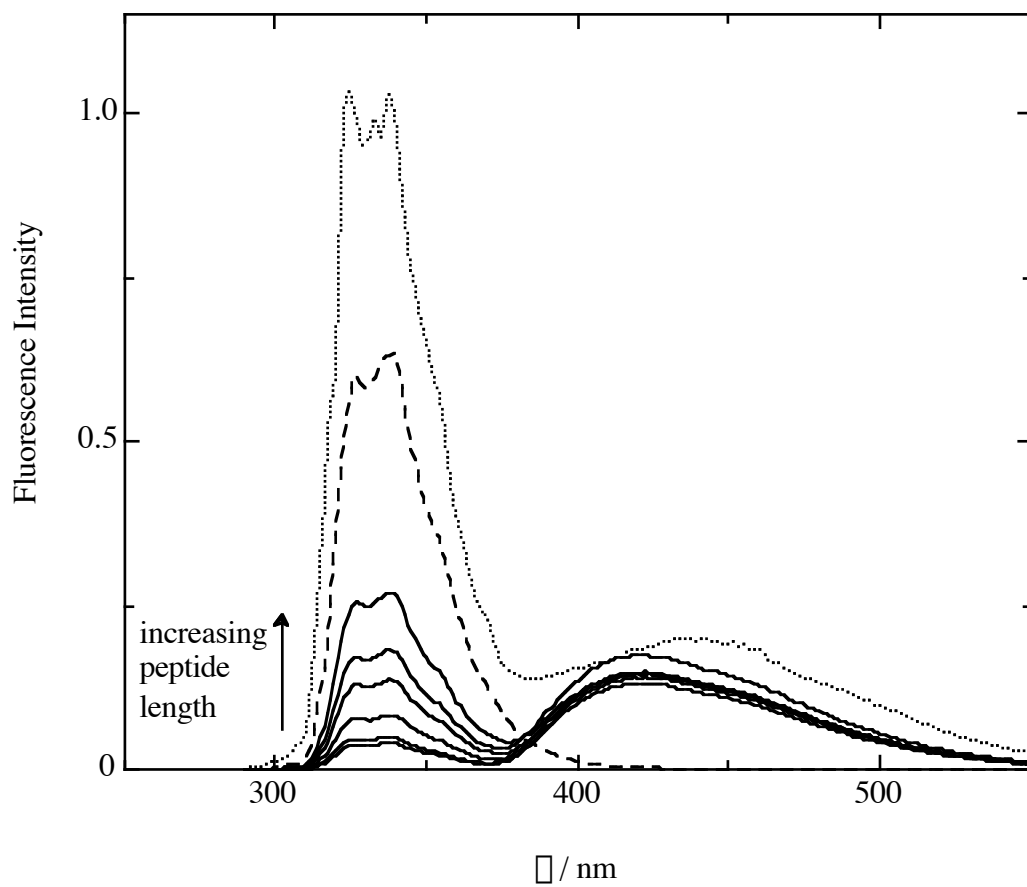


Figure 4

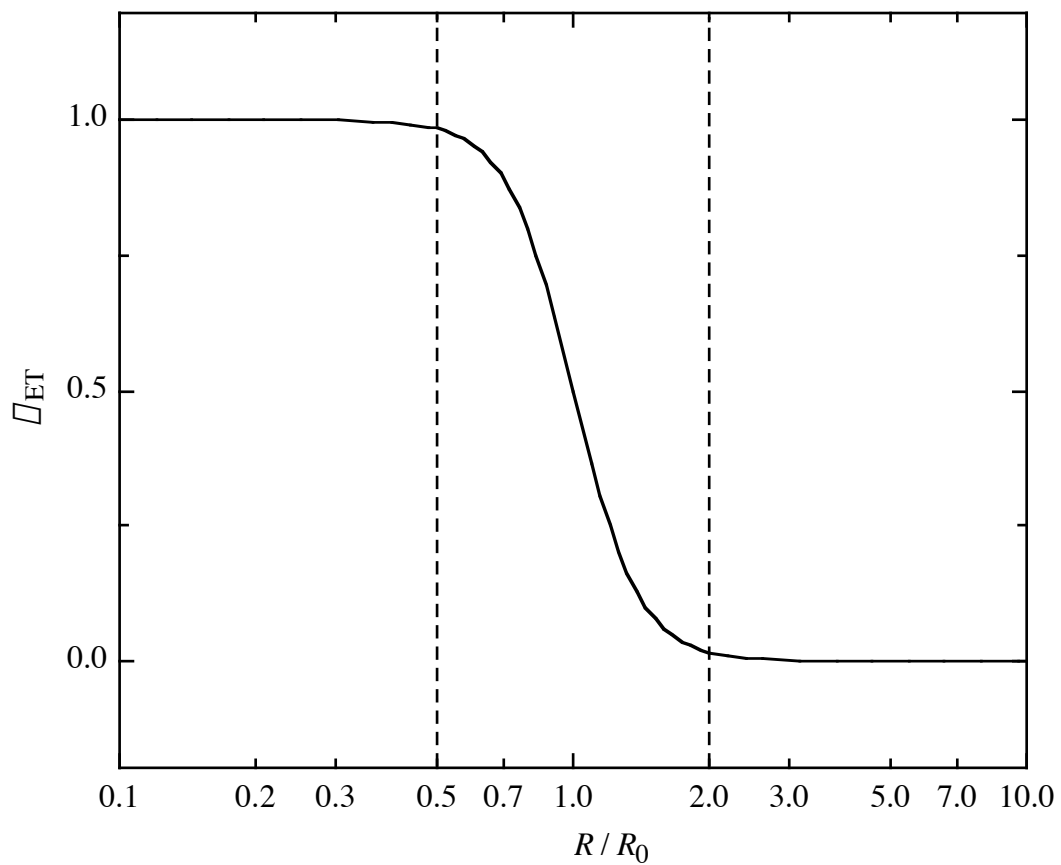


Figure 5

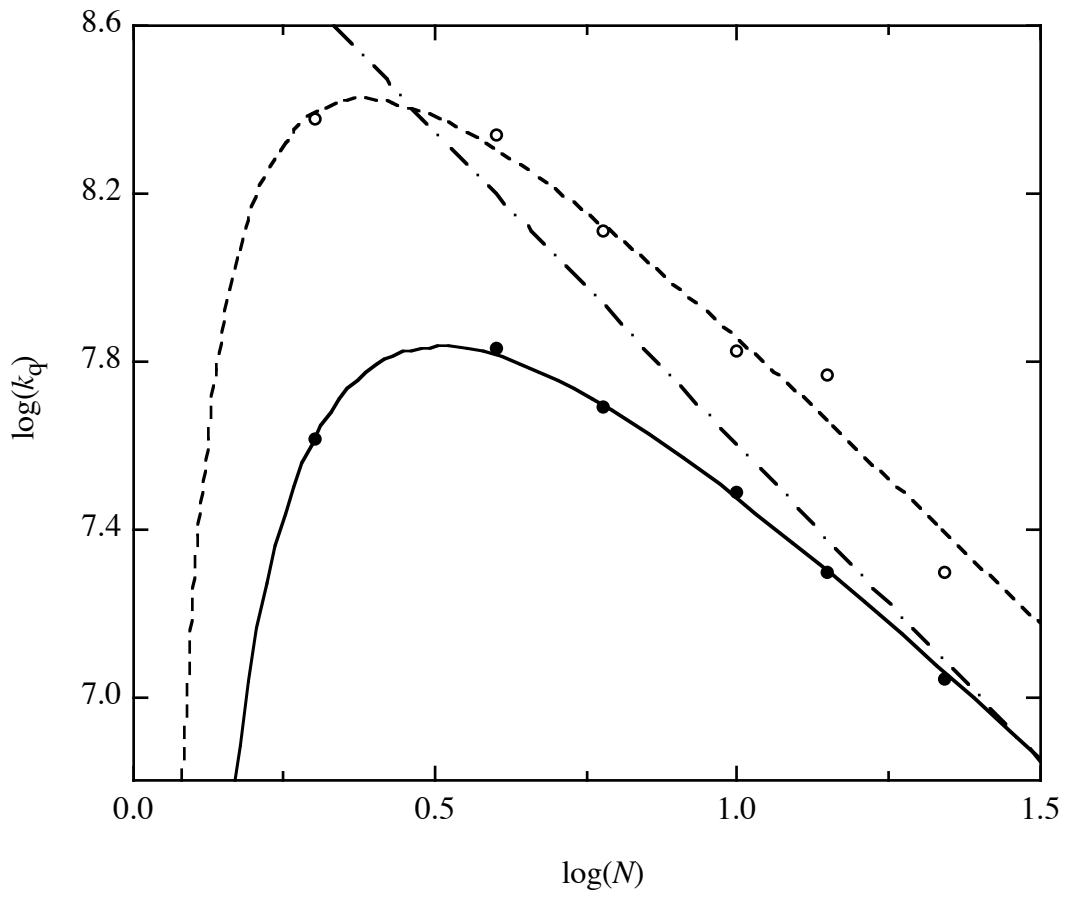


Figure 6

Table 1. Parameters of naphthalene fluorescence lifetimes in donor-only-labeled and donor/acceptor doubly-labeled peptides^a

peptide	N	$\sum(\tau_i)$ (ns) ^b	τ	$\langle\tau\rangle$ (ns) ^c	k_{qET} (10 ⁷ s ⁻¹) ^d	k_q (10 ⁷ s ⁻¹) ^e
Nal-(G-S) ₆		35.5(1.000)	1.01	35.5		
Nal-DBO	2	3.1(0.975), 25.8(0.025)	1.28	3.7	24	4.1
Nal-G-S-DBO	4	3.5(0.966), 22.6(0.034)	1.36	4.1	22	6.8
Nal-(G-S) ₂ -DBO	6	5.0(0.961), 35.4(0.039)	1.09	6.2	13	4.9
Nal-(G-S) ₄ -DBO	10	8.3(0.920), 36.0(0.080)	1.09	10.5	6.7	3.1
Nal-(G-S) ₆ -DBO	14	10.8(0.978), 36.4(0.022)	1.11	11.4	5.9	2.0
Nal-(G-S) ₁₀ -DBO	22	18.2(0.904), 45.0(0.095)	1.12	20.7	2.0	1.1

^a $\lambda_{ex} = 285$ nm and $\lambda_{em} = 335$ nm.

^b Recovered lifetimes (τ) and preexponential factors (τ_i , normalized) of single or double exponential fits to time-resolved fluorescence decay of naphthalene residue in different peptides.

^c Lifetime averages ($\langle\tau\rangle$) for multi-exponential fits.²⁴

^d Apparent quenching rate constants of naphthalene by DBO, calculated from the average lifetime of naphthalene in Nal-(Gly-Ser)_n-DBO peptides.

^e Collision-controlled intrachain quenching rate constants of DBO by tryptophan, taken from Ref. 6.

Table 2. Distance distribution and diffusion coefficient recovered from global analysis for Nal-(GlySer)_n-DBO peptides.

n	N	L (Å) ^a	direct global analysis			model-assistant analysis		
			R _{mean} (Å) ^b	D (10 ⁻⁷ cm ² /s)	χ ²	R _{mean} (Å) ^c	D (10 ⁻⁷ cm ² /s)	χ ²
0	2	7.6	6.14	2.67	1.12	5.4	0.78	1.42
1	4	15.2	6.26	2.76	1.09	7.6	5.44	1.10
2	6	22.8	7.96	4.03	1.13	9.3	11.69	1.14
4	10	38.0	10.39	5.66	1.11	12.0	14.73	1.12
6	14	53.2	10.91	4.91	1.08	14.2	79.0	1.10
10	22	83.6	14.76	4.47	1.16	17.8	4.2	1.16

^a Contour length, $L = N l$, where N is the number of intervening peptide units and l is the length per unit (Kuhn length), taken as 3.8 Å.

^b Experimental average end-to-end distance obtained by FRET measurements and direct global analysis.

^c Root mean square end-to-end distance of each peptide calculated from the relationship

$$R_{\text{mean}} = l\sqrt{N}.$$

Table 3. Energy transfer efficiency and effective end-to-end distance in peptides Donor-(Gly-Ser)_n-DBO with naphthalene and tryptophan serve as energy donor.

<i>n</i>	<i>N</i>	Donor = naphthalene		Donor = tryptophan	
		$\overline{\mu}_{\text{ET}}$	$R'_{\text{mean}} (\text{\AA})$	$\overline{\mu}_{\text{ET}}$	$R'_{\text{mean}} (\text{\AA})$
0	2	0.94	6.2	0.94	6.4
1	4	0.92	6.5	0.86	8.6
2	6	0.87	7.1	0.79	9.5
4	10	0.73	8.3	0.68	10.7
6	14	0.70	8.5	0.65	11.3
10	22	0.61	9.1	0.58	11.0